

ECONOMIC GEOLOGY OF THE
AVOCA MINERALIZED BELT S.E. IRELAND,
AND
PARYS MOUNTAIN, ANGLESEY

by

CHRISTOPHER JOHN VARLEY WHEATLEY

A thesis submitted for the degree of
Doctor of Philosophy in the University of London

Department of Mining Geology,
Imperial College of Science and Technology,
London, England.

September 1971

A B S T R A C T

The stratigraphy, lithology, petrology and structure of the rocks in the Avoca district are described. Graded bedding, a phosphorite horizon and carbonaceous intercalations in a sequence of Lower Palaeozoic sediments and volcanics suggest deposition in a shallow-water volcanic environment. The felsites represent a pyroclastic rhyolitic suite and may be ignimbritic, analyses of the rocks imply that the magma source was potassic.

The ore mineral textures at Avoca and their paragenesis are considered in detail, and the first annotated description of a series of lead-bismuth sulphosalts, gold and ullmannite is presented. The mineralization is divided into a series of ore-types. Conformable, lenticular cupriferous pyritic zones are thought to have formed in a marine environment, possibly during diagenesis, with mineral growth taking place below the sediment-water interface. Trace element contents of the sulphides, sulphur isotope results and the evidence for contemporaneous explosive volcanic activity support the notion that the supply of iron, copper and sulphur was probably fumarolic. Magnetite zones developed under different Eh and pH conditions. Stockworks, containing appreciable copper and, in some cases, lead and zinc were developed stratigraphically below the pyritic zones by hydrothermal metal-rich fluids at a later date. Accompanying wallrock alteration consists of silicification and potassic metasomatism. It is suggested that the hydrothermal fluids were chloride-rich, derived from the aqueous phase of an underlying magma and the metal contents may have been of juvenile or connate origin. Complex lead-zinc-pyrite mineralization resulted from the reaction between the pyritic zones and the final fractions of the hydrothermal fluids.

Crosscutting, vein-type cupriferous mineralization occurs at Bunmahon and lead-zinc veins occur elsewhere in S.E. Ireland. These apparently comprise a pulsatory metasomatic sequence, which is closely related to deformation and plutonism.

The geological environment and mineralization at Parys Mountain are analogous to that at Avoca, and a similar genetic model is proposed.

Comparisons are drawn with comparable deposits elsewhere and the implications of the study are considered.

CONTENTS

	<u>Page</u>
<u>VOLUME I</u>	
Abstract	(i)
List of Figures	(x)
List of Tables	(xii)
Acknowledgements	(xv)
Symbols	(xvi)
SECTION 1 INTRODUCTION	
1.1. General	1
2. Geological Framework	1
3. Distribution of Mineral Deposits	5
4. Present study	5
1.4.1. Purpose	5
2. Scope	5
SECTION 2 AVCCA DISTRICT	
2.1. Regional Geology	8
2.1.1. Introduction	8
2. Previous geological work	8
3. Stratigraphy	8
2.1.3.1. Precambrian	8
2. Cambrian	10
3. Ordovician	10
4. Silurian	12
5. Upper Palaeozoic	12
6. Mesozoic and Tertiary	12
7. Quaternary	12
4. Intrusive Rocks	13
2.1.4.1. Precambrian	13
2. Caledonian	13
a) Acidic	13
b) Basic	13
5. Economic Geology	13
2.1.5.1. Copper	13
2. Lead-zinc	15

SECTION 2 (cont.)	<u>Page</u>
2.1.6. Structure and Tectonic sequence	15
7. Geochronology	17
2.1.7.1. Sedimentary rocks	17
2. Granites	18
3. Mineralization	18
4. Summary	18
2.2. General Geology	18
2.2.1. Introduction	18
2. Stratigraphy	20
2.2.2.1. Clara Series	20
2. Lower Laminated Series	22
3. Upper Volcanic Series	22
4. Intrusive rocks	24
3. Petrography	26
2.2.3.1. Sedimentary rocks	26
2. Volcanic rocks	26
3. Intrusive rocks	28
4. Petrochemistry	31
2.2.4.1. Major oxides	31
2. Trace elements	33
5. Petrogenesis	34
2.2.5.1. Granitic rocks	34
2. Felsites	34
3. Intermediate pyroclastics and intrusives	37
6. Mineralization	37
7. Structure	47
2.2.7.1. Mesoscopic Structure	47
a) Planar	47
b) Linear	52
2. Macroscopic structure	53
3. Stress distribution	55
2.3 Economic Geology	55
2.3.1. Introduction	55
2. History of Mining	55
3. Stratigraphy	57

SECTION 2 (cont.)

	<u>Page</u>
2.3.3.1. The Mine Schists	60
a) Lithology and Petrography	60
b) Wallrock alteration	67
c) Discussion	72
d) Summary	78
2. Intrusive Rocks	78
a) Lithology and Petrography	78
b) Petrogenesis	79
4. Structure	80
2.3.4.1. Mesoscopic Structure	80
a) Planar	80
b) Linear	88
c) Discussion	89
2. Macroscopic Structure	90
3. Stress Distribution	93
5. Nature of the Ore Zones	93
2.3.5.1. West Avoca	93
a) North Orebody	93
b) Pond Orebody	95
c) South Orebody	96
d) Lead-zinc lode	98
2. East Avoca	98
a) Tigroney	98
b) Cronebane	99
c) Connary	100
d) Kilmacoo	100
2.3.6. The ore minerals and their paragenesis	100
2.3.6.1. Introduction	100
2. Ore Mineralogy	101
a) Pyritic zones	101
b) Siliceous zones	103
c) Lead-zinc zones	103
d) Magnetite zones	103
e) Disseminated and vein-type mineralization	103
3. Laboratory Methods	104
a) Indentation Microhardness	104
b) Reflectivity	104
c) Electron-probe analysis	105
d) X-ray diffraction	105
e) Etching	106
4. Primary Minerals	106
a) Pyrite	106
b) Chalcopyrite	115
c) Sphalerite	118
d) Galena	121
e) Magnetite	123
f) Hematite	124

SECTION 2 (cont.)

	<u>Page</u>
2.3.6.4. g) Arsenopyrite	125
h) Chromite	125
i) Pyrrhotite	125
j) Cobaltite	126
k) Tennantite-tetrahedrite	126
l) Bournonite	126
m) Native Bismuth	127
n) Bismuthinite	127
o) Galenobismutite	127
p) Aikinite	128
q) Kobellite	129
r) Lillianite	132
s) Ullmannite	134
t) Gold	135
5. Supergene Minerals	136
a) 'Limonite'	137
b) Goethite	137
c) Hematite	137
d) Covellite	137
e) Marcasite	137
f) Native Copper	138
g) Malachite and chalcantinite	138
6. Gangue Minerals	138
a) Quartz	138
b) Chlorite	139
c) Sericite	140
d) Carbonates	140
e) 'Graphite'	140
f) Apatite	140
g) Leucoxene	141
7. Discussion	141
a) Introduction	141
b) Pyrite	141
c) Chalcopyrite, sphalerite and galena	150
d) Magnetite and hematite	151
e) Minor sulphides	152
f) Tennantite-tetrahedrite	152
g) Precious Metals	152
h) Sulphosalts	156
2.3.7. Trace Element Distribution	156
2.3.7.1. Introduction	156
2. Method of Analysis	156
3. Results	157
4. Interpretation	163
a) Contamination Indicators	163
b) Pyrite	163
c) Magnetite	167
d) Hematite	169
e) Chalcopyrite	169
f) Sphalerite	170
g) Galena	172

SECTION: 2 (cont.)	<u>Page</u>
2.3.7.5. Discussion	173
a) Theoretical predictions of element distribution	173
b) Applications of trace element analysis	174
2.3.8. Mineral Stabilities and phase relations	190
2.3.8.1. Geothermometry and geobarometry	190
a) Pyrite-pyrrhotite	190
b) Arsenopyrite	192
c) Sphalerite	192
d) Exsolution textures	193
e) Thermoluminescence	195
f) Fluid inclusions	195
g) Univariant points	196
h) Sulphur isotopes	196
i) Trace elements	198
j) Summary	198
2. Phase relations as environmental indicators	198
a) Pyrite	198
b) Iron oxides	202
c) Base metals	203
d) Wallrock and base metal assemblage	205
2.3.9. Mineral and Metal distribution	205
2.3.9.1. Mineral distribution	205
a) Pond lode	205
b) South lode	207
2. Metal ratios	208
a) Pond lode	208
b) South lode	208
c) Lead-zinc lode	208
3. Relationship between mineral distribution and lode structure	208
a) South lode	210
b) Pond lode	210
4. Discussion	211
2.3.10. Genesis	214
2.3.10.1. General	214
2. Pyritic zones	214
3. Siliceous zones	216
4. Lead-zinc zones	219
5. Magnetite zones	219
6. Disseminated and vein-type mineralization	219
7. Post-depositional changes	220
8. Summary	220

SECTION 3 OTHER DEPOSITS IN S.E. IRELAND	<u>Page</u>
3.1. Bunmahon, Co. Waterford	222
3.1.1. Introduction	222
2. Stratigraphy	222
3. Lithology and Petrography	222
4. Petrochemistry	224
5. Wallrock alteration	226
6. Environment of deposition	226
7. Intrusive rocks	226
8. Structure	226
3.1.3.1. Mesoscopic structure	226
a) Planar	226
b) Linear	227
2. Macroscopic structure	227
9. Mineralization	227
3.1.9.1. Form	227
2. Ore mineralogy	229
a) Primary minerals	229
b) Supergene minerals	229
c) Gangue minerals	229
3. Trace element distribution	230
4. Genesis	230
3.2. Lead-zinc occurrences	234
3.2.1. Cain and Barrystown, Co. Wexford	234
3.2.1.1. Geology	234
2. Genesis	235
2. Glendalough, Co. Wicklow	235
3.2.2.1. Geology	235
2. Genesis	238
3. General	238
 SECTION 4 ANGLESEY	
4.1. Parys Mountain	239
4.1.1. Introduction	239
2. Stratigraphy	239
3. Lithology	241
4. Petrography	242
5. Petrochemistry	244

SECTION 4 (cont.)	<u>Page</u>
4.1.6. Petrogenesis	244
7. Wallrock alteration	244
8. Environment of deposition	244
9. Structure	245
4.1.9.1. Mesoscopic structure	245
a) Planar	245
b) Linear	245
2. Macroscopic structure	247
3. Stress distribution	247
10. Mineralization	249
4.1.10.1. Nature of ore zones	249
2. Ore Mineralogy	249
a) Primary minerals	249
b) Supergene minerals	255
c) Gangue minerals	255
d) Summary	256
3. Trace element distribution	256
a) Pyrite	256
b) Chalcopyrite	256
c) Sphalerite	256
d) Galena	256
e) Discussion	259
4. Mineral and metal distribution	260
5. Genesis	261
4.2. Rhosmynach	263
 SECTION 5 RELATED DEPOSITS	
5.1. The Southern Caledonides	265
5.1.1. Coniston	265
5.1.1.1. Lithology, petrology and petrogenesis	265
2. Wallrock alteration	265
3. Environment of deposition	268
4. Intrusive rocks	268
5. Structure	268
6. Mineralization	268
7. Trace element distribution	269
8. Genesis	269
5.1.2. Other deposits in the Southern Caledonides	271
5.2. World-wide	271

SECTION 6 CONCLUSIONS AND IMPLICATIONS

	<u>Page</u>
6.1. Avoca mineralized belt	275
2. S.E. Ireland	276
3. Parys Mountain	276
4. Related deposits	276
5. Implications	277

APPENDICES:

1. Whole-rock x-ray fluorescence analytical method, using close standardization.	278
2. Description of samples in table 1, from Co. Wicklow, Ireland.	280
3. Lines used in spectrographic analysis.	281
4. The B/Q logging method.	282

REFERENCES	287
------------	-----

VOLUME II

Plates: 1 ~ 51	306
Maps: 1 - 8	Separate

LIST OF FIGURES

	<u>Page</u>
SECTION 1.	
1.1. Geological framework of the Southern Caledonides.	2
2. Comparative lithostratigraphic sections in the Southern Caledonides.	3
3. Mineralization in the Southern Caledonides.	6
SECTION 2.	
2.1. Stratigraphic relations in S.E. Ireland.	9
2. Radiometric dating in S.E. Ireland.	14
3. Structural elements in S.E. Ireland.	16
4. Geological sketch map, Avoca district.	19
5. Vertical lithostratigraphic sections, Avoca district.	21
6. Variation diagrams of volcanic and plutonic rocks, Avoca district.	35
7. Mineral occurrences in the Avoca district.	38
8. Ballymoneen - plan and section.	43
9. Bedding and cleavage, Avoca district.	48
10. Structural elements, Avoca district.	50
11. Generalized cross-section, S.E. Ireland.	54
12A. Avoca mining district : longitudinal plan and section of workings.	58
12B. Avoca mining district : surface geological plan.	59
13. West Avoca, geological cross-section : 1+00E.	61
14. East Avoca - Tigroney, idealized cross-section.	62
15. Major and trace element variations in an idealized cross-section, West Avoca.	70
16. Nature of chlorite at Avoca.	76
17. Geological map of P ⁴ crosscut south, 1670 level, West Avoca.	81
18. Geological map of 10 ⁴ 7 level crosscut south, West Avoca.	82
19. Cleavage, West Avoca - underground.	83
20. Planar features, West Avoca - underground.	85
21. Faulting, and linear elements, West Avoca - underground.	87
22. Diagrammatic structural evolution, West Avoca.	92

SECTION 2 (cont.)	<u>Page</u>
2.23. Avoca district, distribution of the ore minerals.	102
24. Size distribution of framboidal pyrite, Avoca.	113
25. Bismuth sulphosalts from Avoca.	130
26. Avoca district, paragenetic table.	142
27. Summary of the major ore mineral fabrics, Avoca district.	143
28. Tennantite-tetrahedrite minerals from various deposits.	154
29. Chart of the sulphosalt assemblage at Avoca.	155
30. Co and Ni in pyrite, Avoca - underground.	177
31. Co and Ni in pyrite, Avoca - surface.	178
32. Co and Ni in pyrite from comparative deposits.	179
33. Co and Ni in coexisting pyrite and chalcopyrite, Avoca district.	183
34. Stream sediment sampling, Avoca district.	189
35. Pyrrhotite and arsenopyrite stability relations.	191
36. Iron content of sphalerite.	194
37. Sulphur isotopes.	197
38. Temperature variation during formation of the Avoca deposits.	199
39. Stability relations of iron (I).	200
40. Stability relations of iron (II).	201
41A. Composition of liquid and vapour phases in hydrothermal ore deposits.	204
41B. The field of Avoca ore minerals in the Cu-Fe-S system.	204
42. Fugacity - pH diagram of part of the Cu-Fe-S-O system.	206
43. Metal ratios, West Avoca.	209
 SECTION 3	
3.1. Bunmahon district, geological sketch map.	223
2. Bunmahon district, magascopic metal zoning.	233
3. Glendalough district, geological sketch map.	236

SECTION 4

	<u>Page</u>
4.1. Parys Mountain, geological sketch map and generalized cross-section	240
2. Structural relationships, Parys Mountain.	246
3. Cross-sections, Parys Mountain.	248
4. Mineralization at Parys Mountain.	250
5. Size distribution of framboidal pyrite, Bluestone, Parys Mountain.	251
6. Parys Mountain, paragenetic table.	252
7. Sketch level plans, Carreg-y-doll lode.	262

SECTION 5

5.1. Geological sketch map, Coniston district.	266
--	-----

APPENDICES

A.1. West Avoca, mineral distribution graphs.	286
---	-----

LIST OF TABLES

	<u>Page</u>
1. Chemical analyses and ClPW norms of representative volcanic and plutonic rocks from the Avoca district.	32
2. Partial analyses of representative lithological rock units, West Avoca.	69
3. Partial probe analyses of chlorites from West Avoca.	74
4. X-ray powder diffraction data for chlorite.	75
5. Ore zones in the Avoca mine area.	94
6. Composition of bournonite.	127
7. Composition of galenobismutite.	128
8. Composition of aikinite.	129
9. Comparative x-ray powder diffraction data for aikinite.	131
10. Composition of kobellite.	132
11. X-ray powder diffraction data for kobellite.	133
12. Composition of lillianite.	134
13. a) Composition of ullmannite. b) Comparative x-ray data for ullmannite.	135
14. Composition of gold.	136
15. Grain size of pyrite in the Norwegian Caledonides.	145
16. Characteristics of leached textures in pyrite.	149
17. Probe analyses of tennantite-tetrahedrite from Avoca and other areas.	153
19. Spectrographic analysis of pyrite - Avoca district, underground.	158
20. Spectrographic analysis of pyrite - Avoca district, with comparative samples.	159
21. Spectrographic analysis of magnetite and hematite - Avoca district, with comparative samples.	160
22. Spectrographic analysis of chalcopyrite - Avoca district, with comparative samples.	161
23. Spectrographic analysis of sphalerite and galena - Avoca district,	162
24. X-ray fluorescence analyses of selenium in pyrite.	167
25. Comparative probe and spectrographic analyses of iron content in sphalerite, Avoca district.	184
26. Trace elements in primary and remobilized sphalerite.	186
27. Statistical analysis of trace elements in pyrite, Avoca district.	187
28. Partial analyses of rocks from the Bunmahon district, by x-ray fluorescence.	225

(Tables (cont))

	<u>Page</u>
29. Mineralization at Bunmahon.	228
30. Generalized paragenetic sequence, Bunmahon.	230
31. Spectrographic analysis of sulphides, Bunmahon and Cain.	231
32. Generalized paragenetic sequence: Cain and Barrystown.	234
33. Generalized paragenetic sequence: Glendalough	237
34. Parys Mountain, stratigraphic relations.	241
35. Partial analyses of felsites from Parys Mountain by x-ray fluorescence.	243
36. Spectrographic analysis of pyrite and chalcopyrite, Parys Mountain.	257
37. Spectrographic analysis of sphalerite and galena, Parys Mountain.	258
38. Comparative analysis of iron contents in sphalerite, Parys Mountain.	259
39. Partial analyses of rocks from the Coniston district, by x-ray fluorescence.	267
40. Generalized paragenetic sequence, Coniston.	269
41. Spectrographic analysis of sulphides and magnetite, Coniston.	270
42. X-ray fluorescence operating conditions (PW 1540).	279

ACKNOWLEDGEMENTS

The writer expresses his gratitude to the Institution of Mining and Metallurgy, London, for sponsoring the study through an Edgar Pam Fellowship. Thanks are due to Professor G.R. Davis for continual interest and for making available facilities in the Mining Geology Department. The assistance of every staff member is gratefully acknowledged, especially Dr. Barry Scott who supervised the work.

Cordial thanks are offered to the mining companies who permitted access to their properties and offered essential information, in particular, the management and staff of Avoca Mines Limited.

Discussions and stimulating suggestions from numerous people have improved the manuscript, in particular, Professor A.P. Millman, University College, Cardiff, B.K. Atkinson, R. Berlin, B. Jackaman, J. McM. Moore and Dr. C.J. Morrissey. G.M. Steed provided patient instruction on microprobe techniques and the stream sediment analyses were carried out by D.S. Evans. Dr. A.B. Poole, Queen Mary College, London, kindly made available x-ray fluorescence equipment and introduced the writer to its use.

The technical staff of the Department of Geology helped considerably, notably Mr. B. Foster, Mrs K. Irving, Mr. J.A. Gee, Miss H. O'Brien and Mr. J. Blount. The text was typed by Mrs S. Bird.

This thesis would not have been completed without the endless aid and encouragement of Patricia, the writer's wife, to whom the work is dedicated.

SYMBOLS

Mineralogical

Shown on Fig. 2.23 (p102).

Abbreviations

$^{\circ}\text{A}$	angstrom units.
\sim	approximately.
aq	aqueous state (suffix).
atm.	atmospheric pressure.
bar	pressure equivalent to 750.08mm Hg at 0°C .
c	crystalline state (suffix).
$^{\circ}\text{C}$	degree Centigrade.
cm	centimetre ($=0.0328$ ft).
d	lattice spacing between successive identical planes.
DDH.	diamond drill hole.
dissem.	disseminated.
$\delta^{34}\text{S}$	variation in ^{34}S concentration relative to the $^{34}\text{S}/^{32}\text{S}$ ratio of Canon Diablo meteoritic troilite.
$^{\circ}$	degree.
Eh	potential relative to the hydrogen half cell.
ft } , }	foot ($=30.48\text{cm}$)
FW.	footwall.
gm	gram.
HV	Vickers indentation microhardness.
HW.	hangingwall.
kb	kilobar.
kg	kilogram.
km	kilometre.
L.	mine level.
M	molar.
m	metre.
m.y.	million years.

Abbreviations

mass.	massive.
oz	ounce.
P.	Pond.
pH	negative logarithm of the hydrogen ion activity.
ppb	part per billion (10^9).
ppm	part per million (10^6).
R%	reflectivity.
s.g.	specific gravity.
Sh.	shaft.
T	temperature
t.	long ton.
t.p.d.	long ton per day.
v	volt.
2V	axial angle.
X-c	crosscut.
$Z_{\Delta c}$	angle between slow ray and c crystallographic axis.
>	greater than.
\geq	greater than, or equal to.
<	less than.
\leq	less than, or equal to.
μ	micron ($=10^{-3}$ mm).
σ	Standard deviation.

S E C T I O N 1

INTRODUCTION1.1. General

The mining districts described in this text occur along a northeasterly line cutting obliquely across the British Isles from the Waterford coast in S.E. Ireland northwards to the Lake District in Northern England (Fig 1.1.)

Avoca, the site of the major copper-lead-zinc deposit in S.E. Ireland, situated in Co. Wicklow, is about forty miles south of Dublin. Bunmahon, a former copper producing area on the coast of Co. Waterford, is seventy miles southwest of Avoca and marks the southwestern limit of the mineralization.

Parys Mountain, in northeast Anglesey, was once the major copper mine in Britain.

1.2. Geological Framework

The Caledonian mobile belt in Western Europe includes the Southern Caledonides (104), which collectively describes the Lower Palaeozoic rocks in the British Isles occurring southeast of the Highland Boundary fault. (Fig 1.1.) The Southern Caledonides are part of a paratectonic zone where deformation was less intense than in the northerly orthotectonic region (71), and contain the mining districts. The stratigraphic sequence consists of:(Fig 1.2.)

1.2.1. Precambrian

Basement rocks, tentatively divided into a Lower and Upper Proterozoic sequence (13), are exposed along the axis of a prominent median welt : the Irish Sea geanticline. (Fig 1.1.) The Lower Proterozoic rocks consist of the gneisses of the Rosslare Complex and the Lleyrn in North Wales, with the Arvonian volcanics in Anglesey. The Upper Proterozoic (Monian) slates and greywackes are exposed in S.E. Ireland and North Wales, and accumulated in a Caledonoid trough. Dalradian sediments, underlying Ordovician rocks in Western Ireland may be equivalent to the Monian (201) and were probably deposited in a separate

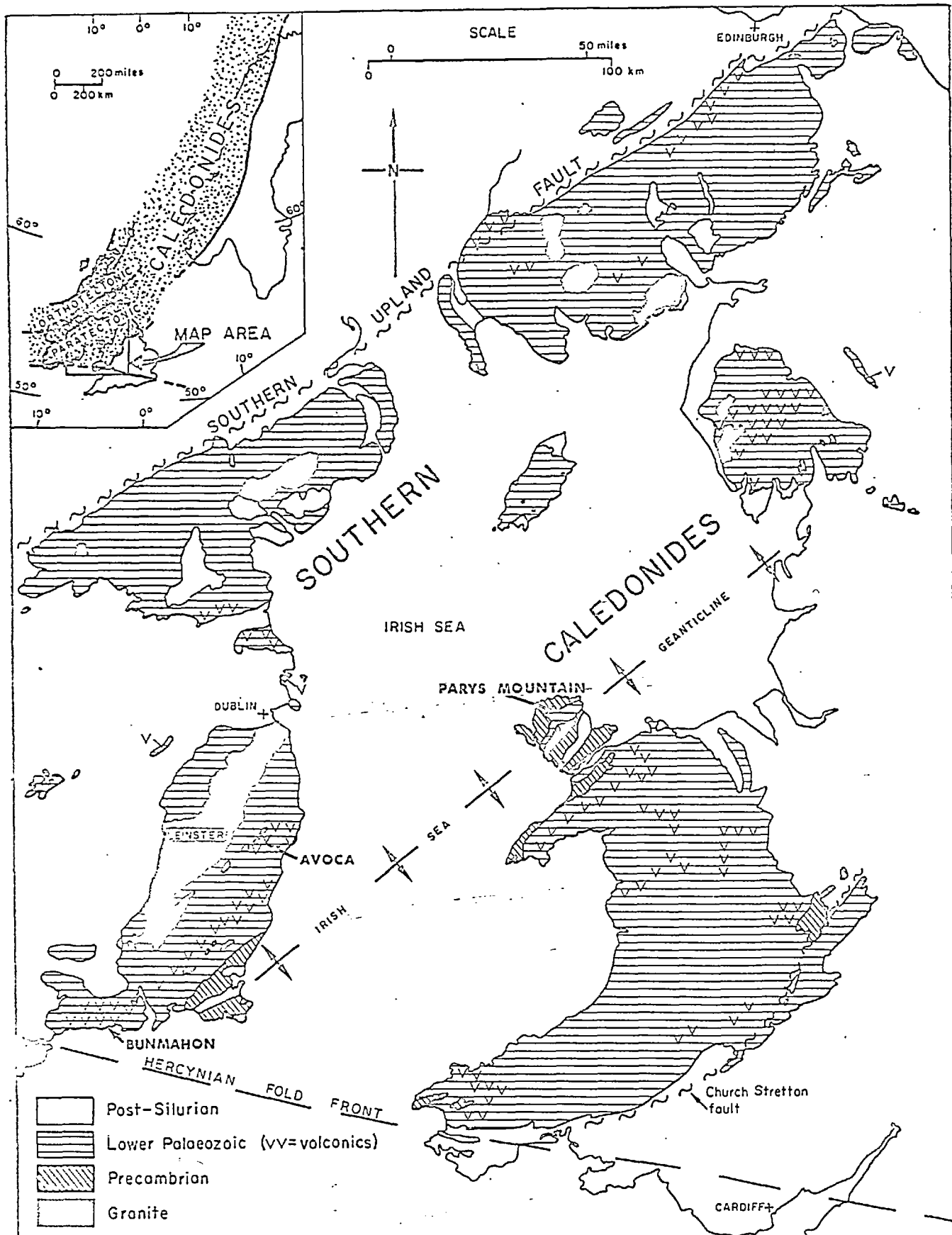
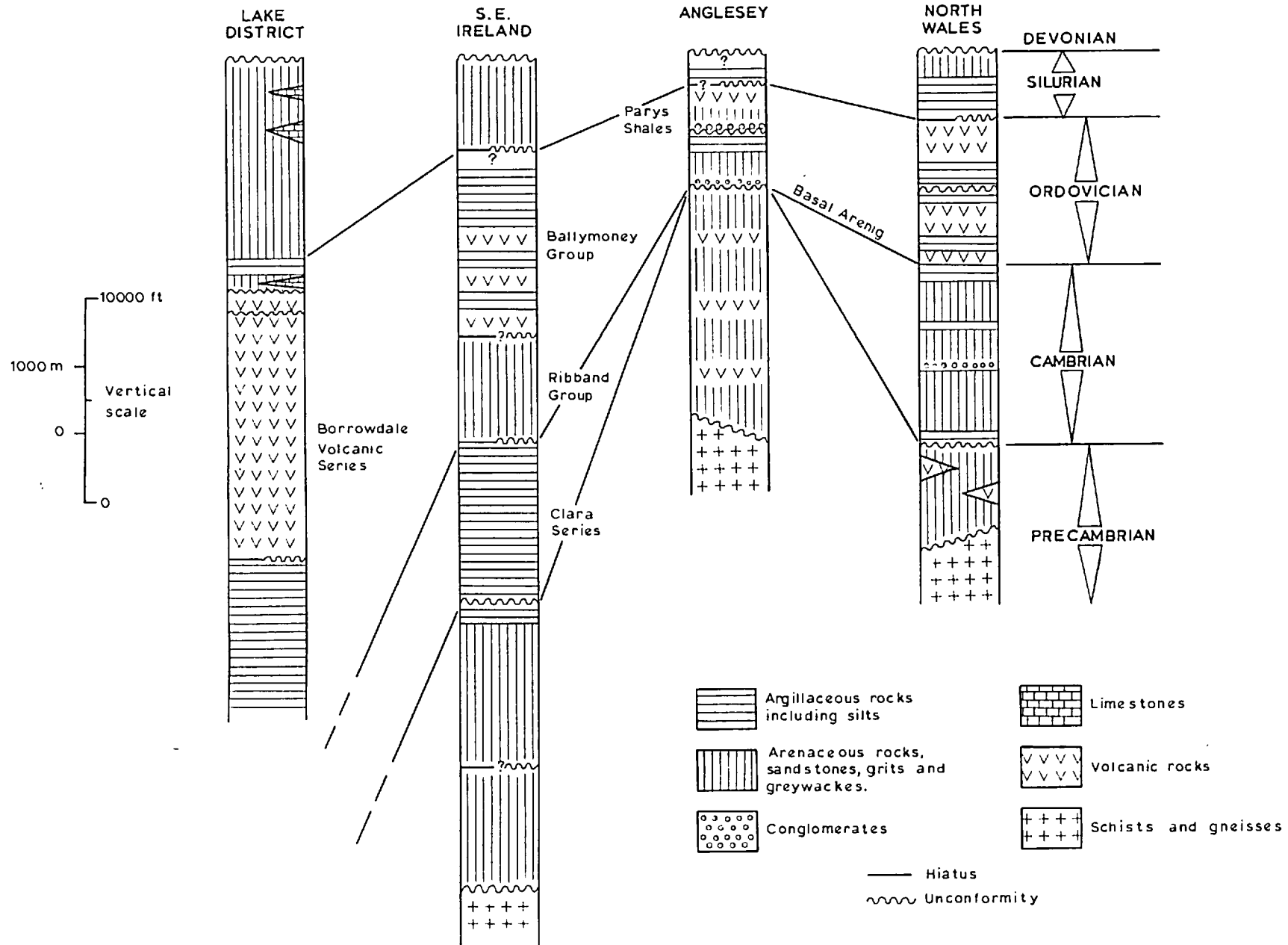


Fig. 1.1 Geological framework of the Southern Caledonides. Geological boundaries after the 25-mile map of the British Islands, 5th edn, 1969, Institute of Geological Sciences, London. Tectonic features after Tectonic Map of Great Britain and Northern Ireland, 1966, 1st edn, Institute of Geological Sciences.

FIG 1.2

COMPARATIVE LITHOSTRATIGRAPHIC SECTIONS IN THE SOUTHERN CALEDONIDES



trough. A major isotopic event about 600 m.y. ago denotes the Monian metamorphism.

1.2.2. Cambrian

Recent work by Downie and Tremlett (73) suggests that the Clara Series is the sole Cambrian representative in S.E. Ireland. In North Wales, the maximum thickness of the Cambrian occurs in the Harlech Dome, but on Anglesey none exists. The Manx slates on the Isle of Man may be the equivalent of the Clara Series, and in the Lake District the presence of definite Cambrian rocks is unestablished.

1.2.3. Lower Palaeozoic

Siluro-Ordovician strata were deposited with minor unconformity on underlying Cambrian in a much enlarged Caledonoid trough. Pulses of igneous activity with concomitant metamorphism occurred during the development of the geosyncline. The Snowdon complex in North Wales and the Borrowdale Volcanic Series in the Lake District demonstrate that volcanic activity accompanied sedimentation. Orogenic activity culminated with the intrusion of the Leinster granite batholith along the axis of the trough.

1.2.4. Upper Palaeozoic

Devonian, Carboniferous and Permian rocks rest unconformably on the preceding strata and occupy a large basin of deposition covering the central British Isles. Tectonic movements associated with the Hercynian cycle in Western Europe terminated deposition.

1.2.5. Post-Palaeozoic

Post-Palaeozoic strata border the site of the Lower Palaeozoic trough and form outliers in N.E. Ireland. Tertiary orogenic activity, volcanism and igneous intrusion took place in the Highlands of Scotland and in Northern Ireland.

The Quaternary glaciation produced the present landscape. Ice moved out from centres on the mountain regions, excavated the valleys, and left the gently rounded highland areas mantled by glacial debris.

1.3. Distribution of Mineral Deposits

In common with geosynclinal deposits in other parts of the world, there are a large number of mineral deposits in the Southern Caledonides (Fig 1.3). These are the southernmost representatives of a metallogenetic province extending from Ireland to Northern Norway.

In S.E. Ireland, deposits in the Avoca mineralized belt are found at 1) Bunmahon and 2) Caim in Co. Waterford, 3) Avoca and 4) Glendalough in Co. Wicklow. In Britain, on an approximately linear extension of the belt, they occur at Parys Mountain, Anglesey and Coniston, Lake District.

Flanking these occurrences there are many small deposits, but detailed consideration of them is beyond the scope of this thesis.

1.4. Present study

1.4.1. Purpose

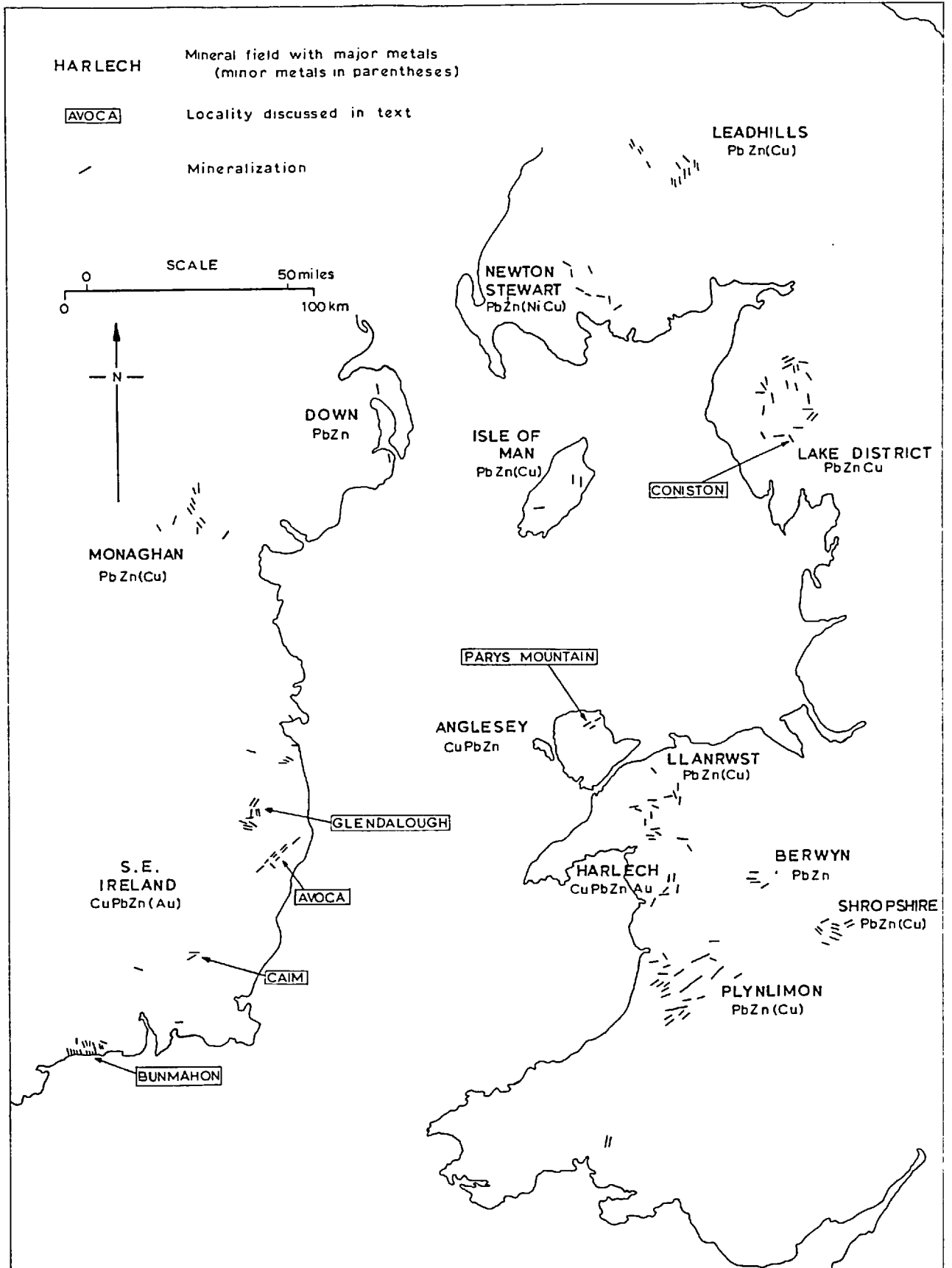
There is considerable doubt about the origin of the conformable pyritic deposits in the Caledonides. A study of the economic geology of the Avoca district, Parys Mountain and certain other deposits in the Southern Caledonides was undertaken to add information to, and possibly resolve, the prevalent ideas on the genesis of the mineralization.

1.4.2. Scope

In the Avoca district, about 40 square miles was mapped at a scale of six inches to one mile (1 : 10,560) providing the first geological map of the mine area. All the ancient workings within the prospecting lease were examined, and at the mine over 30,000 ft of drill core were logged using a statistical method. Accessible underground workings were studied and about 5,000 ft of underground mapping was carried out. A lithological interpretation of the wallrocks is given and structural data are interpreted.

At Parys Mountain, surface exposures and workings were examined and about 5,200 ft of drill core were logged. The flooded underground workings were not studied.

MINERALIZATION IN THE SOUTHERN CALEDONIDES



Reconnaissance work was carried out in the Bunmahon, Caim, Glendalough and Coniston districts.

Examination of the physical and chemical features of the mineralization and country-rocks was carried out in the laboratory. The mineralogy and petrology are described and whole-rock and trace element analyses are presented. Aerial photographs were interpreted and geochemical soil sample analysis results discussed. These aspects were studied in detail at Avoca, but to a lesser extent at Parys Mountain and the other deposits.

A total of nine months was spent in fieldwork during the period 1967-70. Over seven months were spent at Avoca, three weeks at Parys Mountain, two weeks at Bunmahon and one week at Coniston. Prior to beginning research, the writer was employed as project geologist at the Avoca Mine.

S E C T I O N 2

AVOCA DISTRICT2.1. Regional Geology2.1.1. Introduction

The Avoca district surrounds the mining area centred north of the village of Avoca in Co. Wicklow (Map 1). The district straddles part of the belt of Lower Palaeozoic rocks which trend southwestwards across S.E. Ireland.

2.1.2. Previous geological work

Generalized descriptions of the geology of S.E. Ireland by Jukes and Haughton (125), and Smyth et al (207), Bishopp (30) and others, summarized the current data.

Tremlett (225) remapped a large area in Wicklow and Wexford, which included the Avoca district. Although useful, some of the wide-ranging conclusions he reached are highly controversial.

Geological Survey maps of the Avoca district were published in 1856 at the scale of one inch to one mile, based upon six inch to one mile mapping carried out earlier by Kinahan and Du Noyer. A revision was made in 1861 and Kinahan did further work in 1878. The major sheet memoir was published in 1888 (117).

In the mine area, Wynne (257), Odman (169), Jones (124), O'Brien (166), Murphy (158), Gordon-Smith (97), and Lampard (138) made contributions to the local geology, but little work on a regional scale was attempted.

2.1.3. Stratigraphy

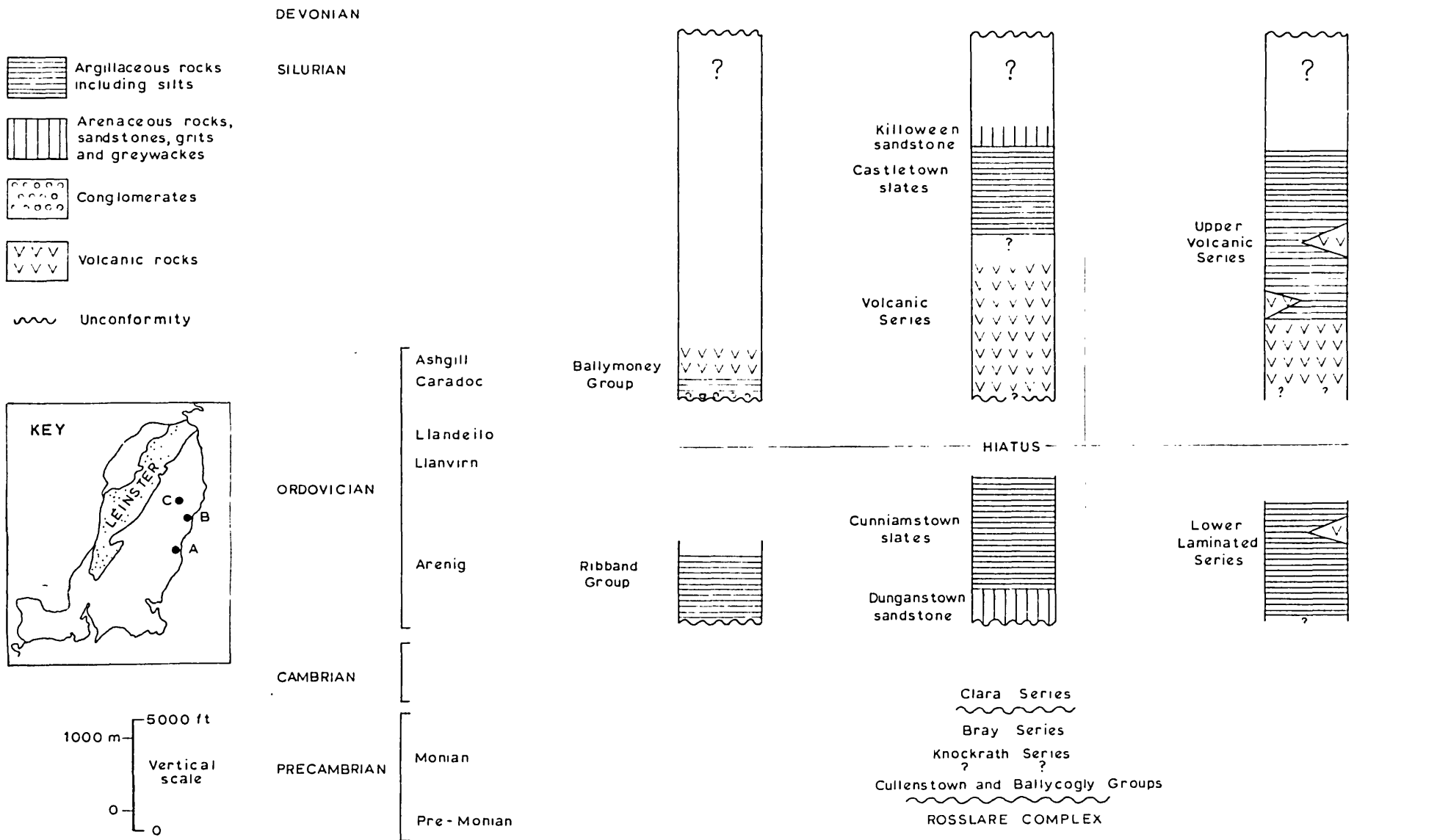
Dearth of faunal evidence and scarcity of diagnostic inland exposure in S.E. Ireland, necessitates the use of litho-stratigraphic correlations. Rocks are well exposed along the coast, and study of these has revised previous theories. (Fig 2.1).

2.1.3.1 Precambrian

The Rosslare Complex (13) is a series of hornblende and biotite nylonite gneisses and other nylonitic rocks, with an

FIG 2.1

STRATIGRAPHIC RELATIONS IN S.E. IRELAND



ENE - WSW trend, occurring in S.E. Wexford.

The Ballycogly and Cullenstown Groups, exposed in Wexford, consist of quartzites, greywackes and pelitic rocks, with greenschist facies metamorphism. The two groups may be equivalent (13).

The Knockrath Series (224), exposed in Wicklow, consists of about 4,000 ft of finely laminated, dark grey and black slates with light grey quartzitic siltstones. Euhedra of pyrite are common. The base of the series has not been identified and relationships with the underlying strata are unknown.

The Bray Series conformably succeeds the Knockrath strata and is more arenaceous, consisting of massively bedded green and grey greywackes, with interbedded purple and grey slates or mudstones (224). Metamorphism of the two series locally developed quartzites from the arenaceous horizons. Isoclinal folding about ENE axes is common, with an associated axial plane cleavage.

2.1.3.2. Cambrian

The Clara Series, about 8,500 ft of black or dark grey mudstones and slates, has a Cambrian microfauna (73). No other Cambrian rocks have been identified in S.E. Ireland.

2.1.3.3. Ordovician

Succeeding strata were not lithologically described by Trenlett and thus an aura of confusion surrounds his succession. Crimes and Crossley (61) and Brenchley and Treagus (38) revised the Ordovician stratigraphy through study of the coastal exposures south of Arklow. In the following description an attempt is made to correlate these studies (Fig 2.1).

The Ribband Group consists of the Kilmichael, Clones and Riverchapel Formations (38). These make up a thickness of more than 3,000 ft. The Kilmichael Formation consists of striped mudstones and siltstones. Sandstones of turbidite character are absent. The Clones Formation is of pale green and grey siltstones, without any diagnostic fossils. The Riverchapel Formation, characteristic of the Ribband Group, contains purple, green and buff interbedded slates and is of early Arenig age.

It is tempting to equate the purple and grey slates of the Ribband Group with the grey, Cunniamstown slates that Trenlett placed above the Dunganstown sandstones. The lithology and thickness is comparable (Fig 2.1) and the lack of fossils similar.

The Ballymoney Group (38) unconformably overlies the Ribband Group. A thin conglomerate at the base of the Courtown Formation is succeeded by calcareous sandstones and silts with a shelly fauna, indicating a possible Caradoc age. Thus, the Upper Arenig, Llanvirn and Llandeilo are missing from the coastal succession.

The Ballintray Formation consists of black mudstones with a sparse graptolitic fauna of Glenkiln age, and exhibits a penetrative cleavage. The basal contact with the Courtown Formation is usually tectonic, but, rarely, appears conformable. Interbedded silts become more numerous in the upper part and tuffaceous intercalations occur.

The Ballymoney Formation is made up of intermediate and acid tuffs having a laharic breccia at the base, with interbedded siltstones and shales. The tuffs show channel features and small slump-structures, grading is common, but the massive pumiceous and feldspathic varieties are poorly stratified. The upper part of the succession is unexposed, and thus a thickness in excess of 2,600 ft is postulated (38). Cleavage is especially marked in the pelitic rocks.

Trenlett's Volcanic Series (225) is above a black shale sequence. Correlation of these shales with the Ballintray Formation is tempting, but there is a great discrepancy in thickness. The Volcanic Series, which is similar to the Ballymoney Formation, consists of rhyolitic pyroclastics and minor basic lavas interbedded with slates, limestones and sandstones. The total thickness, 8,000 ft, is much greater than the figure of >500 ft given for the Ballymoney Formation exposed a few miles to the southeast (38). Despite these differences, correlation is made by the writer (Fig 2.1), because Ordovician strata may be repeated by folds and faults and consist of a thinner sequence

than previously recognized (38).

Overlying the Volcanic Series are about 4,000 ft of strata, grey and black slates, the Castletown slates, and the Killoween sandstone (225). The stratigraphic relationships of these rocks is not known, they may represent an inverted succession of the sequence described above.

2.1.3.4. Silurian

There are no proven Silurian rocks southeast of the Leinster granite, but off the northwestern flank, a series of greywackes and pelites exists. The pelites are buff weathering slates, and psammitic members range from impure chloritic siltstones, a few centimetres thick to typical greywackes. Primary sedimentary structures are widespread; grading, current bedding etc.. The greywackes (on the basis of way-up evidence) overlie the dark phyllites and are >4,500 ft thick (6). The series is overturned, and although dating of the strata is not certain, the fauna appears to be Silurian. Lower Palaeozoic rocks exposed in the Longford-Down massif, range from the Caradoc (Glenkiln) to the Llandovery (Birkhill and Gala). The Silurian on the northern flank of the Leinster granite may thus also range up to the Wenlockian (40).

2.1.3.5. Upper Palaeozoic

Devonian basal conglomerates rest unconformably on the preceding strata. Upper Old Red Sandstone overlaps the southwestern margin of the Leinster pluton.

Carboniferous rocks occur in a synclinal downwarp in S.E. Wexford and border the Palaeozoic strata to the west, forming the central plain.

2.1.3.6. Mesozoic and Tertiary

No Mesozoic or Tertiary rocks occur in S.E. Ireland.

2.1.3.7. Quaternary

Pleistocene deposits, consisting of glacial sand, gravels, moraine and boulder clay are widespread. Recent soil, blown sand, peat, river and lake alluvia cover the bedrocks

2.1.4. Intrusive Rocks

2.1.4.1. Precambrian

The Carnsore Granite in S.E. Wexford, (Fig. 1.1.) although limited in surface extent, may be much larger, from the gravity survey (12). It is a homogeneous biotite adamellite containing xenoliths of the country rocks and a hornfels aureole.

2.1.4.2. Caledonian

a) Acidic

The Leinster pluton is the largest batholith in the British Isles, and intrusion virtually coincided with the climax of the Caledonian deformation. The mass consists of a series of domes, steeply overturned to the west (40), and there is a constant pitch of the roof of the composite body at 15-25° SW. The granites are generally grey biotitic granodiorites, which are partly porphyritic.

Post-tectonic sheet intrusions occur in the Lower Palaeozoic rocks southeast of the granite. They are massive, uniform rocks, ranging from quartz-porphry to microgranite in composition, and are of variable size (Fig. 1.1.).

b) Basic

A group of dolerite-diorite bodies of medium size occur within the Caradocian volcanic belts. They are typically quartz-hornblende-plagioclase rocks with some biotite and pyroxene-bearing varieties. An appinitic suite is also present.

2.1.5. Economic Geology

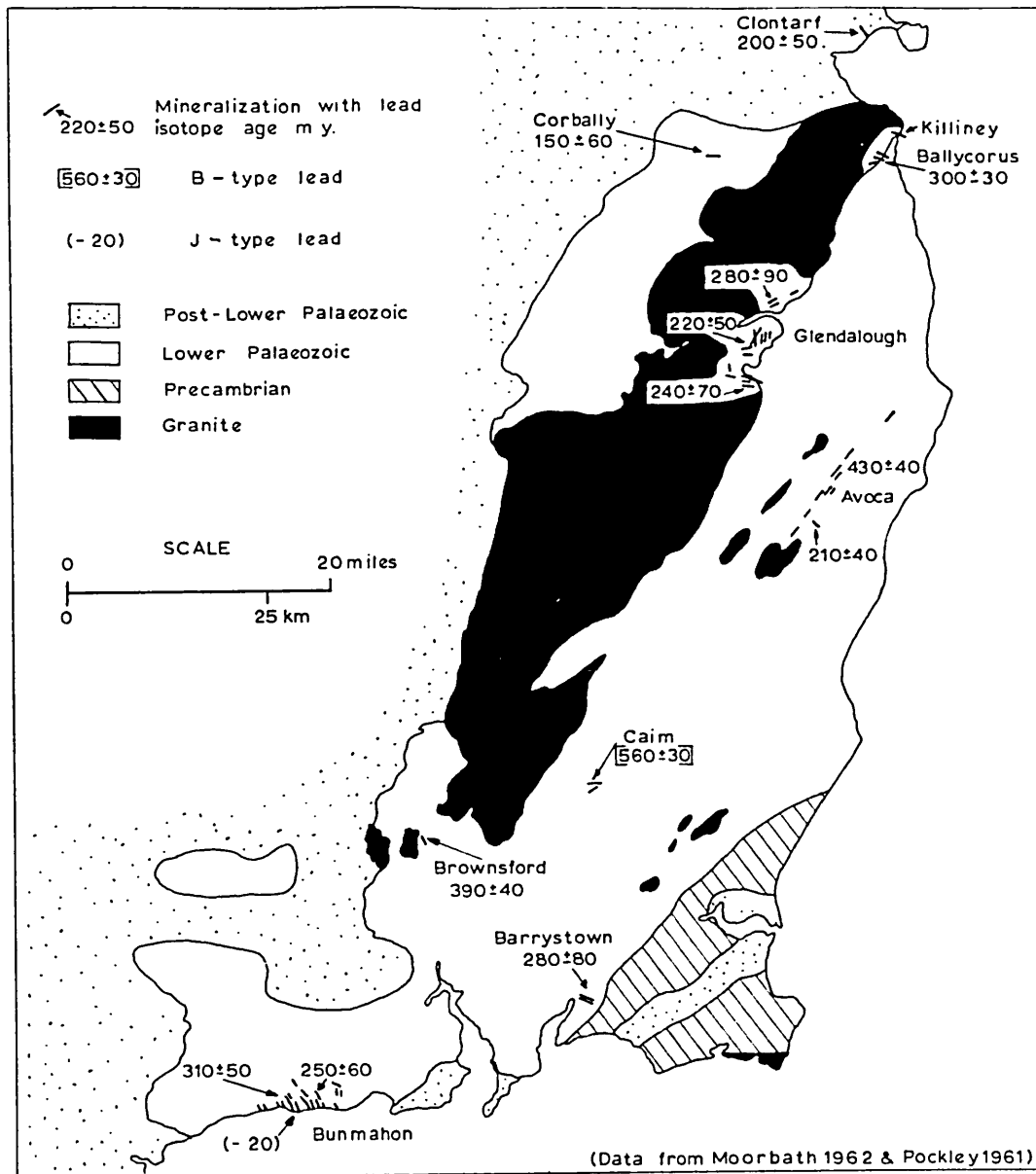
2.1.5.1. Copper

The Avoca mineralized belt is 10 miles southeast of the Leinster granite margin. It is about 10 miles long and more than 1,000 ft wide. (Fig. 2.2A.). The mine is in the centre of the belt. A number of lenticular orebodies occur, seldom possessing sharp contacts, the walls often being assay limits. The ore zones have diffuse pyritic haloes in the wallrocks, where alteration is apparent. The orebodies consist of massive or disseminated sulphides in a siliceous or chloritic matrix. Pyrite, chalcopyrite, sphalerite and galena are the major ore

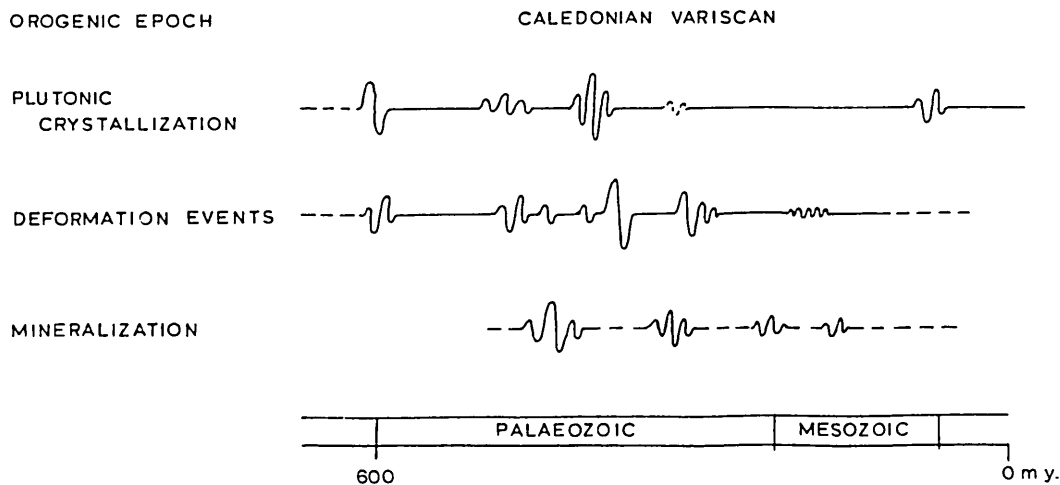
FIG 2.2

RADIOMETRIC DATING IN S.E. IRELAND

A. LEAD ISOTOPE DATING



B. METALLO - TECTONIC SEQUENCE



(Data from Harper 1966, Moor bath 1962 & Pockley 1961)

minerals. The ore zones are conformable with the local foliation, dipping 55° - 65° SE. Sporadic mineralization occurs throughout the belt.

Bunmahon is an abandoned copper mining area. Steeply dipping quartz veins, trending NW - SE cut across the strike of Lower Palaeozoic volcanics and sediments, and carry disseminated chalcopyrite, pyrite, sphalerite and galena. Wallrock alteration is minor.

2.1.5.2. Lead-zinc

At Glendalough, 12 miles northwest of Avoca, on the eastern flank of the Leinster granite (Fig 2.2A), there are steeply dipping sets of N-S and NE-SW trending siliceous veins with galena, calcite, sphalerite and minor chalcopyrite. The veins are within the granite and show minor wallrock alteration. Similar deposits occur at Glenmalure, Ballycorus, Corbally and Brownsford, the latter being on the western flank of the granite (Fig 2.2A.).

Cain is 5 miles east of the Leinster granite margin and 30 miles southwest of Avoca. Ramifying siliceous veins with disseminated galena, sphalerite and chalcopyrite occur in Lower Palaeozoic silts and mudstones. No zone of alteration surrounds the veins.

Barrystown, on the Wexford coast, has country rocks of siltstones. Siliceous veins with an E-W trend, dip 40° S and contain chalcopyrite, galena and sphalerite. Wallrock alteration is absent.

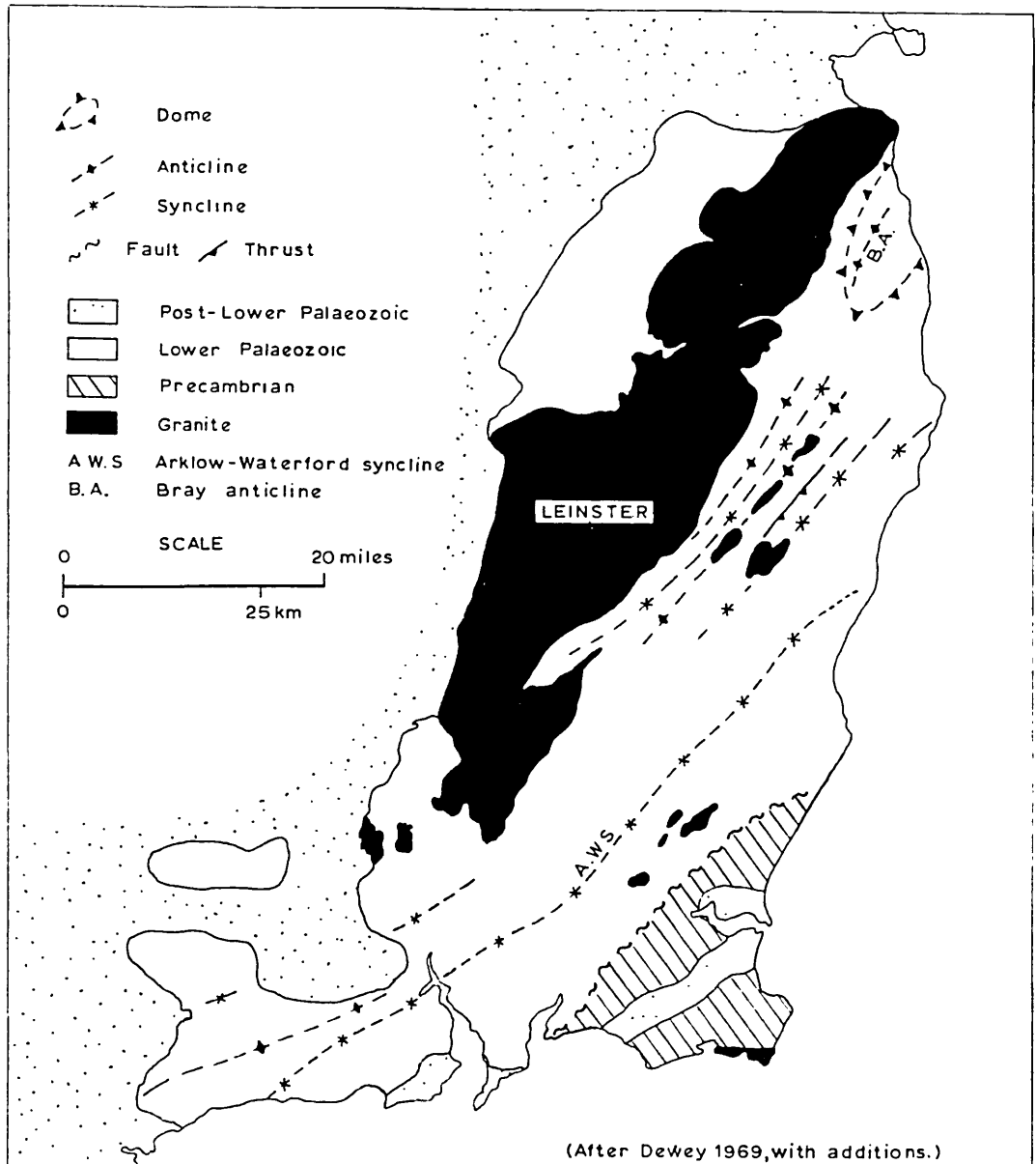
2.1.6. Structure and Tectonic Sequence

A synopsis of the structure and sequence in S.E. Ireland has been presented by Dewey (71) and the following is based largely upon his paper (Fig 2.3.).

The Arklow-Waterford syncline (225) is the major fold in the Lower Palaeozoic rocks southeast of the Leinster granite, and Caradoc volcanic and sedimentary strata exist within its core. The deformed Lower Palaeozoic rocks are fault bounded on the southeast margin by the Wexford Precambrian block, forming

FIG 2.3

STRUCTURAL ELEMENTS IN S.E. IRELAND



part of the complex Irish Sea horst on the line of the Palaeozoic geanticline (Fig 1.1.). The Bray Series outcrops in an anticlinorium to the north, and the Leinster pluton dominates the axial region.

The Arklow synclinorium and its associated Bray anticlinorium developed during an early Caledonian regional deformation, D_1 . The synclinorium, at the northern limit is a closed fold, verging southeastwards whereas to the south it opens and becomes symmetric with a vertical axial surface. A series of open monoclines, facing northwest developed on the southeastern limb (71). This initial deformation produced a steep regional penetrative cleavage, S_1 , with a northeast trend.

A second deformation episode, D_2 , correlates with the main intrusive activity of the Leinster pluton. In the region to the southeast of the granite, folding developed with an associated cleavage, S_2 , ranging from strain-slip to slaty, with an ENE or ESE trend and northward or near vertical dips respectively (71).

The third phase of deformation, D_3 , produced variable structures locally. Folding associated with a moderately intense crenulation cleavage, S_3 , developed in the Kilmichael area south of Arklow (38).

A final stage of deformation, D_4 , characterized by the development of kink bands occurs throughout the region.

In summary, the bulk strain relations in Leinster during the formation of the Caledonian tectogene consisted of an inclined NW-SE shortening coupled with stretching of a variable inclination. These relations suggest origin at a relatively deep structural level.

2.1.7. Geochronology

2.1.7.1. Sedimentary rocks

Harper postulated a sequence of polyphase deformation in the Lower Palaeozoic sediments (104)

- | | |
|--|----------------------|
| a) Early Caledonian cleavage event. | : $437^{\pm} 9m.y.$ |
| b) Late (Silurian) Caledonian cleavage event | : $408^{\pm} 7m.y.$ |
| c) Deformation with accompanying granite intrusion | : $374^{\pm} 10m.y.$ |

Slate from the Knockrath Series gave an age of 450 m.y. and slate from the Caradocian volcanic succession gave 454 m.y. The latter age conflicts with the stratigraphy and Harper inferred that the presence of detrital argon might account for the increased value (104).

2.1.7.2. Granites

Intrusion of the Leinster granite, dated as 386 ± 9 m.y. (135), correlates with the final events denoted by Harper. The Precambrian Carnsore Granite in S.E. Wexford yielded an anomalous isotopic age of 429 ± 7 m.y. (12), presumably a measure of Caledonian overprinting.

2.1.7.3. Mineralization

A great deal of uncertainty surrounds the current interpretation of lead isotope ages. The fundamental constants have recently been revised (170), and when the new constants are applied to the data in Fig 2.2A, most of the ages become J-type.

In the Avoca district, the discordance between the model age of the major mineralization 440-400 m.y. (157) and that of a late stage crosscutting vein at Ballintemple which is a mere 2 miles southwest of the mine, 210 m.y. (176), adds a measure of credibility to the data presented. However, J-type and B-type leads do exist, and this suggests that regeneration, crustal contamination and homogenization were probably significant in giving rise to the discordant ages recorded from the vein-type deposits.

2.1.7.4. Summary

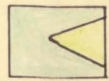
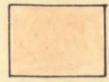



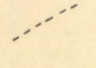
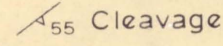
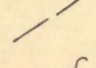
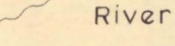

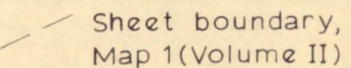

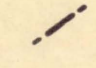
Lead isotope data imply that mineralization has been a pulsatory process, spanning a period from 440-150 m.y., and generally pre-dating periods of plutonic crystallization (Fig 2.2B).

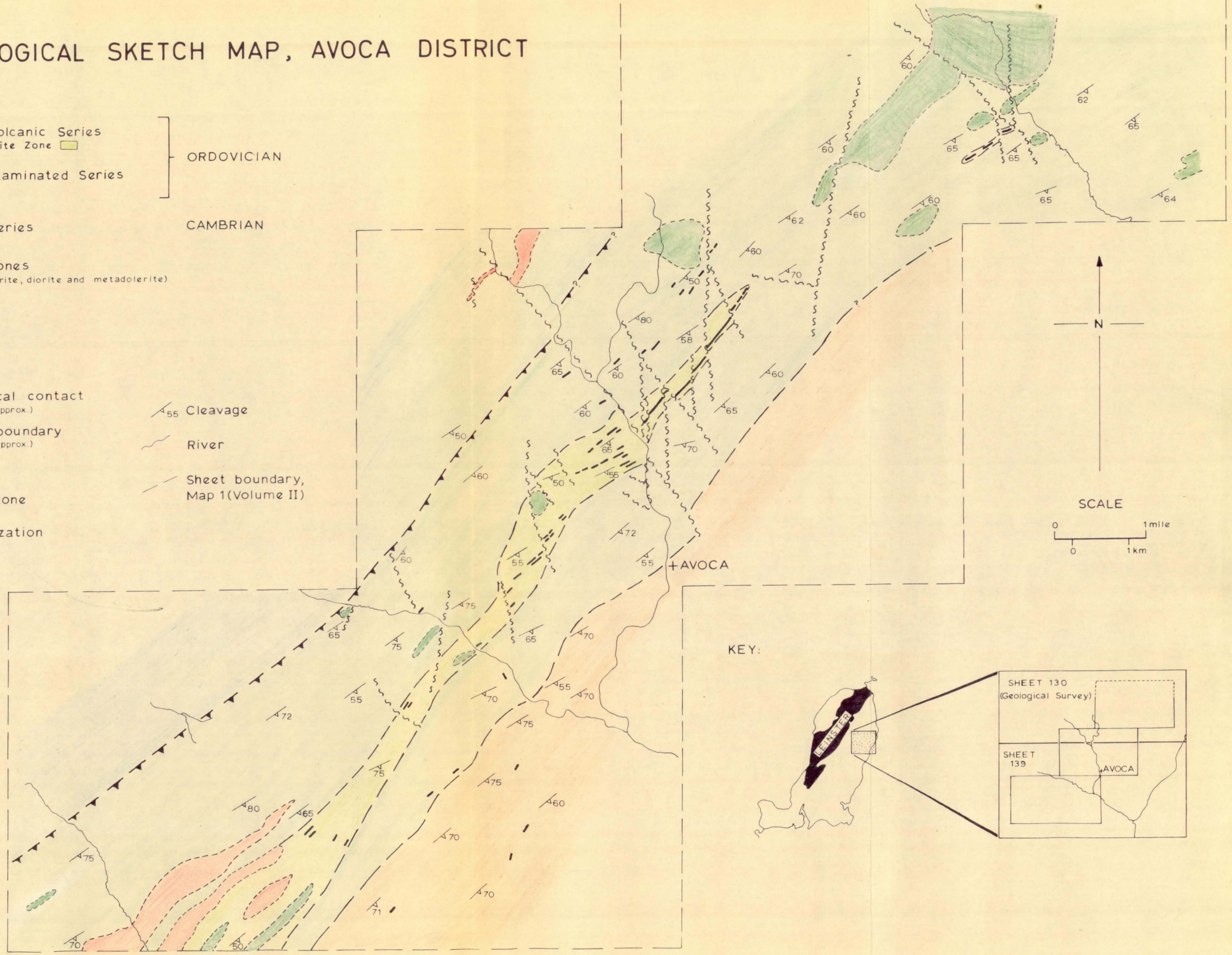
2.2. General Geology

2.2.1. Introduction

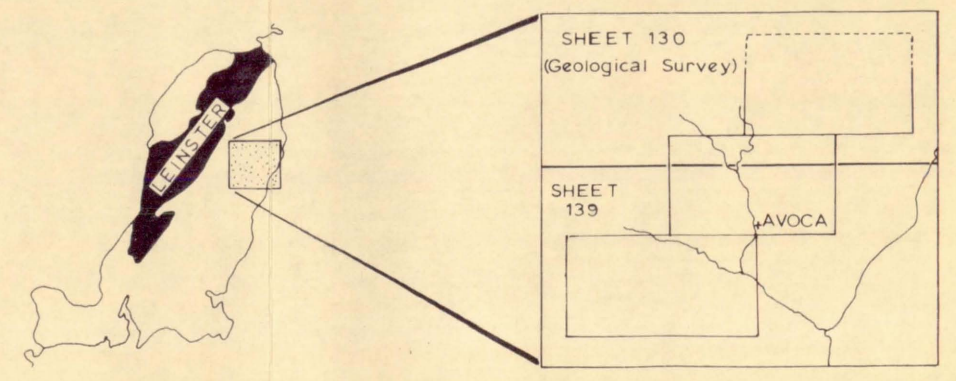
The area mapped during the current study (Map 1) includes portions of sheets 130 and 139 of the one inch series of the Geological Survey of Ireland (Fig 2.4.).

FIG 2.4
GEOLOGICAL SKETCH MAP, AVOCA DISTRICT

	Upper Volcanic Series Chlorite Zone	} ORDOVICIAN
	Lower Laminated Series	
	Clara Series	CAMBRIAN
	Greenstones (Quartz-diorite, diorite and metadolerite)	
	Granite	
	Geological contact (approx.)	 Cleavage
	Series boundary (approx.)	 River
	Fault	 Sheet boundary, Map 1 (Volume II)
	Thrust zone	
	Mineralization	



KEY:



The limits of the prospecting licence held by Avoca Mines Limited, enclose an area of about 40 square miles and contain virtually all the known mineralization. This boundary serves as an approximate limit to the map area.

The varied topography illustrates the effects of the Quaternary glaciation. The summit of Croghan Kinshela (1993 ft), at the southwestern margin of the area is the highest point, and the mean elevation of the lower upland areas is 800 ft. At this and lower elevations, glacial debris, drift and boulder-clay occur, often infilling former drainage channels (Map 1). Glacial striae are preserved on the higher ground. The rivers occupy steep-sided glaciated valleys, with well-wooded slopes.

2.2.2. Stratigraphy

A number of factors hinder elucidation of a precise stratigraphic succession for the map area. There is a marked lack of exposure of sedimentary strata and no fossils have been found. A penetrative cleavage, at a small angle to the bedding, obliterates many primary features of the rock fabric. Faults, often with indeterminate throws, complicate the outcrop pattern.

Representative lithostratigraphic sections, established purely on the basis of lithology and constructed from cross-sections, are shown in Fig 2.5. An Upper Volcanic Series succeeds a Lower Laminated Series, which in turn overlies rocks of the Cambrian Clara Series.

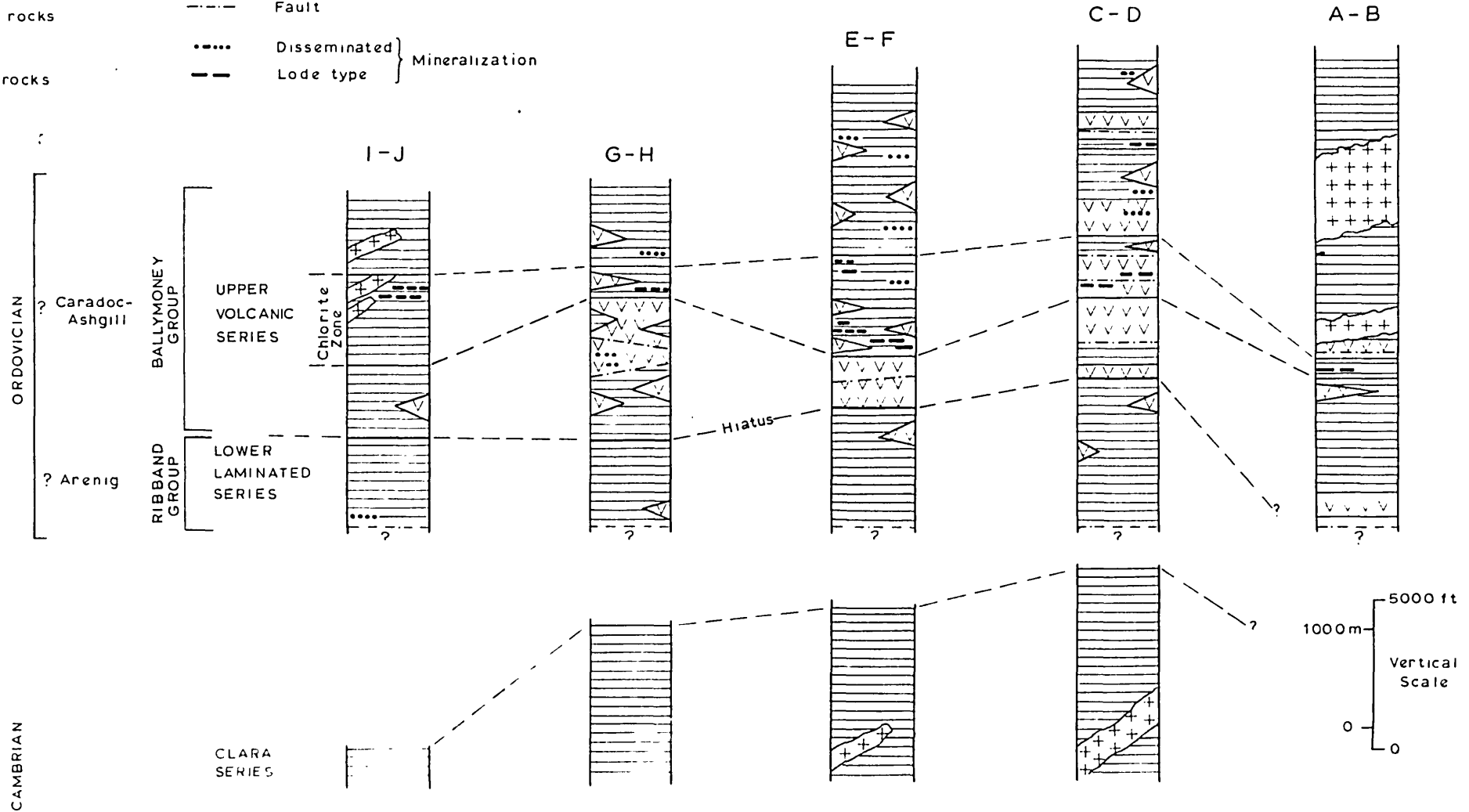
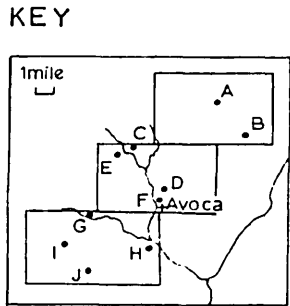
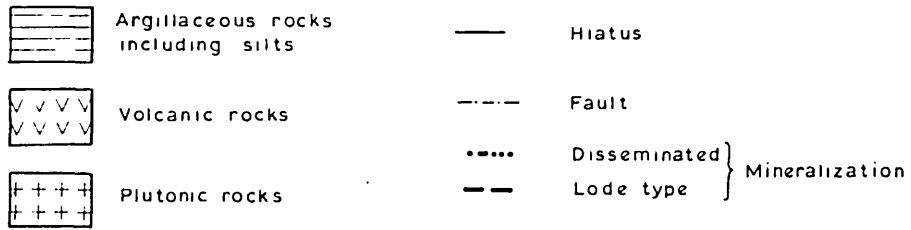
This succession is similar to stratigraphic sequences elsewhere in S.E. Ireland (Fig 2.1.). The Lower Laminated Series is tentatively correlated with the Ribband Group, and the Upper Volcanic Series with the Ballymoney Group. On this basis, the Lower Laminated Series may be early Arenig, and the Upper Volcanic Series Caradocian-Ashgill strata. (It is noteworthy that in rocks similar to the Upper Volcanic Series, occurring northwest of the map area, Jukes and Du Noyer (126) discovered a non-diagnostic Caradocian fauna.)

2.2.2.1. Clara Series

Rocks of the Clara Series bordering the northwestern margin of the map area, consist of blue-grey to black siltstones,

FIG 2.5

VERTICAL LITHOSTRATIGRAPHIC SECTIONS, AVOCA DISTRICT



(Section locations on Map 1)

and mudstones with paler laminae. On the basis of a microfaunal assemblage, found elsewhere, the rocks are Cambrian (73). A prominent strike fault marks the base of the Series in this area making definite correlation impossible, and no fossils have been found.

2.2.2.2. Lower Laminated Series

This series is dominated by a monotonous sequence of light and dark, blue-grey, shaly mudstones and siltstones, containing buff laminae. Purple and grey laminated siltstones and mudstones occur at the base of the series. Individual beds of mudstone are up to 2 cm thick, but generally the laminae range from 1 - 2 mm in width. The more silty layers contain cross-bedding, and the coarsest units are graded. Clay grade material predominates and seams of carbonaceous material are relatively common.

Towards the top of the succession, interbedded fine tuffs and massive tuffaceous horizons become important. These green to buff coloured pyroclastics are generally fine grained, with beds ranging in thickness from less than 1 mm in the fine tuff units to more than 30 cm in the coarser material. Bottom-structures, channelling and cross-bedding occur, and grading is quite common (Plate 2:A,C,E and F). The laminae in the green, fine tuff beds are exceptionally thin, lighter in colour and may originate through reworking of the pyroclastics.

The base of the series is not exposed, but purple and grey thinly bedded siltstones and mudstones, a lithology typical of the Ribband Group, occur at the southeast border of the map area. These are a key to the sequence.

2.2.2.3. Upper Volcanic Series

The Upper Volcanic Series consists of a sequence of interbedded lavas, pyroclastics and sediments and is the host for the major mineralization in the district.

Brenchley and Treagus used a conglomerate at the base of the Courtown Limestone Formation as the basal marker for the Ballymancy Group. This horizon has not been identified in the

Avoca area, and thus the base of the Volcanic Series is arbitrarily taken as the stage at which volcanic detritus assumes a major role in sedimentation (Map 1).

Lithologically, the basal portion of the Series is a sequence of sediments and intercalated tuffs. The thickness of individual beds in the sediments is variable up to 4 cm, and generally the laminae range from 1 mm to 4 mm in width. The pyroclastics are pale to dark green fine tuffs and lapilli tuffs. Fine tuff horizons are dominant and occasionally cross-stratified. The lapilli tuffs are often graded and afford way-up evidence in certain localities (Map 1.). Finely laminated blue-grey to buff siltstones and mudstones succeed the pyroclastics.

Interbedded with this sequence are a series of rhyolitic volcanic rocks, termed felsites. Felsite, is the field name given to a distinctive rock unit - a compact light to dark grey flinty material. These rocks form compound masses greater than 500 ft thick, composed of relatively massive units separated by lenticles of lapilli tuff, occasionally exhibiting grading of the vitric and lithic fragments (Plate 2:B). The felsites occur as relatively isolated outcrops but faulting has disrupted the initial relationships.

The felsites occur at the base of a lithological unit, termed the Chlorite Zone, which consists of light to dark, green and grey rocks and serves as the sole 'marker-horizon'. These rocks are dominantly of pyroclastic origin and consist of fine and coarse crystal-vitric tuffs. Intrusive volcanic and plutonic rocks also occur, forming the bulk of the outcrop at the northeast and southwest limits of the mineralized belt. Grading of the pyroclasts is rare in the tuffs, and alteration has destroyed the primary sedimentary features of the finer grained beds. Interbedded siltstones and mudstones are minor, and finely laminated. Carbonaceous seams are relatively common and are often spatially associated with mineralization.

The Chlorite Zone is succeeded by a series of sediments with pyroclastic intercalations, lithologically similar to the underlying sequence, except for the rarity of felsite. Light

and dark blue-grey siltstones and mudstones are accompanied by lithic and crystal tuffs which are grey-green to buff in colour.

Post-depositional alteration of the volcanic rocks has been intense. The felsites have suffered devitrification and extensive silicification, whereas the intermediate and basic tuffs have been altered into rocks consisting essentially of quartz and chlorite. A penetrative cleavage has affected all the strata; the siltstones and mudstones have been converted into slates and phyllites.

The Upper Volcanic Series contains the bulk of the rocks previously referred to as the 'Avoca Schists' (158). The total thickness is unknown, but is probably greater than 5,000 ft (Fig 2.5.).

2.2.2.4. Intrusive rocks

A variety of intrusive rocks occur in the district, making up a suite ranging from acid to basic. Hatch (106) and Tremlett (225) published descriptions of the rock-types. The pioneering account by Hatch produced a classification which is still pertinent and largely followed in the account below. A tripartite division of the 'greenstones' into diorite, quartz-diorite and meta-dolerite adequately covers rocks of that type in the map area.

a) Granite

There are two occurrences of granite in the district, at Croghan Kinshela and Ballinaclash-Ballinacarrig. The granites are sheet-like minor stocks. They are medium to fine grained and light grey-white to pinkish-grey in colour, containing large orthoclase feldspars. A prominent aureole of biotite andalusite hornfels is adjacent to the Ballinaclash granite, and effects of dynamic metamorphism extend about 250 ft from the granite contact. On Croghan Kinshela, however, no hornfels exists. This factor may be related to the difference in time or mode of emplacement between the two granites.

b) Quartz-porphyry and microgranite

Associated with the main Croghan Kinshela granite are a series of dyke-like minor intrusive sheets ranging in composition from quartz-porphyry to microgranite and aplite. These bodies are broadly conformable to the regional cleavage but show

intrusive marginal relationships. Thicknesses are generally about 40 ft but may be up to 100 ft. Fine to medium grained and grey-white in colour they are of variable composition.

These acidic intrusives generally occur in the upper part of the Upper Volcanic Series.

c) Quartz-diorite

A series of stocks and associated lenticular dyke-like bodies of quartz-diorite concentrate at the north-eastern limit of the map area, but masses of similar composition occur throughout the belt (Map 1.). The rock is light greenish-grey in colour, medium grained, sometimes with dark plates of mica (often chloritized) up to 2 mm in length, in a matrix of light, turbid feldspar and quartz.

d) Diorite

These rocks are green-grey in colour and differ from the quartz-diorites in containing less quartz. Diorites tend to occur as satellites to the major intrusive masses and marginal autometasomatic alteration is conspicuous, forming a dense, dark green, fine grained chloritic rock which often contains specks of sulphide.

e) Metadolerite

Metadolerites occur as elongate, lensoid dyke-like bodies showing minor crosscutting relationships with the country-rocks. Medium to fine grained and dark greenish-grey, they contain laths of amphibole up to 3 mm in length, enclosed in a chloritic matrix. With increasing degree of alteration the rocks become lighter in colour.

f) Appinite

There is a solitary occurrence of appinite at Toberlowagh on the northwest slope of Croghan Kinshela (Map 1.). The body is sheet-like, 100 ft in width and is about 1,000 ft in length. It is spatially associated with a lenticular intrusion of quartz-porphry, 500 ft away, and is enclosed in blue-grey siltstones and mudstones. This occurrence, associated with the Croghan granite, has many similar features to members of the appinitic suite associated with the Leinster pluton (41).

2.2.3. Petrography

2.2.3.1. Sedimentary rocks

The siltstones and mudstones consist of fragments of quartz and feldspar (dominantly plagioclase) in a matrix of finely divided clay minerals, chlorite, sericite and silica. Highly argillaceous seams contain partings of carbonaceous material. Pyrite is common. Magnetite, ilmenite and leucoxene make up the accessory iron oxide 'dust' in the ferriferous laminae.

2.2.3.2. Volcanic rocks

a) Tuffs

The medium and fine grained tuffs consist essentially of feldspar, quartz, chlorite, calcite, epidote with accessory iron oxides, sphene and leucoxene. This assemblage is typical of low greenschist facies metamorphism of intermediate to basic rocks (227). In the relatively unaltered tuffs, the feldspar forms idiomorphic grains (An_{15-35}). Microcrysts of plagioclase (albite) occur in the groundmass with calcite and chlorite. Distortion of twin lamellae in plagioclase indicates post-crystallization deformation. Phenocrysts of quartz are anhedral and chlorite corrodes the grain outlines. Fluid inclusions are invariably present in the quartz which is strain polarized. Granular, microcrystalline, recrystallized quartz, and chlorite occur in pressure fringes surrounding quartz phenocrysts. Grass green, highly pleochroic chlorite occurs as lath-like streaks and wisps, sub-parallel to the foliation. Anomalous brown interference colours suggest that it is a magnesium-rich variety (2). Epidote occurs as subhedral grains included within feldspars and also as individual anhedral grains and clusters in the chloritic matrix. Calcite develops, through albitization and alteration of the feldspars, as irregular allotriomorphic segregations. Leucoxene, sphene and iron oxides occur as scattered grains, from the breakdown of ferromagnesian minerals and magnetite-ilmenite.

Despite extensive recrystallization, the fragmental nature of these rocks is apparent when thin sections are viewed in ordinary light with a partially closed diaphragm (Plate 2:G,H). Positive identification of the nature of the pyroclasts is

impossible, but from the whole-rock analyses material of andesitic, and rhyolitic composition probably formed the bulk of the lithic material. Chlorite-phyllites are the major rock-type. Development of true phyllonites (212) is rare, being confined to those areas where differential movement has taken place along closely spaced slip planes (e.g. the Chlorite Zone in the nine area).

b) 'Felsites'

Microscopically the felsites exhibit a felsophyric texture, with phenocrysts of quartz and feldspar in a felty cryptocrystalline mesostasis of quartz, micaceous minerals and scattered feldspar microlites (Plate 3). Accessory sphene and leucoxene are minor. The quartz phenocrysts consist of multiple subhedral grains, strain polarized and exhibiting mortar texture. Fluid inclusions are ubiquitous. The feldspar is albitic plagioclase (An_5), with simple, albite twin lamellae. Rupture and subsequent rehealing of the feldspar phenocrysts with a granular mosaic of recrystallized quartz occurs, Plate 3:C,D. This implies post-formational deformation. Chlorite and sericite surround the phenocrysts in pressure fringes, and corrode the outlines of the augen grains. Sphene and leucoxene occur as scattered granules in the groundmass, and epidote sometimes lines joint planes.

To discover the nature of these enigmatic deposits, a suite of samples was collected from the margin and main body of representative felsites throughout the district. Nodular structures at the borders of individual felsites consist of knots of siliceous material. Rare spherulitic textures occur (Plate 8:B), and a paraeutaxitic texture develops around quartz macrocrysts (Plate 3: A-F). The latter is probably the 'striae fluxion' observed by Jukes (125). Streaked out lenticles of vitric material now devitrified and silicified may be original fiame.

Hatch (107) described the felsites as lavas, but other writers have carefully avoided any conclusions. Secondary silicification, which followed devitrification, is generally intense making study of the original characteristics difficult. Beavon et al. (21) indicated, that the basal zones of similar rhyolitic bodies are often the only region where diagnostic textural information is retained. The presence of paraeutaxitic

textures at the margins of felsites in the Avoca district and possible original fiame suggest that they are a series of rhyolitic pyroclastics which may be partly welded. Their large aerial extent suggests that they may be ignimbrites.

2.2.3.3. Intrusive rocks

a) Granite

The petrology of the granites was described by Houghton (125), Sollas (209) and Hatch (117) and, although these descriptions are out of date, the fundamentals are established.

The Croghan granite, which has a hypidiomorphic texture, consists of idiomorphic microperthite and anhedral quartz with interstitial plagioclase feldspar (Plate 4:A). The microperthite grains, weakly sericitized, contain subhedral included microcrysts of plagioclase. The microcrysts of microperthite and quartz have sutured margins. Quartz grains are strongly strain polarized and have marginal recrystallized microcrystalline zones. Graphic intergrowth of quartz and potassium feldspar is minor. Plagioclase (An_{25}) occurs as subhedral grains, associated with quartz and biotite, in the interstices between microperthite laths. Anhedral grains of sphene occur in the feldspar megacrysts, but more commonly, accompany biotite. In contact with the enclosing pelitic rocks the granite becomes granophyric, with a marked increase in quartz and the amount of graphic quartz and feldspar (Plate 4:B).

The Ballinaclesh granite has a similar mineralogy and texture, except that the plagioclase feldspar content increases and grains of accessory zircon, surrounded by pleochroic haloes, occur in biotite.

b) Microgranite and quartz-porphyry

This series of rocks is heterogeneous, but typically consists of microperthite and/or microcline, and quartz with accessory biotite (or rarely muscovite), sphene and zircon having a hypidiomorphic to allotriomorphic granular texture. Micrographic intergrowth of quartz and feldspar, is prominent.

The zoning in idiomorphic potassium feldspar is revealed by differential sericitic alteration of cores and margins. All the quartz is strain polarized, anhedral and contains abundant

fluid inclusions. Ragged plates of biotite commonly contain included zircon grains with pleochroic haloes, and are locally chloritized. Granular subhedral aggregates of sphene are associated with the mica.

As the grain size coarsens, the macrocrysts of feldspar and quartz develop mortar texture, the quartz sometimes becomes porphyritic, strain effects become more marked and the degree of feldspar alteration increases.

c) Quartz-diorite

These rocks consist of plagioclase feldspar and hornblende, minor quartz, potassium feldspar and biotite, with accessory apatite and epidote in a hypidiomorphic granular texture (Plate 4:C) Idiomorphic oligoclase grains, weakly zoned, have strongly saussuritized cores. Anhedra l potassium feldspar and quartz occupy the interstices between the plagioclase megacrysts, which are sometimes rimmed by potassium feldspar. Subhedral prisms and anhedral laths of hornblende are interstitial to the plagioclase. Apatite grains occur in the feldspars amphibole, and the groundmass as idiomorphic granules. Ragged chloritized plates of biotite are common, with included limonitic dust. Rare subhedral grains of epidote are disseminated in the matrix.

This rock-type is defined by a modal quartz content in excess of 10%. It grades into diorite as the quartz content decreases.

d) Diorite

The diorites are similar to the rocks described above, being distinguished by a modal quartz content of less than 10% (Plate 4:D). The essential constituents are plagioclase feldspar, potassium feldspar, hornblende, quartz and biotite, having a hypidiomorphic texture. Alteration of the plagioclase laths is more intense than in the quartz-rich rocks and calcite and saussurite develop. Potassium feldspar replaces idiomorphic plagioclase and twin lamellae are distorted. Minor strain polarized quartz occupies the interstices. Biotite is chloritized. Ragged laths and prisms of light brown hornblende are minor. Apatite is common, epidote is rare, and scattered grains of pyrite occur.

e) Metadolerite

The metadolerites are a highly variable suite of rocks, with a petrography that directly reflects their degree of alteration. Hatch (106) described the sequence of alteration from the core of a metadolerite intrusive traced towards its margin. The initial rock consists of uralite, oligoclase, and accessory quartz, epidote and leucoxene. The plagioclase is extensively saussuritized and calcite is present. Uralite occurs as idiomorphic prismatic grains and plates. Interstitial quartz is minor. Accessory anhedral grains of epidote and leucoxene occur (Plate 4:E).

As autometamorphism increases, the rock becomes foliated. Uralite shows partial rim replacement by chlorite, plagioclase becomes increasingly albitic, quartz increases and a cryptocrystalline groundmass develops from the alteration products - saussurite, calcite, epidote and leucoxene. Finally, chlorite completely replaces uralite, quartz becomes an essential constituent, the groundmass is cryptocrystalline, and sphene becomes an accessory with calcite and leucoxene (106).

The petrological similarity of the highly altered metadolerite to a sheared intermediate or basic tuff is evident. Hatch (106) regarded all the greenstone masses, previously designated ashes (130), as intrusives. A compromise between these two views is nearer the true situation (Map 1.). Examination of textures shown in ordinary light by thin sections cut normal to the cleavage facilitates recognition of the fragmentary nature of the tuffs. A marked increase in epidote also characterizes the volcanic greenstones and final proof is given by the field relations.

f) Appinite

The appinite is a typical hornblendite, with ragged ophitic plates of idiomorphic hornblende enclosing altered plagioclase feldspar in a mesostasis of feldspar and chlorite. Accessory apatite, sphene, zoisite, pyrite and leucoxene occur (Plate 4:F). Hornblende exists in two forms; the primary variety ($Z_{Ac} = 28-32^{\circ}$) is marginally altered to a secondary variety ($Z_{Ac} = 21^{\circ}$). The primary hornblende contains inclusions

of apatite and secondary hornblende producing a rude sieve texture. The secondary amphibole is marginally altered to chlorite. The plagioclase (oligoclase) is strongly saussuritized and often zoned. The mesostasis consists of chlorite laths, granules of sphene and apatite, and euhedral microcrysts of hornblende.

Healed fractures in the hornblende megacrysts are evidence of post-crystallization deformation.

2.2.4. Petrochemistry

The first analytical data on the rock types in the Avoca district was presented by Haughton (125). Further contributions to the chemistry of the granites and felsites were made by Sollas (209) and Hatch (107). A suite of felsites and tuffs have been analysed by the writer, the results and their relationship to the earlier data is discussed.

Analyses were carried out by x-ray fluorescence, using the technique described in appendix 1. The results are shown in table 1, with earlier data. Descriptions of the samples are in appendix 2.

2.2.4.1. Major oxides

a) Silica. SiO_2 displays a large variation in the felsites due to the varying intensity of secondary silicification. The composition of the Leinster granite, H1, and the major mass of Croghan Kinshela, H4 is close to the average granite (162), whereas the Ballinaclash granite approaches the average granodiorite. Sample H5 illustrates the increase in silica content at the selvages of intrusive granitic stocks.

b) Alumina. The altered rocks contain more alumina, due to removal of the other constituents. Values vary with the intensity of alteration.

c) Titania. TiO_2 contents are generally low, but increase markedly in altered tuffs, e.g. G.2, where appreciable epidote exists.

d) Iron, manganese oxide and magnesia. These constituents show parallel behaviour, with higher contents in the altered tuffs and intrusives, correlating with increase in ferromagnesian minerals. Sample F.11, showing enrichment in magnesia, is also

TABLE I

CHEMICAL ANALYSES AND CIPW NORMS OF REPRESENTATIVE VOLCANIC AND PLUTONIC ROCKS FROM THE AVOCA DISTRICT

Specimen:	F.1	F.2	F.3	F.4	F.5	F.6	F.7	F.8	F.9	F.10	F.11	F.12	F.13	F.14	JH.1	FH.5	FH.6	FH.8	FH.9	FH.10	G.1	G.2	HG.1	HG.2	H.1	H.3	H.4	H.5	
SiO ₂	76.10	75.30	77.40	71.80	78.60	80.20	71.80	60.80	80.00	79.60	73.00	76.60	76.00	77.70	81.36	70.6	74.8	73.6	73.0	71.2	47.60	48.85	52.08	57.88	72.07	70.80	73.66	80.24	
Al ₂ O ₃	9.74	13.43	10.22	12.57	10.51	10.00	11.40	16.76	9.11	10.55	9.58	9.18	11.96	9.51	7.86	15.3	13.9	13.8	16.7	16.8	14.82	9.62	15.60	15.20	14.81	18.00	13.64	12.24	
TiO ₂	0.25	0.32	0.23	0.45	0.27	0.23	0.37	0.73	0.20	0.24	0.31	0.23	0.33	0.23	-	-	-	-	-	-	0.97	2.59	-	-	-	-	-	-	
Fe ₂ O ₃	1.89	2.25	2.34	2.44	1.33	0.24	0.89	1.65	1.68	1.77	*	1.63	2.01	1.87	3.32	0.7	0.5	0.5	0.5	0.8	0.59	1.29	5.75	7.50	2.22	0.80	2.20	0.72	
FeO	2.39	0.10	0.86	0.37	0.07	0.10	3.70	2.47	0.32	0.66	3.63	3.07	0.22	1.49	-	1.7	1.0	2.4	1.3	1.5	9.63	9.31	2.57	1.35	-	-	-	-	
MnO	0.01	*	*	*	*	*	0.01	0.03	0.01	*	0.03	*	*	*	-	-	-	-	-	-	0.52	0.26	-	-	-	-	-	-	
MgO	0.30	0.03	0.14	0.38	0.04	0.01	0.27	0.32	0.07	0.02	1.95	0.04	0.03	0.10	0.45	0.8	1.1	0.7	0.7	0.9	4.22	6.08	8.40	6.34	0.33	0.24	0.48	*	
CaO	0.33	0.32	0.32	0.32	0.32	0.31	0.32	0.31	0.31	0.32	0.33	0.33	0.31	0.31	0.99	0.8	*	0.6	0.5	0.8	5.33	6.74	6.52	4.81	1.63	2.25	0.67	0.89	
Na ₂ O	0.02	0.22	0.10	0.56	0.10	0.49	0.02	0.37	0.01	0.13	0.25	0.44	0.01	0.02	2.63	2.7	2.2	3.2	4.2	4.7	1.67	3.76	2.92	2.67	3.06	4.08	3.51	5.58	
K ₂ O	6.60	9.02	6.63	8.60	7.68	7.38	8.68	12.90	6.70	7.08	4.12	5.67	8.96	6.86	3.09	6.1	5.7	4.3	2.2	2.0	3.66	0.11	3.80	3.03	4.87	2.40	4.32	0.40	
P ₂ O ₅	*	0.05	0.01	0.02	0.04	0.02	0.01	0.04	0.01	0.02	0.01	0.01	0.01	0.02	-	-	-	-	-	-	0.19	0.61	-	-	-	-	-	-	
Total S	*	0.03	*	*	*	*	*	*	0.25	*	*	*	*	0.18	-	-	-	-	-	-	0.14	0.13	-	-	-	-	-	-	
H ₂ O+	-	-	-	-	-	-	-	-	-	-	-	-	-	-	-	-	-	-	-	-	-	-	-	-	-	-	-	-	-
H ₂ O-	-	-	-	-	-	-	-	-	-	-	-	-	-	-	*	0.9	1.2	0.6	1.2	1.5	-	-	2.24	1.04	1.09	1.00	0.72	*	
TOTAL	97.63	101.04	98.25	97.51	98.96	98.98	97.47	96.38	98.42	100.39	93.21	97.20	99.84	98.11	99.70	99.6	100.4	99.7	100.3	100.2	89.20	89.22	99.88	99.82	100.08	99.57	99.20	100.07	

Trace Elements: ppm

Co	17	1	*	*	*	*	*	5	*	*	*	*	*	*							14	47							
Ni	7	30	27	12	23	19	18	6	21	13	3	10	19	2							20	*							
Cu	93	96	95	93	97	102	85	79	99	102	84	89	97	89							70	67							
Zn	65	47	43	44	*	58	87	245	201	130	145	132	57	52							136	122							
Rb	236	299	250	237	247	281	232	301	205	254	106	177	345	223							116	10							
Sr	10	13	7	47	14	6	6	62	15	15	17	32	8	24							99	132							
Pb	20	319	69	13	15	870	8	29	47	77	11	470	51	24							24	8							

* = not detected

- = not determined

CIPW Norms	* = not detected														- = not determined														
Qz	48.46	38.91	50.58	34.43	47.99	48.48	34.92	7.33	53.56	51.09	49.36	49.82	40.97	50.20	52.39	27.5	37.9	34.4	37.1	32.2	0.00	3.61	-	10.58	31.15	32.52	34.06	44.18	
Or	39.00	53.30	39.18	50.82	45.38	43.61	51.29	76.23	39.59	41.84	24.35	33.51	52.95	40.54	18.26	36.1	33.7	25.4	13.0	11.8	21.63	0.65	22.46	17.91	28.78	14.18	25.53	2.36	
pl	1.81	3.12	2.37	6.20	2.17	5.55	1.69	4.41	1.56	2.56	3.69	5.29	1.56	1.58	22.77	26.8	18.6	30.1	38.0	43.7	36.26	40.86	42.95	43.13	33.98	45.69	33.03	51.63	
co	1.96	2.84	2.32	1.81	1.55	0.69	1.41	1.72	1.30	2.14	4.13	1.74	1.71	1.54	-	2.8	4.1	2.8	6.5	5.5	-	-	-	-	1.54	4.60	1.97	1.01	
di	-	-	-	-	-	-	-	-	-	-	-	-	-	-	-	-	-	-	-	-	-	-	-	-	-	-	-	-	-
wo	-	-	-	-	-	-	-	-	-	-	-	-	-	-	2.42	-	-	-	-	-	2.58	16.76	10.98	2.59	-	-	-	-	
hy	3.18	0.07	0.35	0.95	0.10	0.02	6.14	2.82	0.17	0.05	11.07	4.01	0.07	1.06	-	4.5	4.2	5.7	3.7	4.3	25.09	19.14	2.56	16.48	1.91	0.99	2.27	0.35	
en	-	-	-	-	-	-	-	-	-	-	-	-	-	-	-	-	-	-	-	-	0.51	-	11.81	-	-	-	-	-	
ol	-	-	-	-	-	-	-	-	-	-	-	-	-	-	-	-	-	-	-	-	-	-	-	-	-	-	-	-	
fo	-	-	-	-	-	-	-	-	-	-	-	-	-	-	-	-	-	-	-	-	-	-	-	-	-	-	-	-	
mt	2.74	-	2.10	-	-	-	1.29	2.39	0.48	1.43	-	2.36	-	2.71	-	1.0	0.7	0.7	0.7	1.2	0.86	1.87	8.28	4.35	2.38	0.86	2.36	0.77	
ht	-	2.25	0.89	2.44	1.33	0.24	-	-	1.35	0.78	-	-	2.01	-	3.32	-	-	-	-	-	-	-	0.04	4.50	-	-	-	-	
ap	-	0.12	0.02	0.05	0.09	0.05	0.02	0.09	0.02	0.05	0.02	0.02	0.02	0.05	-	-	-	-	-	-	0.44	1.42	-	-	-	-	-	-	
Il	0.47	0.21	0.44	0.78	0.15	0.21	0.70	1.39	0.38	0.46	0.59	0.44	0.46	0.44	-	-	-	-	-	-	1.84	4.92	-	-	-	-	-	-	
Ru	-	-	-	0.04	0.19	0.12	-	-	-	-	-	-	0.09	-	-	-	-	-	-	-	-	-	-	-	-	-	-	-	
Percent An	90.63	40.38	64.27	23.51	61.05	25.34	89.99	28.96	94.57	56.98	42.63	29.68	94.57	89.27	2.26	14.1	0.0	9.4	6.2	8.6	61.03	22.14	41.0	46.1	22.7	23.4	9.5	8.1	

F.1 - F.14 and G.1 - 2, by x-ray fluorescence. Analyst C.J.V.Wheatley

JH.1, HG.1 and 2, and H.1 - H.5, from Jukes and Haughton (125).

FH.5 - FH.10, from Hatch (107).

Norms calculated on a CDC 6600 computer using programs devised by W.I. Ridley and B.M. Gunn.

(Description of samples in Appendix 2).

the most highly altered felsite.

c) Lime. CaO exhibits a similar distribution to the above.

f) Soda and potash. The felsites are highly potassic and earlier estimates of potash contents appear to have been low (compare Haughton's analysis of the Bell Rock felsite: JH.1, with the three new analyses F.1 to F.3.). Hatch (107) noted sodic varieties FH. 9 and 10. There is no confirmation of this amongst the new analyses, although samples from the same localities were not reanalysed.

g) Phosphorous. P_2O_5 shows a maximum value in the tuffs, probably due to apatite in andesitic lapilli.

The increased sulphur values reflect disseminated pyrite in the more basic pyroclastics.

2.2.4.2. Trace elements

a) Cobalt and Nickel. Cobalt and nickel contents are within the mean abundance figures for the rock-types (228), with nickel generally in excess of cobalt.

b) Copper, zinc and lead. Values of copper and zinc in the tuffs are close to the mean abundance figures (87 ppm Cu and 105 ppm Zn) for basaltic rocks (228). The contents of zinc in felsites are comparable to those in siliceous igneous rocks; 60 ppm (228), with samples F.8 to F.12 showing enrichment. The copper values in the felsites are greater than the mean value for granitic rocks 15 ppm (228). Lead contents are highly variable, the mean abundance figures being 6 ppm for basaltic rocks and 17 ppm for granitic rocks. The anomalous values within the felsites (samples F.2, 6 and 12) may be due to deuteric or hydrothermal solutions accompanying the mineralization.

c) Rubidium and strontium. Rb has a mean value of 243 ppm in the felsites and 63 ppm in the tuffs. These figures reflect the mean abundance of the element (228) which indicates enrichment in granitic rocks. The higher values correlate with high potash content.

Sr is characteristic of early differentiates and the low values in the felsites imply that they are late differentiates.

Increased values in the intermediate tuffs suggest that they are products of an earlier differentiation fraction.

2.2.5. Petrogenesis

The petrogenetic significance of the rock analyses can be considered in relation to a series of variation diagrams. (Fig.2.6). CIPW norms have been calculated for the analyses and are shown in table 1.

2.2.5.1. Granitic rocks

Tuttle and Bowen (229) in a study of the system $\text{SiO}_2\text{-KAlSi}_3\text{O}_8\text{-NaAlSi}_3\text{O}_8\text{-H}_2\text{O}$ at varying pressures, demonstrated that the bulk of granitic rocks are of similar composition and when plotted as normative constituents fall within the area shown in Fig.2.6A. The mean analysis of the Leinster pluton falls within this area and that of the Croghan sheet intrusive is near-by and well within the distribution limits of the Newer Caledonian granites demonstrated by Hall (102). The Ballinaclesh granite is enriched in soda, but grossly conforms to the other data. The anomalous nature of the marginal facies of the Croghan intrusive is apparent and is doubtless due to country rock assimilation.

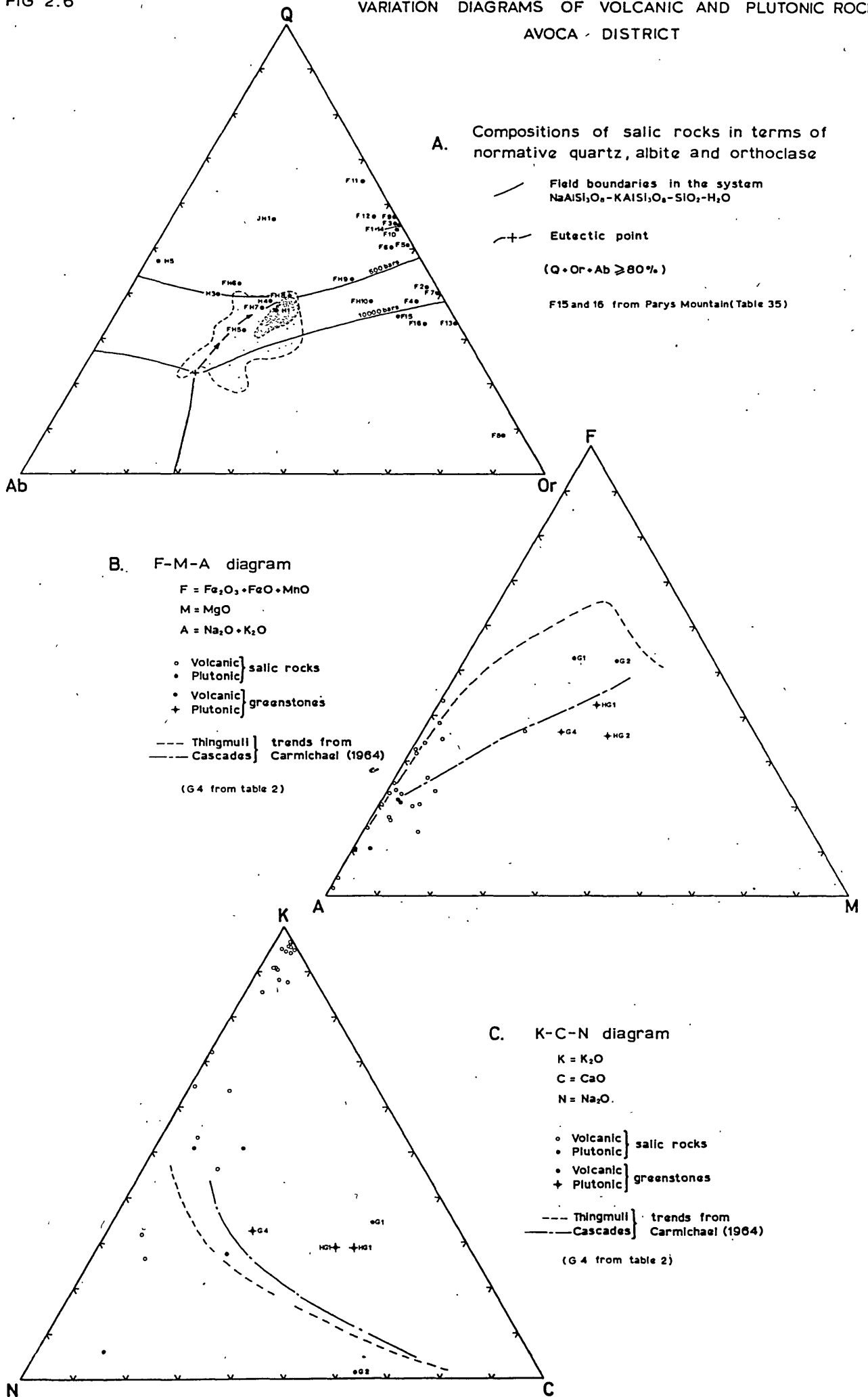
2.2.5.2. Felsites

Analyses of the felsites scatter widely when plotted within the $\text{Q-Or-Ab-H}_2\text{O}$ system: Fig.2.6A. Some of the data gathered by Hatch (107) fall within the field of Caledonian granites, close to the line joining minimum eutectics, suggesting that the felsite and granite magmas may be related. The new analyses however, have a different distribution, concentrating along the Q-Or edge. No magmas with this composition are known, and the felsites cannot have derived from the granitic magma by a normal process of magmatic crystallization. Two of Hatch's samples: FH.9 and 10 plot in the intermediate zone moving towards granitic composition, and support the idea of a connexion between the granite magma and that producing the welded felsic pyroclastics. The felsites also show abnormal enrichment in potash which requires an explanation.

It has been demonstrated by Lacy that, when water is

FIG 2.6

VARIATION DIAGRAMS OF VOLCANIC AND PLUTONIC ROCKS
AVOCA DISTRICT



added to a granitic melt, the structure breaks down with the formation of hydroxyl groups (137). The alkali ions within the melt are more loosely held than their associated anions, and transfer of alkalis only requires a thermal gradient and the presence of a vapour phase (170). The basement below the Lower Palaeozoic tectogene in S.E. Ireland was probably essentially granitic in composition. During the Ordovician the basement was probably tectonically depressed to a level in the crust sufficient to transform it partially into a melt. The accumulating eugeosynclinal pile of sediments and volcanics contained ample pore water. It is proposed that this water acted in the manner envisaged by Lacy to locally break down the structure of the melt. Alkali-ion transfer in this medium aided by the conspicuous thermal gradient, implied by the volcanic activity, would have been considerable and a late stage melt-phase rich in K^+ would have developed (44). This magma phase would rise to the surface through zones of dilatation and on account of its intrinsic high viscosity give rise to explosive volcanicity. Evidence of this process at Avoca is afforded by the rhyolitic pyroclastics, products of just such volcanicity. Devitrification of the pyroclastics was followed by silicification to form felsite. Generation of the potassic rocks by this mechanism is favoured, rather than metasomatism by hydrothermal solutions, because the felsites do not show a local, but regional enrichment in potash and thus a primary source of potassium is more likely. Bodies of Ordovician felsite elsewhere in S.E. Ireland are also potassic, (C.J. Stillman, pers. comm.), confirming the relations deduced at Avoca.

Post-dating the eruption of large volumes of the potassic magma fraction, the Leinster pluton was intruded, having a mean composition lying close to the eutectic at 1,000 bars in the Q -Or-Ab- H_2O system. Finally, granodioritic late stage sheet intrusives were emplaced, and developed marginal assimilation effects.

The two other variation diagrams: Fig. 2.6B,C merely endorse the characteristics of the acid rocks; the high alkali content and enrichment of magnesia in Sample F11 is emphasized

in the F-M-A plot and the anomalous potash contents are striking in the K-C-N diagram.

2.2.5.3. Intermediate pyroclastics and intrusives

These rocks on the F-M-A diagram, Fig. 2.6B appear to lie on a calc-alkaline trend, compared with the typical tholeiitic (Thingmuli) and calc-alkaline (Cascades) trends of Carmichael (51) and are andesitic in composition. This follows reasoning similar to that by Fitton and Hughes (86) who demonstrated the presence of a calc-alkaline province in the southern Lake District and North Wales, and allows projection of that province during the Ordovician across the present Irish Sea area to S.E. Ireland.

The K-C-N plot Fig 2.6C, on which the Thingmuli and Cascade trends are shown, essentially corroborates the above, although the data is minimal and widely scattered.

2.2.6. Mineralization

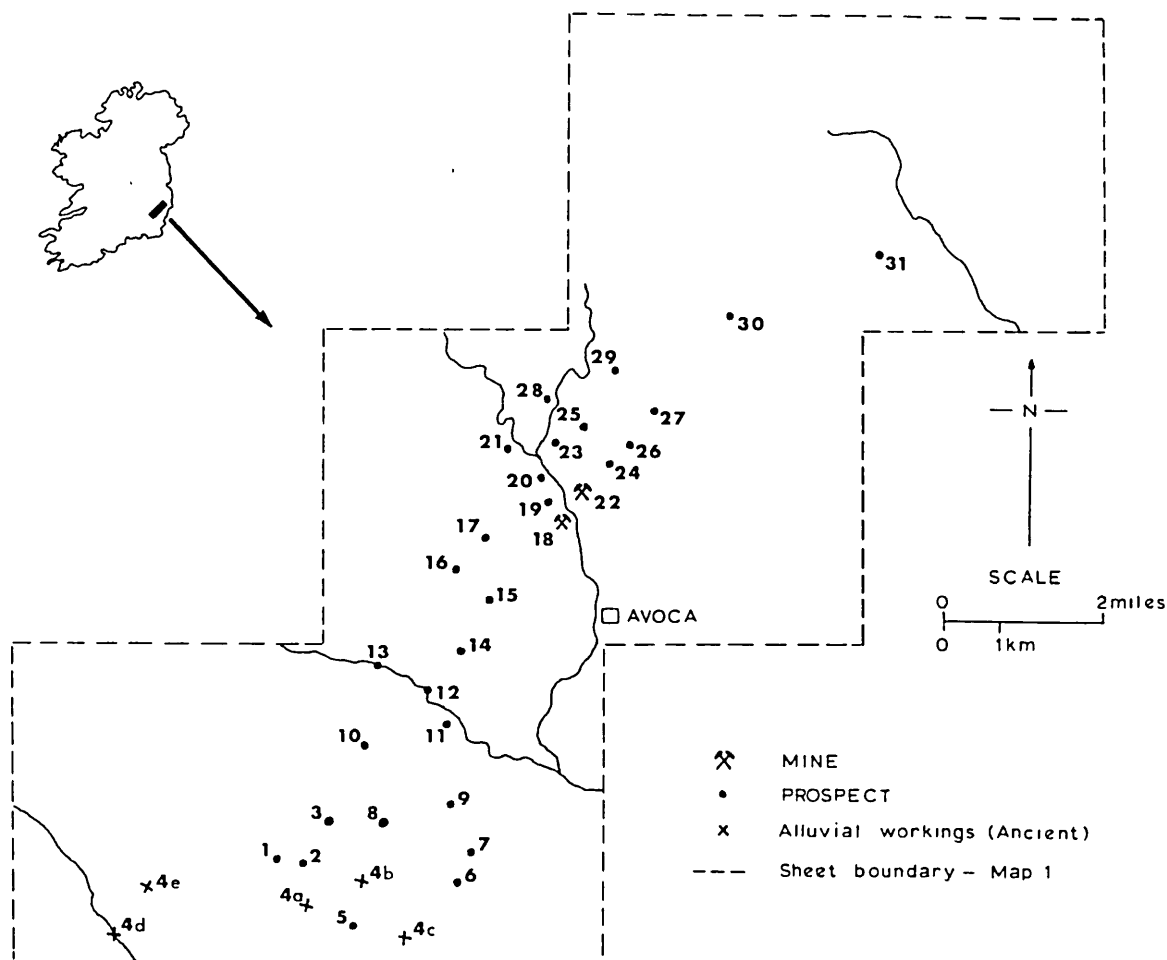
There are a large number of mineral occurrences in the Avoca district. The localities are shown on Map 1, and on a reduced scale in Fig. 2.7.

Moneyteige

Weaver (245) and Smyth (208) record iron ore production from the gossans in this region $5\frac{1}{2}$ miles southwest of the Avoca mine, where there are dumps and caved workings. The outcrops indicate two narrow seams of siliceous magnetite ranging up to 15 ft thick, and about 300 ft in length. Mineralization consists of magnetite, hematite and disseminated chalcopyrite in a siliceous matrix with a grade of about 1.5% Cu in dump material. The wallrocks are green tuffs, highly chloritic, with iron oxide partings (Plate 8:G), locally intensely silicified and typical of the Chlorite Zone. The detailed structure is unknown, but the seams are broadly conformable with the regional strike, and may be epigenetic stockworks of copper-rich siliceous material intrusive into syngenetic iron deposit. No pyrite occurs and no gold exists in polished section.

FIG 2.7

MINERAL OCCURRENCES IN THE AVOCA DISTRICT



KEY:

- | | | | |
|-----|--------------------------------|-------|---|
| 1 | Moneyteige | 18 | West Avoca, Ballygahan and Ballymurtagh |
| 2,3 | Ballinasilloge | 19,20 | Avoca Valley |
| 4 | Ancient alluvial gold workings | 21 | Knockanode |
| 5 | Moreshill | 22 | Tigroney |
| 6 | Knockmiller | 23 | Castle Howard |
| 7 | Clonwilliam | 24 | Cronebane |
| 8 | Ballykillageer | 25 | Connary |
| 9 | Coolgarrow | 26 | Connary |
| 10 | Ballycoog | 27 | Kilmacoo |
| 11 | Ballintemple | 28 | Meetings and Kingston |
| 12 | Aughrim River roadside | 29 | Sroughmore and Rockstown |
| 13 | Ballycoog Ford | 30 | Bolagh |
| 14 | Knocknamohill | 31 | Ballard and Ballycapple |
| 15 | Ballymoneen | | |
| 16 | Killeagh | | |
| 17 | Kilcassel | | |

Ballinasilloge

A series of siliceous veins with sphalerite, galena and minor chalcopyrite occur, about 1500 ft southeast of the Moneyteige deposits. Trial workings consist of a shallow adit and a shaft (~150 ft deep) at the northeastern occurrence. The country-rocks are silicified and chloritized pyroclastics and sediments. The narrow veins crosscut the cleavage but are broadly conformable with the regional trend. Localized high-grading operations took place around 1860.

Alluvial Gold

Wicklow experienced a minor gold rush in 1795 when a 22 oz. nugget purportedly from the Goldmines valley was exhibited in Dublin (130). All the major streams draining the northeast and northwest flanks of Croghan Kinshela were extensively worked until 1803 and 8,000 oz. were recovered (167). On the higher elevations, an adit was driven and a series of trenches were dug (Map 1, sheet 3). The source of the gold remains an enigma as no mother lode was located. A reasonable hypothesis is that the gold derived either from the pre-glacial gossans capping the Moneyteige deposits or from gossans developed at Avoca, where gold exists in the primary sulphide material (p.135).

Moreshill

A solitary shaft was sunk at this locality, in black slates which contain carbonaceous material. The mineralization consists of thin (<2mm) seams of pyrite with minor disseminated chalcopyrite. The pyrite shows post-tectonic metablastic growth, one of the rare examples from the district. Ullmannite, a rare nickel-antimony sulphide occurs in samples from the dumps. Wallrocks are part of the Lower Laminated Series and scattered pyrite euhedra occur within blue-grey to black shales and siltstones. The carbonaceous horizon implies that the metal sulphides may have originated within the sediment and were localized by shearing during folding.

Knockmiller

A series of thin (2-10 cm) seams of siliceous mineralization

within altered siltstones and intercalated pyroclastics is exposed at the roadside. Mineralization consists of arsenopyrite, pyrite, sphalerite and galena in varying proportions within a siliceous matrix. The seams crosscut the cleavage at a small angle. The high arsenopyrite content makes this occurrence unique.

Clonwilliam

Exposed in the western wall of an abandoned slate quarry are a few thin seams (5-10cm) thick, carrying galena, calcite, dolomite and quartz. The country rocks are siltstones and mudstones with intercalated pyroclastics of the Lower Laminated Series. The mineralization is crosscutting and may be contemporaneous with that at Ballintemple, a feature noted by Smyth (208).

Ballykillageer

Spoil from a shallow pit contains disseminated chalcopyrite and pyrite within the altered margin of a silicified metadolerite, and the same minerals occur near a fault plane exposed to the north. This minor mineralization may be the product of marginal alteration of the intrusive, but the prospect warrants further investigation.

Coolgarrow

An adit was driven on ferruginous fault breccia containing disseminated pyrite. The occurrence is minor, appears to wedge out towards the southwest, and probably is a supergene accumulation.

Ballycoog

Cole (58) and others, record active working around 1769 in this district, which is $3\frac{1}{2}$ miles southwest of the mine. A shallow adit and two drifts were driven, but all the workings are caved. The mineralization consists of two en echelon bodies, a northern lode of siliceous magnetite with disseminated chalcopyrite and a southern lens of banded pyrite with minor chalcopyrite. No trace of sphalerite, mentioned by Cole (58) occurs. Grab samples grade $\sim 1.5-2\%$ Cu.

Wallrocks are typical of the Chlorite Zone, green and grey chlorite slates and phyllites. The mineralization is

broadly conformable with the regional trend. The magnetite-rich ore appears to have been replaced by siliceous copper-laden solutions. The bedded pyrite may be syngenetic. A sizeable surface magnetic anomaly exists, but drilling indicates that the lenses wedge out in depth.

Ballintemple

On the southwest bank of the Aughrim River are abandoned workings of an old lead mine, now inaccessible. Mineralization consists of a crosscutting fissure-vein with a strike of 120° , infilled with galena, dolomite and gouge. Smyth (208) recorded that the seam varied from 2-20 cm in width, but this is refuted by others (58). Wallrocks are green-grey siliceous, chloritized tuffs, with intrusive diorites. Isotopic age data on galena from this occurrence (176) indicate an age of 210 ± 40 m.y., which agrees with the geological evidence that the mineralization post-dates that at the mine.

Aughrim River Roadside

A series of intermittent, thin seams, 2-5 cm thick, paralleling the cleavage occur in roadside exposures. Mineralization consists of magnetite, pyrite and disseminated chalcopyrite. Host rocks are dark green chlorite phyllites in the Chlorite Zone.

Ballycoog Ford

At the base of the nearby cliff exposure, minor seams 2-5cm wide occur, containing pyrite, sphalerite and galena in a siliceous matrix. The country-rocks are blue-grey to buff tuffs, with interbedded shales and siltstones of the Upper Volcanic Series. The mineralization crosscuts the cleavage in the tuffs and is related to faulting. The trend of the seams is close to the cleavage. This occurrence is similar to that at Knockmiller, but arsenopyrite is absent.

Knockmohill

Surface pitting has opened up two lenses of siliceous magnetite, which terminate to the southwest against a fault. The lenses vary in width from 1-6 ft. The mineralization consists of magnetite, hematite and quartz with specks of pyrite

and chalcopyrite. Host rocks are iron-rich sediments and tuffs, altered to green chlorite phyllites, typical of the Chlorite Zone, locally intensely silicified. The mineralization is broadly conformable and although the precise structure is unknown it apparently dies out rapidly in depth and may be an extension of the mineralization described below.

Ballymoneen

Dumps and a ruined engine house testify to former working for copper and iron, around 1850, in this area, $1\frac{1}{2}$ miles southwest of the mine.

A series of mineralized seams cross the area, but correlation is difficult due to lack of exposure. The major feature is a prominent fault which separates the area into two halves (Fig. 2.8A).

To the west there are possibly two en echelon lenses of siliceous magnetite with minor pyrite, veined by later carbonates, and indicated by surface pitting. Drilling has shown that the lenses, which are conformable in green chloritic phyllite, are of limited extent. A stockpile of material (~ 200 tons) exists near the adit portal with grades of $\sim 50\%Fe$.

To the east, offset to the north by 600 ft are a series of ore lenses, developed from a shaft and adit (Fig. 2.8B). The configuration of the mineralized zones is remarkably similar to the Avoca mine. A banded pyritic zone stratigraphically overlies a siliceous copper-rich zone which has a felsite in the hangingwall. The mineralogy consists of pyrite, chalcopyrite and sulphosalts (Plate 24:G). The zones are conformable within green chloritic phyllite, their extent is not known and extensions to the mined out zones are excellent exploration targets. The zones probably have the same origin as their equivalents at the Avoca mine.

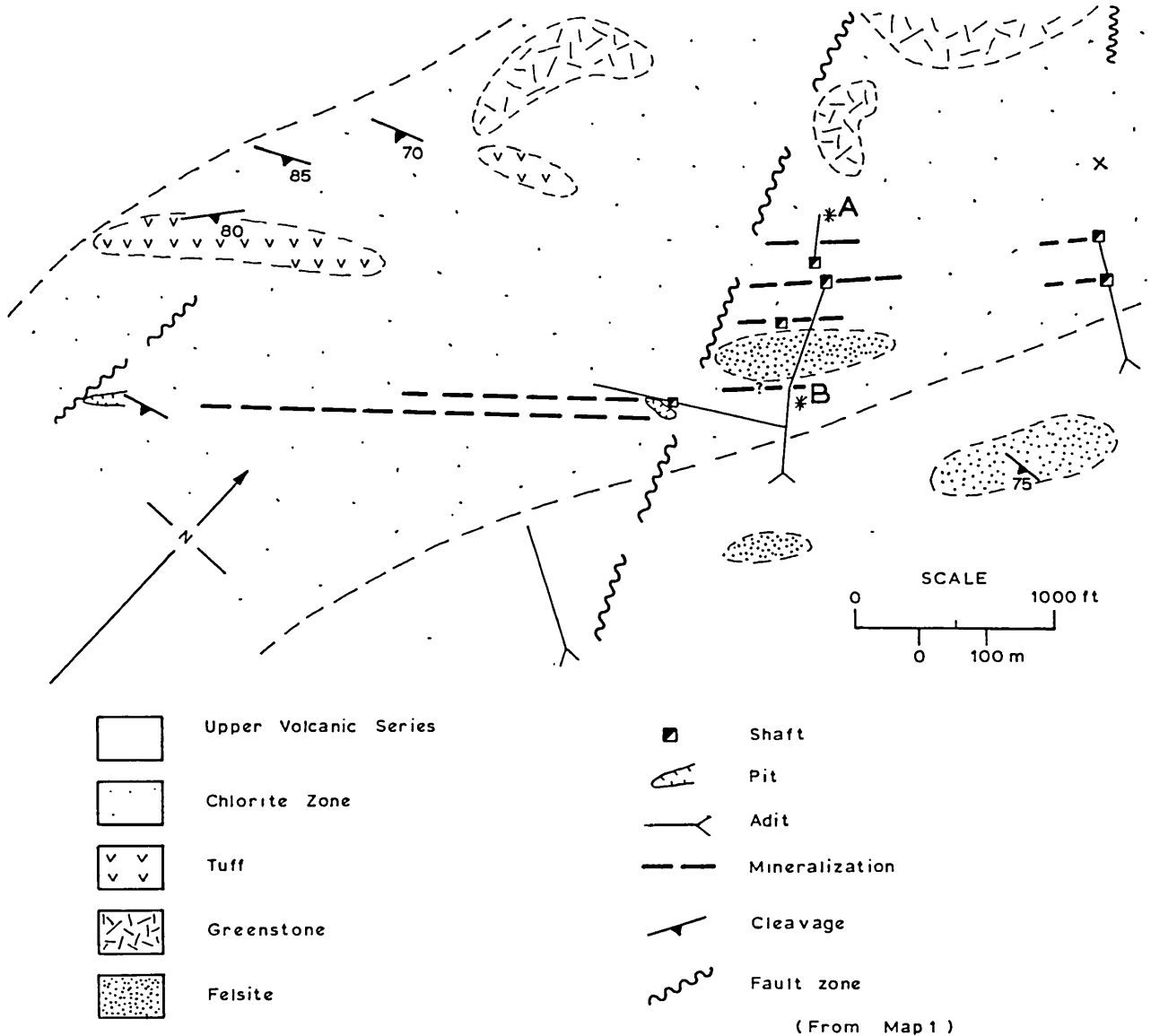
Killcagh and Kilcassel

A series of ancient trial pits 2000ft northwest of Ballymoneen indicate minor seams of siliceous chalcopyrite and pyrite, often at the margins of dioritic intrusives. The country-rocks are blue-grey to buff laminated siltstones and mudstones

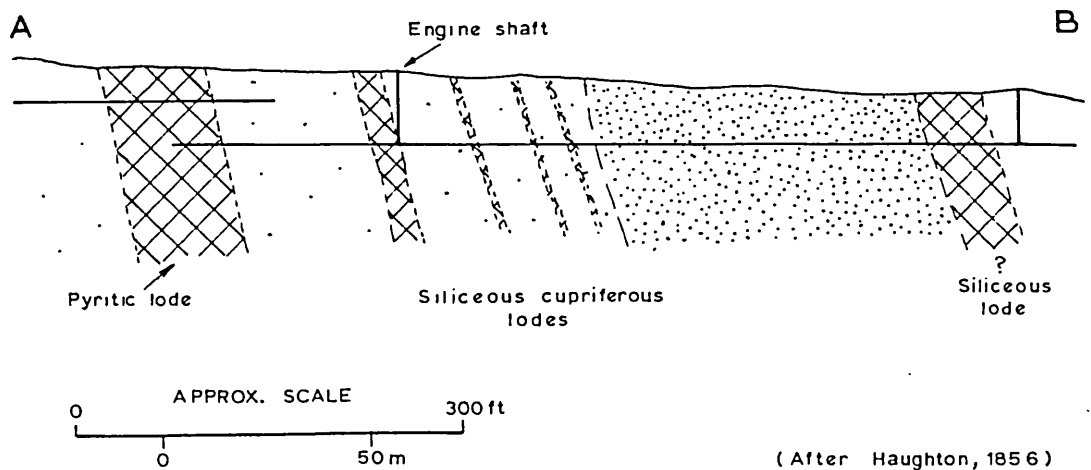
FIG 2.8

BALLYMONEEN - PLAN AND SECTION

A. GEOLOGICAL SKETCH MAP



B. GENERALIZED CROSS-SECTION



with intercalated green tuff beds typical of the Upper Volcanic Series. The structure is not known in detail, but the mineralization is minor.

In Killeagh, a shaft (Cox's) has been sunk on a carbonaceous horizon within shales and tuffs containing disseminated pyrite. This may represent original iron sulphide formation in a carbonaceous shale, and the trace element content of the pyrite supports this notion (p. 176).

West Avoca: Ballygahan and Ballymurtagh

This is the site of extensive former operations, and the present mine. A series of six en echelon lensoid lodes occur, making up the present ore. Amongst the lodes two major ore-types exist; pyritic and siliceous. The pyritic ore consists of fine, medium and, rarely, coarse grained pyrite with disseminated chalcopyrite and minor sphalerite and galena in a highly chloritic host rock. (e.g. North, Pond and Central lodes).

The siliceous material consists of lenticles of quartz with disseminated pyrite and chalcopyrite and traces of galena and sphalerite. Extensive silicification and alteration of the wallrocks produced siliceous chlorite and sericite schists, phyllites and phyllonites. (e.g. North Lode South branch, South and Hangingwall lodes). The geology and mineralization are described in detail in section 2.3.5.

Avoca Valley

Northwest of the mine are a series of short adits and shafts driven on siliceous copper-rich seams. These seams rarely exceed 15 cm in width, and the country-rocks are andesitic tuffs with interbedded siltstones and mudstones. The mineralization is pyrite and chalcopyrite disseminated in a siliceous matrix. These occurrences illustrate the continuity of mineralization in the central part of the belt and although minor, sometimes persist sporadically for thousands of feet along strike.

Knockanode

A series of shallow abandoned workings and dump material indicate scattered siliceous pyritic seams with disseminated

galena in a talcose phyllite. Host rocks are blue-grey siltstones and mudstones and the mineralization is broadly conformable with the cleavage.

East Avoca : Tigroney, Cronebane, Connary and Kilmacoo

This area lying northeast of the Avoca fault, contains extensive former workings and is the prime exploration target for the present operation. At Tigroney and Cronebane, there are two lodes: the northerly Main Sulphur lode consists of banded and massive pyritic ore with significant sphalerite and galena. The southerly, Hangingwall lode is a siliceous pyrite-chalcopyrite ore with sphalerite and galena.

At Connary and Kilmacoo, there are two lodes; a northerly pyritic lode and a southerly lode with sphalerite, galena, and pyrite with disseminated chalcopyrite in a siliceous matrix.

All the mineralization at East Avoca is in the Chlorite Zone, and is described fully in section 2.3.5.

Castle Howard

A zone has been explored by adits and narrow workings. The mineralization is pyritic, consisting of banded pyrite, with disseminated chalcopyrite, becoming siliceous towards the hangingwall. Wallrocks are blue-grey tuffs, and the zone is conformable with cleavage. The host rocks are similar to those of the pyritic zones at the mine. Grab samples indicate grades of $\sim 0.5\%$ Cu over widths of 10-15 ft. The strike extent may be about 300 ft. This occurrence may represent syngenetic pyrite in iron-rich tuffaceous sediments.

North Connary

Two prospect shafts exist in black shale which locally contains disseminated pyrite. The host rocks are blue-grey laminated siltstones and mudstones, with intercalated tuff horizons of the Upper Volcanic Series. Mineralization is essentially pyritic, and the black shale contains specks of carbonaceous material implying an original reducing environment.

Meetings and Kingston

Adits and dumps indicate siliceous crosscutting lead-zinc

veins, which are occasionally dolomitic, in siltstones and mudstones with tuffaceous intercalations. Mineralization consists of galena, sphalerite and minor pyrite and chalcopyrite with quartz. The seams are narrow, of limited extent, and are broadly conformable to the schistosity.

Sroughmore and Rockstown

A series of shallow adits, shafts and pits trace pyritic mineralization. The mineralogy is exclusively pyrite and the host rocks are blue-grey to black siltstone, mudstone and tuff with carbonaceous seams. The latter, with disseminated pyrite, give rise to spectacular geophysical anomalies. Drilling indicates that these are continuous along strike for thousands of feet. Their frequent occurrence within this lithology, makes geophysical interpretation hazardous, unless backed by good ground geological coverage.

Bolagh

A single shaft exists but there is no trace of the dump material. It is on the prolongation of the mineralized belt and may be a barren prospect shaft.

Ballard and Ballycapple

Workings are scattered over a strike length of 500 ft and indicate a magnetite zone which is $2\frac{1}{2}$ miles northeast of the mine. Mineralization consists of banded siliceous magnetite-hematite lenses, up to 10 ft in width in buff and grey-green chloritic mudstones and siltstones. A felsite body occurs in the hangingwall. Murphy (pers. comm.) states that sampling from a small stope returned an assay of 55% Fe over 6-8 ft, and that a mean assay for the ore is: 56% Fe and 4% Mn. The gossans are highly manganeseiferous, with up to 16% Mn (58). This occurrence thins rapidly with depth.

Summary

The conformable mineral occurrences are predominantly in rocks of the Chlorite Zone, and crosscutting vein deposits occur randomly throughout the belt.

Three types of mineralization exist:

- a) Lenticular pyritic bodies, often with associated siliceous cupriferous zones
- b) Conformable magnetite lenses sometimes with associated polymetallic mineralization.
- c) Siliceous polymetallic crosscutting veins.

The operating mine is in the centre of the mineralized belt. Type a) above, predominates and types b) and c) are minor.

2.2.7. Structure

No definitive marker horizons exist in the Avoca district, and the structural scheme is developed from cleavage-bedding relationships and associated minor structures. Poor exposure results in an undue bias towards isolated outcrops, but the effects of this are kept to a minimum.

Salient mesoscopic structural data are on Map 1.

The Avoca district has undergone at least three periods of major deformation, correlating well with the regional sequence (p. 17). Minor structures are superimposed on major features and only the mesoscopic elements can be recognized in the field.

2.2.7.1. Mesoscopic Structure

- a) Planar
 - i) Bedding planes, S_0

The lithological features of the rocks have already been described, and recognition of bedding in the finer grained varieties (of the Chlorite Zone) is often impossible due to the nearly coincident regional cleavage, S_1 . However, in the marginal areas, some measurements of bedding were taken and poles to these planes are shown in Fig. 2.9B. The data are minimal and allow no positive deductions about the nature of the first folds from the spread of the values.

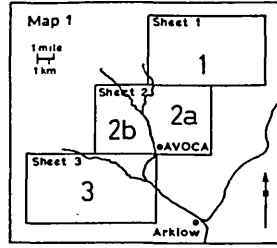
- ii) Regional Cleavage, S_1

A prominent slaty cleavage occurs throughout the district and is penetrative with the exception of the internal zones of

FIG 2.9

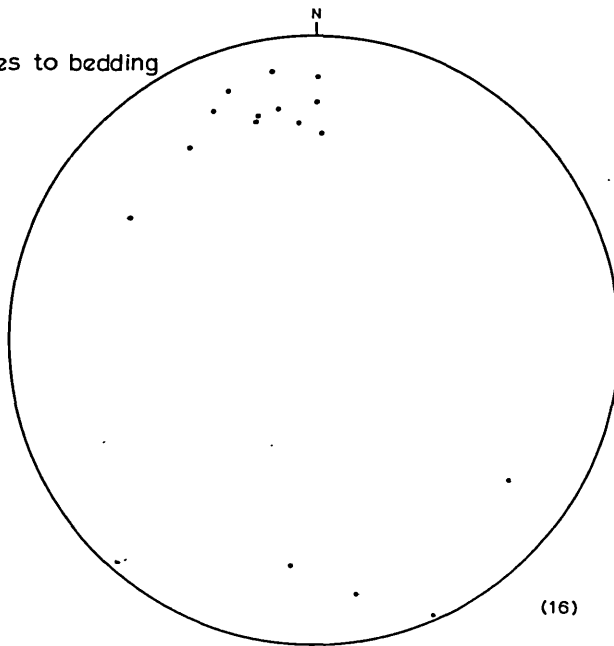
BEDDING AND CLEAVAGE, AVOCA DISTRICT

A.
Key Map, with the sub-areas
for cleavage analysis

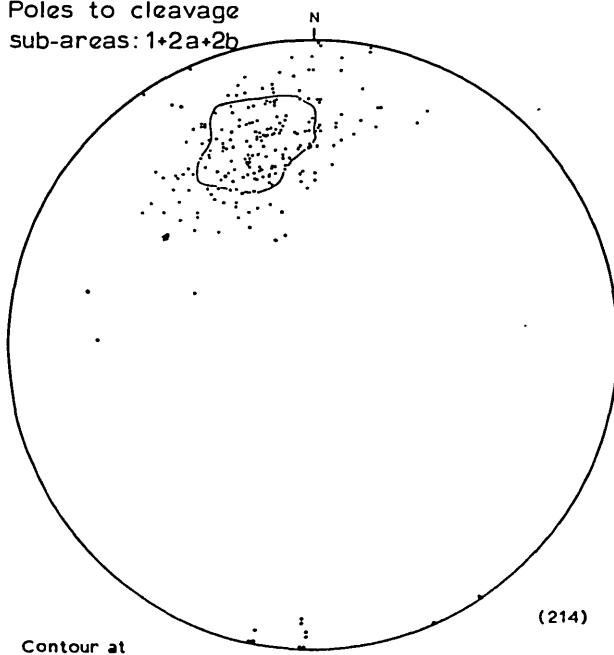


Lower hemisphere equal area stereographic projections:

B.
Poles to bedding

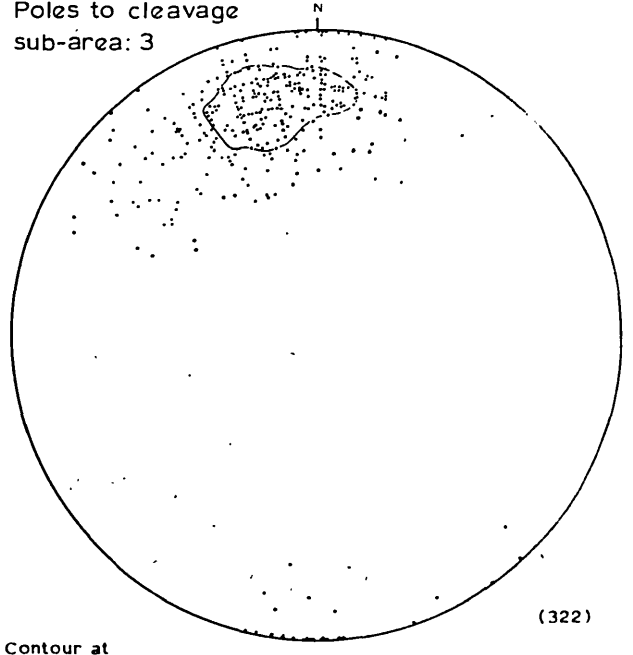


C.
Poles to cleavage
sub-areas: 1+2a+2b



Contour at
1% per 1% area

D.
Poles to cleavage
sub-area: 3



Contour at
1% per 1% area

the intrusive bodies. The cleavage has altered the rocks into slates and phyllites in which the micaceous minerals are orientated sub-parallel to the cleavage. The attitude of the cleavage is remarkably consistent (Fig. 2.9). The average strike is 061° and dips vary from $56-80^{\circ}$ SE. A well developed maxima exists, and the spread of the poles is probably due to small scale superimposed folds

iii) Fracture cleavage, S_2

A fracture cleavage, which crosscuts the minor fold axes, is penetrative in the argillaceous units, but non-penetrative in the more massive and arenaceous beds. This cleavage is always at a moderate angle to the bedding and S_1 , and produces a kinked effect on the chloritic laminae. Few readings of S_2 were obtained due to the scarcity of exposures in the argillaceous units. The available data points to a northwest trend and moderate dips to the southwest (Map 1.).

iv) Axial planes of minor folds

No examples of F_1 folds occur in surface exposures, but data relating to F_2 were collected (Fig. 2.10B). Chevron folds and kink bands are relatively common and with minor folds represent the F_2 fold episode. The kink planes are sometimes arranged in conjugate sets (Plate 5:B) or may merge into one another forming branching fracture systems (Plate 5:A). The shapes of the minor folds are shown in plate 5:C. The form varies from concentric to similar and neither the wavelength nor amplitude is constant. The distribution of the poles to minor folds and kink planes is an excellent conjugate system.

v) Faults

The fault pattern on Map 1 has been deduced from indirect evidence from aerial photographs, coupled with ground observations. Direct evidence is given by offset of geological contacts. It is not possible to determine the magnitude of displacement of the faults due to the absence of marker horizons.

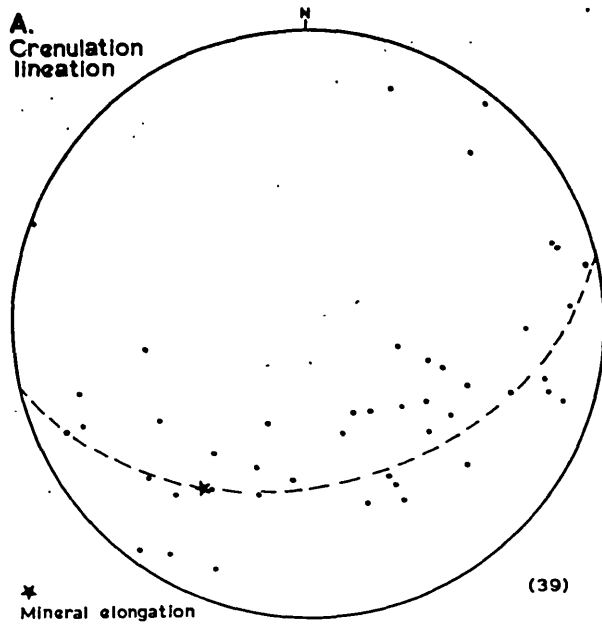
Trenlett (225) elucidated a maze of thrusts and faults in the Avoca district, and assigned them to seven different sets.

FIG 2.10

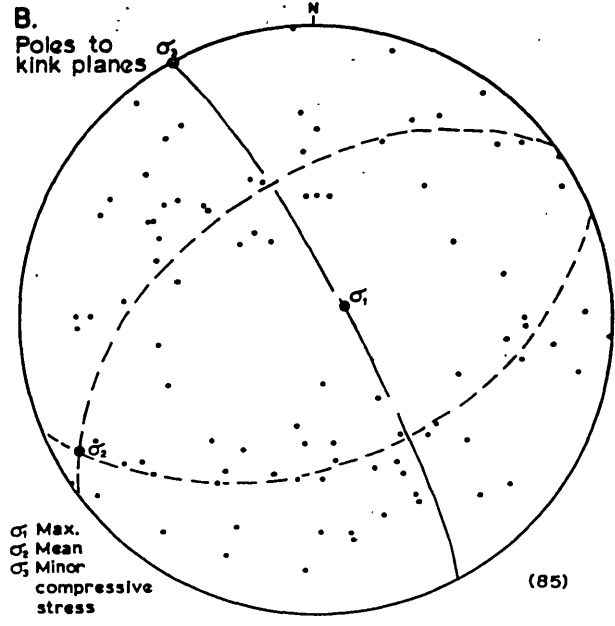
STRUCTURAL ELEMENTS, AVOCA DISTRICT

Lower hemisphere equal area stereographic projections:

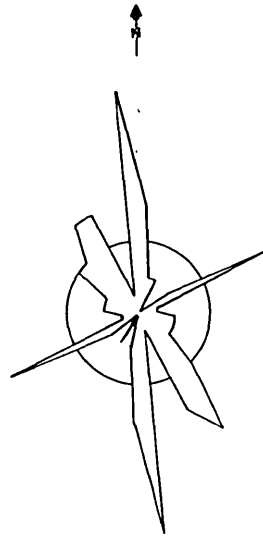
A. Crenulation lineation



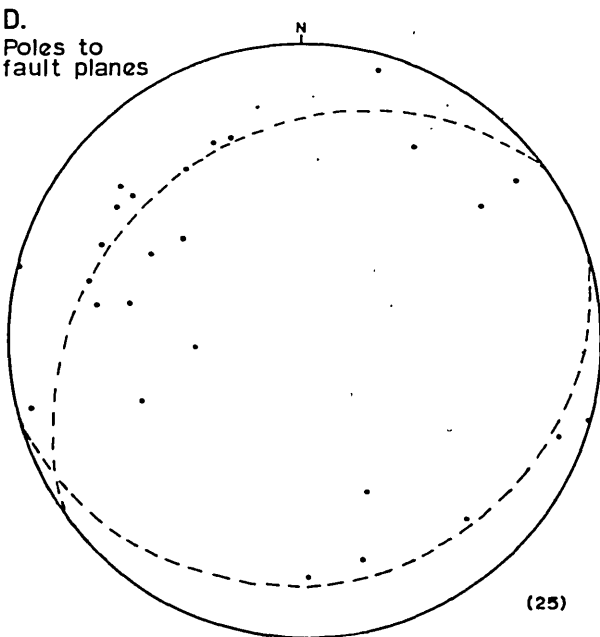
B. Poles to kink planes



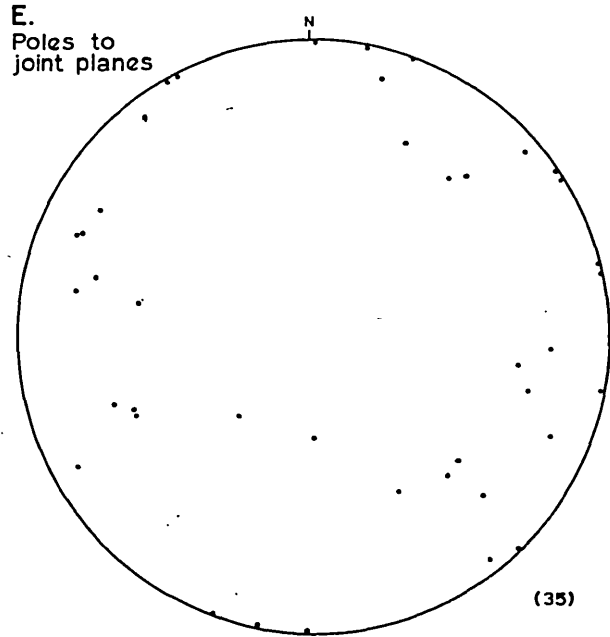
C. Rose diagram of fault planes (unknown inclination)



D. Poles to fault planes



E. Poles to joint planes



The present study simplifies this picture.

The rose diagram, Fig.2.10C, illustrates the distribution of the major surficial faults on which no dip direction can be inferred. Three dominant trends exist:

N-S, trending 174°

Vertical to sub-vertical oblique-slip faults are predominant and often have a sinistral tear component. As noted by Tremlett these faults are cut off by types b) and c) (see below) and tend to occur in pseudo-rift pairs. Faults of this type are prominent at Tigroney, Crenebane and Connary.

N.N.W., trending 144°

These are normal, dip faults, which are vertical to sub-vertical, composed of a zone of multiple fracture, frequently have considerable displacement (dextral or sinistral) and are typified by the Avoca River fault. This fault correlates with the Kirikee fault mapped by Tremlett northwest of the present district.

E.N.E., trending 064°

These high angle strike faults are of minor extent, generally with sinistral displacement. They may be sites for the localization of late stage mineralization: e.g. Knockmiller, Ballycoog Ford etc., and were not recognized by Tremlett.

A major, normal, high angle strike fault is the upper boundary of the Upper Volcanic Series and has an average trend of 035° . This fault, which may have a throw of more than 5,000 ft correlates with Tremlett's northeasterly trending suite. The present study, however, does not substantiate the Limerick or Croghan thrusts postulated by Tremlett, and there is no evidence for the major Castlemacadam or Ballinasilloge faults.

Faults on which inclinations could be measured are shown stereographically in Fig. 2.10D. Data are minimal, but corroborate the trends discussed above. Anderson (4) showed that the redistribution of stresses adjacent to a major fault may give rise to second order faults. The Avoca River fault has a number of associated faults, which may be of second order form.

Chinnery (55) suggested that secondary faulting is confined to the ends of major faults and the fact that the Avoca fault appears to die out when traced southeast of the present area supports his contention.

All the major faulting post-dates S_1 and probably also S_2 , and is therefore referred to a final deformation: D_3 .

vi) Joints

The distribution of joints in various rock types is illustrated in Fig. 2.10E. Joint planes in the incompetent rocks (Plate 5:F) give rise to lineaments which are clearly visible on air photographs. The distribution of the poles to the joint planes exhibit an indistinct concentration paralleling the regional (F_1) fold axis and may be a-c joints. These characteristically develop during the final phase of orogeny, when the regional stress relaxes (28).

b) Linear

i) Intersection of S_1 and S_0

The intersection of the regional cleavage and bedding produces a minor lineation on the cleavage trace. This lineation is a microcrenulation or ribbing (Plate 5:E) with a wide variation in attitude Fig. 2.10A. This variation may be due to overprinting by later deformation. A pronounced girdle is developed in the plane of S_1 and thus the lineation is associated with the axis of the major F_1 folds. (Assuming that S_0 is axial planar to the F_1 folds).

ii) Bedding slip

Associated with the concentric minor folds a fine bedding slip lineation develops.

iii) Intersection of S_2 and S_1

This feature which is rarely seen, gives rise to an indistinct lineation on the trace of S_1 .

iv) Axis of minor folds

There are insufficient exposures to permit accurate determination of the trend and plunge of minor fold axes.

v) Boudinage

Boudin-like structures occur in laminated blue-grey slates at Kilmacrea (Plate 5:D). The structures, with siliceous rods, may be pull-apart structures and not true boudins (180); lack of exposure does not allow a precise definition.

vi) Mineral elongation

Compressed chlorite plates within the lithic tuffs indicate a mineral elongation in the plane of S_1 . Accurate measurements of the trend and plunge were impossible in the surface exposures, but generally conform with the data collected underground at the mine (p. 90).

vii) Slickensides

The majority of fault planes are grooved by slickensides which have variable orientations. As directional indicators of fault movement their use is controversial (177). Several periods of movement have taken place each giving rise to differing sets of striations. The sequence of movements is of little significance to ore localization as faulting is post-ore, and detailed study was not undertaken.

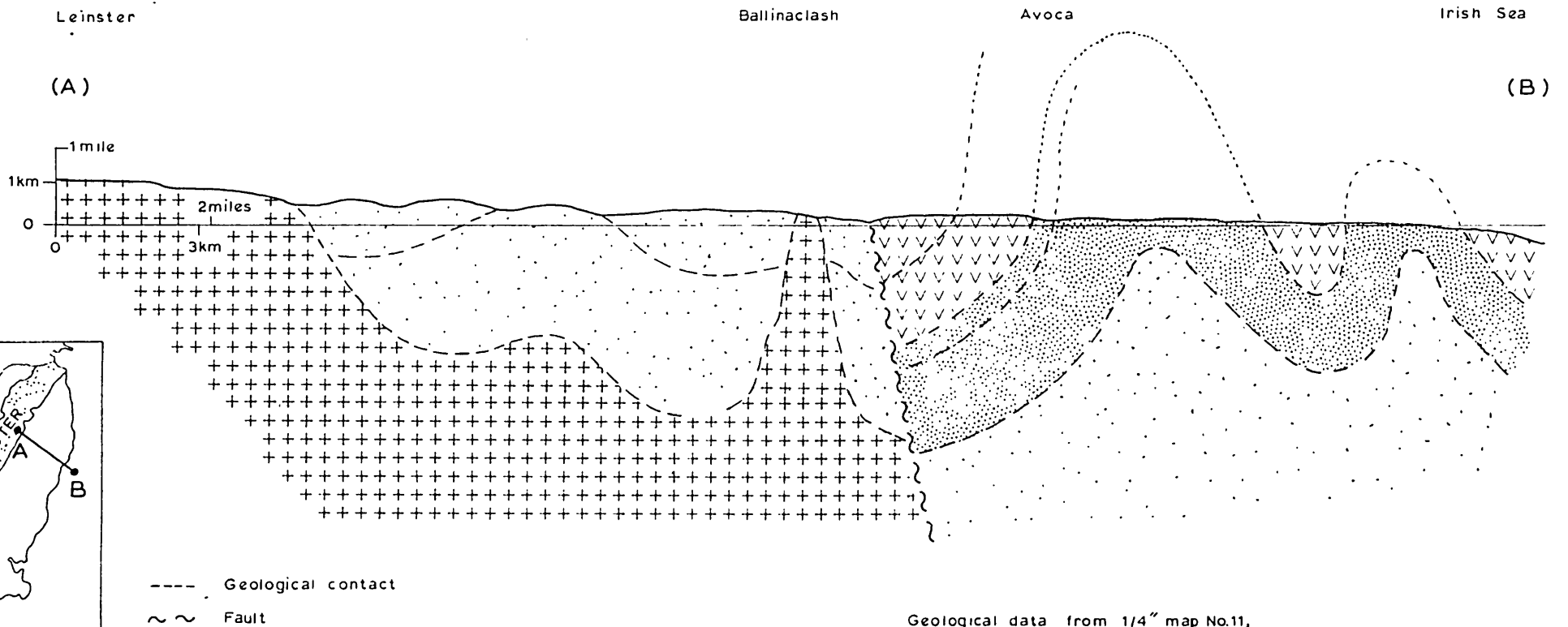
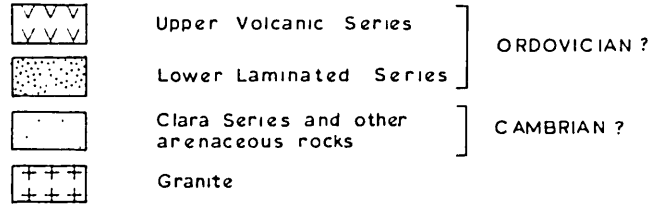
2.2.7.2. Macroscopic Structure

On the basis of way-up evidence and cleavage-bedding relationships, the Avoca district straddles a monoclinial structure which is overturned towards the northwest (Fig. 2.11) At Coats Bridge in Ballymorris townland, the cleavage-bedding angle diverges to $\sim 40^\circ$ Plate 2:D. and thus this point must be close to the zone of closure of the monocline. The other fold closures in the idealized section have been deduced from the regional outcrop pattern. No closures applicable to F_1 were mapped during this study, and the regional picture remains uncertain. The major folds are relatively tight, with amplitudes in excess of 3,000 ft and overturned axial planes.

The intrusion of the Leinster pluton post-dated development of F_1 , was a pulsatory process (40) and took place with later satellite sheet intrusions along a NNE trend. This trend is paralleled by the major strike fault bounding the Upper

FIG 2.11

GENERALIZED CROSS-SECTION S.E. IRELAND



Geological data from 1/4" map No.11,
Geological Survey of Ireland, with additions

Volcanic Series, and thus the two structural events may be interrelated.

2.2.7.3. Stress Distribution

The work of Anderson (4) allows prediction of the stress distribution necessary to produce a set of fractures, once complementary slip surfaces have been recognized. The only set of fractures in this study for which such data are available are the kink planes. Conjugate kink planes, (Fig.2.10B) produce two complementary girdles and the distribution of stresses leading to the production of the kink planes is shown. The maximum stress is vertical, and the minimum and intermediate stresses plot close to the horizontal. This distribution is characteristic of normal faulting (4) and of conditions in the upper levels of the crust (177).

2.3 Economic Geology

2.3.1. Introduction

The Avoca Mine is about one mile north of Avoca Village and seven miles northwest of the port of Arklow. The area is divided into two halves by the river forming an east and west portion and the division is a geological break : the Avoca River fault.

The regional and general geological setting have been described, and in the following section, the stratigraphy, lithology and petrology of the wallrocks is discussed, with the structure, mineralogy, geochemistry and genesis of the mineralization. These factors are essential to understand the controls of ore deposition and they also serve as guides for future exploration.

2.3.2. History of Mining

Goscans were reputedly worked in pre-Norman times (131). Iron ore was extracted at Ballycoog, Moneyteige, Knocknamohill and Ballard (Fig. 2.7), and mining waned in 1761.

Copper Mining, developed in about 1790, on the sides

of the Avoca River and was dominant until 1840. Over 100 shafts were sunk to depths varying from 20 ft to 650 ft using hand moils, hammers and gunpowder. About 4 million tons of ore were produced from the Tigroney Deep Adit. This ore was primary chalcopyrite, with material from the zone of supergene enrichment. Pyrite was rejected as waste. Copper was precipitated from the acidic mine waters in ponds containing scrap iron (172). The ore was transported to Arklow, and shipped to the South Wales smelters in schooners returning with coal for the Cornish pump engines. The ruined engine houses and stacks are a present-day reminder (Plate 1A).

Sulphur became a vital commodity with the industrial revolution in Britain. Sicily, the main producer induced a rise in prices making recovery from pyrite economic. Pyrite production dominated mining until 1880, when competition from mines in Spain and Norway, and engineering difficulties made extraction uneconomic, the mines becoming dormant.

Minor working took place during 1914-18 for copper to supply European war needs, and Mianraí Teoranta, the government mining company extracted pyrite from West Avoca (257) during 1942-45. Intermittant exploration took place from 1917-1949, when work was intensified. The Ballygahan shaft was reopened and deepened to 800 ft. A tunnel was driven 2,500 ft along the strike of the orebodies at West Avoca, in the footwall of their down-dip projection. Underground and surface drilling delimited about 12 million tons at 1.13% Cu. At East Avoca, 2 million tons were proved with additional values in lead and zinc (1.05% Pb and 1.50% Zn) (254).

Mogul Mining Corp. of Toronto took control through St. Patrick's Copper Mines Ltd. in 1956. Sub-level transverse and longitudinal open stope mining methods were employed, using a 12° incline (Knight Tunnel) as access to the upper levels at West Avoca. Development, loading and transportation of ore to the 4,000 t.p.d. mill was mainly trackless, and material from the deeper levels was brought to the surface by a conveyor, via an underground jaw crusher.

A fall in world copper prices added to dilution of the ore in stopes due to breaking against a weak hangingwall and old stopes, caused the company to pass into liquidation in 1962. The mine was maintained by the government, and in March 1969 an option was exercised by Avoca Mines Ltd., controlled by Discovery Mines Ltd. of Toronto. About 7 million tons of ore grading 0.98% Cu, after dilution, was proved. Production at 2,000 t.p.d. began in 1970. Current mining at West Avoca involves longhole open stoping for the South Orebody and mechanized trackless, cut-and-fill for the Pond Orebody. The incline has been extended to the 1670 Level (Fig 2.12A). At East Avoca about 1½ million tons of ore is proved, and will be worked from an open-pit on Cronebane. Production at 500 t.p.d. is due in Autumn 1971.

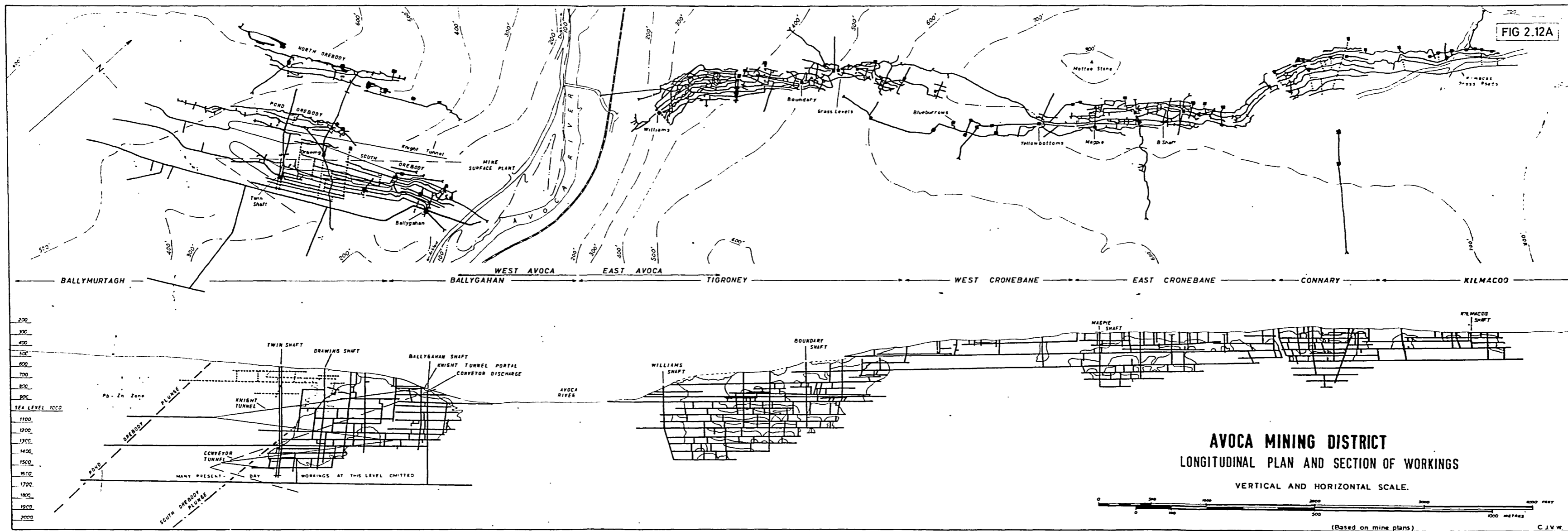
Copper concentrate is shipped from Arklow to Europe, and in addition 80,000 tons per annum of by-product pyrite will be sold to Nitrigin Eireann, at Arklow for fertilizer production.

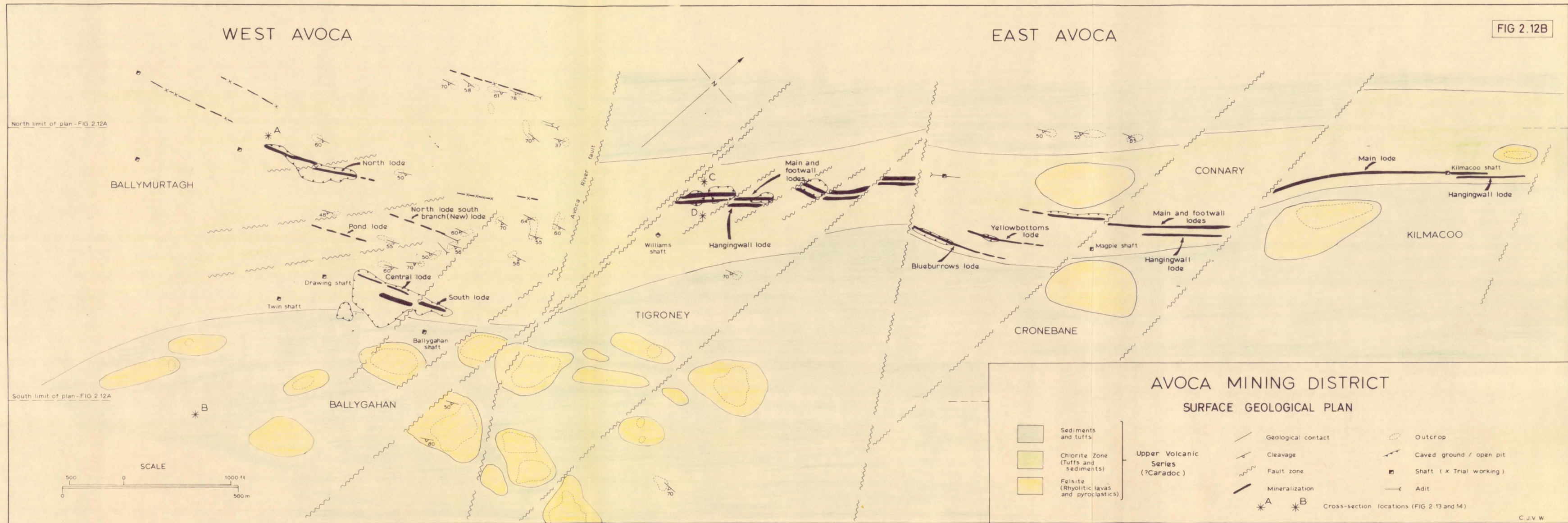
Revision of mining taxation stimulated operations at Avoca. In 1956, the profits generated by new mines working non-bedded deposits were exempt from Income and Corporation profits tax for the first four years of production. In 1967, the 'tax holiday' was increased to twenty years for mines commencing production before 1986.

2.3.3. Stratigraphy

The economic mineralization is in the Chlorite Zone of the Upper Volcanic Series, and Fig 2.12B shows the surface geology of the mine area. The rocks are a series of sediments and volcanics, dominantly pyroclastics. Way-up evidence, from grading of tuff lapilli exposed in the railway cutting south of the mine, indicates that the succession is overturned. (Other localities in Map 1 stress that this phenomenon is not restricted to the mine area.

Lithological variations have been studied from drill cores, and exposures underground at West Avoca. The extent of the recent and former workings is shown in Fig 2.12A.





(N.B. Mine datum is 1,000 ft above mean sea level and the mine levels are numbered positively, downwards from this horizon.)

Rock units have been established and the distribution of these units on three levels at West Avoca is shown on Map 2, and the geological level plans : Maps 3, 4, and 5. In cross-section, changes in lithology are illustrated in Figs 2.13 and 2.14. (The West Avoca cross-section is constructed from drilling and development data; whereas that of East Avoca is idealized, due to a lack of drill-hole intersections.) Access to data gathered by former mine geologists, OBrien, Murphy and Gordon-Smith was provided by the company, but the interpretation presented herein rests largely upon information gathered by the author.

Lanpard(138) recorded that Murphy established a scheme of rock identification, but no information is available. The following description is therefore the first annotated attempt to lithologically define the rocks at Avoca.

Core was logged using a statistical 'S/Q' Logging Method, described in Appendix 4. The mineralogy of the rock units was studied by optical and x-ray diffraction methods and the data was compared with that in the text by Deer, Howie and Zussman(67).

2.3.3.1. The Mine Schists

a) Lithology and Petrography

The mine schists are a series of metamorphosed sediments, pyroclastics and lavas, converted into slates, phyllites and phyllonites. True schists do not occur, but this terminology is adhered to on account of long usage at the mine.

The lithological divisions use two features of the rocks as a basis. a) The proportion and character of the micaceous mineral and b) the degree of secondary silicification. These factors are interrelated through wallrock alteration, a) reflecting the primary rock composition and, b) being the result of secondary alteration.

(N.B. The colours refer to fresh rock, surface weathering of the sulphide and chlorite produce a uniform buff coloured, friable rock.)

FIG 2.13

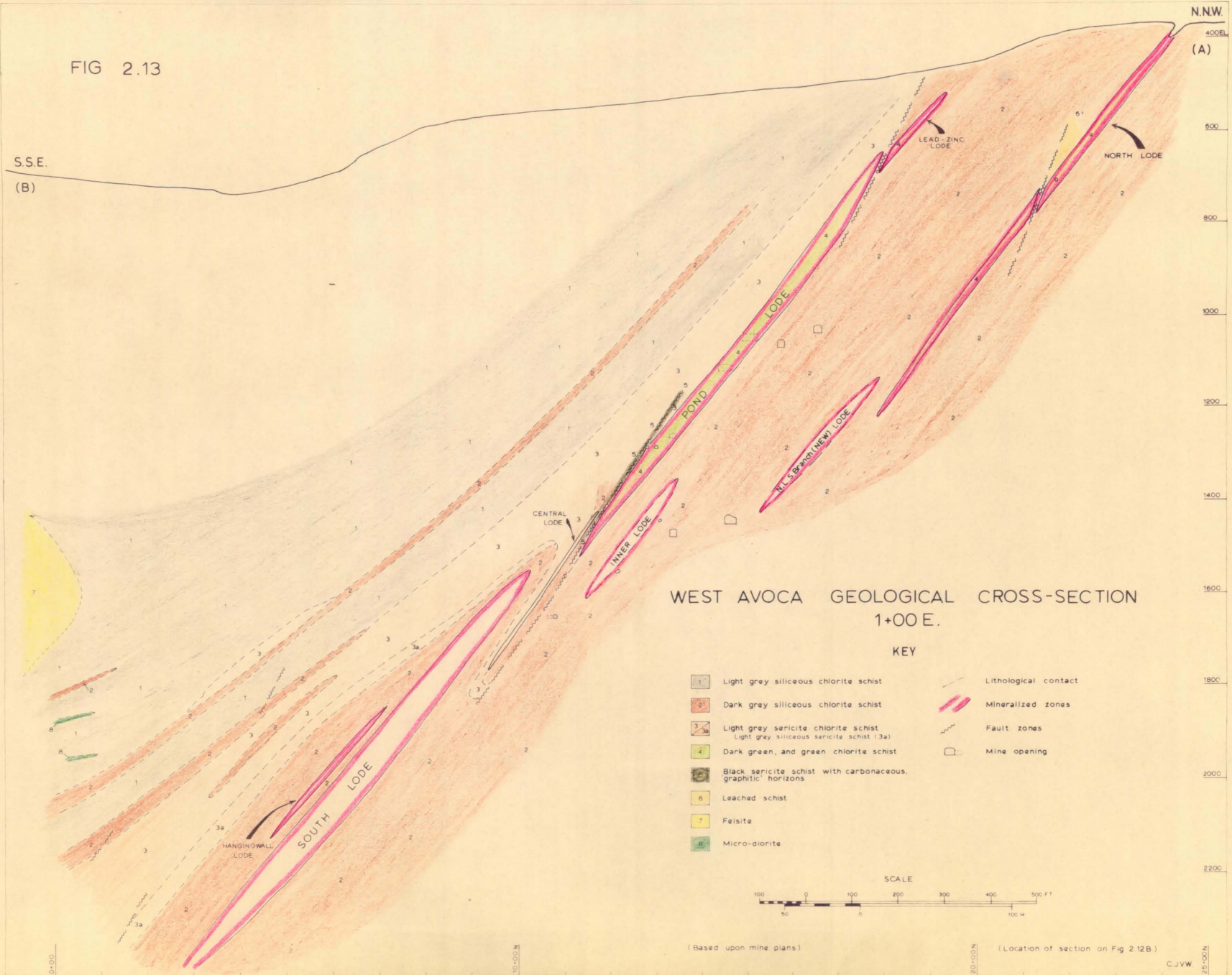
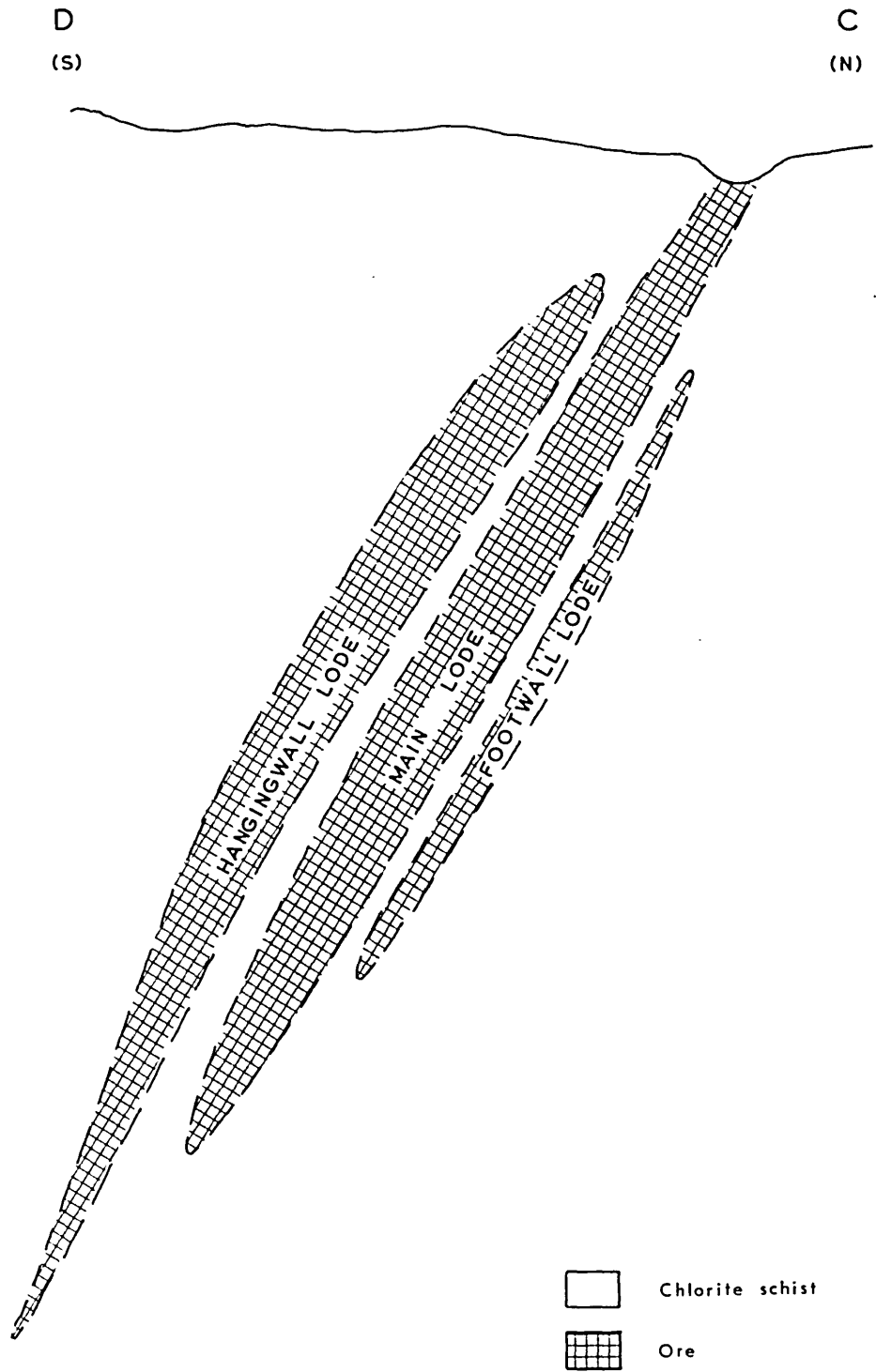


FIG 2.14

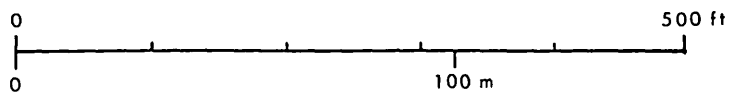
EAST AVOCA TIGRONEY

IDEALIZED CROSS - SECTION



SCALE

(Vertical and horizontal)



(For location see Fig. 2.12B)

(i) Light grey siliceous chlorite schist

This rock type is closely associated with the siliceous zones of mineralization and is common in the wallrocks surrounding the orebodies (Map 2 and Fig 2.13).

Pale tuffaceous layers, 1-1.5 cm thick are interspersed by dark olive green chloritic laminae, from 0.25 - 1 mm in width. Seams of quartz, (1-1.5 mm) crosscut the penetrative cleavage, delineated by the chlorite seams (Plate 6:C). In thin section, the rock consists essentially of quartz with minor chlorite, and disseminated pyrite (Plate 7:F). The quartz is fine grained, and has a saccharoidal fabric in which the grains have sutured margins, contain numerous fluid inclusions and are strongly strain polarized (Plate 7:B,C). The mean grain size of the quartz is 0.2 mm. The chlorite is pleochroic in olive greens, has a small $2V(-)$, shows anomalous violet interference colours, implying that it is a ferroan variety. Disseminated pyrite euhedra are 0.01-0.03 mm in size.

(ii) Dark grey siliceous chlorite schist

This is the major rock type exposed underground and it is the host rock for the siliceous zone mineralization. It differs from (i), in containing more chlorite and this darkens the colour of the rock (Plate 6:B). The chloritic foliae are 0.5-3.0 mm thick and the interstitial tuff layers have a width of 0.5-1.0 cm. Siliceous seams crosscut the foliation at small angles and brecciate the tuff lenticles (Plate 7:E).

The mineralogy and fabric in thin section is similar to (i), but coarser in grain size. The pyrite granules, 0.05-0.2 mm in size, concentrate in chloritic foliae. Slip planes are marked by chlorite and the presence of a crenulation exists on certain foliae (Plate 7:D).

An interesting variety of this schist occurs in the foot-wall of the Pond lode. Medium grey in colour, it consists of chloritic fragments in a siliceous matrix with a rude agglomeratic texture (Plate 6:A). This rock may be similar to the laharc breccia occurring in the area south of Arklow (38).

At Avoca, the fragments range up to 6 cm in length, are about 2 cm thick and may be of andesitic material.

In thin section, the fragments consist essentially of quartz with minor chlorite (Plate 8:D). The quartz shows a recrystallized fabric with sutured grain margins and prominent strain polarization, the texture is fine grained; individual quartz grains ranging from 0.01-0.2 mm in size. The chlorite is olive green and shows features similar to (i) and (ii) above.

(iii) Light grey sericite chlorite schist

This rock-type occurs in the hangingwall of the Pond lode and also in the hangingwall of the South lode (Map 2 and Fig 2.13). Medium to fine grained, the rock consists of closely spaced foliae (0.5-1.5 mm apart) parallel to the cleavage. The foliae are sericitic and contain flattened ovate plates of chlorite; 1 cm by 0.5 cm, and about 0.2 mm thick. Elongation of these plates gives rise to a lineation (Plate 9:B).

In thin section the fragmental nature of the rock is obvious (Plate 7:G,H). Essential constituents are sericite, calcite, chlorite, feldspar and leucoxene with accessory quartz and pyrite. The feldspar grains (~0.15 mm in size) are broken and twin planes are distorted, indicating a pre-cleavage origin. Alteration of the feldspar to sericite is common. Pale green chlorite making up the ovate plates, shows anomalous blue interference colours and does not contain disseminated pyrite grains; these are scattered in the sericitic matrix. Carbonate; calcite and dolomite infill pressure fringes around feldspar grains and occupy crosscutting veins. Leucoxene rims feldspar grains and is disseminated throughout the matrix. Quartz is rare.

(iv) Light grey siliceous sericite schist

Typically occurring on the immediate hangingwall of the siliceous zone mineralization (e.g. South lode), this rock contains highly siliceous tuff layers with sericite laminae, giving a greenish-yellow sheen to the foliation planes. The siliceous seams are 1-15 cm in width and the foliae vary from 0.5-1 mm in thickness. Fine grained pyrite is disseminated in sericite seams, (Plate 6:E) and a slip lineation is visible on cleavage planes.

In thin section, sericite occurs in a matrix of fine grained recrystallized quartz, exhibiting a saccharoidal texture. The sericite is strongly crenulated (Plate 9:D), and much of the quartz is secondary.

(v) Green chlorite schist

This rock type is intimately associated with the pyritic zones throughout the belt, and is prominent at West Avoca as one of the Pond lode host rocks. Consisting almost entirely of chlorite, the rock contains minor quartz and is interbanded with pyritic lenticles, sometimes with other sulphides. There is a pronounced fissility and lustrous cleavage surfaces are common (Plate 12A), and fine slip lineations are conspicuous. The thickness of the individual bands of chlorite and pyrite are generally 1-5 cm.

In thin section, chlorite is the essential constituent, dark olive green in colour, with anomalous blue and violet interference colours. Small euhedral granules of pyrite, from 0.02-0.04 mm in size are disseminated throughout the chloritic areas (Plate 8:E). Within the pyritic lenticles, the grain size of the pyrite increases to 0.1-0.8 mm and occasional porphyritic grains occur.

(vi) Green-black chlorite schist

This rock unit (Plate 6:H) is one of the host rocks for the pyritic zones, and differs macroscopically from the above solely in colour.

In thin section there is an almost total absence of quartz and the grain size of disseminated pyrite increases to 0.05-0.15 mm (Plate 8:F). These factors account for the colour difference.

(vii) Blue-black to blue-grey chlorite schist

This is the third host lithology for the pyritic zones (Map 2). The rock is similar to (v) and (vi), consisting of interbanded chlorite and sulphide lenticles.

In thin section, the chlorite is light olive green with anomalous brown interference colours and a small 2 V(+),

suggesting that it is magnesian (67); a supposition confirmed by the whole rock analysis (sample A.10, table 2). Pyrite granules are again disseminated in the chlorite (0.01-0.5 mm, grain size) and the pyritic lenticles are generally 2-4 cm thick.

(viii) Black sericite schist

This rock unit occurs in the mining hangingwall of the pyritic zones and is a soft, very fissile schistose rock which causes problems in extraction of the adjacent ore as it caves readily. Discontinuous seams of sericite (1-2 mm in width) are interspersed with siliceous laminae 1-3 mm thick, with disseminated pyrite (Plate 6:D).

In thin section, the rock consists essentially of sericite, calcite, and apatite with wisps of chlorite, minor quartz and pyrite. The sericite occurs as small laths, and the apatite is predominantly amorphous (collophane or dahllite) with micro-crystalline grains of true apatite. Calcite extensively replaces the collophane and the pyrite is of variable grain size. This is the first annotated occurrence of a phosphorite rock in the Avoca district.

(ix) Graphite schist

Developed in zones of faulting (e.g. the hangingwall of the Pond lode, West Avoca (Map 4)). The rock is a black fissile slate (Plate 6:F) with metamorphosed carbonaceous partings. Lamination is very fine (Plate 8:H), 5-20 μ in thickness, and the lighter partings, are siliceous and contain disseminated euhedral and spheroidal pyrite.

(x) Leached schist

Leaching of the chlorite schists, described above, by surface and ground waters produces a white friable rock. This occurs on the surface at Cronebane, and underground in the hanging-wall of the North lode at West Avoca (Map 3). The rock consists essentially of silica, with illite and minor montmorillonite. A siliceous boxwork is the sole remnant after extreme leaching.

(xi) Rhyolite

A pale grey aphanitic rock, which rarely possesses a

rude foliation indicated by elongate ragged chloritic laminae, is exposed in No. 7 crosscut south, 1670 level, at its southerly limit, and also in drill core. Considerable secondary silicification by ramifying siliceous veinlets occurs, sometimes with dolomite, and fine grained specks of disseminated pyrite are common (Plate 6:G).

In thin section the texture is porphyritic (Plate 8:C), and spherulites occur (Plate 8:B) in the groundmass. The augen consist of recrystallized quartz and the matrix is composed of altered feldspar laths with sericitic cores.

The rock is texturally and lithologically similar to the felsites, described earlier. Contacts with the enclosing schists are sharp, but there is no clear evidence of intrusion. Lampard(138), and others, remarked on the difficulty of distinguishing between the sheared margin of a felsitic body and silicified pyroclastic, but a mappable contact can usually be found.

b) Wallrock alteration

Many writers have pointed out that alteration of the wallrocks is intense. Murphy described the rocks as products of profound alteration; lit-par-lit quartz veining and permeation, silica metasomatism and chloritization (158). To quantify the alteration effects, partial whole-rock analyses of representative rock units was carried out by X-ray fluorescence, using the method described in appendix 1.

The whole core was assayed during the exploration and development programme at Avoca and thus it proved impossible to obtain sufficient samples to represent a complete transverse section through the orebodies. The lithological rock sequence is based upon macroscopic mineralogical variations, which relate to differences in the bulk chemistry of the rocks. As a measure of continuity exists in the rock units across the ore zones, an idealized cross-strike section at West Avoca, was constructed with samples of representative rock units, which were analysed for major and minor elements (Fig 2.15).

The amount of contained sulphide in each sample was minimized, as the purpose of the investigation was to discover the nature of the host rocks. (The chemistry of the sulphides is considered in a later section.)

The results of the analyses are shown in table 2 with average mineral contents of the rock types. Variations in some of the major oxides and trace elements are illustrated graphically in Fig 2.15.

(i) Major oxides

Silica. SiO_2 contents are generally high, evidence of silicification. Within pyritic zone (Pond lode) host rocks, the amount of silica decreases markedly, to the extent that sample A12 contains virtually none as free quartz.

Alumina. The amount of Al_2O_3 largely depends upon the amount of sericite in the rock, and is low in the silicified units.

Titania. TiO_2 contents are low but increase in samples G3, A7 and A5, which contain appreciable quantities of leucoxene and, demonstrably, are altered pyroclastics.

Total iron. Variation in the amount of total iron, expressed as Fe_2O_3 , is large, and correlates with the proportion of chlorite in the rock. The host rock units characterizing the pyritic zones (and typical of the Chlorite Zone) contain sufficient iron to be classed as iron formation (121). This is a critical point in the genesis of the Avoca ores.

Manganese oxide. Contents of MnO are low but increase slightly in the iron-rich units.

Magnesia. MgO contents show a different behaviour to the other major oxides. This is probably because magnesia distribution is governed by the interplay of two factors: concentration in dolomite, and/or magnesian chlorite. The latter explains the high values recorded in samples A10 and G3.

Lime. The value of CaO is related to the calcite content of the rock unit, exemplified by sample A2.

TABLE 2

PARTIAL ANALYSES OF REPRESENTATIVE LITHOLOGICAL ROCK UNITS, WEST AVOCA

Major Oxides: %	A6	G3	A8	A5	A7	G5	A9	A2	A11	A10	A12	A4	A3	A1	G4
SiO ₂	75.65	46.0	56.80	68.10	42.00	45.00	74.00	38.40	35.75	40.00	28.20	77.70	77.00	77.60	53.90
Al ₂ O ₃	7.56	11.72	24.70	6.47	29.50	25.70	8.95	25.60	10.26	10.04	11.35	5.48	7.26	5.75	13.32
TiO ₂	0.22	2.38	0.55	0.19	4.21	3.54	0.41	0.32	0.32	0.25	0.36	0.13	0.26	0.14	1.32
Fe ₂ O ₃	0.70	1.33				1.57									1.67
FeO	0.14	7.23	3.90	13.60	5.10	5.56	3.90	3.50	37.50	22.85	39.21	9.25	7.95	8.70	4.04
MnO	0.01	0.01	*	0.02	*	0.01	*	*	0.04	0.03	0.04	0.01	0.01	0.01	0.03
MgO	1.80	11.18	2.63	4.53	0.94	2.45	4.64	5.42	6.10	18.90	7.60	1.93	1.77	2.26	5.22
CaO	2.78	2.87	0.33	0.32	1.14	0.33	0.51	8.72	0.33	0.67	0.32	0.32	0.34	0.32	2.80
Na ₂ O	0.01	2.58	0.85	*	1.11	*	0.15	1.00	*	*	0.13	0.01	*	*	4.01
K ₂ O	6.82	1.17	6.33	0.30	9.50	8.22	1.95	6.75	0.09	0.10	0.08	0.45	1.05	0.53	3.26
P ₂ O ₅	0.01	0.26	0.02	0.01	0.70	0.05	0.06	6.28	0.02	0.02	0.01	*	0.01	*	0.75
Total S	1.61	0.15	0.87	1.32	1.63	0.23	1.20	1.43	1.10	3.14	2.37	1.29	0.47	0.25	0.14
TOTAL	97.31	86.88	96.98	94.86	95.83	92.66	95.77	97.42	91.51	96.00	89.67	96.57	96.12	95.56	90.46
S as FeS ₂	3.01	0.28	1.63	2.47	3.05	0.43	2.25	2.68	2.06	5.88	4.44	2.42	0.88	0.47	0.26
Trace Elements : ppm															
Co	24	72	17	50	64	60	190	30	-	-	-	36	24	31	*
Ni	10	70	13	*	70	72	210	58	*	*	*	*	*	7	89
Cu	92	84	100	502	95	986	150	83	50	534	40	81	448	84	88
Zn	230	113	138	128	118	1010	282	204	192	272	215	159	117	156	132
Rb	204	47	268	16	341	305	117	310	*	9	*	25	52	*	69
Sr	*	59	41	*	35	18	*	136	*	*	*	*	*	*	700
Pb	152	52	85	122	4500	211	375	254	78	143	93	49	37	8	18

* = Not detected

- = Not sought

Mineral Composition

Quartz	++++	++	++++	++++	++	+	++++	+	++	++	+	++++	++++	++++	+++
Chlorite	+	++++	+	+++	+	++	+	+	++++	++++	++++	++	++	+++	++
Sericite	+	+	+++	++++	++++	+++	+	++++	+	+	+	+	+	+	++
Pyrite	+		+	+	+	+	+	+	+	++	++	+	+	+	
Calcite	+	++				+		+++							
Dolomite	++	+				++	+								
Graphite							+								
Rutile(Leucos.)					++	++									
Feldspar	++	++				++									+++
Collophane (dahlite)								++							
					++++	30% Modal content									
					+++	10-30%	"	"							
					++	5-10%	"	"							
					+	1-5%	"	"							

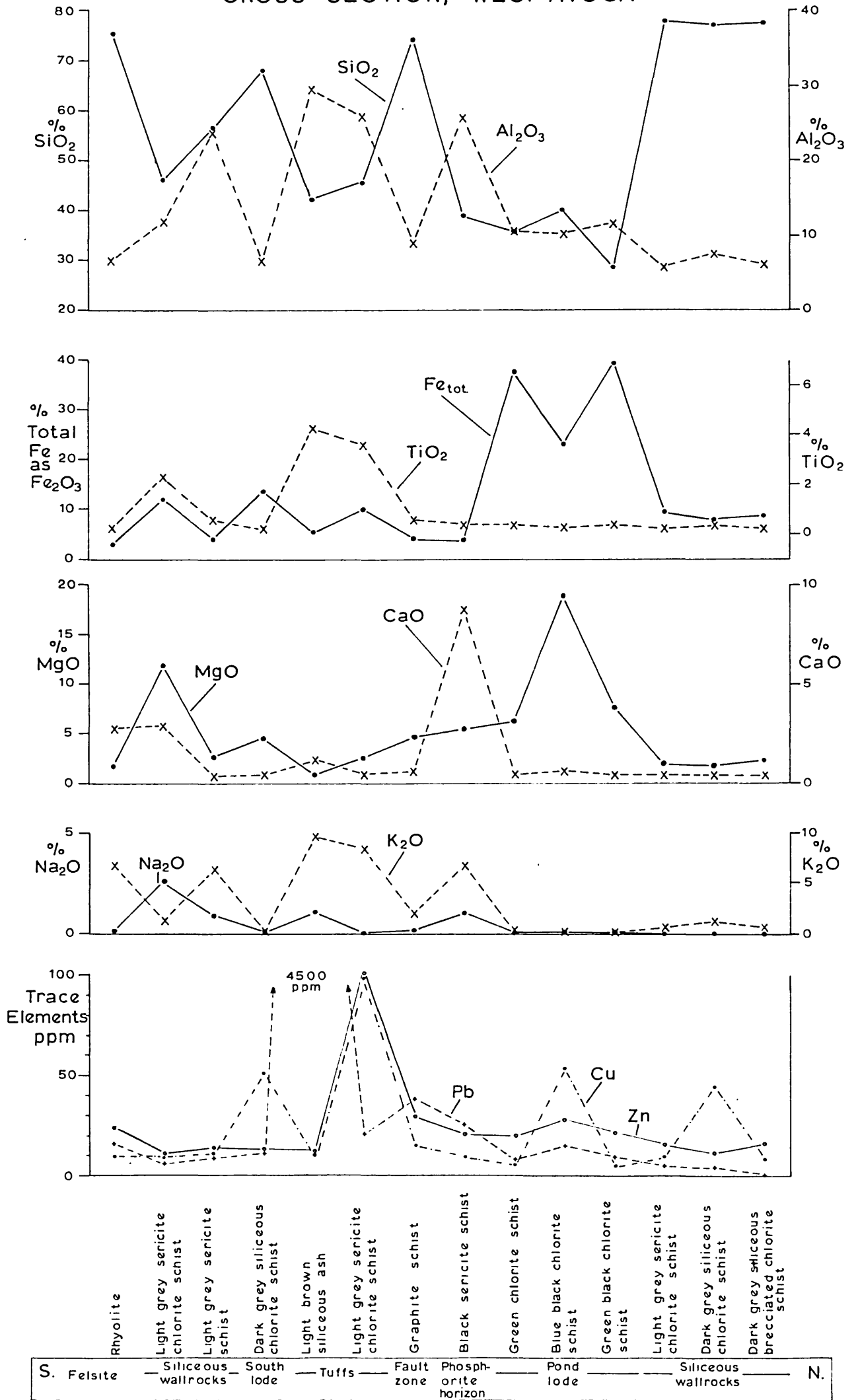
Description of samples :

A6	DDH 1644-15'. Rhyolite	A11	DDH 1353-114'. Green chlorite schist
G3	DDH 1644-236'. Light grey sericite chlorite schist	A10	DDH 1343-67'. Blue-black chlorite schist
A8	DDH 1632-210'. Light grey siliceous sericite schist	A12	DDH 1331-49'. Green-black chlorite schist
A5	DDH 1644-304'. Dark grey siliceous chlorite schist	A4	DDH 1332-16'. Light grey siliceous chlorite schist
A7	DDH 1650-900'. Light brown siliceous ash	A3	DDH 1332-8'. Dark grey siliceous chlorite schist
G5	P.Lode, 720L, W.Ext., HW. Light grey siliceous chlorite schist	A1	DDH 1340-10'. Dark grey siliceous brecciated chlorite schist
A9	DDH 1332-147'. Graphite schist		
A2	DDH 1331-136'. Black sericite schist	G4	1670L, 11 X-c S, 235' from portal. Dyke rock

Analyst : C.J.V.Wheatley

FIG 2.15

MAJOR AND TRACE ELEMENT VARIATIONS IN AN IDEALIZED CROSS-SECTION, WEST AVOCA



Soda. Na_2O contents are low or below detection, but the increase in sample G3 is due to the sodic feldspar in this pyroclastic.

Potash. K_2O contents vary widely and depend upon the sericite and/or feldspar content of the rock. In samples A6 and G5 the potash is dominantly provided by potassic feldspar and in A7, 8, and 2 it is supplied by sericite.

Phosphorous. P_2O_5 is low except for sample A2, which contains appreciable collophane (or dahllite) and apatite.

Sulphur. Contents of S reflect the amount of sulphide in the rock unit.

(ii) Trace Elements

Cobalt and nickel. The erratic values are probably contributed partially by contaminant sulphide. (It is interesting that the cobalt and nickel content of graphite schist (A9) is high for both elements, whereas the contained pyrite shows preferential incorporation of nickel (p. 175) with a content of 184 ppm, which is closely comparable).

Copper. Values are generally low, showing an enrichment in the host rock for the siliceous zone mineralization (A5), part of the pyritic zone (A10) and also the tuffaceous horizon stratigraphically below the Pond lode (G5;-in the mining hanging-wall). An increased content in the brecciated dark grey siliceous chlorite schist on the footwall of the Pond lode suggests that this rock unit may have been altered by deuteric or hydrothermal cupriferous solutions.

Zinc. The background level approximates to the mean abundance figure for the pyroclastics (p. 33). Values tend to parallel those of copper without enrichment in the siliceous zone. A distinctive high value occurs in the tuff horizon (G5).

Lead. A minor enrichment occurs in the pyritic zone host rocks, with a higher value in the graphite schist (A9). The footwall of the siliceous zone shows a marked increase in value, a feature supported by mineral distribution analysis of the South Orebody (Map 6).

Rubidium. The rhyolite (A6) contains 204 ppm, which is comparable to the mean for felsites from the Avoca district (243 ppm). Otherwise, values of Rb correlate with the potassium content of the rocks, represented by sericite.

Strontium. Contents of Sr are often below the detection limit, but a high value is recorded in A2, possibly because of increased calcite content, or due to incorporation in collophane by diadochic replacement of calcium (181).

c) Discussion.

The characteristics of the wallrock alteration can be considered under four major headings:

- (i) Introduction of silica and consequent silicification.
- (ii) Development of chlorite.
- (iii) Potassic metasomatism with the development of sericite.
- (iv) Development of carbonate.

(i) Silicification

Undoubted tuffaceous and marine shale members in the stratigraphic sequence suggest that the rock units represent a sequence of tuffaceous sediments. Within this sequence, three episodes of silicification can be recognized. Although these are locally distinct, similar effects took place at different periods of time, depending upon the stratigraphic level in the sedimentary pile.

a) Devitrification of the pyroclastics probably took place within a system in which the connate waters were highly siliceous. Macroscopic and microscopic observation confirms that extensive post-formational silicification took place within and outside the mineralized zones. This silicification probably took place through the medium of circulating silica saturated connate water. (This produced the 'lit-par-lit' effect mentioned by Murphy (158)).

b) In the siliceous mineralized zones, seams rich in quartz are demonstrably crosscutting and often accompanied by sulphides. The quartz contains abundant fluid inclusions

indicating possible crystallization from a hydrothermal fluid. Hydrothermal solutions, rich in silica and alkalis, with dissolved base metals were probably active and would have given rise to silicification of the type associated with the siliceous zones.

c) The pore waters may have become siliceous during the deformation which produced the regional cleavage, as they were trapped in a eugosynclinal sequence rich in silica. These pore waters migrated into fractures and pressure slacks deposited silica, and produced the third phase of silicification.

(ii) Chlorite

Chlorite is a prime indicator mineral in the rock units, and thus its composition is of interest. Separation of pure chlorite from the whole-rock proved unrewarding, with the exception of samples A.11 and 12, and therefore partial probe analysis of representative, pure grains was carried out on the Geoscan (cf. p. 105 for details). The results are shown in table 3, X-ray powder data are presented in table 4, and a reasonable comparison with thuringite (ASTMS Card No. 7-78) is illustrated.

A number of classifications of the chlorite minerals have been suggested. Application of swelling heating and dissolution tests, combined with X-ray diffraction, established the absence of kaolin-type minerals at Avoca. A classification of the chlorites based upon their optical characteristics was used by Albee (2), and the relationship of the present data to his scheme is shown in Fig 2.16A.

Hey (114) makes a primary subdivision into oxidized varieties on the basis of the Fe_2O_3 content. In order to name the chlorite associated with mineralization at Avoca, pure mineral separates were obtained, using heavy liquid and magnetic methods, from samples A.11 and 12 (2, 3 and 4 on table 3). (The FeO content was determined using the hot titrimetric method.) The results are shown in table 3, indicating that the chlorites are clearly oxidized ($>4\% \text{Fe}_2\text{O}_3$). The data (Fig 2:6B) are scattered, but the analyses generally correspond to a chamosite chlorite.

The presence of chamosite chlorite is the essential

Table 3. Partial probe analyses of chlorites from West Avoca.

	1	2	3	4	5	6
SiO ₂	22.26	22.90	24.02	24.21	22.36	22.37
Al ₂ O ₃	15.98	18.91	16.30	16.95	19.36	20.20
Fe ₂ O ₃	-	5.86	5.91	5.91	-	-
FeO	27.27*	30.16	28.53	28.53	29.11*	32.52*
MgO	12.83	8.75	10.41	10.61	7.45	9.37
Total %	78.34	86.58	85.17	86.21	78.28	84.46

(* Total Fe as FeO.)

Numbers of cations, on the basis of 20(O).

Si	6.41	5.57	6.07	6.01	6.02	5.68	} 8
Al	1.59	2.43	1.93	1.99	1.99	2.32	
Al	6.56	5.73	5.35	5.43	7.23	6.72	} 12
Fe ³⁺	-	1.62	1.68	1.65	-	-	
Fe ²⁺	2.68	3.06	3.01	2.96	3.27	3.44	
Mg	2.75	1.59	1.96	1.96	1.50	1.78	
<u>Fe(Total)</u>	0.49	0.747	0.71	0.70	0.69	0.66	
Fe + Mg							

(Analyst: P Suddaby)

Description of samples:

- (A5) DDH 1644-304' Dark grey siliceous chlorite schist.
- (A11) DDH 1353-114' Green chlorite schist
- (A12) DDH 1331-49' Green-black chlorite schist.
- (A12) " " " " "
- (A4) DDH 1332-16' Light grey siliceous chlorite schist.
- (A1) DDH 1340-10' Dark grey siliceous chlorite schist.

Table 4. X-ray powder diffraction data for chlorite

<u>AVOCA</u>		<u>ASTMS-7-78</u>	
Chamosite	CoKa	Thuringite	CoKa [‡]
4	14.02	9	14.1
10	7.07	10	7.07
-	-	3	4.726
4B	4.70	2B	4.57
7	3.53	6	3.541
1	2.82	3	2.845
-	-	1	2.642
4	2.55	3	2.576
-	-	3	2.529
5	2.45	3	2.434
5	2.39	2	2.371
1	2.27	1	2.254
1B	2.16	0.5	2.062
4	2.01	2	1.998
2	1.885	1	1.878
1B	1.822	0.5	1.818
-	-	0.5B	1.745
1B	1.659	0.5	1.660
1B	1.566	1	1.563
4	1.550	3	1.532
1B	1.516	1	1.497
-	-	0.5	1.458
2B	1.392	1	1.392

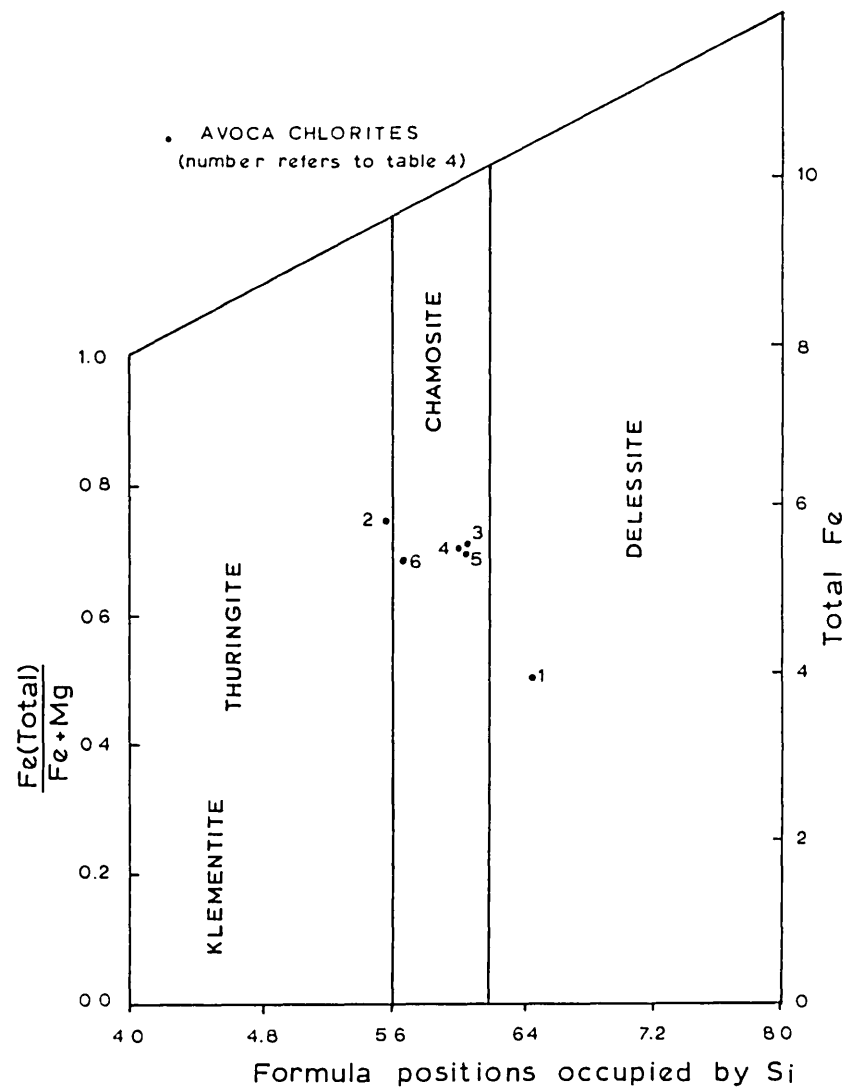
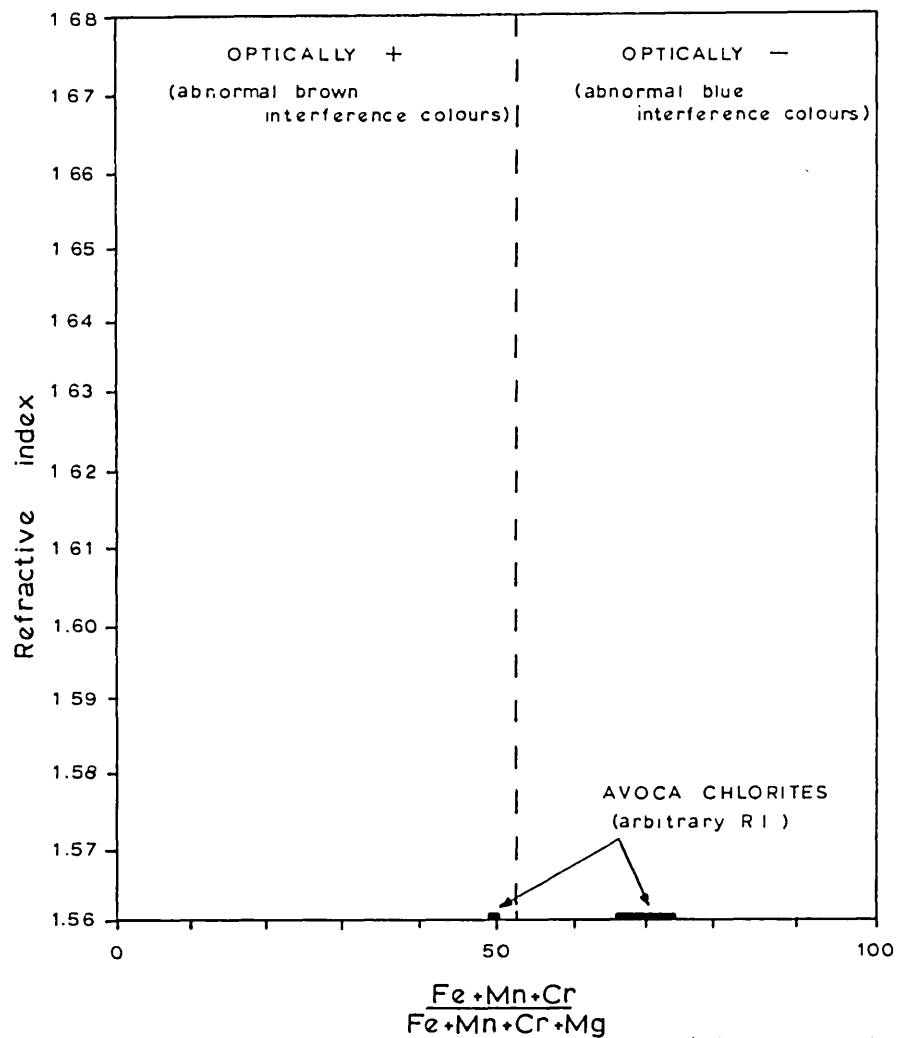
[‡]Thuringite; Nessina, Limpopo, Transvaal.

FIG 2.16

NATURE OF CHLORITE AT AVOCA

A Optical properties and the $\frac{Fe}{Fe + Mg}$ ratio

B Chlorites containing more than 4% Fe_2O_3



(After Hey 1954)

characteristic of the Chlorite Zone, in which the pyritic and magnetite-hematite zones occur. The chlorite is a well crystallized metamorphic form, which could have derived from an authigenic chamosite originating within sediments rich in iron, alumina and silica. There is no evidence of metasomatism during formation of the chlorite.

It is clear that the chlorite of the Chlorite Zone is an environmental indicator, and not an index of metamorphic grade. The Chlorite Zone denotes an intercalated 'iron formation' in the lower part of the Upper Volcanic Series.

(iii) Sericite

Sericite is associated with zones of siliceous mineralization, and has formed either by potassium metasomatism of chlorite or through breakdown of feldspars. It is invariably associated with quartz which contains numerous fluid inclusions and thus hydrothermal solutions rich in silica and K^+ , associated with the siliceous mineralized zones, may have caused the potassic metasomatism. The plates of sericite are orientated parallel to the cleavage (S_1) and are crenulated.

(iv) Development of carbonate

Calcite and dolomite are the predominant carbonates. Extensive dolomitization is associated with the tuff on the hangingwall of the Pond lode, and calcite frequently occurs in altered pyroclastics. Dolomite forms irregular veins and stringers and is evenly disseminated in the groundmass of the tuff. Crosscutting seams of pinkish or white dolomite ($\frac{1}{2}$ calcite) occur in the hangingwall of the lead-zinc rich portion of the Pond lode. The dolomitized rock is associated with the phosphatic and carbonaceous horizons, suggesting that the dolomitization may be authigenic.

A distinctive dolomite-rich phyllite with a spherulitic texture also occurs at the mine associated with the Pond lode (M.V. OBrien, pers.comm.) and has been found elsewhere e.g. at Rockstown (Map 1, sheet 2)

Calcite occurs as an alteration product in the pyroclastic

horizons, developing from the breakdown of feldspars.

Carbonatization of the schists and phyllites is of post-depositional origin. Remobilization and recrystallization of dolomite and calcite probably took place during deformation under high pore-water conditions producing crosscutting veins.

The presence of ankerite, identified by Lampard (138), was not corroborated.

d) Summary

Lithological features and analyses of the wall-rocks indicate that a suite of tuffaceous sediments with an intercalated 'iron formation' exist and chlorite and secondary silica formed during diagenesis. Later hydrothermal activity by metal laden, potassic, siliceous fluids caused sericitization and extensive silicification.

During the subsequent deformation, chlorite, sericite and quartz were partially reorientated and recrystallization took place in pressure slacks.

2.3.3.2. Intrusive Rocks

a) Lithology and petrography

(i) Micro-diorite dykes

Undoubted intrusive rocks are rare in the mine area, but thin (<10 ft in width) dykes have been cut by drill holes and are exposed in the hangingwall of the Pond and North lodes (Map 2). The rock is fine grained, greenish-grey in colour, containing scattered glassy phenocrysts of quartz (up to 1 mm in diameter) which are set in an aphanitic matrix containing specks of pyrite. Contacts, sometimes fault-bounded, are sharp and a minor alteration zone, <1 cm in width, occurs. The amount of pyrite decreases away from the contact, suggesting that diffusion of sulphur took place from the country rocks.

In thin section, the rocks consist essentially of quartz, feldspar and pyroxene. The quartz phenocrysts have overgrowths of microcrystalline silica and feldspar laths in the matrix show a rude trachytic texture (Plate 8:A) in a groundmass of sericite

and chlorite needles. Alteration is of variable intensity, but in no case could the original pyroxene be identified.

Lampard (138), in describing examples of this rock used the term 'sodic microsyenite', however the whole rock analysis (table 2) reveals a dioritic composition. A similar rock, collected and described by Lampard, shows extreme alteration and cuts pyritic material in the Grass Levels area at East Avoca. This rock undoubtedly belongs to the same suite as the dykes at West Avoca. (The dykes appear generally to be stratigraphically below mineralized zones, and occur at their margins.)

(ii) Quartz-porphyry

A quartz-porphyry intrusive described by OBrien (167), cuts mineralization at Connary and the ore is not appreciably altered at the contact. This agrees with the features of intrusive rocks noted above. Mackay (145) described tenorite disseminated in the porphyry. The copper content of the intrusive may be due partly to assimilation, but siliceous seams with chalcopyrite are associated with the margin of the Ballinaclash granite, suggesting that the porphyry magma may have been enriched in copper, which concentrated in the marginal zones of intrusive stocks. Sampling of the porphyry at Connary proved impossible.

b) Petrogenesis

Whole-rock, partial analysis of the microdiorite is in table 2. The composition grossly compares with the average diorite (162) and plots sensibly on the F-M-A and K-C-N diagrams (Fig. 2.6B and C). Trace element contents of copper, zinc and lead are close to the mean abundance figures. The rubidium and potassium content are not high, however, strontium shows a marked increase. This increase implies that the rock is alkalic, but the analysis indicates that this is not so and thus the value is anomalous.

The data supports the contention that the genesis of the dyke rocks is related to the magma which gave rise to quartz-porphyry and granitic intrusive activity during the climax of the Caledonian orogene.

2.3.4. Structure

Interpretation of the structure is critical to discover the control for the location of the ore zones and to predict extensions.

The mineralization has been deformed and pre-dates development of the prominent regional cleavage, S_1 . A study has been made of the deformation elements exposed in the mine workings. Salient mesoscopic structural data are recorded on Maps 3, 4 and 5.

2.3.4.1. Mesoscopic Structure

(a) Planar

(i) Bedding planes, S_0

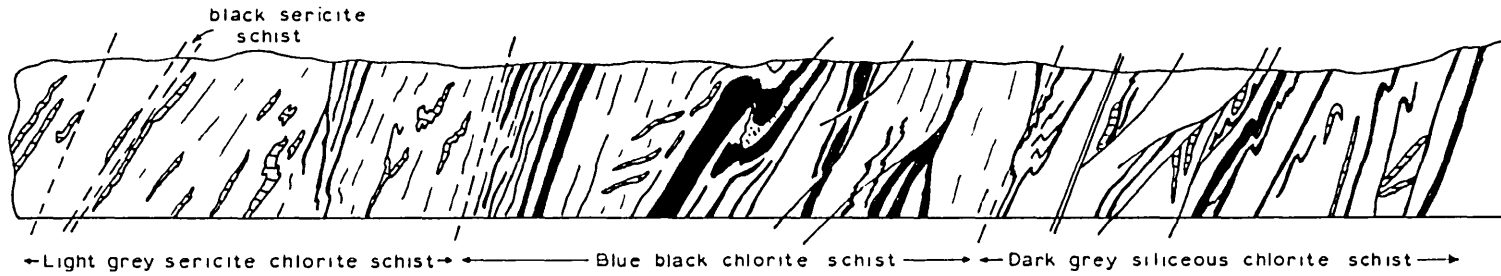
The primary silicate fabric has been almost wholly reconstituted and no original stratification exists. However, as will be demonstrated in section 2.6, primary growth fabrics do occur in the pyritic zones. The individual lenticles of pyrite, incompetent during deformation, may therefore represent the original planar fabric, S_0 . Quantitative measurement of the attitude of discrete lenticles of pyrite was not possible, because they tend to be discontinuous along the strike and up-dip. Qualitatively the attitude of the pyritic horizons can be gauged from detailed mapping of workings within the pyritic zones. During the exploration and development phase, underground workings are concentrated in the wallrocks and thus few clean exposures of pyritic ore are found. Relevant data is shown on Map 4, and mapping of crosscuts in the Pond lode on Figs. 2.17 and 2.18. Interpretation of these 'bedding structures' is considered in the discussion.

(ii) Regional cleavage, S_1



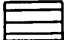







All the rocks in the mine area are affected by a slaty cleavage which is penetrative. Measurements of the cleavage produce a consistent pattern, represented stereographically in Fig. 2.19. The average strike is 061° , and dips vary from $52-69^\circ$ SE. The spread of the values is due to overprinting by later planar fabrics.

FIG 2.17

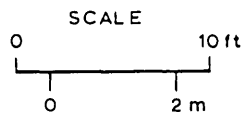
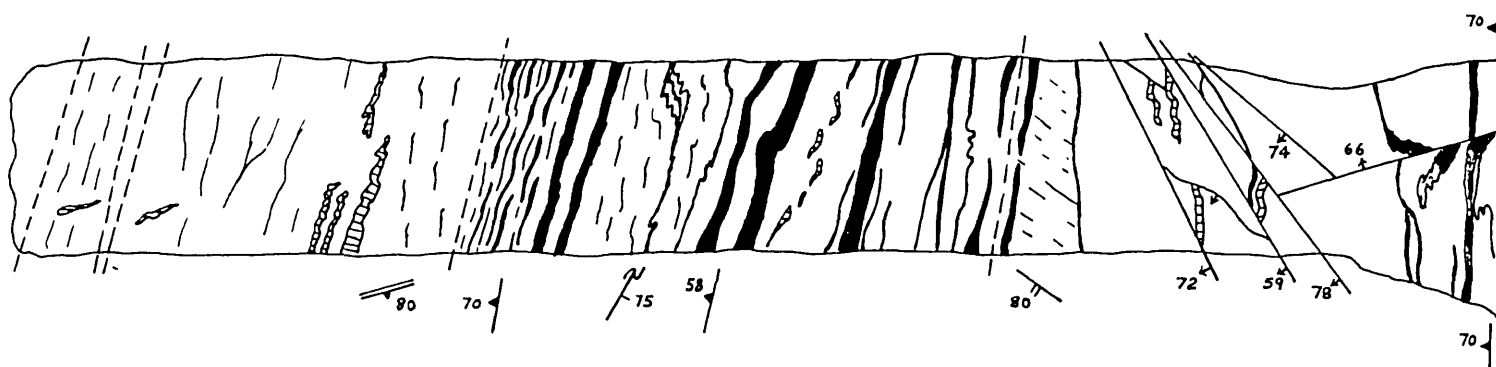
WEST WALL



KEY :

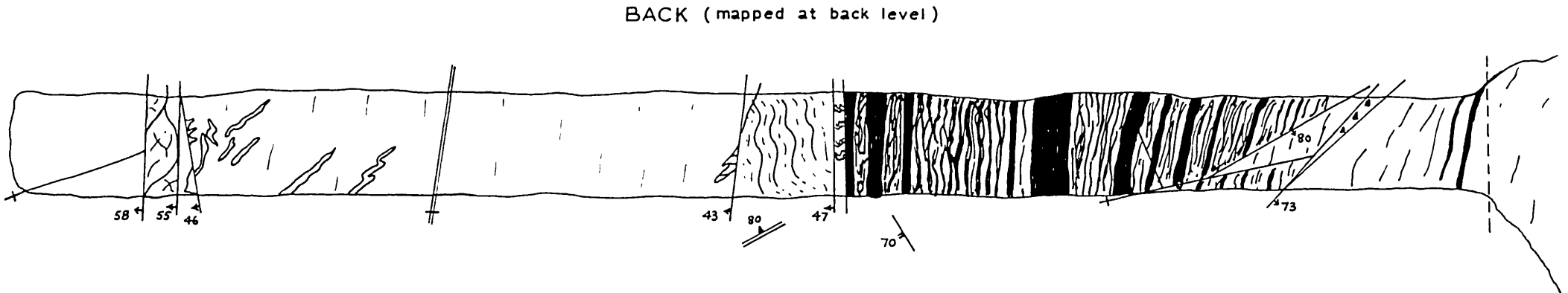
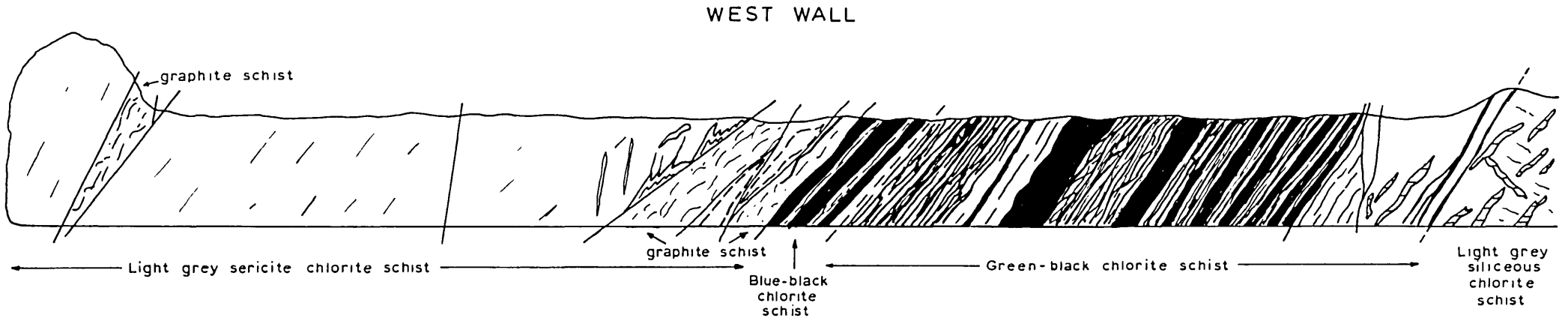
-  Pyrite ± chalcopyrite and quartz.
-  Quartz vein with chalcopyrite
-  Barren quartz
-  Dolomite
-  Lithological boundary
-  Cleavage with dip
-  Fracture cleavage
-  Axial plane of minor fold
-  Kink plane
-  Fault with dip

BACK (mapped at back level)



GEOLOGICAL MAP OF P.4 CROSSCUT SOUTH
1670 LEVEL WEST AVOCA

FIG 2.18



GEOLOGICAL MAP OF 1047 LEVEL CROSSCUT SOUTH
WEST AVOCA

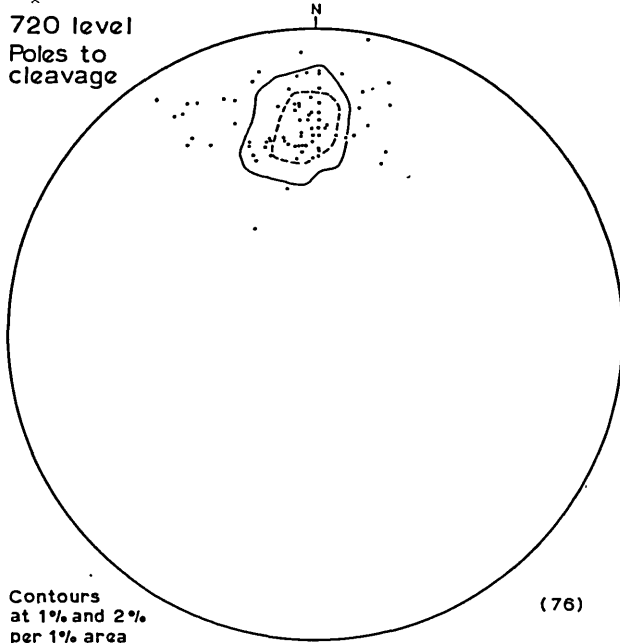
(Key as for FIG 2.17)

FIG 2.19

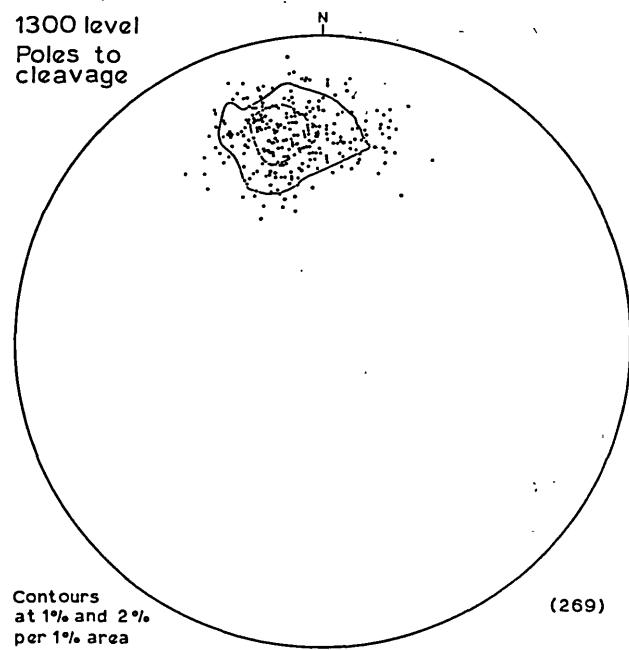
CLEAVAGE, WEST AVOCA - UNDERGROUND

Lower hemisphere equal area stereographic projections:

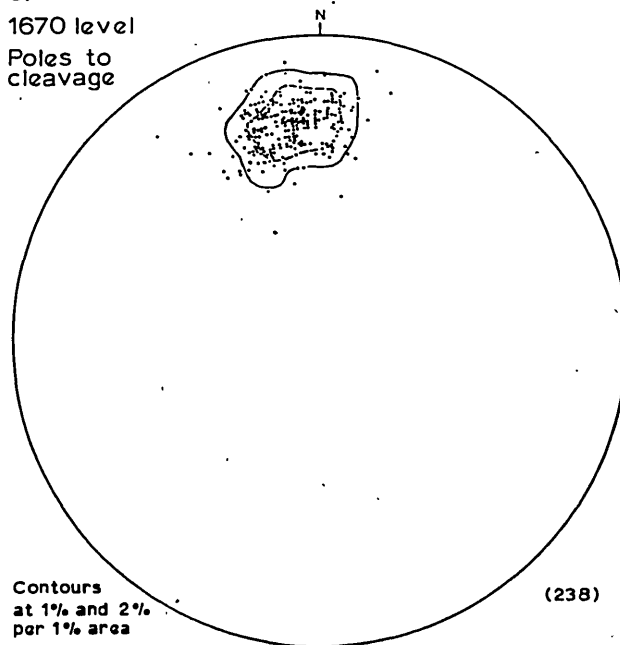
A.
720 level
Poles to
cleavage



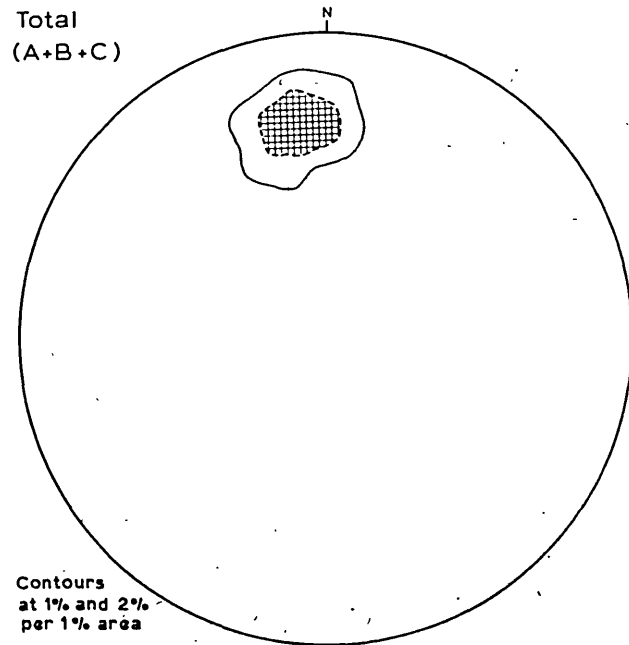
B.
1300 level
Poles to
cleavage



C.
1670 level
Poles to
cleavage



D.
Total
(A+B+C)



(iii) Fracture cleavage, S_2

Fracture cleavage typically develops in highly fissile chloritic units and appears to be non-penetrative in the silicified rocks. (Plate 11:H). Poles to S_2 planes are shown graphically in Fig. 2.20A and a correlation with crenulation cleavage pole distribution is evident (Fig. 2.20B). The sparse data indicates a mean strike of 130° , with dips varying from 70° NE to 70° SW. This corroborates the surface measurements, given in a previous section.

(iv) Crenulation cleavage, S_2

In the siliceous rock units, crenulation of S_1 produces a non-penetrative cleavage. The intersection of this crenulation with S_1 gives rise to a distinct lineation, with a steep pitch. Stereographically, the data illustrate a mean trend of 133° and dips averaging 75° NE. (Fig. 2.20B).

(v) Axial plane of minor folds, F_1

Minor folds, predominantly drag-folds, are found in the pyritic zones, and are well displayed in the 1300 level Drive West (Map 4). Attitudes of the axial planes are plotted on Fig. 2.20C, with the axial surface lineations. The distribution indicates that the average fold axis is vertical, with a trend of 078° and a plunge of 22° E. The form of the minor folds is illustrated in Plates 10, A to E, and 11:F. Wavelengths and amplitudes are variable, from 5 ft to 10 ft and 2 ft to 5 ft respectively. If the pyrite seams are parallel to S_0 , these minor folds are related to the F_1 fold episode.

(vi) Kink planes

Kinking of chloritic foliae commonly develops in the fissile units. (Plate 9:A,C). Conjugate sets of planes occur and poles to the planes are shown in Fig. 2.20D. The points are distributed about two distinct girdles.

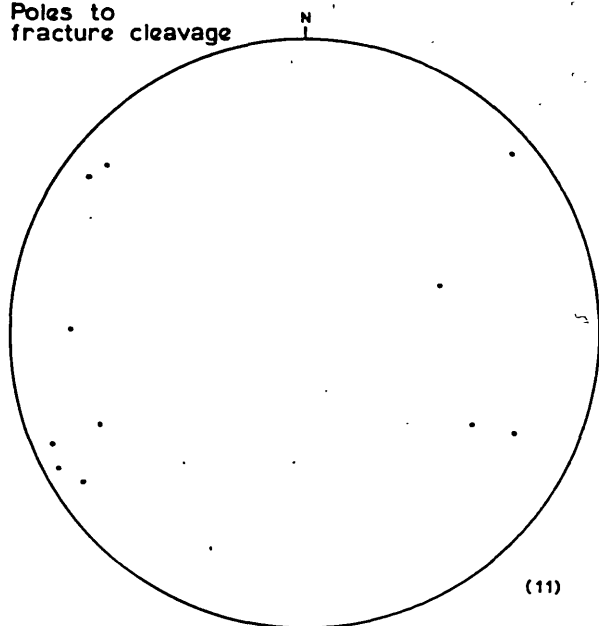
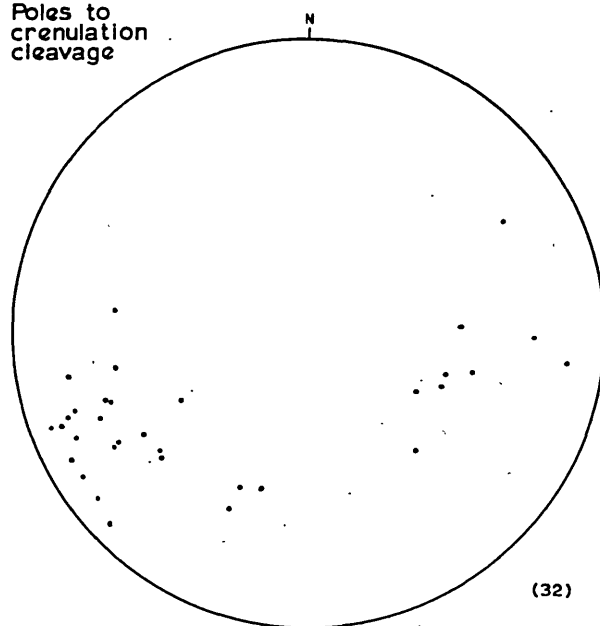
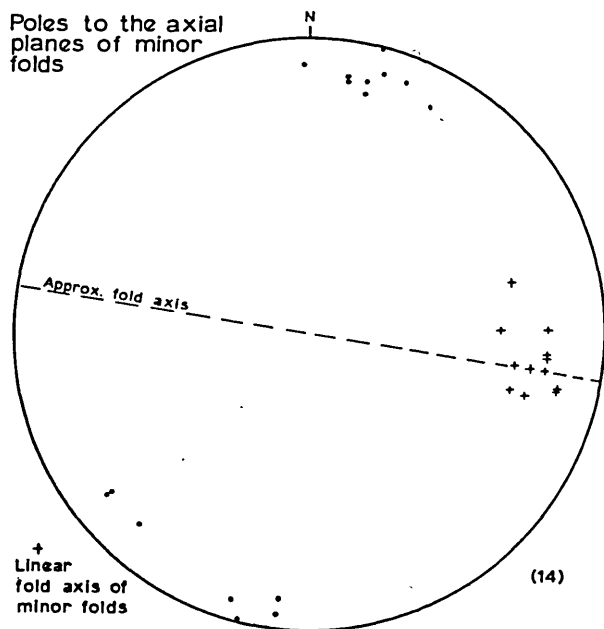
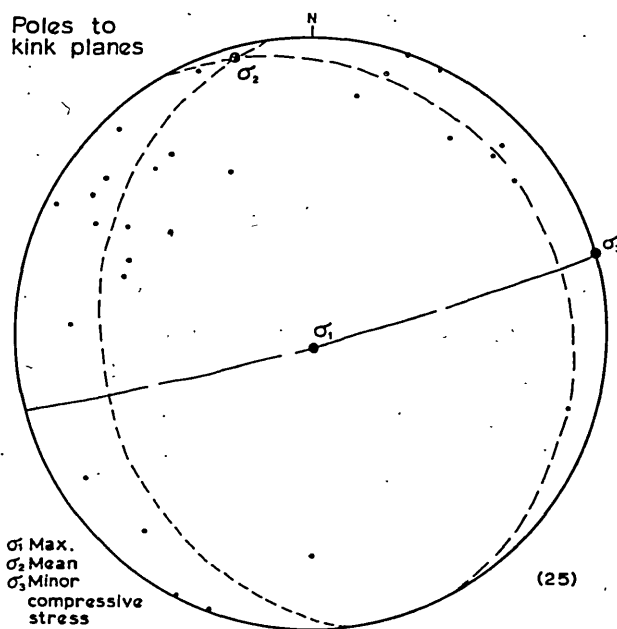
(vii) Faults

Dislocations are common, and three types of faults occur

FIG 2.20

PLANAR FEATURES, WEST AVOCA - UNDERGROUND

Lower hemisphere equal area stereographic projections:

A.
Poles to
fracture cleavageB.
Poles to
crenulation
cleavageC.
Poles to the axial
planes of minor
foldsD.
Poles to
kink planes

1. minor, 2. major and 3. open fissures and breccia zones.

1. Minor

Disruption of the foliation and of the mineralized lenticles is common, and fractures on which displacement is small ($\leq 10\text{cm}$) are classed as minor. Poles to the minor fault planes are shown in Fig. 2.21A. Three major directions of faulting are apparent.

a) The dominant bimodal maximum indicates that the majority of minor faults have an approximate north-south strike. (A feature remarked upon, but not quantified, by Murphy (158)).

Strike, 179° and dip 84°W

Strike, 161° and dip 84°W .

These are normal and reversed oblique strike faults, generally having a minor sinistral component of movement.

b) A series of steep normal faults is represented by maxima, which indicate a strike of 143° and dips varying from 85°SW to 75°NE . These minor faults often group together and collectively cause small-scale displacement of the ore zones. Clay fault gouge occasionally lines the fault planes, sometimes accompanied by remobilized chalcopyrite, and, more rarely, by remobilized sphalerite or galena. Supergene marcasite also occurs.

c) Strike slip faults give rise to a subsidiary maxima with a strike of 047° and an average dip of 68°SE . These are essentially shear faults and, when traced along their length, have a marked tendency to merge into the schistosity.

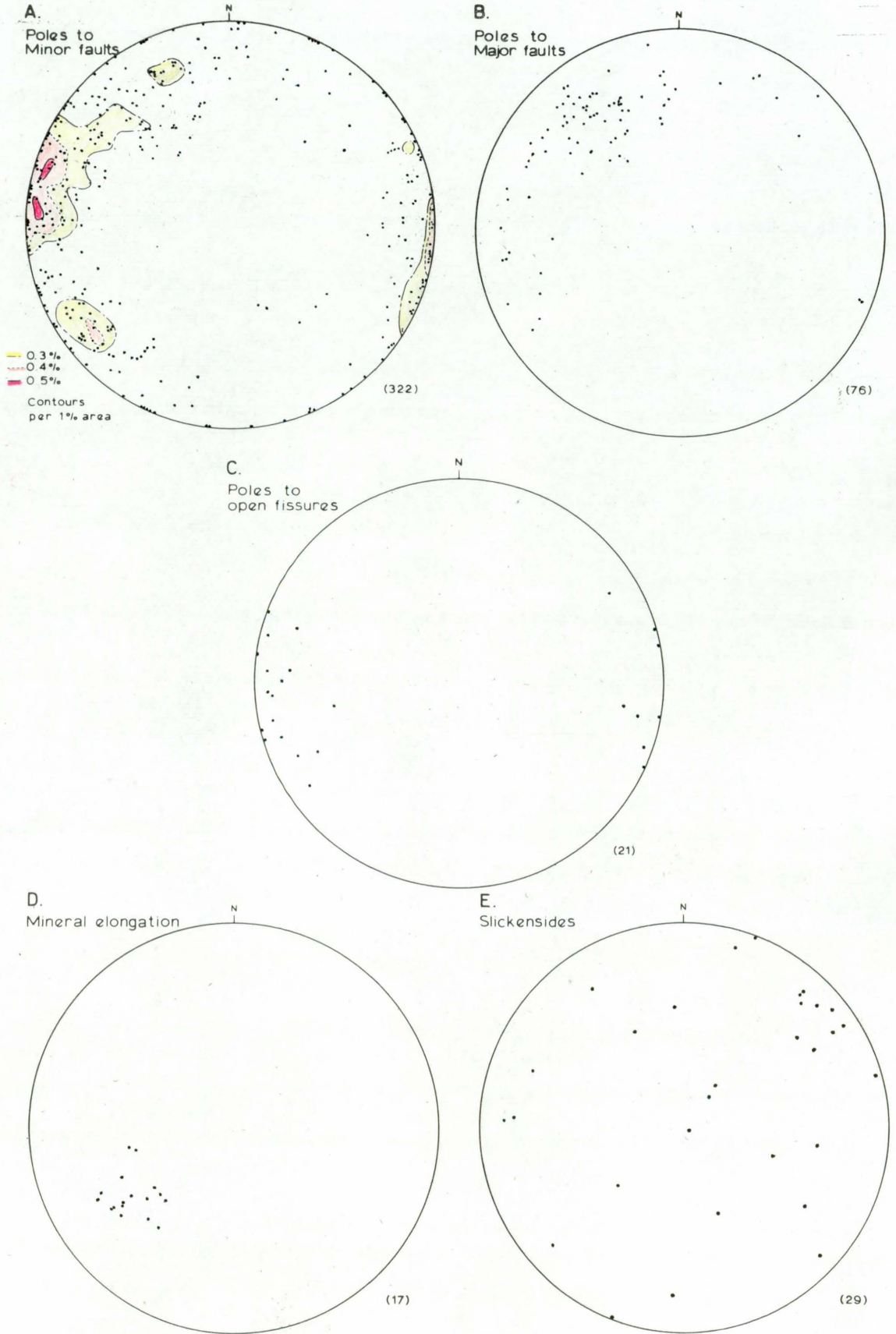
2. Major

The major faults are oblique strike-slip faults with a sinistral movement, either normal or reversed. The fault planes are often smeared by gouge and strongly slickensided. The projection (Fig. 2.21B) indicates an average strike of 026° , and dips of 65°SE . Recognition of these faults is of prime importance, as they may cause considerable displacement of the mineralization. The prominent Pond lode hangingwall fault clearly is reversed (Plate 12:G). Faults of this type are primarily

FIG 2.21

FAULTING, AND LINEAR ELEMENTS, WEST AVOCA - UNDERGROUND

Lower hemisphere equal area stereographic projections.



responsible for the en echelon distribution of the ore zones. (Fig.2.13)

3. Open fissures and breccia zones

A series of faults with a mean strike of 169° and steep dips from 70°W to 75°E develop normal to the regional cleavage (Fig 2.21C). The Great Head fault is a typical example, made up of a silicified breccia zone, up to 15 ft in width. The faults are predominantly normal, but a minor tear component may exist.

Open fissures infilled by angular fragments of broken rock from the fracture walls may be similar to 'a-c joints', and have formed when the regional stress relaxed. Supergene chalcopyrite and granular crystalline quartz encrust the fissure walls and the fault breccia.

(b) Linear

(i) Intersection of bedding and regional cleavage ; S_0 and S_1

Stratification was not positively identified in the wallrocks and thus there is no information about this feature.

(ii) Intersection of S_2 and S_1

A distinct microcrenulation develops on the S_1 cleavage trace, with a steep plunge. The attitude of this lineation was not recorded because accurate measurement was difficult and the attitude can be deduced stereographically, as the point of intersection of the great circles containing the two cleavages.

(iii) Axis of minor folds

Exposures on the 1300 level enable accurate measurement of the axes of drag folds in pyritic material (Map 4). A mean trend of 078° and a plunge of 22°E exists.

(iv) Boudins

Boudins develop in the pyritic ore zones, especially in portions of the Pond lode (Plate 10:F,G and H). The boudins consist of chlorite with disseminated pyrite, and may be classed as micro-boudins. Chalcopyrite infills the necks of the structures and provides macroscopic evidence for remobilization and

recrystallization of chalcopyrite during folding. The form of the boudin-necks, tightly compressed, indicates marked contraction perpendicular to the foliation (180). An indistinct elongation of the boudin cores has a southwesterly trend and a small plunge.

(v) Tension gashes

En echelon sigmoid tension gashes infilled by quartz occur in the siliceous chlorite schists, occupying zones of shear (130). (Plate 11:E). The gashes are often associated with faults, and indicate the direction of movement.

(vi) Mineral elongation

Plates of chlorite in the light grey sericite chlorite schist (tuff) horizon on the hangingwall of the Pond lode, show a marked linear elongation in the plane S_1 (Plate 10:B). In situ measurements of the trend and pitch from exposures on the 720 (Margaret) level are plotted graphically on Fig 2.21D. The distinct maxima, trending 212° and plunging 38° SW, coincides with the overall plunge of the mineralization.

(vii) Slickensides

Slickensides are common on the walls of major faults, and a plot of the attitude of some striations is shown in Fig 2.21E. Sets of grooves occur suggesting that movement was pulsatory and not a distinct event (Plate 19B). A concentration of points exists, trending 027° with a plunge of 12° NE. (Lampard recorded (138) that striations on the walls of the Great Head fault had a similar orientation.).

(c) Discussion

(i) Relationship between cleavage S_1 and bedding, S_0

If the pyrite lenticles in the Pond lode are accepted as representing the sole original stratification to have survived deformation and metamorphism without obtaining a penetrative fabric, then the nature of the first folds can be deduced from the relationship between cleavage, bedding and minor structures.

Detailed mapping of crosscuts driven at right angles to

the foliation illustrates the relationship between folds in the pyritic horizons and the cleavage (S_1), Fig. 2.18. The cleavage dips more steeply than the bedding, implying that the Pond lode, in the 1047 level crosscut south, occupies the right-way up limb of an anticlinal structure.

(ii) Minor folds, F_1

In terrain where there is no repeated folding, the minor folds bear a consistent relationship to the major structures and reflect them in attitude (Pumpelli's Rule). The minor folds in the Avoca area possess a near-vertical axial plane and the axis plunges 22° E. This suggests that the major fold structure plunges at a low angle to the east.

The shape of the drag folds implies that a major fold closure exists in the footwall of the Pond lode in the approximate area north of the Twin Shafts on the 1300 level (Fig. 2.22B).

(iii) Fracture and crenulation cleavage, S_2

The near coincidence of the strike and dip of these two structures indicates that they were produced by a system of forces with a similar orientation (Fig. 2.21A and B).

(iv) Faulting

The analysis of faulting exposed in the underground workings shows good agreement with the results from surface mapping (cf. p. 51).

(v) Mineral Elongation

The direction of mineral elongation is parallel to the mean plunge of the ore grade material, which indicates that the distribution of payable ore is governed by the state of stress existing during metamorphism and deformation. The maximum extension direction is in the plane of the regional cleavage (S_1) but is not coincident with the fold axis (Fig. 2.21D).

2.3.4.2. Macroscopic Structure

Initial recognition of the possible existence of large scale folding at West Avoca was by Murphy (158), who interpreted

the macroscopic structure as a major overturned isoclinal syncline in which the core was occupied by a schistose greenstone sill having an overall plunge to the southwest at a small angle. This view is currently supported by Platt (pers.comm.) who also avers that the major folds have a westerly plunge. Murphy admitted that small scale structures with an equivalent plunge to the major folds are rare, proof that little supporting structural evidence exists in favour of that fold structure. Knowledge of the macroscopic structure is thus somewhat confused.

The present study provides data which enable a fresh interpretation of the macroscopic structure to be made.

The relationship between cleavage and bedding and the form of the minor structures indicates a system of tight to isoclinal folds which plunge to the east at a shallow angle. These folds are parasitic upon the regional monoclinial structure (Fig. 2.11).

The distribution of the mineralization in relation to the macroscopic structure is in Fig. 2.22. The pyritic zones; North, Pond and Central lodes are essentially a single horizon, stratigraphically beneath which occur stockwork siliceous zones, represented by the North lode South branch, Inner and South lodes.

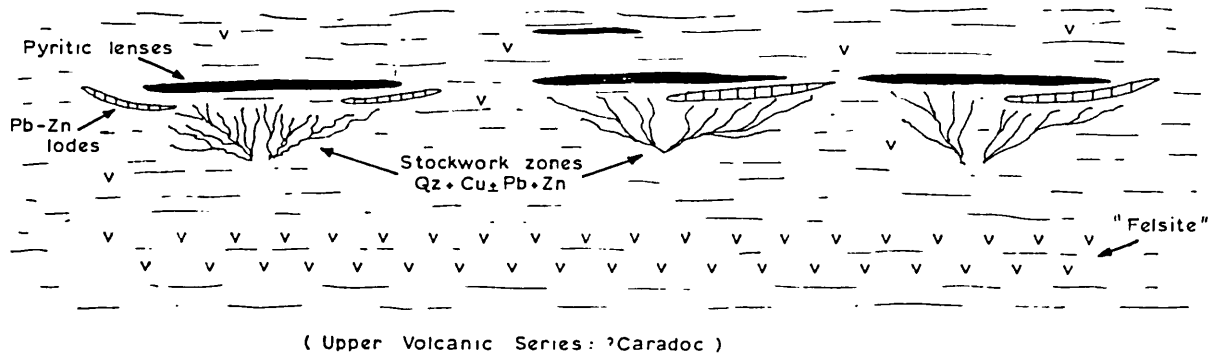
A maximum extension direction in the S_1 cleavage fabric parallels the elongation of the orebodies. Remobilization and recrystallization of the economic sulphides and the silicates (except pyrite) during deformation is evident and thus redistribution of ore grade material parallel to the direction of maximum extension is plausible. (A similar relationship has been demonstrated at Rammelsberg (J.McM. Moore pers. comm.).

The presence of boudinage indicates that contraction occurred perpendicular to the foliation, and the form of the boudins at Avoca illustrates that this contraction is considerable on the limbs of major folds. Silica migrated into tension gashes and the minor folds are tight in style. The mesoscopic structural evidence is therefore consistent with the development of a macroscopic structure similar to that proposed. The structure at East Avoca is not known, but probably corresponds to the

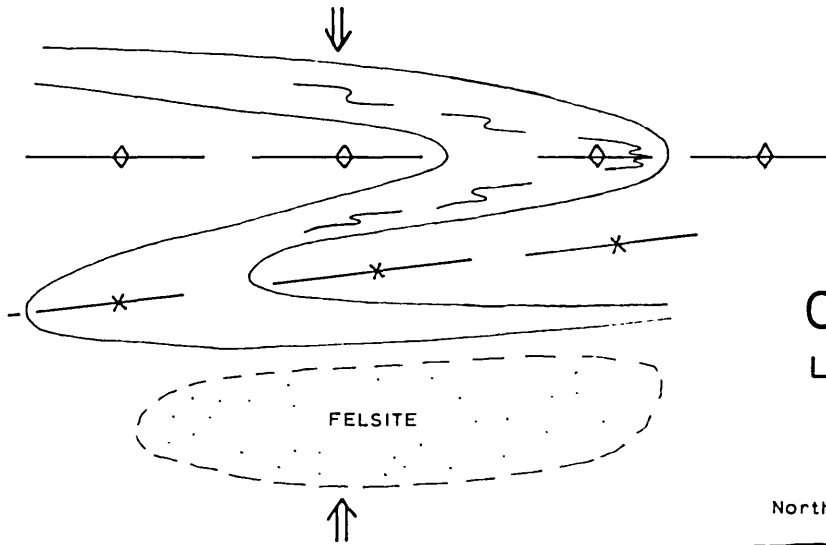
FIG 2.22

Diagrammatic structural evolution, West Avoca.

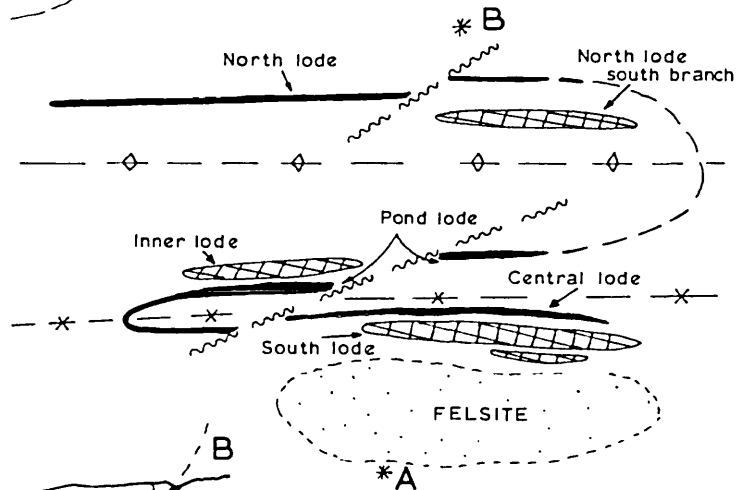
A. SEDIMENTATION AND ORE DEPOSITION (section)



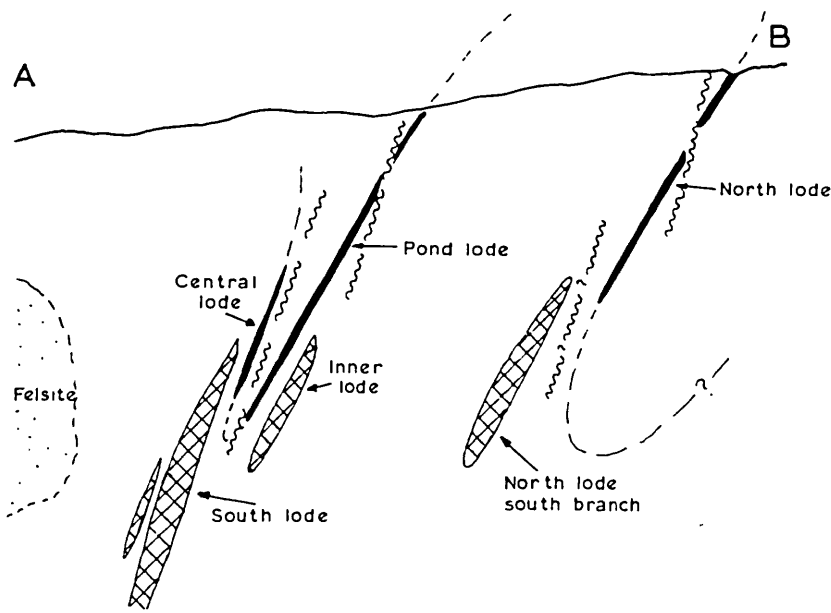
B. EARLY FOLD DEVELOPMENT (plan)



C. LATE FAULTING (plan)



D. CROSS-SECTION: A-B



general picture at West Avoca.

2.3.4.3. Stress Distribution

In common with the surface data the only fracture surfaces for which complementary sets exist are late-stage kink planes (Fig 2.20D). The maximum stress is near-vertical and the intermediate and minimum stresses plot close to the horizontal. Normal faults characterize late-stage displacements and this orientation of stresses supplies the necessary conditions for their formation in the upper levels of the crust (177).

2.3.5. Nature of the Ore Zones

The individual zones of sulphide-rich material are termed lodes, however, they are not true fissure-type deposits and the connotation is a general one, indicating a collection of closely spaced mineralized seams. The local usage, although primarily a miners phrase, has geological application because the zones of mineralization are dominantly 'strata-bound', and can be precisely delineated.

The essential features of the ore zones; surface expression, extent, major mineralogy, representative grade and type, are given in table 5.

2.3.5.1. West Avoca

A series of en echelon lensoid lodes occurring close together make up the present orebodies. Moving from north to south across the belt they are: (Fig 2.13).

North lode	}	North Orebody (undeveloped)
North lode, south branch (New lode)		
Inner lode	}	Pond Orebody
Pond lode		
Central lode	}	South Orebody
South lode		
Hangingwall lode		

a) North Orebody

(i) North lode

This zone provided the bulk of the sulphur mined during

TABLE 5

ORE ZONES IN THE AVOCA MINE AREA

WEST AVOCA

LODE	WEST AVOCA							
	NORTH OREBODY		POND OREBODY		SOUTH OREBODY			
	NORTH	N.L.S.Br. (NEW)	INNER	POND	CENTRAL	SOUTH	HANGINGWALL	LEAD-ZINC
Surface Expression	Open pit + Caved workings	Minor	None	Minor	Caved workings + Open pit	Caved Workings	None	None
Extent :								
Strike length	>2000'	>1000'	~800'	≥2000'	≥1500'	≥2500'	~500'	~500'?
Width	10'-40'	~5'	5'-30'	25'-30'	5'- ≥45'	20'- ≥75'	≤15'	~30'?
Proven depth (or, vertical extent)	≥650'	≥150'	≥200'	≥1500'	≥1200'	≥2000'	≥200'	~300'
Major Mineralogy * (*Symbols in Fig.2.23)	py,cp,sl, (gn)	py,cp, (sl,gn)	py,cp	py,cp,mt, (sl,gn)	py,cp, sl,gn	py,cp, (sl,gn)	py,cp	py,sl,gn,cp
Grade :								
(representative) Cu %	0.5	1.5	≤1.0	1.2-1.3	1.5-2.0	1.0	0.8	0.3
Zn %	0.8	-	-	-	-	-	-	~7.0
Pb %	0.1	-	-	-	-	-	-	~3.0
S %	25	10	-	25	12-18	6.0	4.0	15
Nature (Zone type)	Pyritic	Siliceous	Siliceous	Pyritic	Pyritic	Siliceous	Siliceous	Lead-zinc

EAST AVOCA

LODE	EAST AVOCA												
	TIGRONEY			W.CRONEBANE		E.CRONEBANE			COGNARY			KILMACOO	
	MAIN	FOOTWALL	HANGINGWALL	"DEAD GROUND"		MAIN	FOOTWALL	HANGINGWALL	MAIN	FOOTWALL	HANGINGWALL	MAIN	HANGINGWALL
Surface Expression	Caved workings + open pits			Pits and caving		Shallow pits and caving			Fitting			Trials and workings	
Extent :													
Strike length	≥1500'			~1500'		≥1500'			≥1000'			≥1000'	
Width	15'-50'	~10'	~20'	?		15'-30'	≤30'	?	?	?	?	?	?
Proven depth (or, vertical extent)	≥800'	≥600'	≥600'	~200'		>500'	≥600'	?	?	?	?	?	?
Major Mineralogy * (*Symbols in Fig.2.23)	py,sl,gn, cp	py,cp,sl, gn	py,cp,sl, gn	py,cp,sl,gn		py,cp,sl,gn			py,cp,sl,gn			gn,sl, py,cp	py,gn,sl,cp
Grade :													
(representative) Cu %	1.5	2.0	1.0-1.5	?		1.5	?	0.5	1.5	?	?	Tr.	2.5
Zn %	3.0-5.0	1.0	1.5	?		2.0-4.0	?	1.5	0.5	?	?	14.0	2.0
Pb %	1.0-3.0	0.5	0.5	?		0.5-1.0	?	1.0	0.3	?	?	15.5	3.0
S %	15	12	6.0	?		16	?	5	?	?	?	30	8.0
Nature (Zone type)	Pyritic	Pyritic	Siliceous	Pyritic + Siliceous		Pyritic	Pyritic	Siliceous	Pyritic	Pyritic	Siliceous	Pyritic	Siliceous

the late nineteenth and early twentieth century.

The mineralization is pyritic, massive and banded, with minor disseminated chalcopyrite, sphalerite and rare galena. A significant increase in lead and zinc occurs to the west, but widths decrease.

The host rock is a green chlorite schist, and dark grey siliceous chlorite schist forms the hanging and footwalls, and in certain areas it is strongly leached. There is an overall plunge to the southwest, and faulting disrupts relationships at the western end, causing a thinning in values. Towards the east, the intensity of mineralization decreases (169) and a microdiorite dyke occurs in the hangingwall (Map 3).

(ii) North lode, South branch (New lode)

This lode was developed from the Spa adit (Plate 1:A), to a limited extent.

The mineralization is siliceous, ramifying veinlets carrying disseminated pyrite and chalcopyrite, with rare galena and sphalerite.

The host rock is dark grey siliceous chlorite schist. Very little is known about the mineral distribution and the lode is cut off to the east by the Great Head and the Avoca River faults, whilst to the west the mineralization diminishes.

The paucity of copper in the North lode makes this a poor exploration target in depth, however the character of the mineralization may change. The south branch, lying 300 ft in the footwall, is a prime target, bearing in mind the regional plunge of the mineralization to the southwest. (Recent drilling confirms the existence of the latter in depth as the 'New' lode (J.W. Platt, pers.comm.).

b) Pond Crebody

(i) Inner lode

Murphy (158) and others noted a zone of siliceous mineralization in the footwall of the Pond lode called the Inner lode (Fig 2.13).

This lode appears to develop on and below the 1100 level. The mineralization is essentially made up of disseminated pyrite and chalcopyrite in quartz. The host rocks are dark and light grey siliceous chlorite schists, and in depth it may unite with the South lode.

Extension of this zone in depth may provide further reserves.

(ii) Pond lode

The surface outcrops are insignificant, but the lode widens appreciably below the 600 level and is a source of copper and sulphur. The lode is a banded and massive lenticular pyrite zone with minor disseminated chalcopyrite and lesser sphalerite and galena. In the footwall there are magnetite-rich lenses, with disseminated pyrite and chalcopyrite. The value of sulphur decreases towards the margins of the lode and contents of lead and zinc increase at the western end (an indication of the Lead-zinc lode, see below).

The host rocks are dark green chlorite schists, with dark grey siliceous chlorite schist on the footwall and a 'graphitic zone', or black carbonaceous shale, on the hanging-wall. The hangingwall rocks are partly dolomitized, especially in the west, where a tuff horizon (light grey sericite chlorite schist) assumes importance. (This rock is referred to by Murphy (158) and others, as a 'greenstone'.) A phosphatic horizon occurs within the shale.

The mineralized seams are not parallel to the foliation, but inclined at a small angle, and the plunge of the lode is 35° - 40° W. With increasing depth, the content of pyrite decreases due to permeation by siliceous veins, and to the east the lode terminates against a reversed fault which causes a marked thinning of values (Map 8).

c) South Orebody

(i) Central lode

This is the ore zone predominantly worked by the 'old men' for copper and lies in the footwall of the South lode.

The ancient workings are now marked by an open-pit(Plate 1:A).

The mineralization is banded and essentially composed of pyrite with disseminated chalcopyrite, sphalerite and galena. There are marked concentrations of lead and zinc on the hanging-wall and Kinahan (131) recorded a rich lead-zinc zone (kilmacooite) in the upper levels in this lode, with up to 3.5% Zn and 1.5% Pb over widths of 30-50 ft.

The host rock is a dark green chlorite schist with dark and light grey siliceous chlorite schist on the hanging and footwall, and the mineralized lenticles crosscut the foliation. The ore zone plunges towards the southwest and the lode is interrupted to the east by the Great Head and Avoca River fault system (Fig 2.12B). (Lampard (138) termed this lode 'Pond lode No.1.', and although apt in the present structural context, the name 'Central' is adhered to, in order to facilitate comparison with current mine usage.)

(ii) South lode

This occupies, essentially, the site of the major recent development and mining, producing surface caving along the strike of the lode (Plate 1:A).

The maximum strike length is in excess of 2,500 ft and widths vary considerably being dependent upon the cut-off grade chosen and may exceed 100 ft, but are generally ≤ 75 ft (Table 5). Mineralization consists of ramifying siliceous seams and veinlets with disseminated pyrite and chalcopyrite and trace amounts of sphalerite and galena (Plate 11:A,B). The grade is remarkably uniform with a tenor of about 1% Cu and 6% S, and was an uneconomic source of copper for the ancients.

The host rock is a dark grey siliceous chlorite schist with light grey varieties in the hanging and footwall (Fig 2.13 and Map 5). A discontinuous zone of sericitic schist occurs in the hangingwall. An overall plunge of 35° - 40° SW exists for the centre of the lode which becomes diffuse at its western limits and is cut by the Great Head and other faults at the eastern margin.

(iii) Hangingwall lode

This zone is in the hangingwall of the South lode.

Mineralization is siliceous, with disseminated chalcopryrite and pyrite.

Host rocks are dark and light grey siliceous chlorite schists, sericitized in part, and the lode is discontinuous vertically above and below the 1670 level. (A similar zone occurs in the hangingwall of the South lode at the 1000 level (Fig 2.13)). Felsite, forming the conspicuous surface bluff of the Bell Rock (Plate 1:A) is in the hangingwall.

d) Lead-zinc lode

A zone of lead-zinc enrichment occurs to the west of (and en echelon with) the Pond lode and this is called the Lead-zinc lode (Fig 2.12A). This mineralization, proved by meagre drilling, contains reserves of about 500,000 tons with about 10% combined lead and zinc, and 2.8 oz/ton Ag(261).

Mineralization consists of banded sphalerite, galena and pyrite with minor chalcopryrite, typical of 'kilmacooite' ore.

Host rocks are green and grey chlorite schists, and the lode may be a faulted continuation of the Pond lode.

2.3.5.2. East Avoca.

The mineralized zone at East Avoca extends for a distance of about 8,000 ft along the strike. Few of the workings are accessible and the following description of the area is a summary of previous accounts (7, 131, 257) coupled with the writer's own observations.

a) Tigroney

A series of open-pits and surface caving (Plate 1:B), indicate intensive former working.

Three poorly defined lodes occur : Main, Footwall and Hangingwall.

The Main lode consists of banded and, rarely, massive seams of pyrite, with disseminated sphalerite, galena and

chalcopyrite. The Footwall lode is also a pyritic zone, but enriched in chalcopyrite and depleted in sphalerite and galena.

The Hangingwall lode dominantly consists of siliceous veinlets, with disseminated pyrite, chalcopyrite, sphalerite and galena. Situated in the hangingwall of this lode are discrete siliceous zones which may carry high copper contents over narrow widths.

Host rocks are dark and light grey siliceous chlorite schists with sericitic zones on the hangingwall of the siliceous lodes. Dark green chlorite schists are the host rocks for the pyritic zones. The mineralization plunges 35° - 40° SW and terminates to the east against the Great Fluccan fault, one of the faults in the Avoca River fault system. To the west, values thin due to the presence of a series of faults producing a cumulative offset (Fig 2.12B).

b) Cronebane

In the west, there are minor zones, which received little attention from the ancient miners, being termed 'Dead Ground'. The mineralization consists of a low grade pyritic zone in the footwall of a siliceous zone; The Yellowbottoms and Blueburrows lodes.

The cause of the decrease in intensity of mineralization in this area is not clear, and may be due either to post mineralization structural effects, or simply variations along the strike.

In the east (Magpie-'B' Shaft section), a series of lodes occurs. A main lode, essentially pyritic, has irregular hanging and footwall lodes. The footwall lode is also dominantly pyritic with high copper values and significant galena and sphalerite (similar to the Footwall lode in Tigroney). The hangingwall lode, is a siliceous zone with disseminated pyrite, chalcopyrite, sphalerite and galena.

Host rocks throughout are chlorite schists with varying degrees of silicification. Sericite-rich zones exist on the hangingwall of the siliceous ore, and black shales with carbonaceous horizons locally occur. Dykes of intrusive microdiorite (sometimes porphyritic) cut the footwall ore zones in the Grass

Levels Adit and also the Magpie area.

c) Connary

Three mineralized zones occur: a pyritic main lode, a footwall lode of similar composition and a widespread zone of hangingwall silicification.

The host rocks are a series of siliceous and chloritic schists. Leached schist is common adjacent to fissures and black, sometimes carbonaceous, shale horizons occur.

Intrusive microdiorite dykes have also been recorded (257). The mineralization appears to plunge 35° - 40° SW and the zone terminates to the east against a prominent fault. To the west the intensity of mineralization decreases.

d) Kilmacoo

Two major lodes occur, a Main lode; essentially pyritic and low in copper, together with a siliceous Hangingwall lode. This is the type area for 'kilmacooite', a rock consisting of a dense intergrowth of galena, sphalerite, pyrite and minor chalcopyrite. Grades of this material vary widely but may be >30% combined lead and zinc (Table 5).

The host rocks are green and grey chlorite schists, with sericitic schists associated with the siliceous zones. The mineralization appears to decrease in intensity towards the east and the limits have not been precisely delineated. An interesting feature is that feldspar generally occurs in the hangingwall of the ore zones in East Avoca and at Kilmacoo it also exists in the footwall. Kilmacoo also is the apparent termination of viable mineralization, this may have some structural significance which is not yet clear.

2.3.6. The Ore Minerals and their paragenesis

2.3.6.1. Introduction

Aspects of the mineralogy and paragenesis of the Avoca ores have been studied. Odman reported (168) on polished sections of material from the upper levels at East Avoca and

the lead-zinc zone at West Avoca; his conclusions, in the light of considerable experience of the Scandinavian deposits, are useful. Samples similar to those chosen for metallurgical tests in 1967, were collected by the writer and are included in this description. Lampard's work (138) provides extensive coverage of the West Avoca deposits. Full use has been made of the polished sections from that study as, in many cases, they represent material it is now impossible to sample. A total of over 250 polished sections have been examined including new samples from East and West Avoca together with material from all the known mineral occurrences in the prospecting lease area. The following description is an attempt to present an objective conspectus of the ore mineralogy and paragenesis of the district.

2.3.6.2. Ore Mineralogy

The elements of the mineralogy are shown in Fig. 2.23. Primary minerals are those formed during the initial period or periods of mineralization (19), and those which formed from descending surface solutions, supergene (139). This distinction, illustrated in the generalized paragenetic sequence (Fig. 2.27), cannot be rigorously applied.

The occurrence and distribution of the major primary ore minerals depends upon their spatial arrangement within the mineralized zone. As shown previously, a wide variety of ore types exists, each with its own characteristic mineral association. Five broad divisions are recognized.

a) Pyritic zones (lodes)

Pyrite is the dominant mineral, either banded or as massive lenticles with or without interstitial chalcopyrite, sphalerite and galena in a chloritic matrix. Magnetite, hematite, arsenopyrite, pyrrhotite, bismuthinite and native bismuth are minor, and gold is rare.

Representative examples are: North, Pond and Central lodes at West Avoca, the Main lode in East Avoca, the Castle Howard lode, the North lode at Ballymoneen and the South lode at Ballycoog.

FIG 2.23

AVOCA DISTRICT

DISTRIBUTION OF THE ORE MINERALS

	Symbol	MINERALIZED ZONES				
		PYRITIC	SILICEOUS	LEAD-ZINC	MAGNETITE	DISSEMINATED + VEIN
PRIMARY	Pyrite :					
	Framboidal	•	*	◐	*	•
	Colloform	●	•	●	*	•
	Zoned, crystalline	●	◐	●	*	◐
	Unzoned, crystalline	•	●	•	◐	●
	Chalcopyrite	cp	●	●	◐	•
	Sphalerite	sl	◐	◐	●	• + ●
	Galena	gn	◐	◐	●	• + ●
	Magnetite	mt	◐	*	*	●
	Hematite	hm	•	*	*	◐
	Arsenopyrite	asp	◐	•	◐	•
	Chromite	cm	*	*	*	•
	Pyrrhotite	po	•	•	*	•
	Cobaltite	cb	*	•	*	*
	Tetrahedrite	td	*	•	•	*
	Bournonite	bo	*	•	•	*
	Native Bismuth	Bi	•	•	*	*
	Bismuthinite	bt	•	•	*	*
	Galenobismutite	gb	•	*	*	*
	Aikinite	ak	•	*	*	*
Kobellite	ko	*	•	*	*	
Lillianite	li	*	•	*	*	
Ullmannite	ul	*	*	*	• + *	
Gold	Au	•	*	*	*	
SUPERGENE	Goethite	gt	◐	◐	◐	●
	Covellite	cv	◐	◐	◐	◐
	Marcasite	mc	•	*	*	*
	Native Copper	Cu	•	•	*	*
	Malachite	ml	•	•	*	*
	Chalcanthite	ct	•	•	*	*

● Major

◐ Accessory

◐ Minor

• Trace

* Absent

b) Siliceous zones (lodes)

Major pyrite, chalcopyrite, sphalerite and lesser galena occur within a siliceous matrix. Arsenopyrite, pyrrhotite, bismuthinite, native bismuth, tetrahedrite, galenobismutite and bournonite are minor with cobaltite and lillianite as trace occurrences.

The South lode, South Branch of the North lode and the Hangingwall lode at West Avoca are typical examples with the South lode at Ballymoneen and the Hangingwall lode at East Avoca.

c) Lead-zinc zones (lodes)

Banded sphalerite, galena and pyrite with minor arsenopyrite and chalcopyrite in a chloritic matrix. Tetrahedrite and bournonite are rare. The Lead-zinc lode at West Avoca and the zones at Kilmacoo are representatives, and include the material known as 'kilmacooite'.

d) Magnetite-zones (lodes)

Essential magnetite and hematite occur in a silico-chloritic matrix with minor chalcopyrite and pyrite. Chalcopyrite, sphalerite, arsenopyrite, pyrrhotite and chromite are rare.

The minor magnetite zones in the footwall of the Pond lode at West Avoca and those at Moneyteige, Ballycoog, Aughrim River Roadside, Knocknamohill, Ballymoneen and Ballard, are examples of this category.

e) Disseminated and vein-type mineralization

Throughout the wallrocks and within the stratigraphic sequence, pyrite is ubiquitous. Minor veins with chalcopyrite, sphalerite, arsenopyrite and galena also occur. Pyrrhotite, and ullmannite are rare.

Representatives of this type occur at Moreshill, Ballinasilloge, Knockmiller, Clonwilliam, Ballycoog Ford, Ballintemple, Kilcashel, Knockanode and Sroughmore (Fig. 2.7).

Supergene iron and copper minerals are formed in dump material and open fractures underground. The zone of secondary enrichment extends to a depth of about 200 ft below the surface

but effects are minimal.

The occurrence of the various mineralogical types has been described in a previous section. Each type is not mutually exclusive, gradations and diachronous relationships exist.

2.3.6.3. Laboratory Methods

Physical features and optical properties of the minerals were examined in reflected light using a Reichert Zetopan ore microscope. Identification was by reference to texts by Uytenbogaart (230), Ramdohr (179) and Millman (152). Contrasts with published data are recorded. Quantitative data on the following properties was gathered on certain phases:

a) Indentation Microhardness

Measurement of the Vickers microhardness was carried out with a Leitz Durimet microscope and an indenter attached. A load of 50 gm was used for all the determinations in this work, and applied for 20 secs, using the method of Young and Millman (258). Values were derived from the formula:

$$\text{VHN}_{\lambda} = \frac{1854.4 \times L}{d^2}$$

Where:

VHN = Vickers microhardness number; kg/mm^2

L = Load applied; gm

d = Indentation diagonal of square; μ

Measurements were made on several grains of differing orientation whenever possible.

b) Reflectivity

A Reichert Zetopan equipped with a reflex microphotometer was used, described in detail by Singh (204). Comparative quantitative measurements were made against the RSM Pyrite Standard. Reflectivity is calculated from the formula:

$$R_{\lambda} \% \text{ of mineral} = \frac{\text{Deflection value of mineral}}{\text{Deflection value of standard}} \times K$$

Where:

K = calibrated R_{λ} of standard and λ = monochromatic wavelength - in this case 546 nm, in air. It was not possible to obtain

grains of known orientation and thus approximate figures are given for bireflectance. The degree of dispersion was indicated by comparison with Millman's data at 589 nm (152).

c) Electron-probe analysis

A Cambridge Microscan MK.1 was employed to analyse carbon-coated polished mineral surfaces. A constant accelerating voltage of 25 kV was used throughout. Average counts per ten seconds from the sample were compared with the count rate from standards which were pure metals or analysed samples. The detection limit is 1.0%, or better, and the precision of analyses is within $\pm 5\%$ of the relative value.

Quantitative data were corrected for errors due to instrumental effects: absorption, overvoltage, atomic number and fluorescence, using a semi-empirical method (T.K. Kelly and G.M. Steed pers. comm.).

A few analyses were performed on a Cambridge Geoscan instrument operating at 15kV. The probe current was adjusted to give a maximum count rate on the standards of ≤ 7000 c.p.s. to avoid large dead-time corrections. Synthetic standards were used, and other instrumental corrections were carried out on a CDC 6600 computer using a program written by M.T. Frost. The precision of the analyses is of the order of $\pm 1.5\%$.

d) X-ray diffraction

Small amounts of certain minerals were excavated from polished sections using a fine steel needle and incorporated in a small ball of rubber solution. The ball was mounted on a drawn glass fibre and inserted in a Philips 11.46 cm (dia) Debye-Scherrer powder camera. Either Fe filtered CoK α ($\lambda = 1.7889^{\circ}\text{A}$) or Ni filtered CuK α ($\lambda = 1.5405^{\circ}\text{A}$) radiation was used. Interplanar spacings were determined with the line spacings being read on a Hilger Watts micrometer scale ($\pm 0.05\text{mm}$). A correction was made for film shrinkage, and the relative intensity of the lines was visually estimated. X-ray diffraction angles were tabulated and the d values obtained from tables.

e) Etching

Inter- and intra-granular textures in the ore minerals were revealed by surface etching using various reagents, following techniques applied by earlier workers (230).

Pyrite was electrolytically etched, with 10% chromic acid solution employing a method similar to that described by Lampard(138). Disseminated grains in a non-conductive gangue were treated with fuming nitric acid.

Sphalerite was etched with a 55% solution of hydrogen iodide, and galena with hydrogen bromide solution (s.g., 1.46-1.49).

2.3.6.4. Primary Minerals

a) Pyrite: FeS_2

(i) Pyritic zones

A complete gradation exists between massive, and disseminated pyrite, occurring within a chloritic matrix. The massive seams are made up of closely packed euhedral to subhedral crystal aggregates with a variable grain size: 0.1-1.5 mm, often only revealed after etching. Disseminated pyrite is sandwiched between massive seams, and makes up the weakly mineralized haloes surrounding the massive lenticles (Plate 13), where it has a smaller grain size: 0.001-0.5 mm, however, porphyritic crystals and aggregates do occur.

Slight variations in reflectivity often indicate the presence of zoning in unetched specimens and the non-stoichiometry of the pyrite. Anisotropy is very weak but none-the-less distinct. The crystal morphology is dominantly cubic or semi-cubic, with incompletely developed faces. Corrosion of the crystal outlines and cores is ubiquitous and characteristic.

Zoning

Zoning in pyrite is almost universal and can be detected prior to etching, but is obvious after treatment. Textures are illustrated in plates 14, 15, 16 and 17. Ramdohr (179) stated that zonation effects could be caused by (a) differences in chemical composition between the zones, (b) inclusions of other

minerals or (c) interruptions during crystal growth. Differences in colour and hardness also give rise to zoning, e.g. in bravoite, (233). At Avoca, the sub-grain boundary has a decreased hardness and is initially etched. Inclusions of other minerals, clays etc., during crystal growth may have given rise to sub-grain inhomogeneities, and may also have marked periods of decreased crystal growth. Incorporation of these extraneous particles at sub-grain boundaries creates areas preferentially leached on etching. The cores of zoned crystals often have an octahedral habit (Plates 14, 16), but the observation by Ramdohr (179) that the habit alters progressively to cubic in the outer zones, is only partially substantiated.

Colloform textures

These are common, especially in the upper mine levels in the zones, (Plates 15, 17:A) both botryoidal and reniform types occur. Banded melnikovitic pyrite is characteristic.

Spheroidal textures

Spherical and subspherical aggregates of pyrite concentrate within the lead-zinc rich areas of the pyritic zones (Plates 23:1 and 34).

Deformation textures

Many of the textures formerly ascribed to cataclasis and deformation within the pyritic ores, are now thought to have been produced by leaching and this is considered further in the discussion. Definite deformation fabrics due to mechanical brecciation and brittle failure are shown by pyrite adjacent to slickensides (Plate 12).

Inclusions

Inclusions rarely exist in pyrite from massive seams but increase with increasing matrix sulphide content. They occur as emulsion blebs of chalcopyrite, sphalerite, galena and pyrrhotite intimately related to zone and grain boundaries. This confirms that unmixing of crystals is more complete at grain boundaries than in cores. The minute (10 μ) blebs of pyrrhotite occurring with or without chalcopyrite are often included along zone boundaries.

Grain boundary relations

As noted above, pyrite grains are normally strongly corroded, especially in material from the upper levels or areas exposed to surface oxidation and leaching (Plate 16:A). Zoned crystals and crystal aggregates are replaced and differential replacement is shown by initial attack and embayment along fractures and zone boundaries. Melnikovitic pyrite (dirty colloform pyrite - a very fine grained cryptocrystalline aggregate) is very reactive to weathering (179) and has a brownish colour and decreased hardness in relation to unzoned pyrite. Etching is rapid on material with these properties and produces textures identical to those in material from the upper levels at Avoca, (cf. Fig. 487, in 179) (Plate 17). The 'dirty' nature of the pyrite may be due to minute inclusions of clay grade material, iron oxides and oxyhydroxides. These enlarge the free surface of the pyrite available for reaction and thus increase the rate of reaction with etch reagents.

(ii) Siliceous zones

Disseminated pyrite commonly occurs in the siliceous zones in a silico-chloritic matrix. Lenticular seams of massive pyrite with a siliceous matrix are rare, being dominantly confined to the hangingwall portions of the zones. The grain size varies widely, from 0.001-0.5 mm, depending upon the degree of aggregation.

Weak anisotropy is universal and the morphology is cubic with rare sub-cubic development. Corrosion and embayment of crystal outlines by gangue and other sulphides is marked, producing pseudocataclastic textures.

Zoning

In marked contrast to the pyritic zones, zoned pyrite rarely occurs in the siliceous zones; the majority of grains are euhedral to subhedral unzoned crystals or aggregates. The zonal forms which do exist are shown in plate 18 and only occur within areas of melnikovitic pyrite. The clear pyrite kernals are more resistant to replacement and zonal textures are found in the overgrowths of dirty pyrite. These melnikovitic areas (Plate 18:C,D,E) infill the cores of lattice-works of clear pyrite. These lattice-works may be remnants of former large

zoned, corroded grains. A similar relationship occurs in pyrite from Cyprus (G. Constantinou pers. comm.)

Colloform textures

Colloform textures occur in the rare areas where melnikovitic pyrite overgrows and replaces unzoned pyrite.

Spheroidal textures

Spheroidal textures are uncommon, except for corroded atoll-like forms remaining after replacement of zoned pyrite. At Tigroney, spheroidal pyrite occurs in lead-zinc rich material from the hangingwall siliceous zone.

Deformation textures

Mechanical deformation is shown in plate 19, where slickensided material has been sectioned. Chalcopyrite complicates the relationships and prior to deformation, it undoubtedly replaced the pyrite granules. On deformation, the chalcopyrite behaved in a ductile manner and obtained the bulk of the strain by glide-twinning, followed by recrystallization. Effects of strain on the pyrite were thus reduced, and granulation and cataclasis only locally took place.

Inclusions

These concentrate in fractures or along the boundaries of grains, but because there is much less zoned pyrite in the siliceous zones, inclusions of chalcopyrite, galena, and sphalerite are not as common in pyrite as they are in the pyritic zones. Pyrrhotite inclusions were not observed.

Grain boundary relations

In the absence of chalcopyrite, pyrite grains are euhedral to subhedral. However, in copper-rich material, grains are strongly embayed (Plate 25:A,B). The bulk of the pyrite is unzoned and thus corrosion takes place at grain boundaries and along fractures; where pyrite is zoned, preferential dissolution takes place at the zone boundaries.

(iii) Lead-zinc zones

Pyrite is usually banded sub-parallel to the foliation in the individual lenticles of the lead-zinc zones, as a fine grained matrix mineral to major sphalerite and galena. Anhedral to subhedral grains and granular aggregates occur with a variable grain size: 0.001-0.1 mm. Melnikovitic pyrite is common. Anisotropy is weak, but distinct, and the crystal morphology is sub-cubic to cubic. Embayment of zoned grains is marked.

Zoning

Zoned textures after etching are illustrated in plates 16:C,D and 27. The prominent careous replacement of pyrite by sphalerite is characteristic. It is evident that sphalerite, galena (and chalcopyrite) are later in the paragenetic sequence than pyrite. The grain boundaries of the latter are universally corroded by the matrix sulphides. The coincidence of zones of colloform and spheroidal pyrite accumulation and the lead-zinc rich portions of the mineralization is striking.

Colloform textures

These are common, especially in partially oxidized material from the upper levels at West Avoca (138). Radiating, botryoidal and reniform textures occur, in addition to worm-like and atoll structures.

Spheroidal textures

Unzoned pyrite is found in sub-spherular aggregates. Framboidal pyrite is common, plates 20 and 34.

Deformation textures

The matrix of the pyrite granules is either sphalerite or galena. On deformation the latter minerals are affected due to an increased ductile behaviour. Remobilization is followed by recrystallization, which is the main effect observed in the assemblage. Pressure fringes around pyrite may be infilled by sphalerite or galena (Plates 26:E and 29:G,H).

Inclusions

In common with zoned pyrite from other areas in the

mineralized belt, the zone boundaries sometimes contain inclusions of sphalerite, galena or chalcopyrite, as ovoid blebs or segregations.

Grain boundary relations

Marked corrosion of the grain margins is ubiquitous, pyrite being replaced by the base metal sulphides (Plate 16:C). Preferential corrosion of zoned pyrite is common.

(iv) Magnetite zones

Pyrite is a minor constituent, occurring as disseminated subhedral crystals: 0.001-1.0 mm in size, showing minor replacement by magnetite. It also replaces magnetite.

Zoning, colloform and spheroidal textures are absent.

Inclusions

Inclusions of both hematite and magnetite are common, especially in fractures and at grain boundaries.

Grain boundary relations

Highly careous outlines are common and a poikilitic texture is characteristic.

(v) Disseminated and vein-type mineralization

Disseminated pyrite occurs within a chloritic or graphitic host. The grain size is highly variable: 0.001-1.5 mm. Euhedral or subhedral crystals are common, either solitary or as aggregates and they are often porphyroblastic (Plate 39:A).

Zoning

This is common, and simple, with a few zones in each crystal. Original euhedral cores are surrounded by later anhedral overgrowths.

Colloform textures

These sometimes occur in oxidized material.

Spheroidal textures

The carbonaceous zone on the hangingwall of the Pond lode at West Avoca contains myriads of framboidal pyrite

spherulites (Plates 21 and 22).

Framboids have received much attention during the past two decades (143), and are spherical to sub-spherical raspberry-like aggregates of microcrystalline pyrite with a diameter varying from $<3\mu$ to $>30\mu$. The constituent crystallites range in size from $\leq 0.5\mu$ to 6μ . Agglomeration of framboids produces a variety of shapes, from simple dumbbells to complex clusters, exemplified by material from Avoca (Plates 20, 21 and 22). The characteristics of microscopic framboidal pyrite (143), are examined below.

A) External features

(i) Size. Analysis of the size distribution of pyrite framboids from a pyritic carbonaceous horizon and a lead-zinc rich ore seam are shown in Fig. 2.24.

(Sample traverses were made using a $\times 60$ objective and measurements were taken with a Reichert micrometer ocular; $\times 8$, to $\pm 0.1\mu$)

Framboidal pyrite spheres from the carbonaceous rock have a unimodal positively skewed distribution (Maxima = 3.5μ) and a mean (observed) diameter of 3.8μ (Fig. 2.24A). This corresponds to a true mean diameter of 4.6μ , applying the correction procedure of Jackson (in 143), where :

$$\text{True Diameter} = \frac{\text{Average observed diameter}}{0.8165}$$

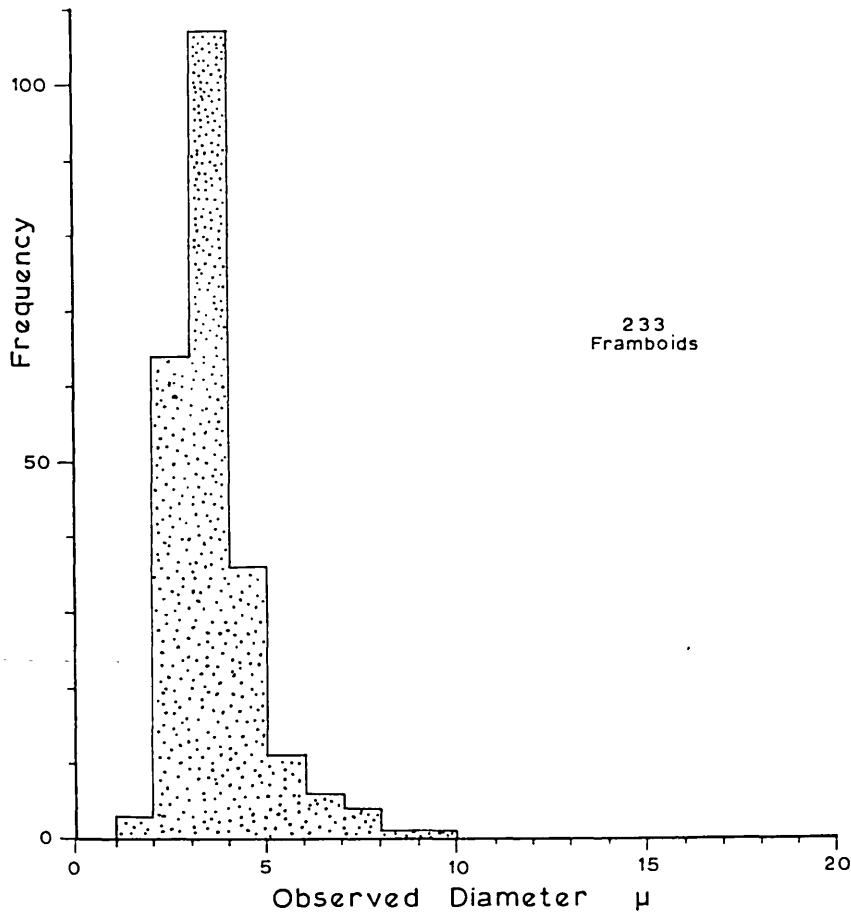
In the lead-zinc seam a more strongly skewed distribution occurs (maxima = 7.5μ) with a mean diameter of 12.1μ , corresponding to a true diameter of 14.8μ (Fig. 2.24B).

The two populations of framboids are from syngenetic (sensu lato) and epigenetic mineralization.

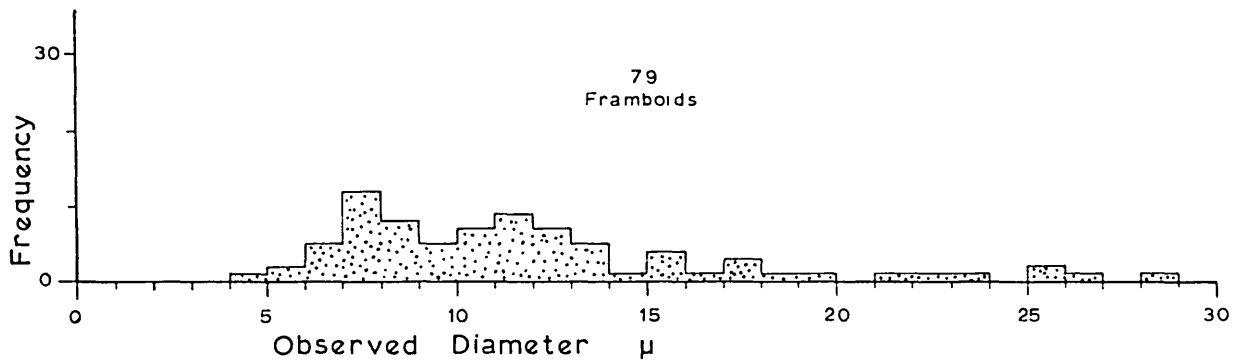
There is a significant difference in size of framboidal pyrite from the two environments. As the two populations are from syngenetic (sensu lato) and epigenetic mineralization, there may be a relationship

FIG 2.24

A Size distribution of framboidal pyrite - Graphite schist, Pond lode hangingwall, West Avoca.



B Size distribution of framboidal pyrite - Lead-zinc seam, Hangingwall lode, Tigroney, East Avoca.



between framboïd size and mode of formation.

(ii) Outline: spherical or sub-spherical.

(iii) Agglomeration

a) single; often with a carbonaceous 'sac' visible (Plate 21:A).

b) Dumbbell; with two units of similar size (Plate 21:D).

c) Cubic; with four units of similar size (Plate 21:E).

d) Cluster; with all units of similar size (Plate 21:F,H,I).

The fact that framboïds of similar size tend to cluster together is confirmed by Kalliokoski and Cathles (127) and Rickard (187).

B) Internal Characteristics

(i) Size of microcrystallites. There is a generalized size differentiation between the microcrystallites in framboïds from the carbonaceous horizon and the lead-zinc seam (Fig. 2.24). In the former it is generally 1.0-1.5 μ , although it may be $\leq 0.5\mu$ (Plates 21:B and 22:A,B), and in the latter 1.5 μ -2.5 μ . Increase in size of the component crystallites is thus accompanied by increased size of the composite framboïd, a conclusion reached elsewhere by Wilson (in 127).

(ii) Structure. The crystallites are often ordered (Plates 21:B,C,F,H and 22:B). This conforms grossly to cubic close-packing and corroborates observations by Kalliokoski and Cathles and Rickard, who postulated that electrostatic surface effects controlled agglomeration (127, 187).

Inclusions

These are common where overgrowths of pyrite are present and probably were trapped during crystal growth.

Grain boundary relations

Euhedra are dominant with well developed crystal faces. Replacement only occurs with zoned and colloform pyrite.

b) Chalcopyrite: CuFeS_2

A greatly increased tendency towards ductile behaviour is shown by chalcopyrite in relation to pyrite. This fact, together with a major affinity for the more siliceous portions of the belt influences the distribution of chalcopyrite. Oxidation and secondary enrichment effects are locally important.

Consideration of the pyrite paragenesis illustrates that textures indicative of leaching and remobilization are present. Although the original textures of chalcopyrite may have been partially or wholly obliterated by recrystallization, the assemblage is described and in the following discussion, tentative deductions about the form and nature of the various concentrations of copper are made.

(i) Pyritic zones

Chalcopyrite occurs as an interstitial cement to pyrite grains and aggregates; infilling the pore spaces formed by leaching activity and partial replacement of primary pyrite (Plate 24). Remobilized, it occurs as infillings in crosscutting fractures and shears (Plates 12:G and 25:F). Rim and zonal replacement of pyrite is common.

Etching reveals the fabric (Plate 25). The grain size is highly variable, but dominantly is 0.1-1.0 mm, as equidimensional grains. In secondary shears and infilling pressure fringes around pyrite, the grains are elongated parallel to the foliation. (There is no evidence of translation during growth of chalcopyrite in pressure fringes, and the equigranular, directional fabric suggests that crystallization took place within a tensional environment.)

Deformation

Twinning is almost universal and both lamellar and polysynthetic types are common (Plate 25). Chalcopyrite,

infilling late stage cross-cutting fractures, is twinned thus the association between twinning and zones of deformation, noted by Ramdohr (179), is substantiated, Lampard (138) demonstrated, however, that twinning could occur in chalcopyrite which had crystallized in an open space, and so precise implications are impossible.

Inclusions

Inclusions are rare and usually consist of blebs of sulphosalts, native bismuth or gold. Chalcopyrite is included in pyrite, intergrown with pyrrhotite.

Grain boundary relations

Covellite replaces chalcopyrite in the zones of oxidation (Plate 41:G). Relationships with galena and sphalerite are considered under the headings of these minerals.

(ii) Siliceous zones

Concentrations of copper show a consistent average tenor of $\sim 1.0\%$ Cu. The optical characteristics, and fabric of chalcopyrite are similar to that in the pyritic zones, but the matrix is siliceous. The textures are illustrated in plate 25:A,B. Replacement of fractures in pyrite grains by chalcopyrite is ubiquitous.

The grain size, revealed on etching, varies about a mean of 0.5 mm (Plate 25:B). The majority of grains are equidimensional, untwinned and recrystallized. The twinning appears to be simple and not translational.

Deformation characteristics in plate 19, illustrate that chalcopyrite in slickensided zones is strongly twinned. Glide and translation twinning is developed in this case, and good examples of shredded and bent twin lamellae exist (Plate 19:F,G,H).

Inclusions of sulphosalts and native bismuth, as ovoid blebs and segregations, are rare.

Grain boundary relations

Mutual boundaries occur against milky quartz (Plate 24:H). Minor threads of chalcopyrite sometimes penetrate the quartz

grain boundaries.

(iii) Lead-zinc zones

The major occurrence of chalcopyrite is as exsolution blebs in sphalerite, and as irregular segregations at grain boundaries between the sulphides, plate 28:B. The grain size is generally less than that in the other zones: ranging from 0.025 mm to 0.1 mm. Equidimensional grains are common and twinning is minor.

Replacement relationships by chalcopyrite against sphalerite are those expected from an exsolution product (Plate 28:B), and mutual boundaries against galena are common. (This may not illustrate a paragenetic feature, but a close similarity in ductile behaviour).

(iv) Magnetite zones

Chalcopyrite occupies the interstices between magnetite crystals and is similar to that in the pyritic zones. The grain size is variable, with a mean value of 0.5 mm (Plate 30:I). Equidimensional, generally untwinned grains are common. In schistose material the grains are elongated parallel to the foliation, having recrystallized in a tensional field. No deformed twin lamellae exist.

Grain boundary relations suggest chalcopyrite is of later generation than magnetite. Poikilitic magnetite crystals are infilled and embayed by chalcopyrite, probably remobilized during metamorphism.

(v) Disseminated and vein-type mineralization

Threads and stringers of chalcopyrite, with pyrite, are disseminated in the country-rocks, in a chloritic, siliceous or graphitic matrix. Grain size is variable; ~ 0.5 mm, and twinning is minor. The grains are often elongated parallel to the foliation.

Grain boundary relations suggest pencontemporaneous crystallization of chalcopyrite and chlorite, although in certain areas chlorite needles cut across grain margins of

chalcopyrite. Inclusions of other sulphides occur as blebs at grain boundaries.

c) Sphalerite: ZnS

The physical properties of sphalerite are one of the principle controls over the mode of occurrence. The tendency towards ductile behaviour is slightly less than chalcopyrite and much less than galena. Sphalerite is the same generation, or slightly later, in the paragenetic sequence than chalcopyrite and obviously later than pyrite (Fig. 2.26). The colour varies from russet to a deep red-brown, remobilized material being lighter in colour. Characteristic reddish internal reflections are common. Neither zoning nor colloform textures occur and no wurtzite was identified.

(i) Pyritic zones

Sphalerite is interstitial to the pyrite grains, infills open spaces and strongly replaces zoned crystals (Plate 26:A,B). Internal replacement of zoned pyrite by sphalerite produces striking textures (Plate 27).

Etching reveals a variable grain size, dominantly within the range 0.1-1.0 mm, occurring as aggregates of rounded to polygonal grains. There is a tendency for the finer grained material to concentrate at seam margins.

Deformation produces granulation and a decrease in sphalerite grain size, and has been referred to be McDonald (146). Porphyroblastic undeformed sphalerite within sericite schist, sometimes occurs with pressure fringes infilled by galena (Plate 28:E,F), illustrating the difference in ductile behaviour between the two sulphides.

All sections of sphalerite show marked twinning. Normally, simple and polysynthetic twin lamellae (parallel to (111)) are developed. Evidence for dislocation of twin planes is minor, but examples are in plate 28.

Inclusions of chalcopyrite are universal in primary sphalerite and are absent in remobilized material (Plate 26:F). This factor may explain the anomalously high iron contents

recorded in the spectrographic analyses of primary sphalerites and may be the reason for the close correspondence between spectrographic and probe analyses of remobilized sphalerite (p. 184).

Plates 28:B,C and G indicate that chalcopyrite inclusions concentrate at grain boundaries. This is in contrast to Stanton (215) and Ramdohr (179) who stated that twin planes were the site of preferential exsolution. (It can however, be argued that original exsolution along twin planes at Avoca was followed by diffusion to the grain boundaries.) The inclusions are minute, sub-spherical blebs 0.5μ in size, which often coalesce to produce larger allotriomorphic masses. Amounts of exsolved chalcopyrite increase at sphalerite seam selvages, where cooling during crystallization, would have allowed less interstitial iron to be tolerated within the sphalerite lattice.

Replacement relationships at sphalerite grain boundaries are shown by chalcopyrite, galena and tetrahedrite; and discussed under the headings of the specific minerals.

(ii) Siliceous zones

Sphalerite is a minor constituent of the siliceous zones at West Avoca, with irregular hangingwall and footwall concentrations. At East Avoca the content of sphalerite rises appreciably and it becomes a major mineral. Concordant and crosscutting relationships occur within primary and remobilized material respectively (Plate 26:E,G). Textures are similar to those in the pyritic zones (Plate 26:E and F). The grain size is variable, 0.1-1.5 mm, making up an interlocking mosaic. Twinning is ubiquitous.

Deformation is not common, although twin lamellae are occasionally bent.

Ovoid exsolution blebs of chalcopyrite occur, ranging from sub-microscopic to 1.5μ in size, and concentrate at grain boundaries. Remobilized sphalerite rarely contains inclusions of chalcopyrite. Generally, sphalerite associated with chalcopyrite possesses a large number of inclusions, but, associated with pyrite or quartz, the number is less.

Replacement of sphalerite by exsolved chalcopyrite is

common. Pyrite exists as rounded granules, and when zoned (Plate 26:C) is deeply embayed along zonal boundaries. Characteristic atoll textures develop in intensely corroded (leached) pyrite (Plate 27). In unzoned pyrite the grain boundary is replaced.

(iii) Lead-zinc zones

Sphalerite is the major constituent of these zones and exhibits textures similar to those already described. Primary sphalerite is invariably banded parallel to the foliation and shows minor discordant effects (Plate 12:F). Remobilized material crosscuts earlier structures (Plate 12:I).

The grain size is variable, and in monomineralic seams, the grains may reach diameters of 2-5 mm. At the borders of individual seams the grain size decreases, often spectacularly. An even aggregate of rounded to polygonal grains is common.

Twinning is almost always present, and simple sectorial twins tend to develop, however, polysynthetic twinning on (111) is still predominant. Dislocation and distortion of twin planes is rare.

Inclusions of chalcopyrite, as ovoid segregations at grain boundaries, are common and of a variable size.

Chalcopyrite, galena and tetrahedrite all replace sphalerite, which in turn corrodes the outlines of pyrite and chalcopyrite.

(iv) Magnetite zones

Trace quantities of sphalerite occur with chalcopyrite (Plate 26:H). The grain size is small: ≤ 0.1 mm euhedral to subhedral and polysynthetically twinned. Minute exsolution blebs of chalcopyrite are common. Deformation textures do not exist, and sphalerite crystallization probably overlapped that of chalcopyrite.

(v) Disseminated and vein-type mineralization

Sphalerite is a major constituent of siliceous vein-type mineralization outside the main mine area, occurring with galena

and chalcopyrite. The grain size is variable (Plate 29:D), about a mean of 100μ , and equidimensional grains are common. A decrease in grain size occurs near vein margins. Twinning is present, but not distinct.

Deformation textures are not present and the assemblage appears to represent a close approach, or reapproach, to equilibrium.

Inclusions of chalcopyrite are frequent, as ovoid blebs and marginal segregations, but they are not as numerous as in sphalerite from other zones. Rare elongate inclusions of pyrrhotite occur in sphalerite at Ballinasilloge, associated with chalcopyrite and galena (Plate 33:D).

Mutual boundary relations occur against galena. Brecciation of included wallrock fragments testifies to the intrusive nature of this mineralization.

d) Galena: PbS

This is the most ductile of the primary minerals. On metamorphism and folding galena tends to migrate into pressure slacks and zones of dilatation, and this influences the mode of occurrence. Galena is one of the final minerals to crystallize, and replaces every other major primary mineral. Sheared 'steel' galena was absent; even in the most highly crenulated material galena has recrystallized with an equilibrium (?annealed) fabric.

(i) Pyritic zones

Almost invariably intergrown with sphalerite, galena forms cusped bodies at the grain boundaries of the enclosing minerals.

Relatively uniform granular mosaics are the common mode, no elongate grains exist. Zoning is absent and the equigranular texture suggests that it is the result of annealing and recrystallization. (Plate 29).

Inclusions do not occur in galena. A careous boundary is often shown by galena against chalcopyrite, and there is

corrosion of sphalerite grain margins, and interruption of twin boundaries. Remobilized supergene galena encrusts a fracture plane in the pyritic zone on 1300 level at West Avoca, associated with chalcopyrite and pyrite.

(ii) Siliceous zones

The grain size ranges from $\leq 0.1-0.5$ mm, but in every case is larger than that of adjacent sphalerite (Plate 29:F). No elongate grains were identified and isolated segregations have cusped outlines. Inclusions and zonal textures are absent. Replacement textures are rare, however, the cores of spheroidal pyrite (Plates 23:I and 34) are occasionally infilled by galena.

(iii) Lead-zinc zones (kilmacooite)

Galena is intimately associated with sphalerite, pyrite and chalcopyrite (Plates 26, 27 and 28). Textures correlate with those in the pyritic zones; the galena occurs as allotriomorphic segregations composed of a polygonal grain aggregate. The mean grain size is 200μ . No inclusions or deformation textures were observed. Cusped outlines are common and pyrite granules have rounded margins.

(iv) Magnetite zones

No galena identified.

(v) Disseminated and vein-type mineralization

Galena is a major mineral in the siliceous vein type deposits (e.g. Ballinasilloga) associated with, or without sphalerite and dolomite (e.g. Ballintemple). Disseminated galena occurs in sericitic and talcose schist at Knockanode. Allotriomorphic masses with a mean grain size of 150μ are common, and cusped outlines are shown against other sulphides and gangue. Complex paragenetic relationships exist, but, in general, galena crystallization post-dates development of chlorite and the wallrock alteration, and is probably contemporaneous with late stage milky quartz. At Ballintemple, galena is encrusted by dolomite.

Zoning and deformation textures were not observed. At

Ballinasilloga an ovoid inclusion of pyrrhotite occurs in galena (Plate 33:E), but otherwise the samples are free of sulphide and sulphosalt inclusions.

e) Magnetite: Fe_3O_4

Magnetite occurrences concentrate in prospects outside the mine area. The effects of metamorphism make dogmatic conclusions about the origin of the magnetite hazardous. The textural relationships are described and tentative deductions made in the later discussion.

Exsolved ilmenite lamellae are absent and the colour is pinkish-brown, implying that the minor amounts of titanium indicated by spectrographic analysis (section 2.3.7.) are held within the lattice. Zoning was not observed within individual grains, but at Knocknamohill cores of chromite with overgrowths of magnetite were identified (Plate 33:F). Martitization often occurs, generally due to incipient weathering, in the grab samples studied.

(i) Pyritic zones

At West Avoca, magnetite occurs as two seams in the footwall of the Pond lode, exposed in the 1047 level W. Drive, extending to the 1300 level, from drill-hole data. Ragged subhedral grains: 0.5-3.0 mm in size exist (Plate 30:A) and appear to have been involved in tectonic events (Plate 30:B) during which the grain boundaries were replaced. The occurrence of magnetite may illustrate former oxidation effects. Inclusions of rounded pyrite granules infill fractures, and chalcopyrite and siderite embay the grain boundaries. Replacement of magnetite by pyrite, chalcopyrite, goethite, siderite and quartz occurs.

(ii) Siliceous zones

Absent.

(iii) Lead-zinc zones

Absent.

(iv) Magnetite zones

Siliceous and more rarely dolomitic, banded iron ores occur in a chloritic schist.

honeyteige: banded magnetite-hematite ore is found, with interstitial chalcopyrite and quartz. Magnetite occurs as subhedral to euhedral crystal aggregates 0.15-0.25 mm in size, and as tabular crystals, pseudomorphing hematite. Wispy hematite replaces magnetite (Plate 30:F), especially in zones of secondary shearing. Interstitial chalcopyrite as allotriomorphic masses infills fractures, cleavages and corrodes the magnetite grains. Selvage alteration to covellite is marked.

A number of occurrences exist on either bank of the Aughrim River Valley. Euhedral and subhedral grains and aggregates of magnetite with a variable grain size; 0.05-0.5 mm, are characteristic. Complex and contradictory relationships between pyrite and magnetite (Plate 30) grains exist; magnetite replaces pyrite and overgrowths of pyrite on magnetite occur (Plate 30:D,J,). Magnetite replaces hematite and is itself replaced by hematite.

A synthesis of the relations appears to be as follows: alteration of primary pyrite, possibly by leaching, produces hematite and hydrated iron oxides (limonite). Metamorphism, to give magnetite, is followed by later overgrowths of pyrite and subsequent martitization.

At Dallard, the ore is banded (Plate 31:H,J) and consists of euhedral to subhedral grains of magnetite which vary in size from 0.02-0.1 mm, siliceous matrix. Banding is due to changes in grain size. Pseudo-graded bedding is illustrated in plate 31:H. Alteration along cleavage planes (martitization) to form hematite laths is rare (Plate 31:I). Grain boundaries are replaced by jasperoid quartz which contains sub-microscopic inclusions of hematite.

f) Hematite : $\alpha\text{-Fe}_2\text{O}_3$

Typically found as a secondary oxidation product, it also occurs as a primary mineral in the magnetite zones, indicated above. Twinning is beautifully developed (Plate 30:G and 31:D), and there is no evidence of zoning.

Euhedral to subhedral tabular laths are common, with an

average grain size of 0.5 mm by 0.1 mm. Deformation of the laths by the pervasive foliation (S_2) is almost universal (Plate 30:H and 31:F). Magnetite pseudomorphs of hematite, are common, and alteration of magnetite produces a second generation of hematite (Plate 30:F).

g) Arsenopyrite: $FeAsS$

Occurs in the pyritic zones, especially the lead-zinc rich areas (kilmacooite) particularly in the upper levels at West Avoca. At Knockmiller a minor pyritic seam occurs, rich in arsenopyrite. This is some distance from the mine, and the paragenetic implications are not fully understood. Elsewhere, the mineral is rare. (Fig. 2.23).

Plate 32 illustrates the textures. The grain size, although variable, approximates to 40μ . Euhedral or subhedra develop and there is zoning (Plate 32:G). Inclusions of galena chalcopyrite and pyrite were probably trapped during crystal growth (Plate 32:D,H). Grain boundaries are planar, but at Knockmiller, corrosion (due to incipient weathering) has been intense.

h) Chromite: $FeCr_2O_4$

Trace quantities occur in the iron ore prospect at Knocknamohill. Rounded subhedral grains are surrounded by an overgrowth of magnetite and the grain boundary is bleached, indicating iron enrichment (Plate 33:F). The grain size is dominantly 0.15 mm. Evidence of zoning, twinning and deformation is lacking.

i) Pyrrhotite: $Fe_{1-x}S$

A rare mineral, which occurs as minute inclusions in other sulphides. In pyritic zones the inclusions concentrate at zonal boundaries in pyrite, with or without associated chalcopyrite (Plate 33:A-C).

Pyrrhotite occurs as allotriomorphic blebs up to 50μ in diameter, in pyrite. Inclusions in sphalerite and galena are confined to Ballinasilloge (Plate 33:D,E). Neither twinning nor zoning were observed. Deformation textures and lamellae

characteristic of unmixing hexagonal and monoclinic forms are absent. The structure and chemical composition are discussed on p.190.

j) Cobaltite: CoAsS

In a single sample, this mineral occurs as a subhedral overgrowth on pyrite (Plate 34) in a matrix of sphalerite. The grain size prohibited detailed study. Trace cobalt contents exist in pyrite (cf. Section 2.3.7.) suggesting that the cobaltite may have originated through unmixing during crystallization or metamorphism.

k) Tennantite - tetrahedrite: $(\text{Cu,Zn,Fe,Ag,Hg})_{12}(\text{As,Sb,Bi})_4\text{S}_{13}$

Argentinian tetrahedrite occurs in the lead-zinc rich portions of the siliceous zones. Characteristic textures are illustrated in plate 35:A-D. Allotriomorphic granular aggregates exist with a variable grain size, with a mean of 30μ . No inclusions are present, twinning and deformation effects are absent, and the grains are associated with chalcopyrite, sphalerite, galena and bournonite.

The composition of tetrahedrite at Avoca is considered further in the discussion.

l) Bournonite: PbCuSbS_3

Rare, always closely associated with tetrahedrite, bournonite occurs as a marginal, and sometimes graphic, intergrowth. The grain size is variable ($20-40\mu$) (Plate 35:A,B) and allotriomorphic grains are common. Twinning and zoning are absent and no indication of deformation exists.

The composition is close to that indicated by stoichiometry (Table 6 see overleaf):

Table 6: Chemical composition of bournonite

Element %	PbCuSbS ₃	1.	2.
Pb	42.4	44.6	43.8
Cu	13.0	13.6	14.2
Sb	24.9	22.7	22.7
S	19.7	19.3	20.5
Total %	100.0	100.2	101.2

1. } E. Avoca, Tigroney, 850L, HW. lode,
 2. } No.1A drawpoint: 5' from entrance. (VW24)

m) Native Bismuth: Bi

A minor accessory mineral occurring as minute blebs within chalcopyrite and pyrite in the copper-rich portions of the pyritic and siliceous zones (Plate 36:A-C). Twin lamellae are obliterated by polishing scratches in the smaller grains but twinning is visible in the larger grains. Zoning is absent and there are no inclusions. An intimate association with other bismuth sulphosalts is evident. Probe analysis confirmed the purity of the mineral. (Plate 36).

n) Bismuthinite: Bi₂S₃

Closely associated with native bismuth, galena and other bismuth sulphosalts, bismuthinite occurs as allotriomorphic grains of variable size (Plate 36:B,C,) included in chalcopyrite. It shows normal optical properties, and is greyish white in colour with a strong anisotropy, becoming more marked under oil immersion. Lamellar twinning sometimes occurs. Inclusions of native bismuth are common and it occurs at the selvage of aikinite grains (see below). Identification was confirmed by probe analysis and x-ray diffraction.

o) Galenobismutite: PbBi₂S₄

Trace quantities occur associated with bismuthinite (Plate 36:D) and also rimming aikinite. Bright grey-white in colour, strong pleochroism and anisotropy are shown. Skeletal

intergrowths with bismuthinite occur (also in Ramdohr(178)). The grains were too small for x-ray study and the composition by probe analysis is tabulated below:

Table 7: Composition of galenobismutite

Element %	PbBi ₂ S ₄	1.
Pb	27.5	24.7
Bi	55.5	58.0
S	17.0	17.0
<hr/>		
Total %	100.0	99.7
<hr/>		

1. Ballycoog; dump at lower adit portal (VW623)

p) Aikinite: PbBiCuS₃

Associated with bismuthinite and native bismuth as selvage minerals, aikinite occurs in one sample from Ballycoog in a matrix of chalcopyrite and pyrite (Plate 35:G,H). Bright, light bluish-grey in colour with a moderate bireflectance of 6.2, from olive-grey to light bluish-grey in air, becoming more marked under oil immersion. Anisotropy is strong with sectorial twinning, well shown under oil immersion. The reflectivity range is 35.0-41.2% at 546nm, and the agreement with Millman's data at 589nm illustrates low dispersion (7). The HV₅₀ range is 159.0-164.4 Kg/mm², determined from six indentations with a load of 50 g on grains of random orientation. This value compares well with published values (152, and 160). There is no prominent cleavage, only allotriomorphic bleb-like segregations occur.

The composition of aikinite from Avoca (determined by probe analysis) is tabulated below, with reference to that of the ideal formula and samples from Sweden (249).

Table 8: Composition of aikinite

Element %	PbBiCuS ₃	1.	2.	3.	4.	5.
Pb	36.0	29.8	28.2	33.5	26.0	22.1
Cu	11.0	8.4	7.6	10.0	7.5	6.5
Bi	36.3	44.4	45.9	37.0	44.5	53.0
S	16.7	17.6	17.8	19.5	22.0	18.4
Total %	100.0	100.2	99.5	100.0	100.0	100.0

1. Aikinite, Ballycoog; dump at lower adit portal (VW623).
2. " " " " " " " "
3. Aikinite, Gladhammer, Sweden, from Welin (249).
4. Hammarite, " " " " " "
5. Lindstromite " " " " " "

X-ray diffraction data are given in table 9.

The diffraction data compared with Welin's results indicate that aikinite from Avoca has an intermediate composition between lindstromite and aikinite from Gladhammer, and this is corroborated by the probe analyses. A correlation was found by Welin (249), between composition and the d_{220} spacing for minerals in the bismuthinite-aikinite series, and the Avoca analyses are plotted in relation to the data in Figs. 2.25A and B.

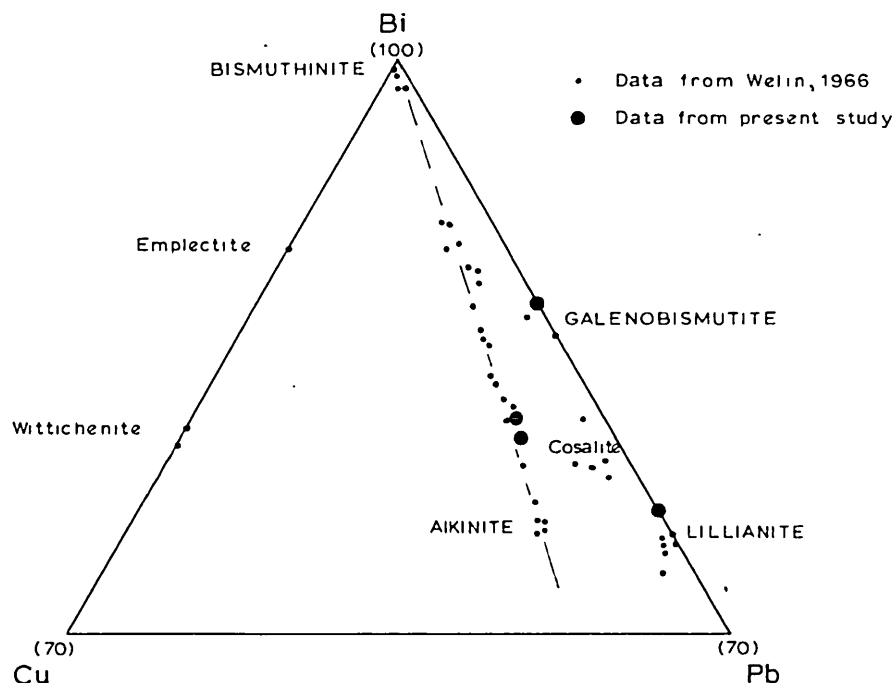
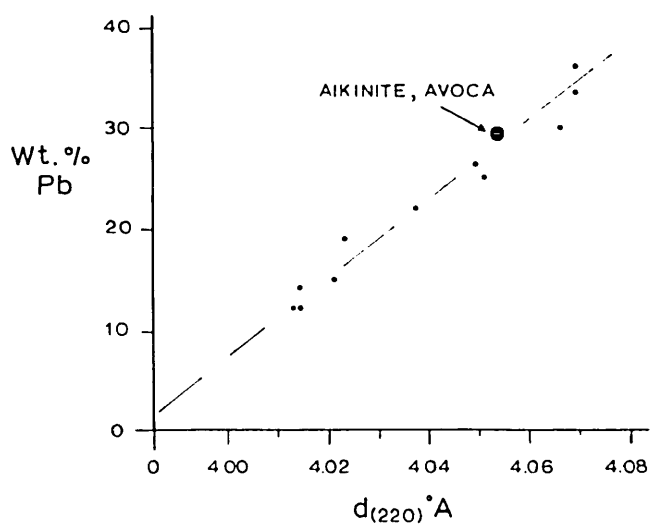
q) Kobellite: $\text{Pb}_2(\text{Bi,Sb})_2\text{S}_5$

Kobellite is a rare bismuth sulphosalt which occurs with native bismuth, bismuthinite and tetrahedrite, or alone, in a matrix of chalcopyrite or sphalerite (Plate 35:E,F). It is bright, light grey-white in colour, with a reflectivity range of 32.9-38.7 % at 546 nm, agreeing well with Millman's data at 589 nm and illustrating a non-dispersive nature. Bireflectance in air is 5.8, becoming more marked under oil immersion. The anisotropy is less than that for aikinite, but distinct. The HV_{50} range is 132.1-136.2 kg/mm^2 . These values agree with data from Millman (152) at 100 gm, and confirm the results in (105). Sectorial twinning is conspicuous. Allotriomorphic blebs and lath-like grains contain inclusions of chalcopyrite, native

FIG 2.25

BISMUTH SULPHOSALTS FROM AVOCA

A. Compositional diagram: (Wt %)

B. Lead content and the $d_{(220)}$ spacing in the bismuthinite - aikinite series:

(After Welin, 1966)

Table 9. Comparative x-ray powder diffraction data for aikinite

Lindstromite (249)		Aikinite Avoca: CuKa		Aikinite (249)		hkl [#]
d(Å)	I	d(Å)	I	d(Å)	I	
4.836	2	-	-	4.862	1	-
4.037	4	4.05	4	4.069	4	220
3.790	3	3.81	1(b)	3.820	3	101
3.656	8	3.67	9	3.716	9	130
3.603	7	-	-	3.626	6	111
3.568	8	3.59	9	3.600	8	310
3.305	3	3.31	1(b)	3.328	2	021, 201
3.172	8	-	-	3.194	9	121
3.151	10	3.17	10	3.171	9	211
2.898	1	-	-	2.915	1	040
2.849	10	2.85	9	2.870	10	221
2.809	1	-	-	2.840	1	140
2.743	2	2.75	1(b)	2.764	2	301, 410
2.668	6	2.68	6	2.713	6	131, 330
2.578	6	2.59	6	2.594	5	240
2.528	3	2.53	2(b)	2.553	3	420
2.497	3	2.51	1(b)	2.513	4	231, 321
2.351	4	2.36	3	2.366	3	041
2.298	3	2.30	3	2.314	2	141
2.258	4	2.27	3	2.278	5	340
2.235	1	-	-	2.250	2	510
2.168	2	-	-	2.183	2	241
2.140	3	-	-	2.157	4	421
-	-	-	-	-	-	250
-	-	-	-	-	-	520
2.011	6	2.02	4	2.024	6	440
1.979	5	1.977	4	1.993	5	431, 341
1.961	1	-	-	1.979	2	501, 151
1.943	3	1.947	4	1.959	5	112, 530

[#] Indices from (249)

bismuth and bismuthinite. A distinct cleavage exists, parallel to included chalcopyrite lamellae.

The composition of kobellite, by probe analysis, is shown below in relation to the ideal formula:

Table 10. Composition of kobellite

Element%	$Pb_2(Bi,Sb)_2S_5$	1.	2.	3.	4.
Pb	44.4	47.1	53.1	51.4	53.2
Cu	≠	0.9	1.9	2.4	1.0
Bi	29.9	32.1	19.8	22.3	37.6
Sb	8.6	4.5	8.2	7.1	9.6
S	17.2	15.7	17.3	16.4	18.6
Total %	100.0	100.3	100.3	99.6	100.0 [*]

1. West Avoca, South Lode, 995L. (collected by W.J. Lampard).

2. " " DDH 1670-35A-163'. (VW.235B)

3. " " " " "

4. Hvena, Sweden (Anal. J.C. Rucklidge in (105))

≠ (0.5% Ag and 0.6% Fe also found)

X-ray diffraction data obtained from sample 1 are given in table 11.

Harris, et al (105) demonstrated that kobellite is a member of a solid solution series with the general formula $5 PbS.4(X_2)S_3$ where X is Bi and/or Sb. The Bi:Sb ratio in the Avoca sample is >1.1 and thus, it is a true kobellite.

Diagnostic d spacings, with intensities in parentheses, compared with material from Hvena, Sweden are as follows:

Hvena (105)	:	3.54(10)	3.41(10)	3.27(4)	2.72(5)
Avoca	:	3.57(2)	3.42(10)	3.29(7)	2.74(2)

r) Lillianite: $Pb_3Bi_2S_6$

Lillianite occurs (Plate 38) in a single sample from the Central lode at West Avoca, with chalcopyrite and sphalerite, enclosed in tetrahedrite within fractured pyrite. The lillianite

Table 11. X-ray powder diffraction data for kobellite

Kobellite			
Avoca		- CuK α	
<u>d(\AA)_{meas}</u>	<u>I</u>	<u>d(\AA)_{meas}</u>	<u>I</u>
4.54	3(b)	1.908	3
4.23	3(b)	1.863	2
3.93	3	1.819	3
3.82	3	1.788	4
3.77	3	1.745	4
3.65	2	1.711	4
3.57	2	1.685	$\frac{1}{2}$ (B)
3.42	10	1.643	1(B)
3.29	7	1.536	$\frac{1}{2}$ (B)
3.18	2	1.482	2(B)
3.14	2	1.460	$\frac{1}{2}$
3.03	3	1.443	2
2.96	6(b)	1.427	$\frac{1}{2}$
2.89	4	1.325	3
2.82	4(b)	1.308	$\frac{1}{2}$ (B)
2.74	2(b)	1.288	$\frac{1}{2}$ (B)
2.62	$\frac{1}{2}$ (b)	1.227	$\frac{1}{2}$
2.56	$\frac{1}{2}$ (b)	1.209	1
2.37	2	1.191	$\frac{1}{2}$
2.32	2		
2.27	2		
2.15	6		
2.09	6		
2.03	6		
1.988	1		
1.961	1		

grain is ragged and allotriomorphic, bright light grey-white in air, with a reflectivity range of 36.4-41.0% at 546 nm, and shows a moderate bireflectance of 4.6. Anisotropy is strong in both air and oil, and twinning exists. No microhardness determination was possible due to the limiting size of the grain.

Probe analysis of several points within the grain gave the composition set out in Table 12, contrasted with other published data:

Table 12. Composition of lillianite

Element %	Pb ₃ Bi ₂ S ₆	1.	2.	3.
Pb	50.5	48.2	45.2	41.8
Bi	33.9	34.4	36.9	36.6
Cu		1.1		2.8
Ag			1.1	1.5
S	15.6	15.8	16.7	15.7
Total %	100.0	99.5	99.9	98.4

1. Lillianite, Gladhammar, Sweden from Palache et al (172).
2. Lillianite, W. Avoca; DDH. 1670-32-65'. (VW234B)
3. Neyite, Alice Arm, British Columbia, from Drummond et al.(74).

Neyite is a recently identified Pb-Cu-Bi sulphosalt from British Columbia (74). The similarity of the analyses of neyite and lillianite from Avoca imply equivalence, but x-ray data are necessary for confirmation, as lillianite from Gladhammar was shown to be a mixture of galenobismutite and galena (25).

The size of the grain at Avoca hindered x-ray identification, and a very indistinct pattern was obtained, on which only the following four lines could be measured (intensities in parentheses): 3.41^oA(4), 3.03^oA(3), 2.92^oA(2) and 2.81^oA(10). These lines do not permit positive identification.

s) Ullmannite: NiSbS

This rare mineral occurs in one sample from disseminated mineralization found at Moreshill (see Map 1, sheet 3).

Ullmannite (Plate 39) forms a selvage to chalcopyrite within

poikiloblastic pyrite in black, carbonaceous, slate (Plate 39:A). The mineral is bright white in colour with reflectivity in air at 546 nm of 43.2%, agreeing well with Millman's data at 589 nm and showing it to be non-dispersive. It is isotropic under crossed nicols and there is no zoning.

The composition determined by probe analysis and the x-ray results are in table 13:

Table 13 (a) Composition of ullmannite

Element %	NiSbS	1.	2.
Fe		0.2	0.6
Ni	27.6	28.2	27.0
Co		tr	0.2
Sb	57.3	55.7	54.0
As		0.8	1.9
S	15.1	14.6	15.1
Total %	100.0	99.5	98.8

1. Ullmannite, Sardinia, in Palache et al. (172).
2. Ullmannite, Avoca, Moreshill shaft dump. (VW520B).

(b) Comparative x-ray data for ullmannite

A		B	
I	d Å ^o (meas.)	I	d Å ^o (meas.)
vw	2.89	6	2.88
w	2.60	10	2.59
w	1.73	8	1.74

A = Ullmannite from Avoca district. (Sample 2, above)

B = Ullmannite from Berry and Thompson (25)

The presence of significant iron, cobalt and arsenic in ullmannite confirms the statement by Palache et al. (172), that substitution by these elements is common.

t) Gold: Au

A trace amount of gold occurs in one sample from the hangingwall of the Main Sulphur lode at Tigroney as an ovoid

bleb of electrum included in chalcopyrite infilling a fracture within pyrite (Plate 40). The minute size of the grain precluded the possibility of obtaining any reliable data on zoning, deformation and other internal properties. Probe analysis of the grain was carried out and the results are shown below:

Table 14. Composition of gold

Element	%
Au	72.5
Ag	17.4
⌘ Cu	0.7
⌘ Fe	4.8
⌘ S	4.6
<hr/>	
Total	100.0
<hr/>	

(⌘ Contaminants)

E. Avoca, Tigroney, M. lode, 850L, Nol.dwp. (VW10)

This analysis confirms Gay's (90) statement that gold may contain many trace elements, the commonest amongst which are Ag, Cu, and Fe. Amounts of Fe and Cu are usually <1% and the combined total of any others also <1%. The anomalous iron and sulphur values are probably explained by the gold occurring at the pyrite grain boundary, included in chalcopyrite, and scattered radiation is the source of the values.

2.3.6.5. Supergene Minerals

The major primary mineral in the Avoca district is pyrite, with or without chalcopyrite, sphalerite, galena, and magnetite. Thus, hydrated iron oxides and covellite are the dominant supergene assemblage. Outcropping mineralization gave rise to extensive surface gossans, but ancient iron ore (ochre) workings have removed the majority of this material. (One large boulder of gossan occurs close to the ancient tramway from Ballymurtagh to Avoca). Subsurface oxidation has not been intense, but effects exist to a depth of about 200 ft below the surface and also in and

adjacent to fissures exposed in underground workings at considerable depths. The fissures are often waterfilled below the water-table (approximately equivalent, in the West Avoca Mine workings, to the 1500 level) and above this, supergene minerals encrust the fracture walls. Within the mined ground, there is intense leaching on the 720 level at West Avoca (Map 3). At East Avoca supergene effects are more marked and have been recorded at depths of 200 ft, whilst old mine records note a steatic clay layer below the ochre gossan.

a) "Limonite" : $\text{FeO.OH.nH}_2\text{O}$

Limonite is the ubiquitous product of oxidized sulphide material, and consists dominantly of goethite with minor to trace amounts of hematite. Characteristic of the oxidized zones, limonite coats the roofs and walls of old mine workings.

b) Goethite : $\alpha\text{-FeO.OH}$

Goethite occurs as botryoidal and reniform masses and isolated acicular crystals. Colloform textures are common and pseudomorphs of pyrite and magnetite sometimes exist.

c) Hematite : $\alpha\text{-Fe}_2\text{O}_3$

Supergene hematite, is a product of the oxidation of magnetite through martitization, and commonly occurs along the octahedral cleavage (Plate 31:I).

d) Covellite: CuS

The major product of the oxidation of copper-rich zones (Plate 41:G). Covellite replaces chalcopyrite as allotriomorphic granular masses at grain borders and fractures, and also occurs as a cementing medium in highly oxidized pyritic ore. Guided replacement of chalcopyrite is rare, and no twinning or zoning of grains exists. Ramdohr noted (179) that covellite occurs at the limits of the zone of oxidation - giving rise to the "black copper ore" of the ancients. This is often mentioned in old reports at Avoca (e.g. 169).

e) Marcasite: FeS_2

Characteristically, marcasite encrusts fracture planes

within the pyritic zones (Plate 41:B-F). A minor supergene mineral, it occurs only in dry fissures (mainly above the level of the present water-table). The grain size is variable, 0.1-0.3 mm, euhedral to subhedral, and marcasite encrusts all the primary minerals.

f) Native copper: Cu

The sole occurrence is within a fissure above the present water-table at West Avoca (Pond lode, 1300 L - in the haulage incline) with quartz and clay gouge. In mine openings, where track is left, native copper precipitates on the iron, as filiform masses, from the acidic mine water (e.g. 850 level at East Avoca and 1300 level at West Avoca). The grain size is highly variable, 0.5-1.0 mm, and well formed crystal terminations often exist (Plate 39:A).

g) Malachite: $\text{Cu}_2(\text{CO}_3)_2\text{OH}_3$

Chalcanthite: $\text{CuSO}_4 \cdot 5\text{H}_2\text{O}$

These minerals are surface coatings on copper-rich sulphide ore exposed in the mine workings. Chalcanthite also forms reniform masses and is characteristic of the dryer areas of the workings, probably originating by evaporation of copper sulphate-rich solutions before they intersected the water-table. These minerals are both common in post-mine openings, e.g. southwestern U.S.A. (172).

2.3.6.6. Gangue Minerals

Lampard (138) described the gangue minerals at West Avoca, and this description is still valid. New observations coupled with a synthesis of previous work is given below.

a) Quartz

It has already been shown that three (and possibly more) relatively distinct periods of silicification exist within the wallrocks and these are also present in the ore zones.

(i) Early quartz, which is disseminated and forms seams that parallel the foliation, is dominantly murky white (grey), fine grained: 0.01-0.05 mm, with a granular (saccharoidal)

recrystallized texture. Individual grains have sutured margins and contain scattered fluid inclusions, grains of chlorite, and are strongly strain polarized. Quartz of this type forms the matrix in all the silicified schists and the colouration is thought to be due to admixed chlorite plates. (cf. 34).

(ii) Milky, ramifying seams of quartz which are slightly discordant with the foliation are characteristic of the siliceous zones. The grain size shows an overall increase in relation to the early quartz (0.02-1.0 mm), but a similar granular texture is exhibited. Conspicuous sutured margins are common, the grains are crowded with bubble inclusions and strain polarization is marked.

(iii) Late stage veinlets of quartz, produced during the deformation, are the products of solution, mobilization and recrystallization of silica in fractures and open spaces. The grain size is coarse, 0.5-2.5 mm, and mutually interfering boundaries are common. Strain polarization is shown and bubble inclusions are frequent. The quartz veinlets are characteristic of the siliceous zones and their wallrocks. A number of overlapping periods of faulting accompanied by later quartz infilling are evident.

Etching basal sections of crystalline quartz from open spaces in the mineralized zones, Lampard (138) demonstrated that low quartz was ubiquitous. All the quartz probably formed below its inversion temperature in the Avoca deposits.

b) Chlorite

The nature of the chlorite associated with the mineralized zones has already been discussed (Section 2.3.3.1.,b). Optical properties and analytical data indicate that ferroan and magnesian chlorites are present, with the former being dominant as an oxidized chamositic form. The ease of solution and recrystallization of chlorite explains its occurrence in pressure fringes around pyrite (Plate 9:E) coating late stage foliation planes.

c) Sericite:

Associated with the marginal areas of the mineralized zones and with disseminated medium to coarse grained pyrite, this metasomatic product has been discussed (Section 2.3.3.1.,b). It is a variety of muscovite and occurs as wisps and streaks along the foliation, in addition to infilling the pressure fringes of pyrite grains.

d) Carbonates:

(i) Dolomite occurs as a gangue mineral on the hanging-wall of the lead-zinc rich western portion of the Pond lode at West Avoca, associated with late-stage crosscutting veinlets. Although a remobilized sphalerite and galena occur admixed with dolomite, the dolomite is not thought to be genetically associated with the lead-zinc mineralization, resolving a previous dilemma(138).

(ii) Calcite is rare accessory mineral within the siliceous zones and may have originated through breakdown of the feldspathic constituents.

(iii) Siderite is also rare, and occurs in association with magnetite on the foot wall of the Pond lode on 1047 level at West Avoca. It probably implies a change in Eh and pH conditions during formation of the magnetite zones (discussed further on p.203).

(iv) Smithsonite, recorded by Lampard (138) encrusting pyrite on a fracture plane, is not substantiated by x-ray study of the material; which indicates hydrated iron oxides.

e) "Graphite"

Disseminated pyrite, often exhibiting spheroidal textures, is found with seams of metamorphosed carbonaceous material in the hangingwall of the Pond lode. No carbonaceous partings occur in the ore zones. Crystalline graphite is absent.

f) Apatite

A phosphate-rich horizon occurs in the hangingwall zone of the Pond lode, and whole-rock analyses (Table 2) indicate that contents of apatite within the ore zones are minimal.

g) Leucoxene

Scattered grains of leucoxene occur in the siliceous schists and anomalous concentrations (Table 2) may represent leached (?) basic pyroclastics. Within the ore zones, leucoxene is rare.

2.3.6.7. Discussiona) Introduction

The paragenetic sequence deduced from the mineral textures in the Avoca district is shown in Fig. 2.26. Precise time relations are obscured by the overprinting effects of metamorphism, and a series of interconnected, overlapping events are envisaged.

Intergranular and intragranular features of the mineral fabric are discussed within the context of the ore mineralogy in the following section, and the fabrics of the major minerals are summarized in Fig. 2.27.

b) Pyrite

This is the major ore mineral in the district, making up over 90% of the sulphide material. A number of contrasting morphologies occur and when these are related to ore type and paragenesis, significant facts emerge.

(i) Zoned crystalline pyrite

This is the commonest morphology, and characteristic of the pyritic zones. Euhedral zoning, a ubiquitous feature, is a primary growth fabric and not a product of metamorphic recrystallization.

In a study of the deformation at Rio Tinto, Read (182) experimentally demonstrated the thermal instability of zoning in pyrite by heating at 600°-700°C. At 700°C, under both static and stress-annealing conditions, there was a marked tendency for zoning in pyrite to be obliterated, but at lower temperatures the zoning survived. Graf and Skinner (98) in a recent paper, support this contention. At Avoca (as at Rio Tinto) the temperature indicated for the metamorphism by the wallrock assemblage is $\leq 350^{\circ}\text{C}$, and this is far below the region in which zoning in

AVOCA DISTRICT

PARAGENETIC TABLE

		NATURE OF THE ORE FORMING PROCESS					
		SYNGENETIC	EPIGENETIC	REMOBILIZATION	SUPERGENE		
ORE MINERALS	PRIMARY	Pyrite :					
		Framboidal	—————				
		Colloform	———	-----			
		Zoned, crystalline		—————			
		Unzoned, crystalline		-----	-----		
		Chalcopyrite		—————	—————		
		Sphalerite		—————	-----		
		Galena		—————	-----		
		Magnetite	———				
		Hematite	———				
		Arsenopyrite		-----			
		Chromite	-----				
		Pyrrhotite		-----			
		Cobaltite			-----		
		Tetrahedrite		———			
		Bournonite		-----			
		Native Bismuth		———			
		Bismuthinite		———			
		Galenobismutite		———			
	Aikinite		———				
	Kobellite		-----				
	Lillianite		———				
	Ullmannite		———	-----			
	Gold		-----				
	SUPERGENE	Goethite			—————		
		Covellite			—————		
		Marcasite			—————		
Native Copper				—————			
Malachite				—————			
Chalcanthite				—————			
GANGUE	Quartz :						
	Grey	-----	-----				
	Milky		-----				
	Clear			-----			
	Chlorite	———	-----				
	Sericite		-----	———			
	Dolomite	-----	-----	———			
	Calcite		-----	—————			
	Siderite	-----					
	Graphite	———		———			
	Apatite	-----					
Leucoxene		-----	———				
TECTONIC SEQUENCE		Sedimentation	Hydrothermal activity	D ₁	D ₂	D ₃	Erosion+Uplift

FIG 2.27

SUMMARY OF THE MAJOR ORE MINERAL FABRICS, AVOCA DISTRICT

		MINERALIZED ZONES				
		PYRITIC	SILICEOUS	LEAD-ZINC	MAGNETITE	DISSEMINATED + VEIN
A. PYRITE :						
Grain size(mm)	0.1 - 1.5(Mass) 0.001-0.5(Diss)	0.001-0.5	0.001-0.1	0.001-1.0	0.001-0.5	
Zoning	Common	Rare	Common	Absent	Rare	
Colloform textures	Common	Rare	Common	Absent	Rare	
Spheroidal textures	Common	Rare	Common	Absent	Common	
Deformation textures	———— Minor cataclasis ————			———— Minor brecciation ————		
Inclusions	cp,sl,gn & po	cp,sl & gn	sl,gn & cp	cp,hm,mt	cp,sl,gn	
Grain boundaries	———— Marked corrosion ————			———— Rare corrosion ————		
B. CHALCOPYRITE :						
Grain size(mm)	0.1-1.0	0.5	0.025-0.1	0.5	0.5	
Deformation textures	———— Twinning common ————		———— Twinning minor ————			
Inclusions	———— Sulphosalts ————		Absent	Rare sulphides + sulphosalts		
Grain boundaries	Repl. by cv	Mut.bdy.ag. qtz	Replaces sl Mut.bdy.ag. gn	Replaces mt	Repl. by chl.	
C. SPHALERITE :						
Grain size(mm)	0.1-1.0	0.1-1.5	0.5-5.0	≤ 0.1	0.1	
Deformation textures	———— Twinning + > in grain size ————			Absent	Twinning	
Inclusions	cp	cp	cp	cp	cp, + po(rare)	
Grain boundaries	Replaces py Repl.by cp,gn, + td	Replaces py Repl. by cp	Replaces py+cp Repl.by,cp,gn, +td	———— Repl. by cp ————		
D. GALENA :						
Grain size(mm)	0.2	0.1-0.5	0.2	—	0.15	
Deformation textures	———— Recrystallization ————			—	Recrystallization	
Inclusions	———— Absent ————			—	po (rare)	
Grain boundaries	———— Replaces all other sulphides ————			—	Replaces all other sulphides Repl. by chl.	

pyrite is destroyed. Thus, preservation of original growth zoning in pyrite at Avoca is expected. The results of trace element partition between coexisting pyrite and chalcopyrite (cf. Section 2.3.7.) suggest that non-equilibrium conditions exist in the assemblage, and that complete metamorphic homogenization is absent.

(ii) Colloform pyrite

Botryoidal and reniform growths of layered 'clear' and 'dirty, melnikovitic' pyrite are common in the pyritic zones, especially the oxidized portions. A large variety of textures occur and these display no wide-spread evidence of deformation, such as brecciation etc.. Ruptures which do exist are of late stage origin and were not produced during the major metamorphic episode. Preservation of delicate colloform banding is further evidence that the pyritic layers have been largely unaffected by the metamorphism, a feature noted elsewhere by Stanton (216) and Read (182).

(iii) Framboidal and sub-spherical pyrite

This form represents <5% of the pyrite at Avoca. Framboidal pyrite occurs in the hangingwall carbonaceous schist horizon of the Pond lode at West Avoca. This horizon, involved in a complex reversed fault system, is in a deformation zone, however, the framboidal forms are not altered into elliptical shapes. This feature is also recorded from Rio Tinto (182). Framboidal pyrite occurs within a matrix of sphalerite and galena at East and West Avoca in siliceous zone mineralization. The matrix sulphides have recrystallized, but the framboids are unaffected. Corrosion of framboid outlines is rare, but cores are sometimes replaced by galena.

The resistance of framboidal pyrite to metamorphic effects in matrix sulphides has been noted by Stanton (216) and Croxford (63). Vallentyne (231) demonstrated that the maximum temperature which recent pyrite spherules could withstand without destruction of their morphology was $\leq 440^{\circ}\text{C}$. It is thus unlikely that this temperature was exceeded during the post-depositional history at Avoca.

Sub-spherical microcrystalline pyrite aggregates occur in massive pyrite (Plate 23). This occurrence differs from the framboidal forms discussed above, as there is an increase in size of individual microcrystallites and of the overall aggregate. The pore space in the aggregates far exceeds that in characteristic framboids. The textures suggest that the microcrystallites grew in an 'open space', post-dating formation of primary pyrite, possibly in a fossil supergene environment. Deformation of these aggregates is not observed.

(iv) Unzoned crystalline pyrite

This is characteristic of the siliceous zones. The absence of zoning indicates near-equilibrium conditions at formation. Large grains are rare and thus growth was probably rapid in an unsaturated media (slow growth in a supersaturated media produces large crystals, see below). There is no correlation of unzoned crystalline pyrite with a diagnostic trace element assemblage. Increased resistance to replacement relative to zoned pyrite reflects the intracrystalline homogeneity of unzoned pyrite. Overgrowths of pyrite on zoned material are of clear unzoned pyrite (Plate 14:A,G).

(v) Grain size

The metablastic nature of pyrite in metamorphosed ores has been advocated by Vokes (240) and elaborated by Templeman-Kluit (222). The basis of the hypothesis is the crystalloblastic series: quite simply, a series reflecting the relative internal structural stability of minerals. Many European workers uphold the view that metablastic grains are ubiquitous in metamorphosed Caledonian deposits. Vokes (240) suggested that there was clear evidence that increase in pyrite grain size was parallel to an increase in metamorphic grade within the Norwegian Caledonides, indicated in table 15.

Table 15. Grain size of pyrite in the Norwegian Caledonides

Occurrence	Size	Grade
1. Leksdals	5 μ	Lower chlorite
2. L�kken and Grong	50-200 μ	Greenschist
3. Follidal, Roros and Sulitjelma	mm-cm	Upper Amphibolite

Increase in size of component crystals with equilibrium at progressively higher temperatures is well known in the study of ceramics. Equilibrium conditions are a pre-requisite, however, Vokes applied this criterion to types 1 and 2 above, which have certainly been metamorphosed to temperatures well below the level at which zoned pyrite is homogenized and equilibrium reached. In these cases a different explanation must exist.

The large grains of pyrite in the fahlbands (disseminated zones) surrounding the massive pyrite lenticles in Norwegian deposits indicate slower crystal growth within a system supersaturated with iron sulphide, and are probably not evidence of the dispersal of suitable nucleation sites, as Vokes suggested. The major factor in low greenschist terrain, responsible for increase in size of pyrite grains which are zoned and cannot have been metamorphically reconstituted, is not metamorphic thermal energy, but stable conditions during formation which allowed slow growth of pyrite megacrysts. A study of etch textures in Norwegian ores would probably confirm that zoned pyrite exists in types 1 and 2 in table 15.

Stanton (215) pointed out that paragenetic sequences for stratiform ores were simply a reflection of the crystalloblastic series demonstrating a natural tendency towards attainment of minimum interfacial free energies and equilibrium at grain boundaries. Disseminated pyrite is generally euhedral to subhedral at Avoca, but matrix sulphide-rich seams contain pyrite with strongly embayed outlines. Vokes (241) stated that at Eleikvassli, the order of increasing corrosion between sulphides and gangue was sphalerite, galena, gangue, thus corroborating this study. Stanton, expressed this in a different way (215), by stating that the presence of galena decreased the idiomorphic development of pyrite. The absence of euhedra within matrix sulphides was attributed to recrystallization during metamorphism. In the present context, and probably in the more general one also, the decrease in idiomorphism of pyrite is due to replacement by solutions containing the matrix sulphides developed during ore formation or succeeding deformation periods.

(vi) Cataclasis

The Avoca deposits, long been reputed to lie along a 'shear zone', have been described (138) as showing ample evidence of cataclasis in the mineral textures. Cataclastic features have been ascribed to pyrite. The present study indicates that evidence of true cataclasis is rare, being confined to areas adjacent to slickensided fracture surfaces. These surfaces are coated with a black granular pyritic dust, and if chalcopyrite is also present this has been smeared out along the grooved surface (Plate 19:A). This surface has a recrystallized fabric, generated by mechanically induced ductile deformation. Similar features occur at Rio Tinto (182) and in massive pyrite ore at Skorovass, Norway, as mirrored surfaces.

Cataclasis requires the brittle fracture of pyrite. Robertson (188), Graf and Skinner (98) and others, have presented pertinent data on the behaviour of pyrite and concluded that little evidence existed for plastic behaviour. Pyrite is an extremely brittle substance and has a tendency at confining pressures $>2.5-3$ kb to obtain moderate irrecoverable strains by homogeneous cataclasis. It is relatively insensitive to temperature variation and minor intracrystalline deformation takes place. The strain is obtained by grain fracture and rotation together with compaction of the pore volume. (B.K. Atkinson, pers.comm.). The current work of Price (178) illustrates that crustal deformation must take place at strain rates of 10^{-10} to 10^{-12} sec^{-1} or faster, which are considerably below those predicted from measurements along the San Andreas fault. In addition, the stress available to drive deformation processes under crustal conditions will be <50 bars for faulting, and certainly <1 kb for folding. Under geologically meaningful conditions it is thus unlikely that pyrite will exhibit more than a minimal amount of strain before fracturing, even in the presence of the high pore water pressures thought to have existed in the present environment. Quite large confining pressures are needed to promote homogeneous cataclasis even at temperatures up to 400°C . The pore water pressure in the present

context is close to the confining load pressure in value. Very deep burial and a stress >5 Kb is then necessary for cataclasis. Wholesale cataclastic deformation of pyrite is therefore unrealistic within the geological environment at Avoca. (The effects of chemical mobility have not been enumerated, but are believed to be of minor significance). The large divergence of differential strain rates between pyrite and the other major sulphides, chalcopyrite, sphalerite and galena makes it reasonable that the latter may well have been deformed and recrystallized (see below). Localized brittle failure however, exemplified by slickensided shear planes, occurs and may be caused by a non-uniform stress environment close to the upper limit of the elastic region. This changes suddenly when traced laterally confirming the strictly transient nature of these shears and the inhomogeneity of the mineralization. A feature also noted at Rio Tinto (182) and Skorovass (241). The essential characteristics of a cataclastic texture are illustrated in plate 19:C-E. The majority of textures previously termed cataclastic are therefore now considered to be the products of leaching or, replacement.

(vii) Leached Textures

The recognition of textures indicative of leaching activity in pyritic ores is of relatively recent origin. Read (182) sparked off the hypothesis, and current workers on the etch textures of pyrite, are demonstrating and widening the scope of this theory.

The key factor is the relative porosity shown by pyrite grains and aggregates. (Porosity in this context being equivalent to void volume). Banding in the pyritic zones is due to variations in grain size of the constituent pyrite and to intercalations of chloritic laminae. Within massive sulphide lenticles, when a series of sections is taken normal to the foliation, variations in porosity become noticeable. The magnitude of the porosity is proportional to the amount of leaching that the pyritic material has undergone since formation. Leaching effects are beautifully shown in plates 15 and 16. In zoned

crystalline pyrite the zone boundaries are the lines of least resistance to replacement and, consequently, initial embayment takes place along them. If the grains are unzoned, replacement concentrates at the grain boundary. When melnikovitic pyrite is present in the zonal scheme, this suffers preferential dissolution once the zone boundary has been breached. Cataclasis could not produce similar textures, as fracturing would randomly cut across zonal boundaries and not be controlled by the inhomogeneity of the pyrite granules. Following a scheme devised by Read (182) the characteristics of leached textures are laid out below:

Table 16. Characteristics of leached textures in pyrite

WEAK LEACHING	STRONG LEACHING
1. Low porosity.	1. High porosity.
2. Replacement of zonal boundaries	2. Replacement and often complete obliteration of melnikovitic pyrite and zone boundaries producing atoll textures. Embayment of unzoned crystal margins.
3. Straight sided narrow corrosion channels.	3. Careous, wide corrosion channels.

The overall porosity at Avoca is highly variable, but a crude qualitative zonation across the pyritic lodes can be deduced. An apparent increase in porosity occurs from footwall to hangingwall. Superimposed upon this are many local variations. At the scale of individual lenticles, it is sometimes noticeable that the porosity in the footwall region is greater than that in the hangingwall. Lead-zinc rich zones in the hangingwall of the Pond lode at West Avoca and at Kilmacoo in East Avoca show a notable increase in porosity relative to the corresponding pyritic zones. In siliceous zones the porosity of pyrite is much greater than that in the pyritic areas, and it remains remarkably consistent throughout the zones.

This spatial distribution of leached areas may have some genetic significance (cf. Section 2.3.10). Leached textures are critical in the interpretation of pyritic mineralization, but are

also conspicuous in the zones rich in matrix sulphides, described in the following section.

c) Chalcopyrite, sphalerite, and galena

Each of these minerals shows replacement features against zoned and unzoned, colloform and framboidal pyrite in the major deposits at East and West Avoca, and they are thus considered together.

The tenor of copper is variable, and the presence of leached textures in the pyrite suggests that the copper-rich seams may represent zones of former secondary enrichment. These enriched zones would have succeeded an initial quasi-homogeneous distribution. (The uniform tenor of copper in the siliceous zones may be significant in this respect). Metamorphism resulted in recrystallization of the chalcopyrite and, in certain areas, remobilization into crosscutting fractures.

In the siliceous zones, chalcopyrite replaces pyrite grain boundaries - evidence of the leaching activity of the copper-rich solutions.

The fabric of chalcopyrite in the outlying prospects conforms to that in the central mine area; it is generally interstitial to, and replaces, pyrite or magnetite, having a recrystallized grain mosaic.

Sphalerite and galena occur in the siliceous zones and in the marginal areas of the pyritic zones. The pyrite granules show characteristic leached textures and provide convincing evidence that the lead-zinc rich solutions differed markedly in composition from those that gave rise to the pyritic zones, and were highly corrosive to pyrite.

Atkinson (pers.comm.) has demonstrated that deformation of galena, chalcopyrite and similar minerals is dependent upon temperature. Deformation is largely obtained through intracrystalline mechanisms; gliding and twinning etc., thus, plastic deformation of galena, sphalerite and chalcopyrite may be expected at Avoca. Stanton (215) and Stanton and Gorman (217) indicated that the effects of this deformation are often

obscured by recrystallization, and the textures of the ore minerals at Avoca support this.

In the outer prospects, similar fabric relations occur, but at Ballintemple, late stage dolomite encrusts galena. At West Avoca dolomite on the Pond lode hangingwall crosscuts earlier structures and probably crystallized later in the paragenetic sequence than galena.

d) Magnetite and hematite

At West Avoca, magnetite-rich seams occur in the footwall of the pyritic Pond lode; which, stratigraphically, correlates with the base of this pyritic zone. The magnetite is replaced by siderite which in turn is replaced by the later iron and copper sulphides. The stability relations of the iron minerals are summarized in Fig. 2.32, and a minor change in Eh and pH, with increase in dissolved carbonate could account for this association. The creditability of this increases as growth must have taken place in the near-surface environment, where conditions probably fluctuated.

At Moneyteige, Ballycoog, Knocknamohill and Ballymoneen, siliceous magnetite seams occur. The trace element assemblage (Section 2.3.7.) in the magnetite does not imply a definite origin hydrothermal and the field relationships are not diagnostic. These occurrences may thus be considered with the banded magnetite of Aughrim River Roadside and Ballard. In all cases, the chloritic host rock may be the product of metamorphism of an iron formation, and the oxides sedimentary deposits related in time and space, to the mine area sulphide accumulation. The location of the deposits, marginal to the central area, suggests that they are a differing depositional facies. James (121) in a major study of the environments of iron ore formation, deduced four 'facies': sulphide, carbonate, silicate and oxide. The sulphide facies is represented by the pyritic zones, which occur in a non-granular silicate host rock (chlorite). The magnetite and hematite occurrences may represent the two oxide facies: magnetite and silicates (Moneyteige etc.,) and hematite and jasper (Ballard).

e) Minor Sulphides

Arsenopyrite is closely associated with lead-zinc mineralization and conflicting textural relationships occur with pyrite (Plate 32:A,B,C,E and F). Pyrrhotite universally occurs as an exsolved phase. The sole occurrence of cobaltite has been documented, and it may derive from metamorphism of cobaltiferous pyrite.

f) Tennantite-tetrahedrite

The importance of the tennantite-tetrahedrite mineral series in the Irish base metal province has been high-lighted by the discovery of mercurious tennantite at Gortdrum (256). Tetrahedrite has long been known as a host for silver (172), and thus its occurrence at Avoca is of interest.

Probe analysis of representative samples of tetrahedrite from Avoca is shown in table 17, in relation to analyses from Silvermines, Co. Tipperary, and other Irish polymetallic deposits, at Bunmahon, Tynagh and Keel.

A compositional break exists between material from Avoca, Bunmahon and Silvermines and that from Tynagh and Keel suggesting that tetrahedrite might be a metallogenetic indicator. Samples of tetrahedrite-tennantite from other deposits were analysed and the results are given in table 17, with other published data.

The pilot study suggested that the Irish lead-zinc deposits in Lower Carboniferous strata contained tennantite and that the Caledonian copper-rich deposits contained tetrahedrite. As demonstrated in Fig. 2.28, although a grouping of the data exists, no precise metallogenetic inferences can be made. It is clear, however, that silver concentrates in tetrahedrite, and is absent from tennantite.

g) Precious Metals

The precious metal content of the ore at Avoca has been studied cursorily in the past. There is a dearth of analytical data, but O'Brien (166) concluded that gold showed a statistical correlation with chalcopyrite and sphalerite. This is corroborated

Table 17. Probe analyses of tennantite-tetrahedrite from Avoca and other areas.

Element%	1	2	3	4	5	6	7	8
Cu	34.4	36.7	34.9	34.6	35.5	35.0	39.8	20.4
Fe	4.9	2.2	3.9	3.7	0.6	2.1	2.6	2.5
Zn	2.6	3.9	2.5	2.6	6.5	4.3	5.0	5.1
Ag	1.8	2.2	2.6	2.3	1.6	1.7	≠	18.2
Sb	29.8	29.4	29.8	29.7	28.4	27.3	8.7	25.5
As	1.1	≠	0.8	0.3	0.5	1.9	16.6	≠
S	25.0	26.0	24.7	24.8	24.7	24.2	28.2	28.3 ^a
Total	99.6	100.4	99.2	98.0	97.8	96.5	100.9	100.0

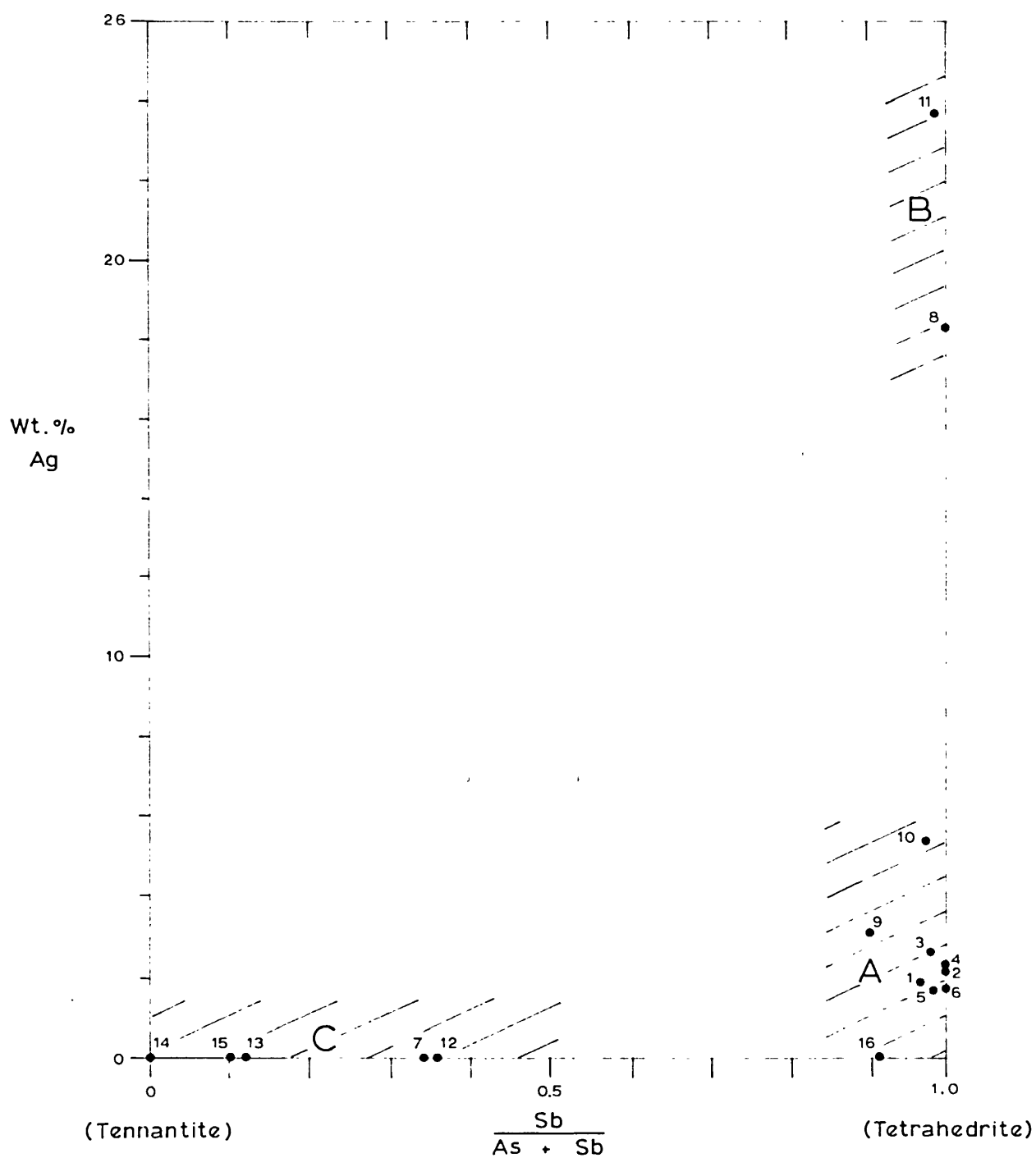
Element%	9	10	11	12	13	14	15	16
Cu	34.7	32.6	16.4	37.9	41.9	41.3	42.3	37.8
Fe	1.7	1.3	0.3	0.6	3.3	6.6	5.6	3.0
Zn	5.7	6.1	≤1.0	8.2	4.3	1.0	1.9	4.4
Ag	3.1	5.4	23.7	≠	≠	≠	≠	≠
Sb	25.1	28.2	30.4	9.1	2.8	≠	2.2	25.0
As	2.7	0.8	0.4	16.2	20.1	23.8	18.9	2.4
S	25.2	24.5	24.1	29.0	29.7	29.1	28.5	25.6
Total	98.2	98.9	≤96.3	101.0	102.1	101.8	99.4	98.2

a = Sulphur calculated by difference
(Analyses 1-5,9,10 and 12-14 by the writer)

1. West Avoca, S.lode, DDH 1670-35A-162'. (VW235A)
2. " " " DDH 1670-35A-163'. (VW235B)
3. East Avoca, Tigroney, HW lode, 850 level, No 1A dwp. (VW24)
4. " " " " " " " " " " "
5. Bunmahon, Ballynarrid, Cliff section. (B.50)
6. Silvermines, Co.Tipperary. (Steed in (173))
7. Tynagh, Co.Galway. (193)
8. Keel, Co.Longford (173)
9. Parys Mountain, Anglesey, Hillside opencast, Bluestone adit dump(38)
10. " " " Morfa-du, Ida shaft dump (P71)
11. Dolgellau, Merionethshire, N.Wales. (91)
12. Buchans mine, Newfoundland. (RSM.2130)
13. Skorovass mine, Grong, Norway, HW of orebody. (Specimen from F.M.Vokes)
14. Bleikvassli mine, Norway, Nordland opencast. (Specimen from F.M.Vokes)
15. Sulitjelma mine, Norway (211)
16. Rio Tinto mine, Spain. (211)

FIG 2.28

TENNANTITE - TETRAHEDRITE MINERALS
from various deposits

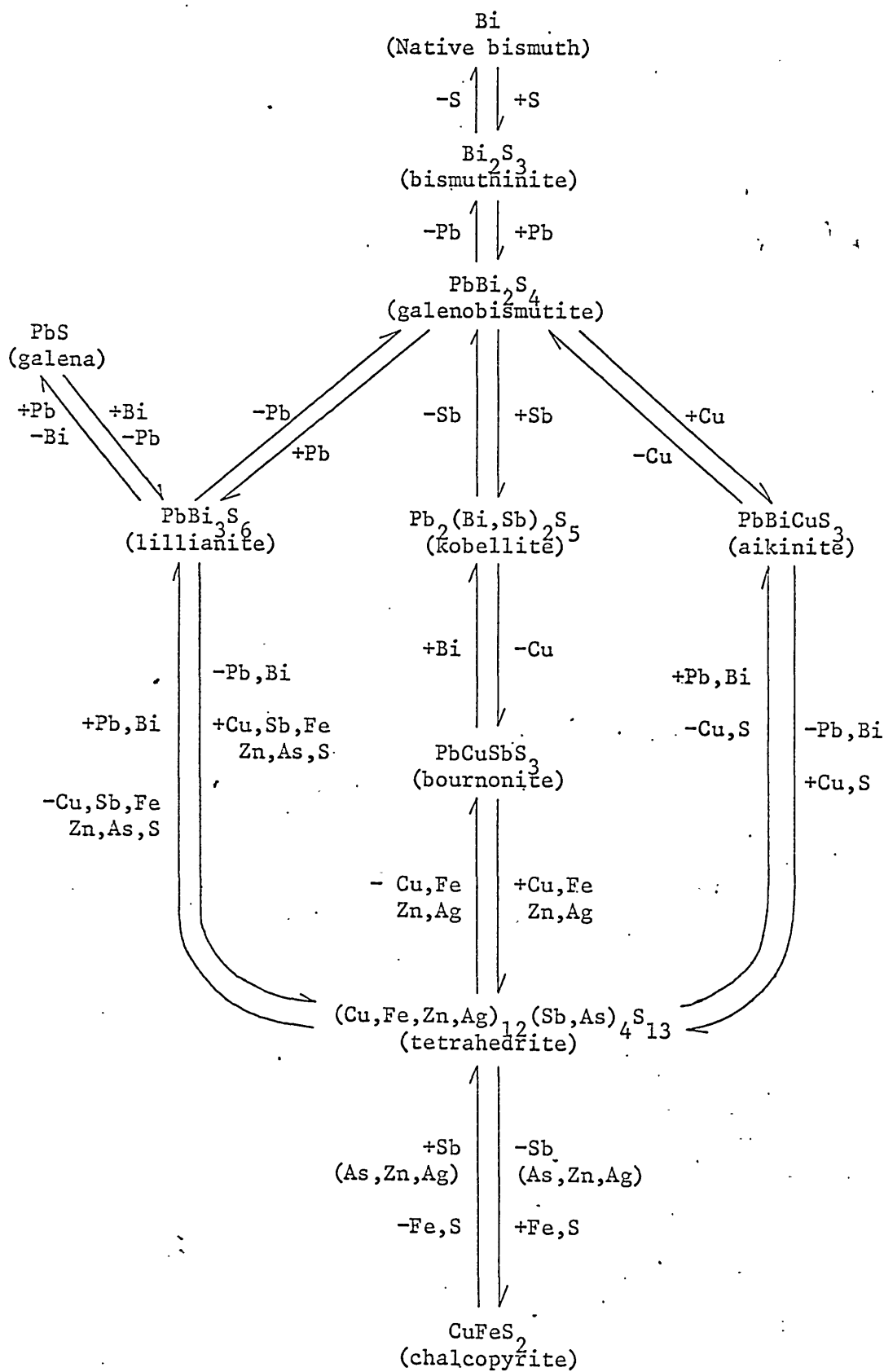


- A Conformable polymetallic pyritic deposits
 B Hydrothermal replacement deposits
 C Tennantites from conformable deposits

(Numbers refer to table 17)

FIG 2.29

CHART OF THE SULPHOSALT ASSEMBLAGE AT AVOCA



in the current study (Plate 40). OBrien also found an association between silver, chalcopyrite and galena. Spectrographic and probe data suggest that the bulk of the silver at Avoca is in galena and tetrahedrite, with traces in bismuth sulphosalts (lillianite). Haughton (108) noted a lead-zinc seam at Connary, supposedly with tetrahedrite, carrying 6-12 oz/ton Ag and 0.5 oz/ton Au.

The textural relations suggest that gold was one of the final ore minerals to crystallize, confirming the stability data.

h) Sulphosalts

Intimately associated with the matrix sulphides, the sulphosalts crystallized during the final stages and the inter-relationships are summarized in Fig. 2.29. The occurrence of a varied suite of bismuth phases and tetrahedrite is a distinctive feature.

2.3.7. Trace Element Distribution

2.3.7.1. Introduction

Applications of the trace element content in sulphides concentrate on the following facets of economic geology:

1. Indicators of ore genesis.
2. Temperature of crystallization of ore assemblages.
3. Distinction between primary and remobilized sulphides.
4. Delineation of metallogenetic provinces.
5. Mineral Exploration.

Information on the distribution of trace elements in the ore minerals from the Avoca district has been obtained in the past from both raw ore and mineral separates. Previous analyses by Lampard (138) of pure samples of pyrite, galena and sphalerite, and by Butler (46) of mine concentrates do not provide satisfactory conclusions to the points above. A series of 140 new analyses have been made by the writer in an attempt to clarify the situation.

2.3.7.2. Method of Analysis

Quantitative determination was made of the following

elements: Ti, V, Cr, Mn, Co, Ni, Ga, Ge, As, Mo, Ag, Cd, In, Sn, Sb, Pt, Au, and Bi with Fe, Cu, Zn and Pb which were sought as contaminant indicators. Ba, and Hg, were determined qualitatively. A D.C. arc optical emission spectrographic method after Bray (37) was employed, using a Hilger Large Quartz spectrograph, E.742. Pure mineral separates were mixed with an equal weight of high purity carbon powder containing 0.04% Pd as an internal standard and burnt to completion at 9A. Spectra were recorded on Kodak B10 plates. A seven-step sector (ratio 2:1) was used for plate calibration. The lines used are given in appendix 3 and densities were read on an A.R.L. microphotometer and converted to relative intensities by means of the self calibration procedure (1). Standards for pyrite, marcasite, chalcopyrite, magnetite and hematite were made by diluting 'specpure' mixes of the elements to be determined, in a ZnS-FeO base. Sphalerite and galena standards were made in a pure ZnS and PbO base respectively. The precision of the method, expressed as a relative deviation, is within $\pm 15\%$. Analysis of the CAAS standard sulphide ore number 1 (A. 1763) is in good agreement with the recommended value (246).

A series of semiquantitative analyses of selected pyrite samples were carried out for selenium by x-ray fluorescence. Approximately 2 gm of pure pyrite powder was pressed into a disc (Appendix 1), and an infinitely thick sample was obtained (165). Analyses were made on a Philips vacuum x-ray spectrograph: PW 1540 using the conditions summarized in table A1 (Appendix 1). Count rates for the samples were compared against those obtained from standards, consisting of spiked Q.M.C. Rock Standards. Matrix effects are admittedly present, making the data semi-quantitative at best, but the constant grain size reduces enhancement effects to a minimum.

2.3.7.3. Results

The results are presented on tables 19-23 (specimen numbers refer to the R.S.M. Spectrographic collection).

TABLE 19/

SPECTROGRAPHIC ANALYSIS OF PYRITE - AVOCA DISTRICT, UNDERGROUND

WEST AVOCA

Sample No.	Locality	Description	Contamination Indicators %			Trace Elements ppm										
			Cu	Zn	Pb	Ti	Cr	Mn	Co	Ni	Mo	Ag	Sn	Bi	Co/Ni	
A.1636	N.lode, 720L; Marg.Adit X-c, HW.	Mass.py, dissem.cp	1.0	*	0.25	1250	*	390	660	22	310	*	150	*	30.00	
1648	" " ; " " " " " "	Dissem.py	0.5	*	*	220	5	620	145	*	30	12	25	*	-	
1944	" " ; 150'W.,X-c, Centre	Mass.py, dissem.cp	2.0	*	0.25	*	*	21	290	6	*	2	99	*	48.33	
1941	" " ; " " " " " "	Mass.py, dissem.gn, cp and sl	*	*	1.5	*	*	68	*	2	30	10	*	*	-	
A.1686	N.lode, S.Branch; 720L Drive E	Dissem.py, cp with qtz	0.5	*	*	47	*	37	135	*	320	6	*	890	-	
1741	" " ; " " " " " "	" " " " " "	6.0	*	*	25	5	60	180	2	660	2	*	500	90.00	
A.1637	P.lode, 720L; Marg.Adit X-c, HW.	Mass.py, dissem.cp	0.5	*	0.25	800	*	54	56	2	38	2	25	*	28.00	
1652	P.lode,1047L; W.Drive, FW.	Mass.mt/hm, dissem.py with qtz	*	*	*	25	5	8	77	*	*	*	*	*	-	
1685	" " ; " " " " " "	" " " " " "	0.5	*	*	68	*	70	142	2	37	*	58	560	71.00	
1843	" " 1300L; W.Drive, FW.	Dissem.py and sl, with qtz	0.5	*	0.5	*	5	42	34	3	30	47	36	12000	11.33	
1730	" " ; " " " " " "	" " " " " "	0.5	*	1.0	33	*	5	120	2	30	19	37	9200	60.00	
1638	" " ; DDH 1332-10'	Banded py, dissem.cp	1.5	*	0.25	730	80	190	*	34	420	2	92	*	-	
1759	" " ; DDH 1332-66'	" " " " " "	1.0	*	*	48	5	50	94	2	215	2	*	500	46.00	
1760	" " ; DDH 1332-79'	" " " " " "	1.0	*	*	48	8	60	98	2	30	4	25	500	49.00	
1761	" " ; DDH 1332-130'	" " " " " "	0.5	*	*	490	8	56	64	2	30	2	25	500	32.00	
1649	" " ; DDH 1338-251'	Dissem.py and mag.	0.5	*	*	230	5	17	83	2	150	2	*	*	41.50	
1905	" " ; DDH 1347-164'	Dissem.py and gn with qtz	*	*	*	88	5	142	10	190	1550	*	*	*	0.05	
1842	" " ; DDH 1354-111'	Dissem.py in graphite schist†	*	*	*	78	*	20	10	178	1000	*	*	*	0.06	
1883	" " ; DDH 1352-143'	" " " " " "	0.5	*	*	38	5	22	28	*	53	*	*	*	-	
A.1653	P.lode,1300L; W.Drive, FW.	Crustiform supergene py, with qtz†	0.25	*	*	55	*	34	102	*	100	6	25	500	-	
1947	" " ; " " " " " "	Crustiform supergene mc, with qtz†	0.25	*	*	44	*	175	147	*	96	*	*	*	-	
A.1727	P.lode, S.Branch; 720L Drive E	Banded py, dissem.cp	0.25	*	0.25	38	*	108	200	*	1200	6	*	*	-	
1728	C.lode, 1670L; DDH 1670-32-65'	" " " " " "	1.5	*	*	34	5	22	175	*	320	6	37	590	-	
A.1737	S.lode, 1670L; 3 X-c S, FW.	Dissem.py and cp, with qtz	0.5	*	0.25	51	5	71	10	*	51	8	*	*	-	
1871	" " ; DDH 1670-15-186'	Dissem.py with cp, gn, sl, and qtz	0.5	*	1.0	*	*	205	*	*	30	41	30	500	-	
1626	S.lode, 1670L; DDH 1670-40-333'	Mass.py	*	*	*	25	5	110	10	*	72	*	*	*	-	
1729	" " ; DDH 1670-35A-163'	Banded py, dissem.cp	1.5	*	*	25	*	98	*	5	53	2	*	*	-	
1845	" " ; DDH 1670-P1-244'	Dissem.py, with sl and gn	*	1.0	1.0	370	5	290	*	*	30	*	25	*	-	
1723	P.lode, 1670L; BWT.Extn.11 X-c S	Dissem.py in micro-diorite dyke†	*	*	*	3750	16	145	600	650	30	2	*	*	0.92	

EAST AVOCA - TIGRONEY

A.1745	Main lode, 850L; No 1 dwp; HW	Banded py & cp, with sl & gn	2.0	1.0	0.75	25	5	94	165	2	320	56	*	300	82.50
1746	" " ; " " " " " "	Banded py, dissem.cp	1.5	*	*	66	*	62	28	2	71	4	*	*	14.00
1747	" " ; " " " " " "	Mass.py, dissem.cp	1.5	*	*	78	*	120	82	2	52	4	*	810	41.00
1748	" " ; " " " " " "	Banded py, cp with qtz	2.0	*	*	57	*	42	115	2	51	10	49	*	57.50
1749	" " ; " " " " " "	Banded py	0.5	*	*	128	*	68	156	2	86	7	34	*	78.00
1750	" " ; " " " " " "	Banded py, dissem.cp	1.0	*	*	62	*	64	172	2	630	10	*	*	86.00
1751	" " ; " " " " " "	Mass.py, dissem.cp	0.5	*	*	25	*	51	285	2	330	5	*	600	142.50
1752	" " ; " " " " " "	Mass.py, dissem.cp	1.5	*	*	29	*	82	203	*	106	10	*	500	-
A.1753	HW.lode,850L ; No 1A dwp; HW	Dissem.py, with qtz	*	*	0.25	590	*	132	23	*	105	7	*	*	-
1754	" " ; " " " " " "	Dissem.py, with qtz	0.25	*	*	330	*	33	10	*	66	2	25	*	-
1755	" " ; " " " " " "	Mass.py, with cp, sl & gn	0.25	1.0	0.25	93	5	48	10	*	190	12	25	*	-
1756	" " ; " " " " " "	Banded py & cp, with qtz	0.5	2.0	0.5	82	*	235	55	*	235	26	25	*	-
1757	" " ; " " " " " "	Mass.py, dissem.cp	2.0	*	0.25	69	*	185	32	*	66	8	25	*	-
1758	" " ; " " " " " "	" " " " " "	2.0	1.0	0.5	25	7	175	37	2	76	14	25	500	18.50
		Detection Limit	0.25	1.0	0.25	25	5	5	10	2	30	2	25	500	

All samples have a matrix of chlorite schist, except †

The following elements were below detection : (limits in ppm) Ga(60), Ge(20), Cd(100), In(700), Sb(100), Ba(100), Pt(50), Au(350) and Hg(500). V. was found in 1649(75 ppm), but was otherwise below detection(50). As. was found in A.1638(2900 ppm), but was otherwise below detection(800).

* = not detected

TABLE 20

SPECTROGRAPHIC ANALYSIS OF PYRITE - AVOCA DISTRICT, SURFACE, WITH COMPARATIVE SAMPLES

AVOCA DISTRICT - SURFACE

Sample No	Locality	Description	Contamination Indicators %			Trace Elements ppm										
			Cu	Zn	Pb	Ti	Cr	Mn	Co	Ni	Mo	Ag	Sn	Bi	Co/Ni	
A.1687	Ballinvalley,E., Sh.dump	Dissem.py, in black slate	*	*	*	880	26	5	137	47	30	2	*	*	2.91	
1724	Moneyteige;SE., Sh.dump	Dissem.py, in grey phyllite	*	*	*	8200	14	66	167	120	30	*	*	*	1.39	
1725	Coolbawn;NE., dump	" "	*	*	*	9500	22	100	220	165	30	*	*	*	1.33	
1762	Ballinvalley;N., dump	Dissem.py, in sericitic tuff	0.5	*	*	127	10	920	50	51	30	2	25	500	0.98	
1672	Knockmiller;W., roadside	Banded py, with asp in sericitic tuff	0.5	2.0	1.0	2220	18	2000	61	130	*	3	*	*	0.47	
1673	Ballycoog;S., lode,dump	Banded py, dissem.cp +	1.5	*	*	98	*	360	900	8	78	2	96	500	112.50	
1674	Ballycoog; " "	Mass.py, dissem.cp +	0.5	*	0.25	118	*	310	260	38	2150	2	*	*	6.84	
1675	Knocknamohill;NE., pit	Dissem.py, in sericitic tuff	*	*	*	120	*	27	680	8	*	*	*	500	85.00	
1676	Killeagh;Cox Sh. dump	Dissem.py, in graphite schist	*	*	*	*	*	69	10	235	*	*	*	*	0.04	
1773	Ballymoneen;Stockpile	Mass. mt/hm, dissem.py +	0.5	*	*	78	5	800	143	98	30	*	*	500	1.46	
1774	Ballymoneen;Eng.Sh.dump	Mass. py, dissem.cp +	1.5	*	*	210	5	5	110	2	43	4	28	500	55.00	
1726	Kilcashesl;W., dump	Dissem.py, in sericitic schist	*	*	*	215	*	46	146	*	97	*	82	*	-	
1742	Kilcashesl;E., dump	Dissem.py, " " "	*	*	*	25	5	16	150	2	71	2	105	*	75.00	
1743	Kilcashesl;E., dump	" " " "	*	*	*	255	5	49	760	2	110	*	470	630	380.00	
1782	Ballymurtagh;E., dump	Dissem.py " " "	*	*	0.25	84	5	18	465	2	115	*	*	*	232.50	
1870	Ballymurtagh;E., dump	" " " "	*	*	*	*	5	5	250	2	30	*	*	*	125.00	
-	-	-	-	-	-	-	-	-	-	-	-	-	-	-	-	
A.1650	Castle Howard;N.lode, adit	Mass py, dissem.cp +	*	*	*	147	5	14	*	*	*	*	*	*	-	
1781	Kilmacoo;Cross Roads Sh. dump	Banded py, with gn & sl +	*	*	*	99	5	23	10	2	30	8	*	*	5.00	
1677	Sroughmore;Glebe Adit dump	Dissem.py, in sericitic schist	*	*	*	345	*	5	10	*	*	2	*	*	-	
1684	Sroughmore;Road Adit dump	" " " "	*	*	*	660	*	310	*	2	90	*	*	*	-	
-	-	-	-	-	-	-	-	-	-	-	-	-	-	-	-	
A.1948	Ballinacarrig; Quarry	Dissem.py, with cp and qtz	*	*	*	1150	5	150	10	98	30	*	*	*	0.10	
-	-	-	-	-	-	-	-	-	-	-	-	-	-	-	-	
A.1731	Glendalough;Van Diemen's lode dump	Dissem.py, with sl, gn & qtz	*	2.0	1.0	1270	*	48	760	270	77	45	*	*	2.81	
<u>COMPARATIVE SAMPLES</u>																
A.1769	Løkken, Norway; 400m L., Hovedgruben	Mass.py, dissem.cp	*	*	*	25	*	500	*	13	39	20	*	*	-	
A.1768	Folldal, Norway;Copper orebody, Tverrfjellet	Banded mt/hm py, with qtz	*	*	*	25	*	35	20000	54	520	18	*	*	370.37	
A.1771	Skorovass, Norway; 680m L.	Mass.py, dissem.cp and sl	0.5	4.0	*	54	*	36	*	2	35	2	*	*	-	
1772	Skorovass, " "	Mass.py, dissem.cp	0.5	*	*	25	*	18	285	2	33	*	*	*	142.50	
A.1770	Røros, Norway;Storvarts Mine, dump	Banded py, with po	0.5	*	*	110	*	13	255	5	52	5	*	*	51.00	
A.1736	Elba, Italy;	Pyritohedron	*	*	*	880	10	33	320	360	30	*	*	*	0.89	
A.1763	CAAS, Standard Recommended Value(246)	Sulphide Ore - 1	0.5	*	*	8100	1350	2700	500	10000	30	2	*	*	-	
			0.8	*	*	8000	360	1100	510	14000	10	4	3	4	-	
		Detection Limit	0.25	1.0	0.25	25	5	5	10	2	30	2	25	500	-	

+ Samples with matrix of chloritic schist

The following elements were below detection(limits in ppm) : Ga(60), Ge(20), As(800), Cd(100), In(700), Sb(100), Ba(100), Pt(50), Au(350), and Hg(500). V. was found in 1724(115 ppm), 1725(195 ppm), and 1948(200 ppm), 1763(660 ppm), but otherwise was below detection(50).

* = not detected

TABLE 21

SPECTROGRAPHIC ANALYSIS OF MAGNETITE AND HEMATITE - AVOCA DISTRICT, WITH COMPARATIVE SAMPLES

MAGNETITE

Sample No	Locality	Description	Contamination Indicators %			Trace Elements ppm									
			Cu	Zn	Pb	Ti	V	Cr	Mn	Co	Ni	Mo	Sn	Bi	
A.1689	W.AvoCa; P.lode; 1047L; FW	Mass.mt/hm, dissem.py with qtz	0.25	*	*	43	*	*	1775	*	*	*	820	*	
1688	" " " "	" " " " " "	*	*	*	25	*	*	1175	*	2	59	1000	3600	
1786	" " ; 1300L; DDH 1338-251'	Dissem.py and mt	0.5	*	*	110	*	5	3050	*	*	120	25	*	
A.1660	Moneyteige; E.shaft dump	Mass. mt/hm, with qtz & cp	0.5	*	*	260	*	*	250	10	*	45	*	*	
1788	" " "	Mass. mt/hm with qtz	*	*	*	175	50	*	225	10	4	41	*	*	
1661	Ballycoog; N. dump	Mass. mt/hm with qtz	*	*	*	680	100	5	2200	10	2	44	*	*	
1789	" " "	" " with qtz & cp	0.5	*	*	500	290	*	1825	10	10	*	*	*	
1662	Knocknamohill; NE. dump	Mass. mt/hm with qtz	*	*	*	480	570	*	1000	10	16	40	31	*	
1790	" " "	" " " "	*	*	*	400	355	*	1375	*	22	48	*	*	
1663	Ballymoneen; S. dump	Mass. mt/hm with py & dolomite	*	*	*	130	150	55	1500	10	10	68	*	*	
1784	" " "	" " " " " "	*	*	*	750	135	20	3100	30	13	40	*	*	
A.1665	Ballard; dump at opencast	Banded mt,hm, qtz	*	*	*	90	210	10	170	10	18	380	*	*	
1791	" " " "	" " " " " "	*	*	*	25	250	*	290	*	12	78	*	*	
A.1775	Folldal,Norway;Copper orebody,Tverrfjellet	Banded mt/hm, py with qtz	0.5	*	*	25	100	5	530	28	2	610	*	*	
A.1783	Skorovass, Norway; Adit level	Mass.py, mt/hm, dissem sl	0.5	2.0	*	25	63	*	200	*	2	*	*	*	
A.1785	Kiruna, Sweden; Rektor dump	Mass. mt/hm	*	0.5	*	3250	3000	5	1000	41	150	*	*	*	
A.1664	Ballard; dump at opencast	Banded mt, hm, qtz	*	*	0.25	800	116	*	2250	10	2	40	*	*	
A.1787	Kiruna, Sweden; Rektor dump	Mass. hm/mt	*	*	*	94	1700	5	455	*	2	*	*	*	
		Detection Limit	0.25	1.0	0.25	25	50	5	5	10	2	40	25	500	

The following elements were below detection : (limits in ppm) Ga(60), Ge(20), As(800), Ag(2), Cd(100), In(700), Sb(100), Ba(100), Pt(50), Au(350) and Hg(500).

* = not detected

TABLE 22

SPECTROGRAPHIC ANALYSIS OF CHALCOPYRITE - AVOCA DISTRICT, WITH COMPARATIVE SAMPLES

AVOCA DISTRICT

Sample No	Locality	Description	Contamination Indicators %										
			Zn	Pb	Ti	Mn	Co	Ni	Mo	Ag	Sn	Bi	
A.1807	W.Avoca; N.lode S.Branch; 720L	Dissem.py, cp with qtz	*	*	110	29	*	*	30	*	400	500	
A.1818	W.Avoca; P.lode; DDH 1332-66'	Banded py, dissem.cp	*	*	230	210	110	*	1250	5	25	500	
1825	" ; " ; DDH 1332-130'	" "	*	0.25	1000	860	136	2	50	14	113	500	
1803	" ; " ; DDH 1338-251'	Dissem.py, and mt	*	*	138	265	75	2	480	10	25	*	
1641	" ; " ; 1300L W.Drive	Mass.cp in fault zone	*	*	25	5	*	*	30	2	760	3500	
1876	" ; " ; " "	Crustiform crystalline cp & qtz	*	*	*	5	*	2	30	2	620	*	
A.1793	W.Avoca; C.lode; DDH 1670-32-65'	Banded py, dissem.cp	*	*	110	350	10	*	94	4	470	500	
A.1804	W.Avoca; S.lode; 1670L; 3 X-c S	Dissem.py, cp with qtz	*	0.25	52	18	*	2	140	10	335	2000	
1875	" ; " ; DDH 1670-15-186'	Dissem.py, with cp, gn, sl & qtz	*	0.5	230	225	26	2	34	4	310	*	
A.1809	E.Avoca; Tigroney; M.lode, 850L, No 1 dwp	Banded py, cp with sl and gn	*	0.5	93	350	42	*	140	45	135	500	
1810	" " " " " "	Banded py, dissem.cp	*	*	175	340	135	*	120	10	25	670	
1811	" " " " " "	Mass.py, dissem.cp	*	*	125	190	10	*	40	5	340	*	
1812	" " " " " "	Banded py, cp with qtz	*	*	25	15	*	3	30	8	260	*	
1813	" " " " " "	Banded py, dissem.cp	*	0.25	74	300	115	*	620	6	150	500	
1814	" " " " " "	Mass.py, dissem.cp	*	0.25	37	43	*	2	30	21	420	*	
A.1815	E.Avoca; Tigroney; HW.lode, 850L, No 1A dwp	Mass.py, with cp, sl & gn	1.0	0.25	25	30	*	2	30	150	190	*	
1816	" " " " " "	Mass.py, dissem.cp	2.0	0.25	66	360	10	2	126	35	335	500	
1817	" " " " " "	Banded py, dissem.cp, gn, sl & qtz	3.0	2.0	25	220	10	2	30	22	265	*	
A.1792	Moneyteige; E.Shaft dump	Mass. mt/hm with qtz & cp	*	*	97	150	*	*	30	20	*	*	
1690	Ballycoog; S.dump at adit	" " " "	*	*	25	690	40	*	30	5	*	1750	
1829	Ballymoneen; N.Shaft dump	Banded py, cp, in sericitic schist	*	*	82	49	*	*	30	3	400	760	
1694	Kilcashel; E.dump	Dissem.cp in chloritic schist	*	0.25	135	3000	10	36	30	66	275	*	
A.1891	Glendalough; Van Dieman's lode, dump	Dissem.cp in qtz	*	0.25	25	5	*	2	30	10	210	*	

COMPARATIVE SAMPLES

A.1826	Løkken; Norway; 400m L., Hovedgruben	Mass.py, dissem.cp.	*	*	100	70	42	2	48	72	*	*
A.1828	Skorovass; Norway; 680m L.	Mass.py, dissem.cp	*	*	51	5	*	*	30	3	25	*
A.1827	Røros; Norway; Storvarts mine dump	Cp. segregation in chlorite schist	*	*	91	49	51	6	30	28	*	*
		Detection Limit	1.0	0.25	25	5	10	2	30	2	25	500

The following elements were below detection : (limits in ppm) V(50), Cr(10), Ga(60), Ge(20), As(800), Cd(100), In(700), Sb(100), Ba(100), Pt(50), Au(350) and Hg(500).

* = not detected

TABLE 23

SPECTROGRAPHIC ANALYSIS OF SPHALERITE AND GALENA - AVOCA DISTRICT

SPHALERITE

Sample No	Locality	Description	Contamination Indicators %			Trace Elements ppm									
			Cu	Pb	Fe	Ti	Mn	Co	Ga	Ag	Cd	In	Sn	Sb	Bi
A.1882 1894	W.Avooca; P.lode; 1300L.W., Drive(FW.)	Dissem.py & sl with qtz Crustiform sl on fracture	1.0 0.75	0.25 *	6.4 6.3	10 48	320 1000	10 10	47 74	15 14	720 1740	10 205	30 134	100 *	3850 *
1884 1898 1893	W.Avooca; S.lode; DDH 1670-P1-244' " " DDH 1670-15-186' " " DDH 1670-50-750'	Dissem.py with sl & gn Dissem.py with cp, gn, sl & qtz Sl, infilling fracture	1.0 *	0.5 *	4.7 7.1 1.9	660 14 120	1750 280 120	10 80 *	15 10 90	2 9 2	1040 940 1480	10 50 210	215 *	1700 *	* * *
A.1896 1895 1881	E.Avooca; Tigroney; 850L, HW.lode " " " "	Banded py, dissem.cp, gn, sl & qtz Crustiform sl on fracture	0.25 2.0 *	0.5 *	12.9 12.3 0.4	260 60 10	1200 970 46	125 31 10	21 16 10	26 48 11	500 330 2350	132 94 127	350 190	100 100	* * *
A.1877 1892 1878	Ballinasillog; dump at adit Knockmiller; W., roadside Kilmacoo; Cross-roads Sh. dump	Dissem.gn, & sl with qtz Dissem.asp, py, sl & gn in sericitic tuff+ Dissem.sl, gn, py & cp in qtz+	* * 0.5	0.5 0.25 0.5	5.4 6.9 7.8	10 10 66	1000 2200 760	24 *	10 *	33 2	1650 560 1260	340 10 35	* *	* *	* *
A.1885	Glendalough; Van Dieman's lode dump	Dissem.sl in qtz+	0.25	0.25	0.73	10	35	*	150	260	3800	262	*	860	*

SPHALERITE and GALENA

A.1937	W.Avooca; N.lode; 720L, HW.	Banded py, with dissem.cp, sl & gn	M	M	18.0	10	108	127	10	295	*	245	200	*	245
A.1940	" ; Lead-zinc lode; DDH 1047-46'	Banded py, sl & gn Detection Limit	0.25 0.25	2.0 0.25		2240 10	1175 30	*	*	*	10 100	10 10	88 30	100	*

All samples except +, with a chloritic matrix

The following elements were below detection : (limits in ppm) V(10), Cr(5), Ni(5), Ge(10), As(500), Ba(100), Pt(50), Au(350), and Hg(500). Mo was found in A.1895 (68 ppm), but was otherwise below detection when Fe > 10%, 30 ppm and when Fe < 3%, 10 ppm.

GALENA

Sample No	Locality	Description	Contamination Indicators %			Trace Elements ppm									
			Fe	Cu	Zn	Ti	Mn	Co	Ga	Ag	Sn	Sb	Bi		
A.1935	W.Avooca; P.lode; 1047L; HW.	Crustiform gn, with py & mc.	3.7	*	*	17	550	10	10	167	152	570	*		
A.1865	W.Avooca; C.lode; DDH 1670-P8B-123'	Dissem.gn & sl, in sericitic schist	4.0	*	1.0	82	91	*	10	190	300	*	*		
A.1900 1903	W.Avooca; S.lode; DDH 1670-15-186' W.Avooca; P.lode; DDH 1347-164'	Dissem.py with cp, gn, sl & qtz Dissem.py, gn with qtz	10.5 1.5	*	0.5 *	10 *	60 40	27 *	10 15	112 1100	*	30	10000	1300	66
1901 1864	E.Avooca; Tigroney; 850L. HW.lode " " " "	Banded py, dissem.cp, sl, gn & qtz Crustiform gn, with sl	1.5 0.05	0.25 *	1.0 2.0	10 10	360 9	225 *	14 *	41 820	*	30	200 180	*	*
A.1861 1862 1863 1860	Ballinasillog; adit dump Ballintemple; Shaft dump Knockanode; Adit dump Kilmacoo; Cross-roads Sh. dump	Dissem.gn & sl, with qtz Crustiform gn, dolomite and qtz Dissem.gn Dissem.sl, gn, py & cp in qtz	1.4 0.46 2.9 5.3	*	*	73 5000 120 10	41 400 3500 51	*	*	270 500 175 1550	*	*	1000 *	245 1000	*
A.1866	Glendalough; Van Dieman's lode dump	Dissem.gn and sl in qtz Detection Limit	* 0.05	* 0.25	* 1.0	56 10	5 5	10 10	*	185 2	56 30	1250 100	*	50	

The following elements were below detection : (limits in ppm). V(10), Cr(10), Ni(5), Ge(10), As(500), Cd(100), Ba(100), Pt(50), Au(350) and Hg(500). Mo was found in A.1901(96 ppm), but was otherwise below detection(10-30). In was found in A.1864(18 ppm), but was otherwise below detection(10).

M = Major

* = not detected

2.3.7.4. Interpretation

a) Contamination Indicators

Polymetallic base metal deposits often exhibit an intimate association between sulphides. Ore microscopy reveals that pyrite, magnetite, chalcopyrite, sphalerite, and galena at Avoca are closely related. In a paragenetic sequence involving crystallization, solution, mobilization and recrystallization (Fig. 2.26), contaminants in mineral separates are expected.

Recently, Einaudi (80) challenged Fleischer's (87) conclusion that the bulk of the copper in pyrite analyses occurred as admixed chalcopyrite or other copper minerals, by revealing copper zoning in pyrite from Cerro de Pasco. Similar zonation of nickel in pyrite is reported by Constantinou (pers. comm.) from Cyprus and Steed (pers. comm.) from Holloford, Co. Tipperary, Ireland. However, these pyrite samples are unmetamorphosed, and the vast bulk of analysed pyrite has come from deposits similar to Avoca which have been metamorphosed. Metamorphism in the Avoca district has not reached chemical equilibrium, but expulsion of trace copper and other elements to form exsolved phases at grain boundaries, occurs (cf. p.126). Fleischer's contention may apply with metamorphosed pyrite, provided that the grade of metamorphism is below that for homogenization (cf. p.141). A similar deduction can be made for the contaminants in magnetite, chalcopyrite, sphalerite and galena. Values are in per cent, but with the exception of zinc, the elements were determined to their detection limits (Tables 19-23). An excellent correlation exists between the contaminants and the mineral associations in the original specimens. In general, separation has been effective.

b) Pyrite (Tables 19 and 20)

Titanium. The mean value is 92 ppm. Titanium normally concentrates in independent oxide and silicate minerals. Ilmenite (FeTiO_3), titaniferous magnetite, and rutile (TiO_2) account for the bulk of the element associated with basaltic rocks. Titanium values in pyrite may be contributed by ilmenite or rutile inclusions along the zonal boundaries of individual grains,

and trace amounts may be in impurity silica. The high values however, strongly suggest that pyrite can contain appreciable titanium.

Pyrite (A.1723) from the micro-diorite dyke contains 3,750 ppm titanium. The host rock is enriched in titanium (228), implying that the pyrite crystallized within the dyke. There is no previous data on the titanium content of pyrite at Avoca.

Vanadium. The detection limit is rarely exceeded, but 75 ppm was found in A.1649, 115 ppm in A.1724, 195 ppm in A.1725 and 200 ppm in A.1948. Titaniferous iron oxides and magnetite are often enriched in vanadium, and enrichment in titanium occurs with A.1724 and 1725. However, because magnetites at Avoca generally contain <300 ppm titanium and contamination of pyrite by magnetite is <1% it is inconceivable that the titanium in the pyrite is the result of contamination by titaniferous iron oxides or magnetite. Lampard (138) obtained similar results, as did Butler (46). Fleischer (87) admitted that only scanty information on vanadium contents was available.

Chromium. Values in pyrite are generally below the detection limit. A strong octahedral site preference and consequent enrichment in early crystallates from silicate melts is shown by crystal-field theory (64). Concentration in chromite $(\text{Fe,Mg})(\text{Cr,Fe,Al})_2\text{O}_4$ and diopside results in only minor amounts being available for sulphides. The sole high value, A.1638, with 80 ppm may be inherited from the original sediment, due to an increased availability of chromium. On weathering, where the soluble complex ion $(\text{CrO}_4)^{2-}$ is formed, precipitation takes place with metallic ions, especially lead, by adsorption on hydroxides, or, within muds under reducing conditions. Chromium may thus be contained in the pyrite lattice. Enrichment of arsenic and lead in A.1638, emphasizes the possible presence of reducing conditions in the sediment, supporting this suggestion. Butler (46), obtained low values, and the element was not detected by Lampard (138). No independent sulphides of chromium exist, but trace quantities within sulphides have been reported (181).

Manganese. The mean value is 64 ppm. Manganese is not

known to enter iron sulphide. The rare high values are probably either due to incorporation of surface films of MnO_2 during diagenesis, in response to changes in Eh and pH conditions, or to incorporation during metamorphism, as discrete inclusions at crystal and zonal boundaries of silica impurities.

The single sample of marcasite, A.1947 contains 34 ppm which does not corroborate Fleischer's statement (87) that manganese is absent in this mineral. However, the value is low and thus of little significance. Lampard obtained random qualitative values (138), and Butler (46), the higher mean expected from a sulphide mix.

Cobalt. Values are distributed around a mean of 41 ppm. Independent sulphides of cobalt, linnaeite, (Co_3S_4) and cobaltite, $(\text{CoAs})\text{S}$ as occlusions cause high contents in magmatic iron ores and hydrothermal sulphides. Cobaltite occurs in polished section, and inclusions of this mineral may account for the anomalous values. Significant variations are considered further in the discussion.

Nickel The mean is 18 ppm. A low value is implied by the elemental geochemistry of nickel, which indicates concentration in ores associated with early formed magmatic rocks, particularly norites and peridotites.

The significance of absolute nickel values and the Co/Ni ratio are considered in the discussion.

Arsenic. Generally undetected, with the exception of A.1638; 2,900 ppm. This value is due to admixed arsenopyrite, which occurs in polished section. Lampard (138), made no direct determinations because of the insensitive method, and the common presence of arsenopyrite in the upper levels at West Avoca. Butler records (46) arsenic values, and Fleischer regards arsenic in pyrite as indicating impurity (87).

Molybdenum. The mean is 44 ppm. Molybdenum virtually always occurs as the individual sulphide MoS_2 , however, the covalent radius Mo^{4+} (1.291 Å) is close in size to Fe^{3+} (1.165 Å) and Ti^{4+} (1.324 Å) suggesting possible diadochic substitution of molybdenum for iron and titanium. There is no molybdenite, so the element is probably present as a diadochic

substitution for iron in the pyrite lattice. The higher values are close to the upper limit (300 ppm) found in black shales by Vine (235).

Samples from graphite schist, A.1842 and 1883, show an enrichment. This may be similar to the high value quoted by Kaplan et al. (128) in pyrite from a nodule, and also confirms Vine's correlation of molybdenum with carbon content. Wedepohl's note of increased accumulation in near-shore clays (247) is satisfied if the carbonaceous horizon originated as an anaerobic mud in a localized basin of pyroclastic deposition. Fleischer's (87) mean value (10-30 ppm) is of the same order as that at Avoca. No significant spatial variation was detected, adding support to Lampard's (138) conclusion that a vertical decrease in value did not exist in the deposit. Results from concentrates by Butler (46) are similar to those in this study.

Silver. The mean is 6 ppm. Silver dominantly concentrates in the sulphide phase during magmatic evolution, forming sulphides and sulphosalts. The influence of contamination by included galena and/or tetrahedrite is shown by a correlation of high values with lead. Neglecting these anomalous values, the conclusion of Lampard (138), Butler (46) and Fleischer (87) that values of silver in pyrite are low, is confirmed.

Tin. Values are generally below the detection limit. This supports the conclusion of former workers that contents of tin in pyrite are generally low. At high temperatures sulphides can contain appreciable tin, and the results therefore suggest that pyrite at Avoca crystallized at a relatively low temperature. The residue of sample A.1743 (470 ppm), was examined by ore microscopy and microprobe for included tin minerals, but none were detected. Stannite, as inclusions along zonal boundaries in pyrite or within impurity silicates remains a possible source(87).

Bismuth. The majority of the results are below the detection limit, and values are highly erratic. Anomalous values, A.1843 and 1730, are from samples in which native bismuth and bismuthinite are visible in polished section, and a correlation with lead content is evident. This amplifies conclusions of Butler (46), Lampard (138) and Fleischer(87), each of whom invoked contamination.

Selenium. A table of semi-quantitative values is given below:

Table 24. X-ray fluorescence analyses of selenium in pyrite

Sample No.	Locality	Description	Se ppm
A.1636	N.lode,720L;HW at Marg. Adit X-c	Mass.py,diss.cp.	20
1648	" " " " "	Diss.py.	20
1637	P.lode " " " "	Mass.py,diss.cp.	15
1638	P.lode,1300L;DDH 1332-10'	Banded py,diss.cp	≠
1759	" " DDH 1332-66'	" "	10
1626	S.lode,1670L;DDH 1670-40-333'	Mass.py.	≠
1650	Castle Howard lode:Upper Adit	Mass.py,diss.cp.	10
1748	Main lode,850L; Tigroney, Nol dwp	Banded py,cp+qtz	10
1757	HW lode, 850L; Tigroney, Nola dwp	Mass.py,diss.cp.	≠

(≠ not detected)

The results confirm Anderson's (3) conclusion, that selenium contents in pyrite are low.

Ga, Ge, Cd, In and Sb were below the detection limit, confirming theoretical predictions of their absence in pyrite. Boyle (35) reported minor amounts (<10 to 400 ppm) of antimony in pyrite from Keno Hill, however, the presence of coexisting antimony-rich galena and sphalerite implies contamination.

The detection limits for Ba, Pt, Au and Hg were high, and their absence in the analyses is therefore expected.

In table 20 analyses of comparative pyrite samples from other pyritic deposits are shown with results from the CAAS Standard Sulphide Ore-1. Values largely conform to the pattern at Avoca, but there is a wide variation in cobalt and nickel content, and tin is absent. Metallogenetic implications of these facts are considered in the discussion.

c) Magnetite (Table 21)

Titanium. Values surround a mean of 282 ppm. This figure is greater than that in pyrite and reflects enrichment in

the magnetite lattice, there being a continuous relationship between magnetite and the ulvospinel molecule Fe_2TiO_4 (67). The titanium value in magnetite from Kiruna A.1785 (3,250 ppm) is high on account of ilmenite lamellae in the magnetite. At Avoca, samples from unweathered underground material have lower titanium contents suggesting that submicroscopic ilmenite alteration lamellae contribute some of this element.

Vanadium. A mean value of 162 ppm illustrates the known enrichment of vanadium in magnetite with respect to pyrite. Crystal-field theory indicates that there is no octahedral or tetrahedral site preference, so that diadochic substitution of Fe^{3+} (0.64°A) by V^{3+} (0.74°A) may take place. However, camouflage by Fe^{2+} (0.74°A) is the probable explanation for concentration of vanadium in magnetite rather than ilmenite (64). Studies on the Skaergaard minerals confirm this (242). A marked increase occurs in the Kiruna sample: A.1785 (3,500 ppm) illustrating enrichment in titaniferous iron-ores.

Chromium. The mean value of 7 ppm is slightly greater than that in pyrite.

Manganese. The mean value of 1070 ppm is that expected from magnetite forming in a sedimentary environment, as shales contain 850 ppm manganese (228). Rare high values may be due to surface films of MnO_2 incorporated during crystal growth.

Cobalt. The majority of the values are below the detection limit (10 ppm).

Nickel. As with cobalt, the bulk of the values are below the detection limit (2 ppm).

Molybdenum. A mean value of 74 ppm is comparable with the content in magnetite forming in a sedimentary environment. Enrichment in the samples from Ballard and Folldal, Norway, A.1665 and 1775 (380 and 610 ppm respectively) has no identified source, as molybdenite does not occur in polished section. Increase in organic matter in the sediments might give rise to anomalous values. Possible line interference by iron cannot be discounted, and the results are thus of minor significance.

Tin. A mean value of 144 ppm illustrates concentration

of tin in magnetite with respect to pyrite. High tin values are known from many magnetite deposits (69). Polished sections were studied for tin minerals but none were observed.

The elements Ga, Ge, As, Ag, Cd, In and Sb were below detection and Ba, Pt, Au, and Hg were absent.

d) Hematite

Trace elements in hematite from Ballard and Kiruna, Sweden, are given in table 21. Contents resemble those in corresponding magnetites and confirm the elemental geochemistry.

e) Chalcopyrite (Table 22)

Titanium. The mean value of 131 ppm is close to that for samples of pyrite and confirms the similarity in chemistry of the two sulphides.

Manganese. The mean of 359 ppm is much higher than that quoted by Fleischer (87) (10-49 ppm), and the value is excessively weighted by anomalous results which may be due to incorporation of MnO₂ surface films.

Cobalt. The mean value, 33 ppm, is similar to that for pyrite. Auger (10) refers to an increase of cobalt in chalcopyrite with depth at Noranda, however, there is no evidence of this at Avoca.

Nickel. The mean value of 3 ppm is close to the detection limit, and conforms to the distribution shown by nickel in coexisting magnetite and pyrite.

Molybdenum. A definite increase of the mean value, 155 ppm, over that in pyrite. Polished section study failed to reveal molybdenite, and thus chalcopyrite from Avoca contains minor molybdenum.

Silver. The mean, 20 ppm, is unduly weighted by a few high values which correlate with lead content, indicating inclusions of galena or tetrahedrite. The ductility of chalcopyrite is near that of galena, and during metamorphism they will migrate into low pressure areas. Mechanical separation of individual phases may be difficult, and zones of low pressure

containing fine grained sulphide intergrowths may also explain the variations found by Auger (10).

Tin. The mean value of 265 ppm is greater than that in pyrite and magnetite. No tin minerals were identified in polished section, but the high values may be due to minute crystals of exsolved stannite (87).

Bismuth. The intimate association of bismuth sulphosalts and native bismuth with chalcopyrite has been described (Section 2.3.6.) and this gives erratic results.

The elements; V, Cr, Ga, Ge, As, Cd, In, Sb, Ba, Pt, Au, and Hg, were undetected.

Analyses of comparative samples from deposits at Glendalough, Lokken, Skorovass and Roros are also given in table 22. The trace element assemblages show only minor differences from those at Avoca. Titanium and manganese contents are low and the tin value at Glendalough is close to the mean already quoted. The Norwegian samples show no tin enrichment.

f) Sphalerite (Table 23)

Titanium. A mean value of 115 ppm is similar to that in coexisting sulphides. Fleischer (87) suggested that titanium was contributed by silicate gangue, and this is possible in the current samples.

Manganese. The mean value, 880 ppm, is relatively high, but there is a wide scatter. Fleischer (87), Boyle (34) and others, suggested that increase in manganese content paralleled that of iron. At Avoca, remobilized sphalerite (low iron) has a mean content of 390 ppm manganese, and primary material (high iron) contains 1050 ppm, confirming this postulate (Table 26). The reason may be fundamental; remobilized sphalerite, containing less iron than its primary parent, crystallized at a lower temperature. The thermal stability of the zinc blende structure increased at this lower temperature, and acceptance of manganese in the lattice decreased.

Colour variations in sphalerites have been ascribed to changes in iron content, but Manning (147) deduced that the

reddish colour is due to interstitial Fe^{3+} ions. Manganese content has also been suggested as giving colouration. At Avoca, increase in both iron and manganese are paralleled by darkening in colour of sphalerite, thus little further can be deduced.

Cobalt. A mean value of 32 ppm exists. In the past, Fleischer (87) and others, invoked contaminant chalcopyrite as the source of cobalt in sphalerite. At Avoca, chalcopyrite contains a mean of 33 ppm cobalt, and as contamination of sphalerite is generally $\leq 5\%$, this suggestion is not feasible. Sphalerite at Avoca must therefore contain minor amounts of cobalt.

Gallium. A mean value of 27 ppm confirms theoretical predictions of gallium occurring in the sphalerite lattice, on account of a relatively high tetrahedral crystal field stabilization energy (221). Lampard's data (138) gives a higher but similar result, and Fleischer's (87) indication of an increase in gallium with decrease in temperature has some support from table 26.

Molybdenum. 65 ppm was found in A.1895, and Fleischer notes (87) that molybdenum is almost always present in sphalerite in small amounts. (This statement may have originated because of line interference, as sensitivity depends upon the iron content of the sphalerite, as indicated on table 23).

Silver. The mean value, 16 ppm, is probably due entirely to contamination by inclusions of galena or tetrahedrite, and a good correlation with lead exists. Lampard (138) and Fleischer (87) reached the same conclusion.

Cadmium. This is the characteristic element which occurs in sphalerite. The covalent radii of cadmium and zinc are comparable: Cd^{2+} (1.48 $^{\circ}$ A) and Zn^{2+} (1.31 $^{\circ}$ A), and the crystal field stabilization energy for tetrahedral coordination is high, accounting for diadochic substitution of cadmium in the zinc sulphide lattice. The mean value of 1150 ppm for sphalerite at Avoca, confirms these theoretical predictions. Fleischer notes (87) increase of cadmium in light sphalerite with reference to darker varieties. At Avoca, primary sphalerite is burgundy

red, whereas the remobilized form is russet. The mean cadmium value for primary sphalerite is 880 ppm, and remobilized material contains 1850 ppm (Table 26). Groves and Loftus-Hills (101) found no significant correlation between cadmium and iron in sphalerites from Tasmania and the significance of this is considered in the discussion.

Indium. This element is geochemically similar to cadmium, the mean value is 106 ppm, and its presence is also characteristic of sphalerite. Fleischer (87) remarked on a decrease in indium content with increase in iron. The present study corroborates this, however, line interference by iron makes any precise conclusions hazardous.

Few values are available for tin contents and the erratic distribution of results is probably strongly influenced by contamination. Similarly, antimony and bismuth show irregular distributions expected from contamination.

The elements V, Cr, Ni, Ge, As, Ba, Pt, Au, and Hg, were below detection.

g) Galena (Table 23)

Titanium. The mean value, 530 ppm, is high on account of some anomalous values, which are possibly due to inclusions of rutile in impurity silica.

Manganese. The mean value of 510 ppm is high and similar to the titanium content. Fleischer (87) suggested that admixed sphalerite gave rise to anomalous manganese values in galena. Amounts of contaminating sphalerite in galena at Avoca are $\leq 5\%$, and manganese contents are generally significant, so that manganese in galena could not be supplied only by sphalerite impurities. The manganese content is due, perhaps, to included surface films of MnO_2 .

Cobalt. Values are predominantly below the detection limit and are unduly weighted by A.1901, with 225 ppm, and a sample contaminated by pyrite and chalcopyrite.

Gallium. Generally not detected, suggesting that the recorded values may be due to contamination by sphalerite; a

conclusion also reached by Fleischer (87) and Lampard (138).

Molybdenum. Only found in A.1901, 96 ppm and, as previously stated, this sample is contaminated.

Silver. This is the characteristic element occurring in galena; with a mean value of 490 ppm. Inclusions of tetrahedrite, which is argentian, may cause an enrichment, but the size of the values indicate that there is undoubtedly some silver present in solid solution in galena. Covalent radii: $\text{Ag}^+(1.339^{\circ}\text{A})$ and $\text{Pb}^+(1.358^{\circ}\text{A})$ imply that diadochic substitution of silver in galena is possible.

Indium. This element only occurs in A.1864 (18 ppm), and the sample is contaminated by zinc indicating that the indium may be included in impurity sphalerite.

Tin. The mean value of 51 ppm, is low and may be due to included silicate impurities. Fleischer states (87) that contents generally are ≤ 100 ppm and this is confirmed. Inclusions of stannite are common, especially in association with tetrahedrite (103) and this may explain Fleischer's higher values.

Antimony. Erratic results are due to intergrown tetrahedrite, noted from polished section study. This seems to be the explanation for commonly reported antimony in analyses of galena (87).

Bismuth. An erratic distribution exists, and as galenobismutite and other sulphosalts have been described from polished sections, values are probably due to impurities.

A comparative sample of galena from Glendalough, A.1866, contained a similar trace element assemblage to samples from Avoca (Table 23).

2.3.7.5. Discussion

a) Theoretical predictions of element distribution

Trace element distribution in mineral phases must take into account the geochemical character of the elements. Goldschmidt's rules (94,95), successively modified by various workers allow a measure of prediction of the trace element

distribution within ionically bonded phases; oxides and silicates. However, sulphides have covalently bonded structures and thus the rules are inapplicable. Recently, Nickel (159) has applied crystal-field theory to the vagaries of sulphide solubilities and structural stabilities. This is the first attempt to explain sulphide behaviour, and illustrates the lack of study on sulphide solid solutions. Burns' monograph (45) summarizes current theoretical predictions, and describes the evolution from Goldschmidt's original postulates.

None of the existing hypotheses, alone, are capable of explaining the behaviour of complexly bonded compounds. The controls of sulphide solid solution are not yet fully understood, and theoretical predictions of trace element distribution are severely limited.

b) Applications of trace element analysis

Trace elements may enter a mineral during crystallization from the parent fluid phase, and as such may be fingerprints of the original environment. This clue may give diagnostic information on the genesis of the mineral.

Mechanisms of incorporation of trace elements are varied; by inclusion as discrete phases along zonal boundaries, either captured during growth, or exsolved during cooling. The elements may be adsorbed into lattice defects in the crystal, or taken into solid solution through diadochic substitution at interstitial lattice sites. Each of these modes of entry into the lattice and subsequent incorporation probably operated during formation of the mineral assemblage at Avoca, and this factor is considered in the discussion. A review of the relevance of trace element studies to sulphides has been given by Loftus-Hills and Solomon (140) with a geochemical treatment by Taylor (221). The standard texts of Goldschmidt (96), Krauskopf (133), Runkama and Sahama (181) and Wedepohl (248), have been used for general reference.

(i) Indicators of ore genesis

This has been the prime application of the mass of data accumulated to date. A wide variety of elements and element

ratios have been used with divided results; at present there is no known diagnostic trace element indicator, but by judicious consideration of the several criteria, tentative conclusions may be reached.

Cobalt, nickel and Co:Ni ratio in pyrite

Noddack and Noddack (163,164) indicated that magmatic sulphides generally contained in the region of 2,100 ppm Co and 31,400 ppm Ni, with a Co:Ni ratio of 0.07. Berg and Friedensberg (22) suggested that hydrothermal sulphides had a Co:Ni ratio >0.1 , and often >1.0 , they also stated that the ratio rose to 830 in hydrothermal pyrite. Several workers have noted that where sedimentary pyrite and magmatic pyrite occur together, the sedimentary pyrite shows a much lower ratio (53, 112, 191). Hawley and Nichol (111) showed that hydrothermal pyrite had a higher ratio than pyrite from ultrabasics. In basic rocks, the Co:Ni ratio rises with increasing acidity, reflecting the difference in geochemical nature as nickel is extracted more rapidly into the solid phase during differentiation.

Davidson(66) proposed the Co:Ni ratio as an indicator of ore genesis, and maintained, that since in normal sediments the ratio was always <1.0 , ratios >1.0 were characteristic of granites. This hypothesis was based upon the behaviour of cobalt and nickel in silicates, and as sulphide structure is totally different it must have very little relevance to the Co:Ni ratio in sulphides. The pioneer study of cobalt and nickel in pyrite was by Hegemann (112), on 780 samples from Central and Northern European ores. This was followed by Cambel and Jarkovsky (48 and 50) on 800 samples of pyrite from Czechoslovakian deposits and by Loftus-Hills and Solomon (140, and pers. comm.) reporting on the initial phase of a study of about 1,000 samples from Tasmania. The current results form a contribution to this global pool of information.

Absolute values of cobalt and nickel in relation to the lode-types are shown in Fig.2.30. The graphs illustrate that the Co:Ni ratios at Avoca are generally high. The lower values contain high nickel contents and occur in pyrite from carbonaceous schist; A.1842, 1883 and 1676. This corroborates Davidson's

(66) noted enrichment of nickel in black shales, and the results correspond remarkably well with the average values of 20 ppm Co, and 200 ppm Ni, quoted by Hegemann (112) as characterizing sedimentary pyrite.

The sample from the intrusive dyke rock, A.1723, with Co:Ni = 0.92 is close to the average ratio for igneous rocks of that composition. Velikoborets, in a study of the relationship between cobalt content and pyrite morphology, has recently demonstrated (234) that contents are invariably higher in pyritic zones which are readily leached i.e. composed of melnikovitic pyrite. The present study broadly substantiates this, the results illustrating that pyrite from pyritic zones at Avoca, which contain abundant melnikovitic pyrite, is enriched in cobalt (Fig. 2.30 and 31).

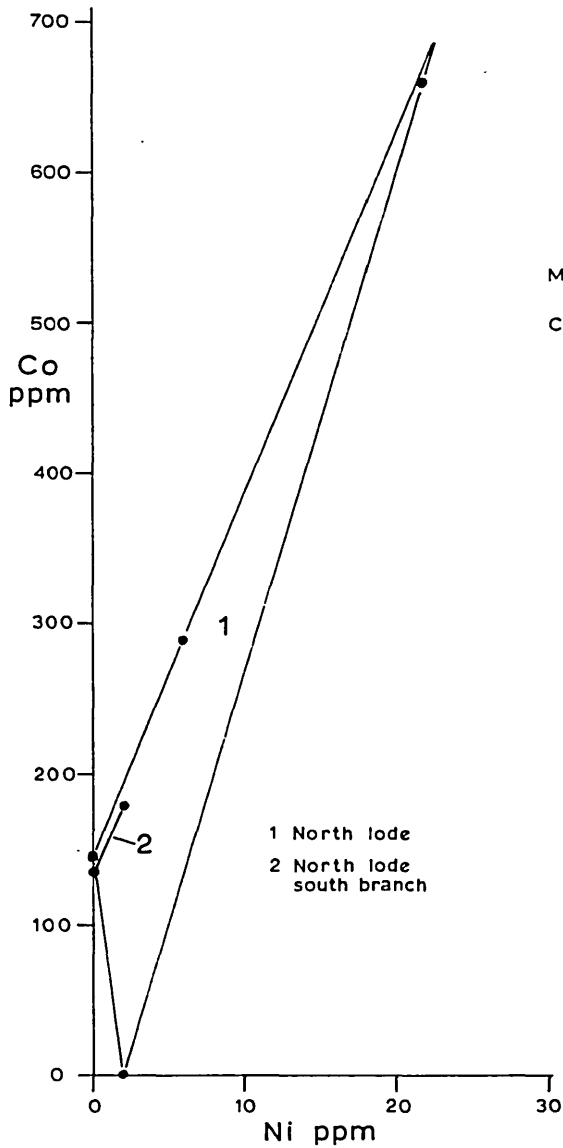
In relation to data from other deposits, some inferences may be drawn (Fig. 2.32). Correlation with deposits in the Norwegian sector of the Caledonides is made using Hegemann's (112) results coupled with the writer's. Lokken, Stordo and Skorovass, with similar degrees of metamorphism, and broadly equivalent ore types and environment to that at Avoca, show comparable Ni:Co ratios (Fig. 2.32A). Values given for Roros, Follidal and Sulitjelma have greater cobalt contents which equate with a markedly higher degree of metamorphism (Amphibolite facies). An increase in cobalt with increasing metamorphic grade was also suggested for the Czechoslovakian ores by Cambel and Jarkovsky (50). However, Velikoborets (234) concluded that increasing metamorphic grade resulted in decrease of cobalt content. Strict interpretation is therefore obviously impossible.

Two pyrite samples from Lokken with high nickel contents fall within the field of pyrite occurring in graphite schist at Avoca, and although Hegemann does not mention any carbonaceous material in the Lokken sample, it may have been present, finely divided, in the chloritic matrix. This fact may be cited as support for a syn-sedimentary origin of the Lokken deposit.

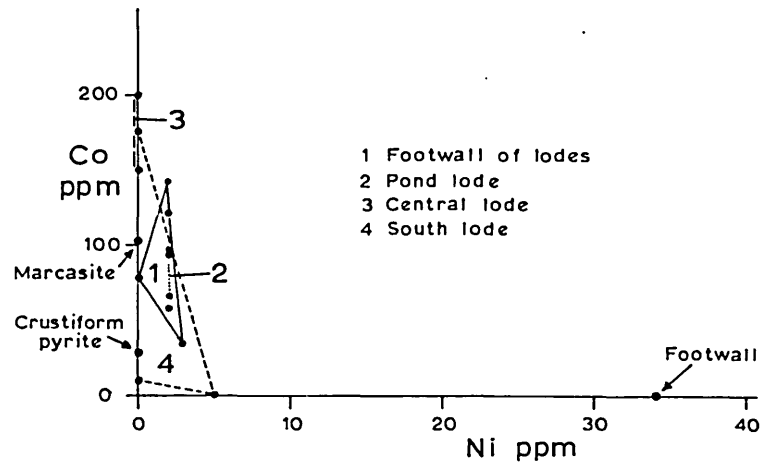
The Tasmanian results, (Fig. 2.32A) indicate that a high Co:Ni ratio exists in pyrite from ores associated with Cambrian volcanics. This feature is also shown at Avoca, where pyrite

Co and Ni in pyrite - Avoca
Underground

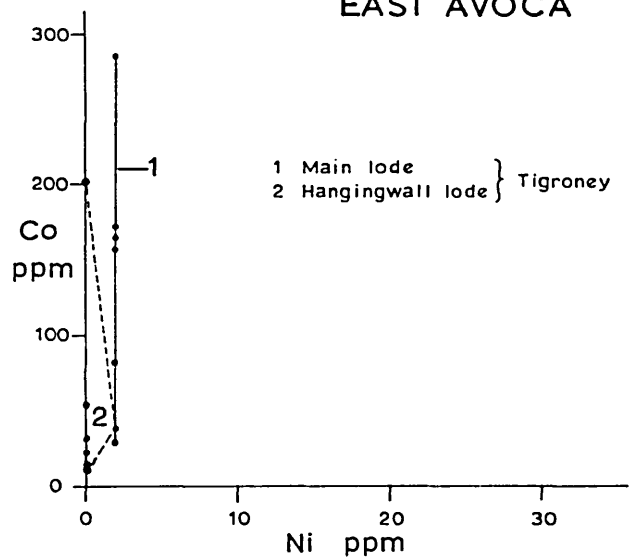
A. NORTH LODES



B. POND, CENTRAL AND SOUTH LODES



C. MAIN AND HANGINGWALL LODES, EAST AVOCA



D. WALLROCKS, WEST AVOCA

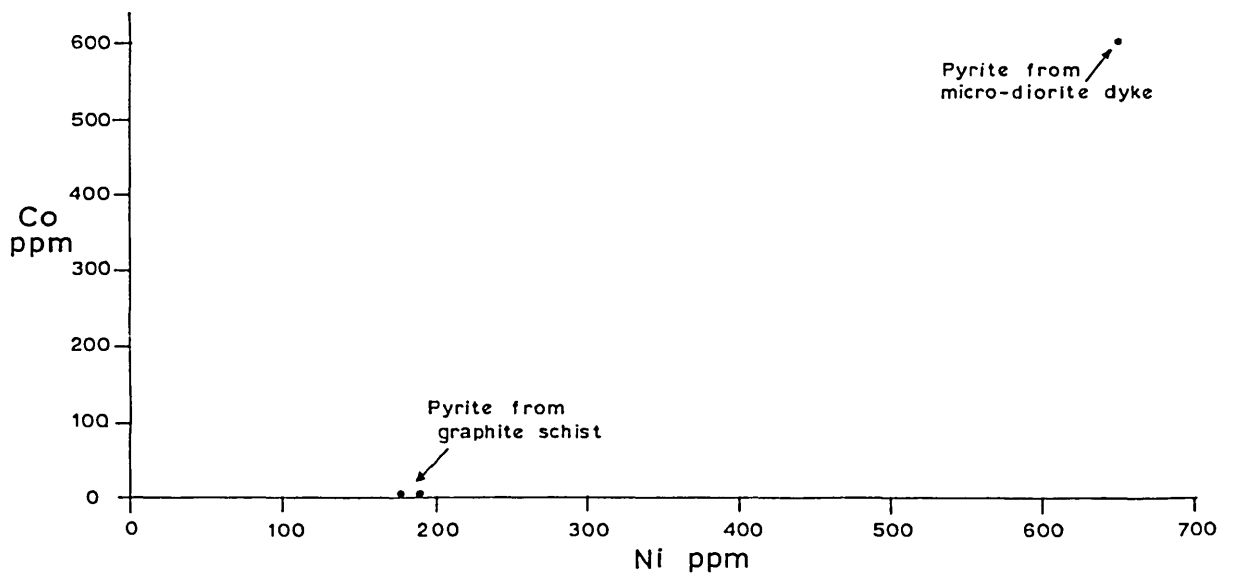


FIG 2.31

Co and Ni in pyrite - Avoca Surface

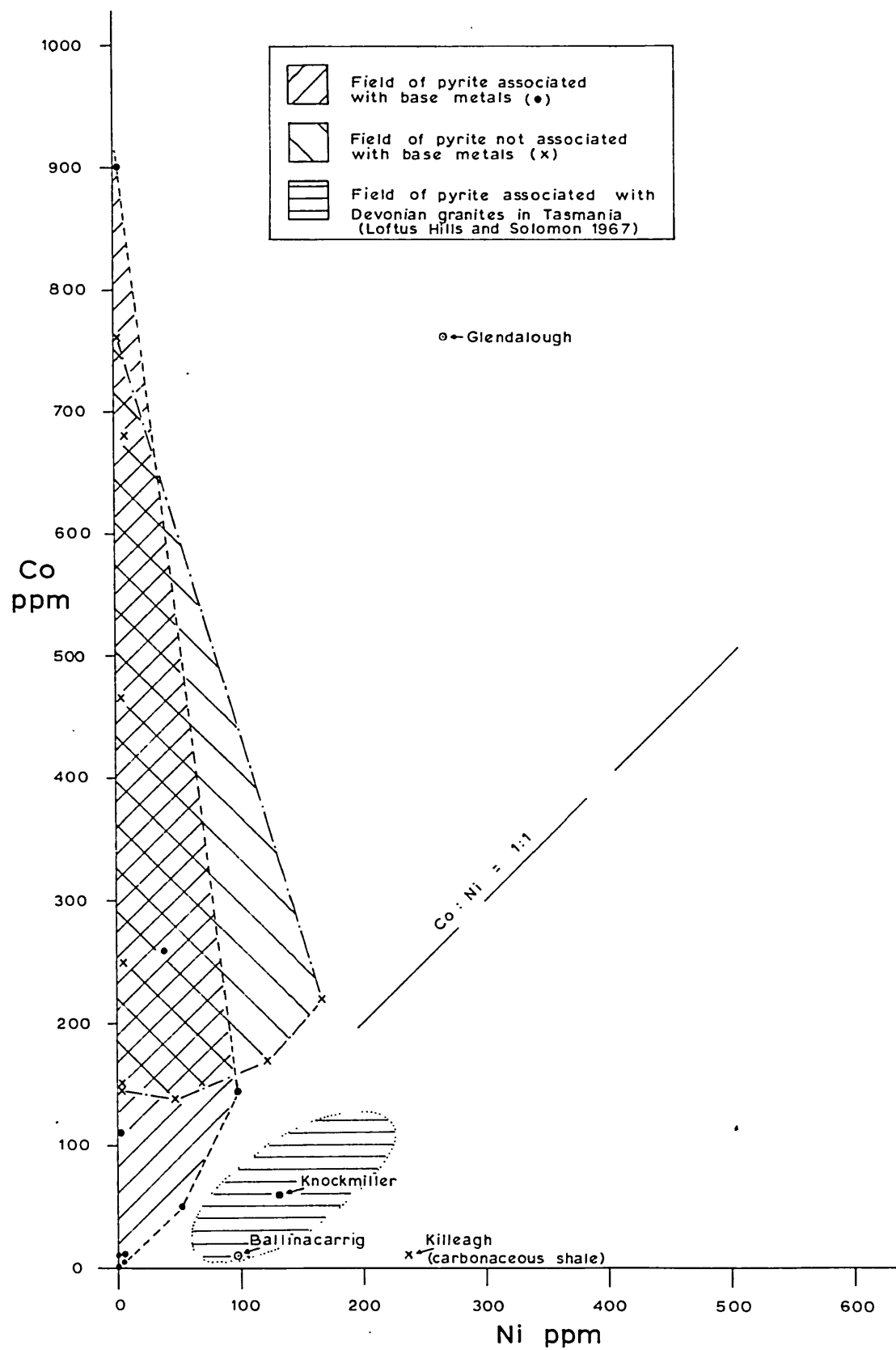
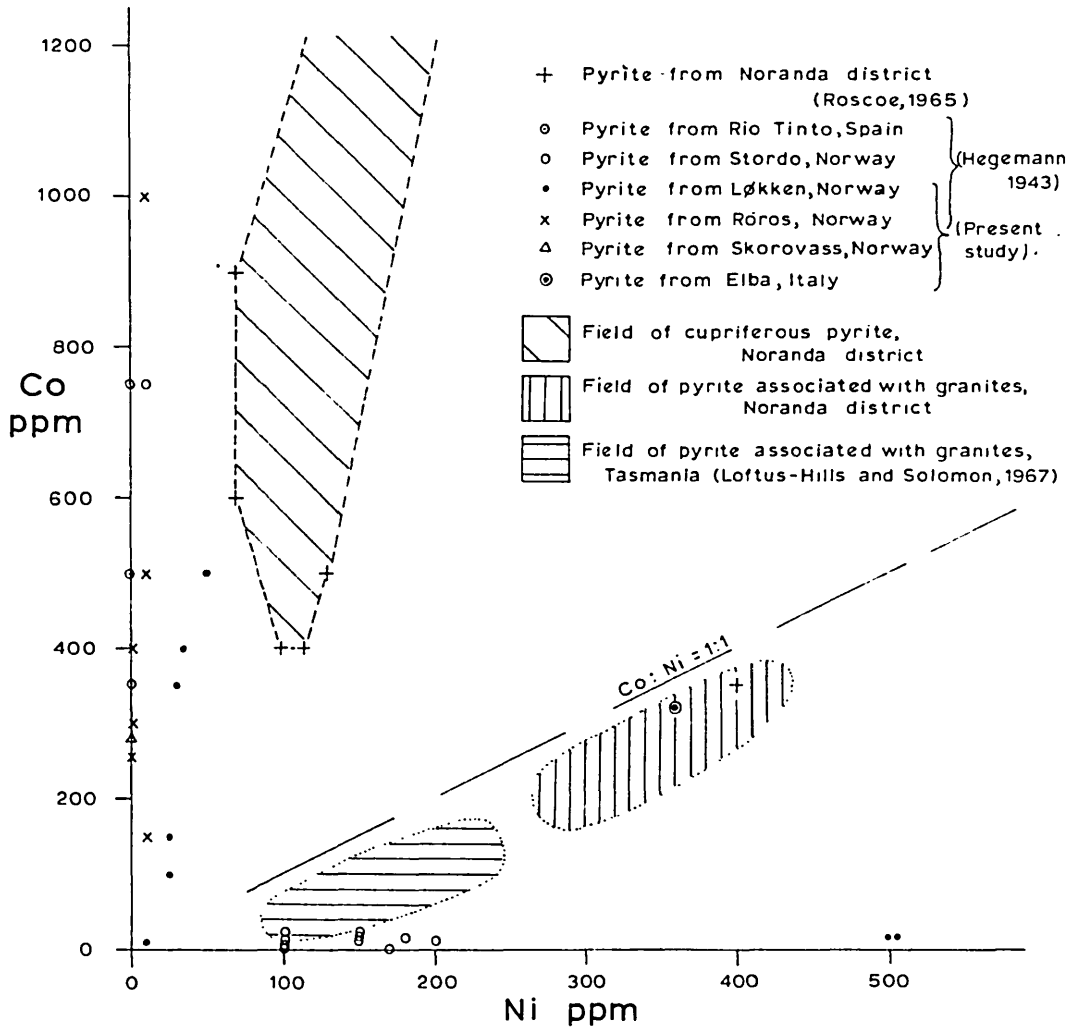


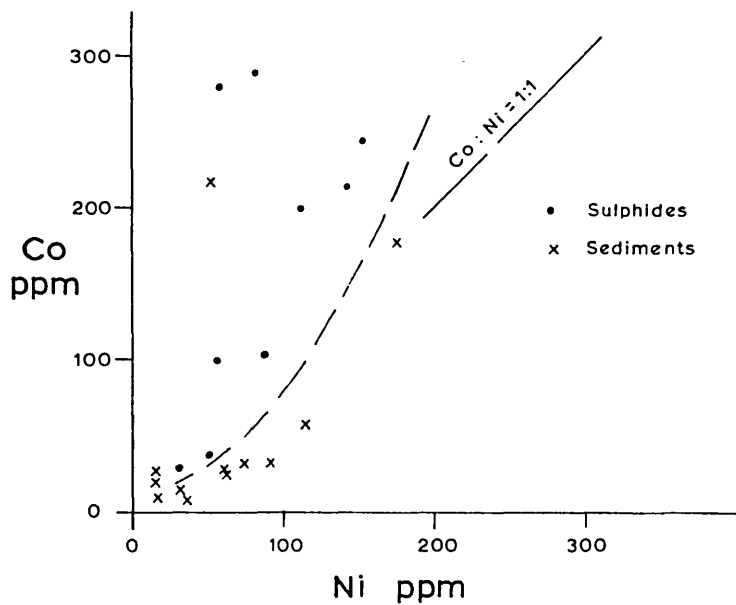
FIG 2.32

Co and Ni in pyrite from comparative deposits

A. Conformable deposits



B. Red Sea geothermal brine area



(Data from Kaplan et al., 1969)

falls into a similar field as the pyrite from the Mount Lyell and Rosebery-Hercules ores. Pyrite from the Ballincarrig Granite (A.1948) is in the field of the Devonian granite (in Tasmania), which post-dates the Mount Lyell mineralization, in the same way as the Caledonian Ballincarrig granite post-dates the Avoca mineralization.

Pyrite from the Noranda district (191) shows an equivalent distribution (Fig. 2.32A), and has been ascribed to the products of volcanism by Roscoe. Samples of sulphide from the Red Sea thermal brine area (128) show enrichment in cobalt (Fig. 2.32B). These sulphides are unmetamorphosed, and after metamorphism the Co:Ni ratio would no doubt rise, placing the value in a field implying a correlation with volcanism.

Gavelin and Gabrielson (89) stated that solution to genesis was impossible on the basis of analyses of nickel and cobalt because minor changes in the chemical parameters, Eh and pH, had a greater effect upon trace element distribution than the nature of the environment, the temperature of formation, or the degree of metamorphism. Considering current studies of the factors which influence trace element distribution (192) certain inferences may be made about the Co:Ni ratio in pyrite at Avoca:

1. The Co:Ni ratios do not allow any dogmatic conclusions about genesis.
2. A marked similarity is shown to pyrite from other deposits, which exhibit similar degrees of metamorphism, comparable ore types and have related lithological settings. Many of these are thought to have originated through a process of volcanism.

Selenium, and the S:Se ratio in pyrite

Goldschmidt and Hefter (92), Goldschmidt and Strock(93) and Carstens (52) suggested that contents of selenium in pyrite related to genesis. Edwards and Carlos (78) reported that in sedimentary pyrite selenium was generally low; 1 to 10 ppm. Carstens found that sedimentary pyrite had S:Se ratios of 1:500,000 to 1:40,000, whereas hydrothermal pyrite had S:Se ratios of 1:10,000 to 1,20,000. Coleman and Delevaux (59)

pointed out that this did not hold in the presence of volcanic matter. Thus, discrimination must be made in every case, between selenium enrichment on a provincial and on a local scale.

Loftus-Hills, Groves and Solomon (141) concluded that Tasmania was a low selenium province and that the selenium content of pyrite was an unsatisfactory genetic indicator. Cambel and Jarkovsky reached no definite conclusions, but found some evidence of an increase in selenium with increasing depth at Smolnik (50). Anderson (3) presented a review of earlier data.

At Avoca the selenium contents are low, with S:Se ratios >30,000 and they are not typical of deposits associated with volcanism found elsewhere (3). Mount Lyell in Tasmania (141) shows a similar enrichment and from that area the conclusions have already been stated. At Follidal, in Norway, Waltham (243) noted that fine grained pyritic ore contained 10 to 20 ppm Se, increasing to 40 ppm in coarse grained ore. The current study points to higher Se contents in massive lenticular pyrite seams than in cross-cutting siliceous ores. This provides an interesting corollary between the Irish and Norwegian deposits.

The results of the analysis of selenium in pyrite tend to mitigate against a truly hydrothermal origin for the siliceous ores at Avoca, but do not disprove a volcanic origin for the pyritic seams. Any conclusions based upon such approximate and meagre data can only be regarded with extreme caution, especially as the selenium content of pyrite may be influenced by the crystal form (50).

Titanium, vanadium, manganese and molybdenum in pyrite

Cambel and Jarkovsky (49) suggested that Ti, Mn and Mo were enriched in sedimentary, relative to hydrothermal, pyrite. The current data is inconclusive, but the relatively low values of these elements in Avoca pyrite adds a small measure of support for a sedimentary origin. Carstens (52) noted the reverse relationship for vanadium in pyrite. The absence of vanadium in pyrite from Avoca thus correlates with a hydrothermal origin, but Carstens' example of a hydrothermal deposit was

Lokken and the author, in common with other writers, contends that it is partly syn-sedimentary and thus little value can be attached to the relationship.

Cadmium in sphalerite

Ivanov (118) found that sphalerite from Cu-Zn-pyrite deposits and from Pb-Zn-pyrite deposits in extrusive volcanic sequences have lower than average cadmium contents. Thus, Groves and Loftus-Hills (101) concluded that low cadmium contents in sphalerite might indicate a genetic association between the ores and volcanism.

The mean cadmium content of sphalerite at Avoca is 1,140 ppm and that at Glendalough, in mineralization associated with the Leinster granite, is 3,800 ppm. This shows a striking similarity to the results from Tasmania (101) where the mean cadmium content in sphalerite from Pb-Zn deposits associated with volcanics is 1500 ppm, and that in mineralization associated with Devonian granites is 2,900 ppm. A clear distinction exists in both regions between the two varieties of sphalerite. By comparison, it can thus be inferred that the deposits at Avoca are related to volcanism.

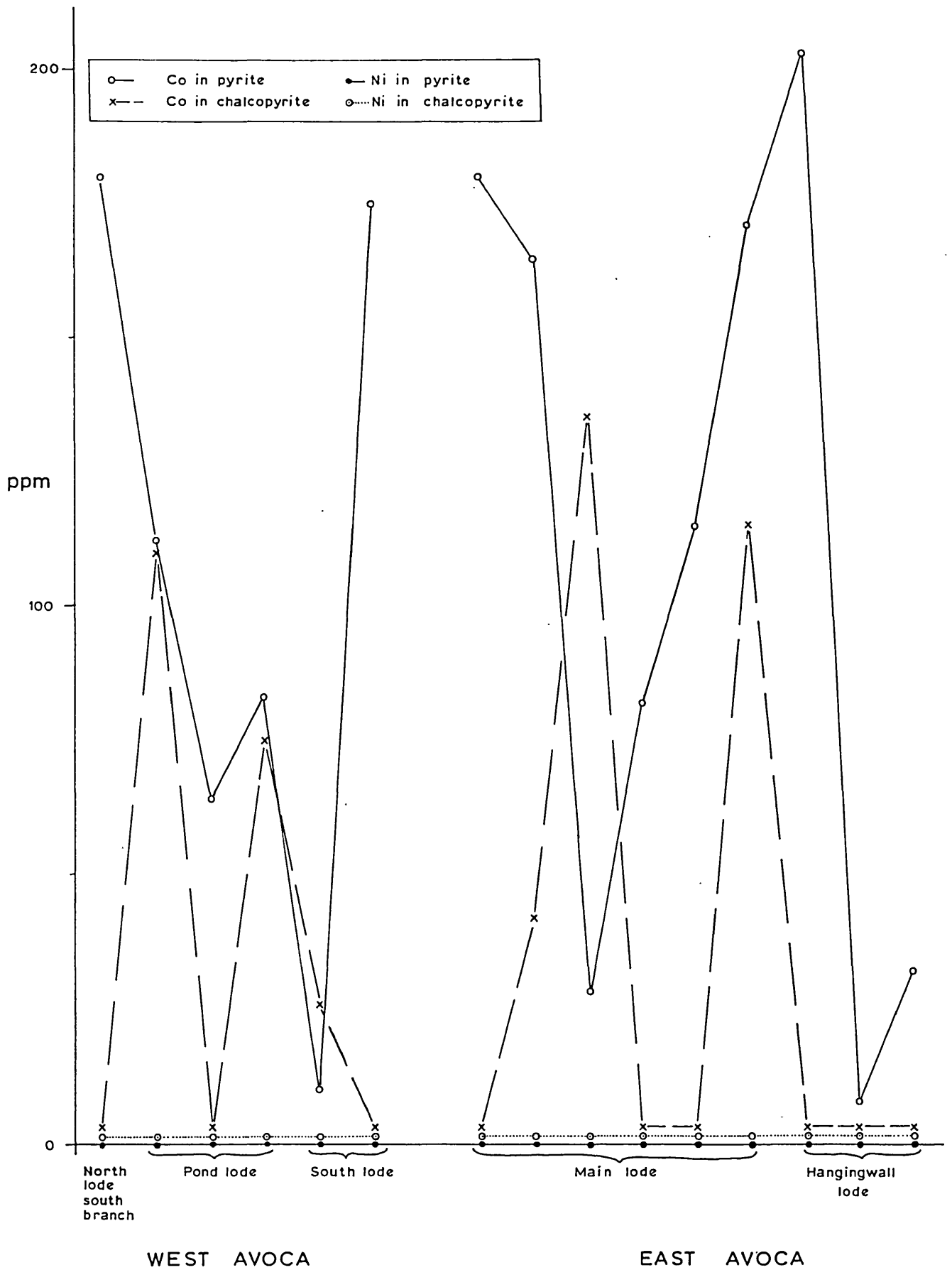
Summary

Evidence from trace element contents in sulphides from the Avoca district indicates that the pyritic zones accumulated within tuffaceous sediments and that the source of the metals and sulphur may be volcanic. The siliceous zones do show typical magmatic-hydrothermal features and may be of hybrid origin.

(ii) Temperature of crystallization of ore assemblages

Studies on ore thermometry involving trace element partition or incorporation depend upon equilibrium conditions being reached. Troshin and Troshina (226) postulated that any consistent partition of elements between coexisting minerals probably indicated equilibrium conditions in an essentially diadochic substitution. To test this hypothesis, Fig. 2.33, illustrates Co and Ni contents in coexisting pyrite and chalcopyrite.

Co and Ni in coexisting pyrite and chalcopyrite,
Avoca district



A constant partition does not exist implying that complete equilibrium was not attained during metamorphism. (Minor inhomogeneities; zoning, twinning, etc., which occur in polished section, also indicate incomplete chemical equilibrium.).

Iron content of sphalerite

The major geothermometer has been based upon the iron content of sphalerite within the ZnS-FeS system. Kullerud (134) presented data which has since largely been discounted (17). Iron contents determined spectrographically in sphalerite from Avoca produce excessively high results. Some of the samples are impure, and thus this is expected. To check the data, probe analysis of pure sphalerite (as free from inclusions of chalcopyrite as possible) was carried out. The results are shown in the following table, compared with the spectrographic data:

Table 25. Comparative probe and spectrographic analyses of iron content in sphalerite, Avoca District.

A. Primary sphalerite

		%Fe	
		Probe	Spec.
A.1937	W.Avoca; N.lode, 720L, HW	3.5	18.0 [*]
1882	" ; P.lode, 1300L, FW	5.7	6.4
1884	" ; S.lode, DDH 1670-P1-244'	3.3	4.7
VW 823	" ; Pb-Zn lode, DDH 1047-46'	1.2	-
VW 6A	E.Avoca; Tigroney, 850L, Main lode	6.0	-
1896	" ; " " HW lode	7.9	12.9 [*]
1895	" ; " " " "	4.8	12.3 [*]
1877	Ballinasilloge; dump at adit	7.8	5.4 ^a
1892	Knockmiller; W., roadside	8.4	6.9 ^a
VW 822	Ballycoog Ford; cliff exposure	8.8	-
1878	Kilnacoo; Cross-roads shaft dump	3.2	7.8

B. Remobilized sphalerite

A.1893	W.Avoca; S.lode, DDH 1670-50-750'	1.3	1.9
--------	-----------------------------------	-----	-----

^{*}Specimen contaminated with CuFeS_2 and FeS_2

^aValue diluted by contaminant quartz.

Agreement between the two analytical methods is good when the samples for spectrographic analysis are clean, but discrepancies exist with impure samples. Difficulty in mineral separation indicates that microprobe analysis is the most effective method of analysing iron content in sphalerite.

Cadmium content of sphalerite

Groves and Loftus-Hills (101) summarized evidence for the application of increasing cadmium content in sphalerite as a geothermometer, but conclusions are at present divided, as Roedder (189) and Sawkins (196) correlated increase of cadmium content with falling temperature and an increase in salinity of the parent media.

Silver and bismuth in galena

Van Hook (232), in a study of the $\text{Ag}_2\text{S}-\text{Bi}_2\text{S}_3-\text{PbS}$ system, noted that the solubility of silver in galena, in the presence of bismuth, could be extensive even at low temperatures. One sample containing 3.76% Ag was reported. In the absence of bismuth, up to 0.4 mol.% Ag_2S is soluble in galena at 700°C , and in the absence of silver, up to 9.0 mol.% Bi_2S_3 is soluble in galena at 800°C . The solubility decreases rapidly with decreasing temperature, and the degree of solid solution may be of use as a geothermometer.

At Avoca, the mean content of silver in galena is 490 ppm Ag (equivalent to 0.06 % Ag_2S). Bismuth occurs in the assemblage, and as other sulphide and silicate geothermometers indicate a maximum temperature of $\leq 350^\circ\text{C}$ during metamorphism, the silver content of galena is well within predicted limits. Bismuth contents in galena are erratic and may be due to contamination.

Selenium in sulphides

The possible use of selenium as a geothermometer was put forward by Goldschmidt and Strock (93), but available data is scanty. Bergenfelt and Sineeveva claim (23,203) a general correlation of selenium content with temperature, and Suzuki, through measurement of selenium within a fumerole, showed that increasing content was proportional to temperature (220). Hawley

and Nichol (110) reported that availability was a more important factor than temperature. In a survey of Tasmanian results Loftus-Hills, Groves and Solomon concluded that the selenium content was an unsatisfactory geothermometer (141). The meagre data in the current study do not allow any specific deductions.

(iii) Distinction between primary and remobilized sulphides

In a specific mineral deposit, remobilized sulphides will probably have a depleted trace element assemblage in relation to primary material.

A comparison of the mean trace element contents of primary and remobilized sphalerite is given below:

Table 26. Trace elements in primary and remobilized sphalerite

		Trace Elements - ppm							
	no.	Ti	Mn	Co	Ga	Ag	Cd	In	Fe %
Primary	(8)	136	1060	42	16	19	880	78	5.9
Remobilized	(3)	59	390	7	58	9	1860	180	1.4

A decreased thermal instability in the sphalerite lattice reduces the available sites for trace elements. This fact is confirmed by the elements Ti, Mn, Co, Ag and Fe, of which only iron and manganese are theoretically predicted to occur in sphalerite. However, Ga, Cd, and In are acceptable in the lattice and contents at Avoca increase with decrease in temperature of crystallization. Statistically, the data has extreme drawbacks because of the small number of analyses.

It was not possible to obtain sufficient primary and remobilized material of any other sulphide.

(iv) Metallogenetic Provinces

Metallogenetic provinces contain certain elements in excess of their mean crustal abundance and they are often related to tectonic elements (27). Warren and Thompson (244) and Burnham (43) noted that enrichment of certain trace elements in sulphides could characterize specific provinces. The data

from Avoca sulphides indicates that in the Caledonian geosyncline, the sole diagnostic trace elements of the Southern Caledonides are possibly tin and molybdenum, both of which are absent in sulphides from Norwegian deposits.

(v) Mineral Exploration

General

To establish whether there was a characteristic trace element in pyrite which could be used in mineral exploration, a statistical analysis was made of trace elements in pyrite from Avoca associated with base metal mineralization and that in pyrite in the country-rock. Logarithms of the trace element values were taken, and means and standard deviations calculated. The results are in table 27 below:

Table 27. Statistical analysis of trace elements in pyrite, Avoca District

	A		B		C	
	Mean	Std. Devn.	Mean	Std. Devn.	Mean	Std. Devn.
Ti	1.830	0.674	2.313	1.119	1.963	0.820
Mn	1.842	0.491	1.696	0.804	1.809	0.571
Co	1.539	1.077	1.878	1.008	1.614	1.064
Ni	0.069	1.034	0.897	1.114	0.252	1.106
Mo	1.841	0.894	0.948	1.298	1.642	1.054

(Values in logarithms)

Number of samples

n=49

n=14

n=63

A= Samples of pyrite associated with base metal mineralization.

B= Samples of pyrite unassociated with base metal mineralization.

C= Pool of samples.

It is clear that no statistical difference exists between the groups, with the conclusion that pyrite associated with base metals and that unassociated with base metals probably originated from the same source. The country-rock sequence is pyroclastic

and thus a volcanic origin for the iron and sulphur in pyrite at Avoca is probable.

Mercury

It is now well known that anomalous quantities of mercury are often associated with sulphide deposits (119), especially those which contain appreciable zinc and/or sulphosalts. In Ireland, discovery of mercurian tetrahedrite at Gortdrum in 1968 (256) stimulated enquiry into mercury haloes surrounding other ore deposits.

Mineralization at Avoca contains abundant zinc in certain zones, and tetrahedrite occurs, so that anomalous mercury contents and a resultant halo are likely. The spectrographic method used in this study has a high detection limit for mercury and this precludes detection of trace quantities in separated sulphides. In order to provide some information, a reconnaissance suite of stream sediment samples were collected.

A total of 14 samples have been analysed for mercury using the method described by James and Webb (120) on minus 80-mesh fractions. To check the significance of the results the samples were also analysed for arsenic, as this element is characteristically associated with mercury in dispersion haloes, using the Gutzeit (modified) method.

The results are shown in Fig. 2.34. The data is minimal, but anomalous values in streams draining known mineralization are encouraging, as they show enrichment of several orders of magnitude over the apparent 'background level'. The highest values are accompanied by anomalous arsenic content, which adds weight to the relevance of this pattern.

Stream sediment sampling has not been applied to any extent in the Avoca mineralized belt, due to fear of contamination by ancient workings. This pilot study demonstrates that analysis of trace mercury content in stream sediments may well prove to be a valuable exploration tool.

2.3.8. Mineral stabilities and phase relations2.3.8.1 Geothermometry and geobarometrya) Pyrite-pyrrhotite

Arnold (8) demonstrated the variation in composition of pyrrhotite with temperature. In addition, the increase in value of the d_{102} spacing of pyrrhotite is sympathetic with iron content, and antipathetic with the temperature of formation. Measurement of the d_{102} spacing of hexagonal pyrrhotite coexisting with pyrite can thus be used to estimate the formational temperature. The following conditions must first be satisfied:

(i) Equilibrium between pyrite and pyrrhotite must be proved and if not, only a minimum temperature can be estimated.

(ii) The pyrrhotite must be hexagonal, because many natural pyrrhotites are monoclinic or a combination of hexagonal and monoclinic forms (47) and these cause large errors in the d_{102} spacing. Arnold (9) and Yund and Hall (60) summarize the current status of the method.

The size of pyrrhotite grains at Avoca (Plate 33) made isolation and measurement by standard x-ray diffraction techniques (8) impossible. Probe analysis (using the Geoscan) of representative pyrrhotites gave the following result:

Composition of pyrrhotite

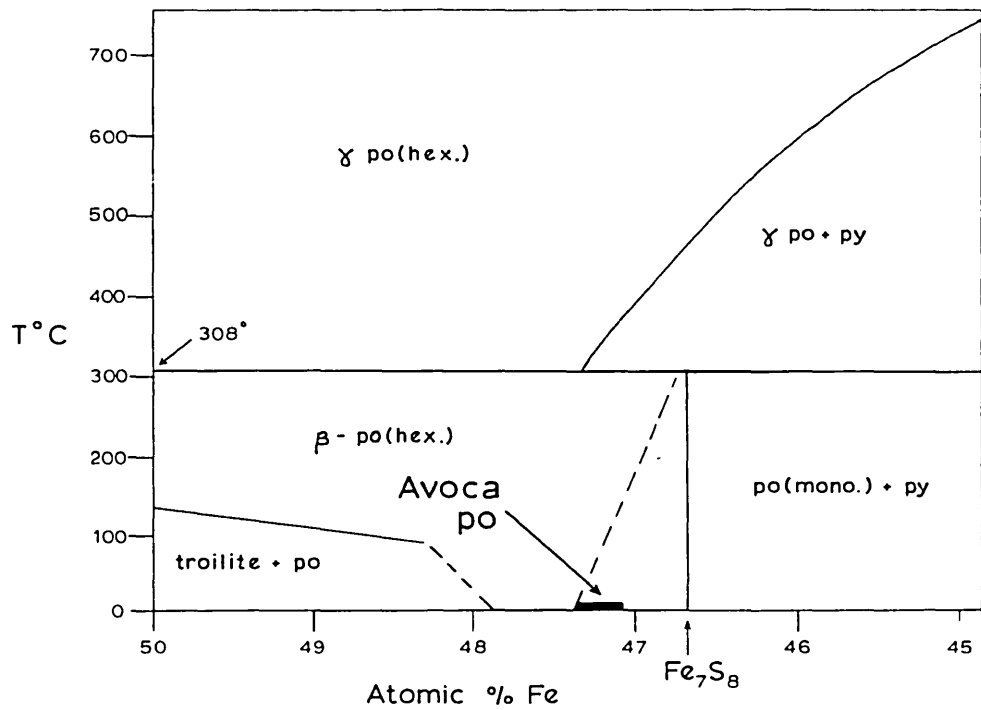
Element %	1.	2.	3.
Fe	60.93	60.30	61.18
S	39.32	38.79	38.96
Total	100.25	99.09	100.14

1. E.Avoca, Tigroney, 850 L. Main lode.
2. Castle Howard, stope off upper adit.
3. " " " " "

This data, in relation to the stability field of pyrrhotite (Fig.2.55A), indicates a low temperature form, either monoclinic or hexagonal. The formation of pyrrhotite at Avoca may well

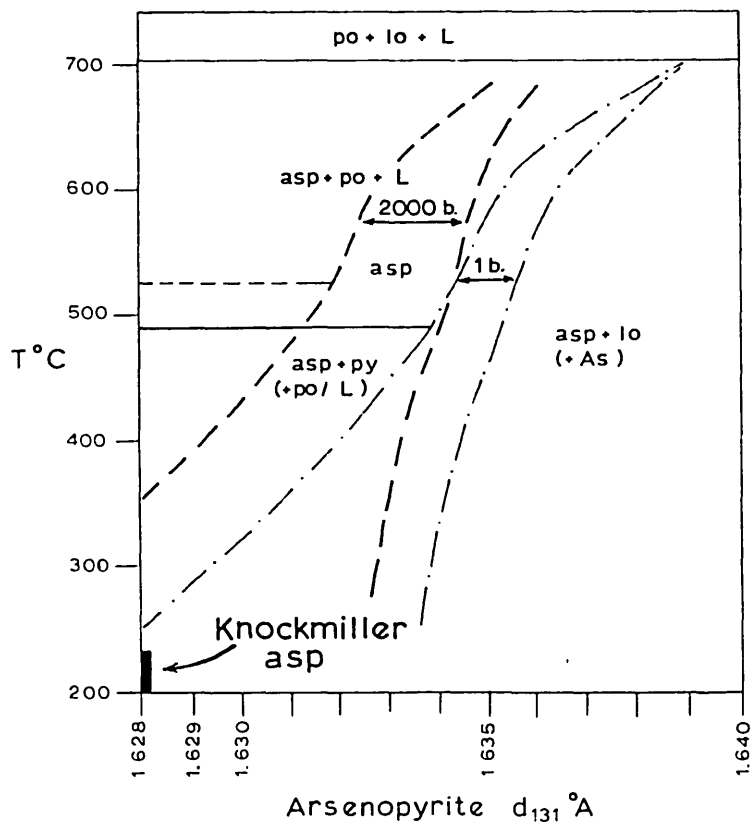
PYRRHOTITE AND ARSENOPYRITE STABILITY RELATIONS

A. Composition of pyrrhotite in relation to the Fe-S system.



(After Desborough and Carpenter, 1965)

B. Phase relations of arsenopyrite at various pressures with reference to temperature and composition.



(After Clark, 1960)

have taken place at $\leq 304 \pm 6^\circ\text{C}$, and Arnold (9) demonstrated that under these conditions pyrrhotite could form from components with a composition between pyrite and pyrrhotite in the presence of pyrite, therefore the results from Avoca are plausible. Desborough and Carpenter (68) deduced that applications of the composition of pyrrhotite might be completely meaningless, and thus no precise geothermometric deductions can be made.

b) Arsenopyrite

The use of arsenopyrite as a geobarometer was suggested by Clark (56) and (57), who presented curves relating pressure variation to the d_{131} spacing. Barton (15) confirmed the phase relations. The temperature must be independently determined and the arsenopyrite must have formed at its arsenic or sulphur-rich limit, the pressure of the assemblage can then be estimated by x-ray study of coexisting arsenopyrite. The d_{131} spacing is a function of the As-S ratio. The method (56) involves powdering arsenopyrite with fluorite (1 : 1) under acetone and making into a smear mount. It was not possible to obtain sufficient material from the Avoca mine, but at Knockmiller, arsenopyrite is a major mineral phase. Zoning in the arsenopyrite suggests inhomogeneity and slight temperature variations, applying the determinative curve, give rise to huge pressure changes. The d_{131} spacing was determined (Fig. 2.35B) and, assuming a temperature of crystallization of $200\text{-}300^\circ\text{C}$ for this vein-type occurrence, a low pressure is indicated (1-50 bars), corresponding to ore deposition in the near surface environment.

Arsenopyrite melts at $702^\circ \pm 3^\circ\text{C}$ (57) and the upper limit of stability of arsenopyrite and pyrite is $491^\circ \pm 12^\circ\text{C}$. These provide useful temperature limits (see below) for the formation of the epigenetic minerals in the mine area.

c) Sphalerite

The sphalerite geothermometer, first postulated by Kullerud (134), later suffered modifications by Skinner, (205) Einaudi (79) and others, to the extent that Barton and Toulmin (18), suggested that the method should be discarded. In spite of this condemnation, the iron contents of sphalerites from Avoca

are shown on Fig. 2.36, illustrating the relationship of values to the various determinative curves. A separation between primary and remobilized sphalerite exists.

Kelly and Turneaure (129) noted an equally distinct separation between 'iron-rich' and 'iron-poor' sphalerites from Bolivia. The composition break occurred at 19 mole % FeS and this was correlated with the abundance of exsolution products. At Avoca primary sphalerite contains exsolved chalcopryrite whereas remobilized material is barren. At Keno Hill (36) Boyle and Jambor demonstrated unrealistically high formational temperatures by applying Kullerud's curve to sphalerites and, interestingly, his values are comparable with those at Avoca.

d) Exsolution textures

The geothermometric applications of exsolution textures must be judiciously applied and Brett (39) has cast severe doubt upon the validity of any interpretations.

Initially it must be shown that true exsolution has taken place; the solvent phase must have exsolved from the solute to form an exsolved phase on rapid cooling of a bulk composition within a solid solution field.

(i) Chalcopryrite from sphalerite

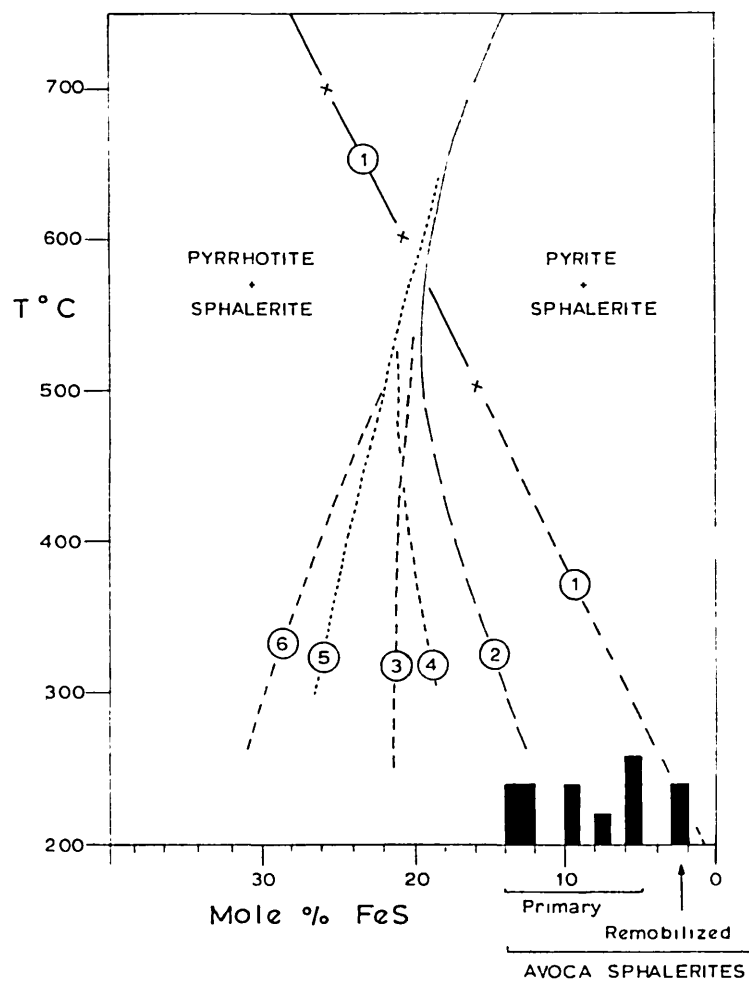
This texture originates below the deposition temperature of the host sphalerite. Forchert (33) and Buerger (42) estimated a temperature range of 350° - 400° C at 1 bar. (With increasing pressure the lower temperature is approached). Marmo's data (150) added evidence in favour of the lower temperature. Brett (39) illustrated that the texture might form over a wide range of temperature and much lower than previously indicated. Any precise geothermometric implications are therefore impossible, but Vokes (237) and Shreyer et al., (198) presented meaningful results. The indicated temperature of $\leq 350^{\circ}$ C for the Avoca ores, is not contradicted by this evidence.

(ii) Pyrrhotite from sphalerite

This relationship only occurs in one outlying prospect; Ballinasilloge. Kullerud (134) postulated a temperature range

FIG 2.36

IRON CONTENT OF SPHALERITE



- 1 Kullerud (1953)
- 2 Barton and Toulmin (1966)
- 3 Boorman (1967)
- 4 Scott and Barnes (1967)
- 5 Einaudi (1968)
- 6 Chernyshev and Anfilogov (1968)

(After Kelly and Turneaure 1970)

of $138-894^{\circ}\text{C}$ at ≤ 1 atmos. pressure for this texture. The temperature of $\leq 350^{\circ}\text{C}$, indicated by the wallrock assemblage, thus appears realistic. Pyrrhotite cannot exsolve from sphalerite unless excess sulphur is added from an external source (16). The spatial association of pyrrhotite (Fe_{1-x}S) with chalcopyrite (CuFeS_{2-x}) confirms that simultaneous exsolution from sphalerite without any change in the metal-sulphur ratio is possible.

(iii) Pyrrhotite from chalcopyrite

Yund and Kullerud (259) revealed that a change in the tie-lines in the Cu-Fe-S system occurred at $334^{\circ} \pm 17^{\circ}\text{C}$. Isometric cubanite and pyrite give way to pyrrhotite and chalcopyrite. This reaction is very slow and the assemblage of pyrite with or without cubanite might be expected at Avoca, but it does not exist. However, pyrrhotite and chalcopyrite intergrowths occur and they do not appear to be high temperature conversion products, and therefore probably developed $\leq 334^{\circ} \pm 17^{\circ}\text{C}$, but could have exsolved at a higher temperature.

e) Thermoluminescence

Lampard (138) reported the results of a study on samples of carbonate from Avoca. Calcite, from the tuff horizon and dolomite from the hangingwall of the Pond lode at West Avoca gave no distinct peaks; indicative either of deposition at a temperature $> 300^{\circ}\text{C}$ or the insensitivity of the method.

f) Fluid Inclusions

The application of fluid inclusion studies to thermometry is well established. Two methods of approach exist (190):

(i) The homogenization method; which consists of determining the filling temperature of the inclusion by observation on a heating stage.

(ii) The decrepitation method; in which a sample of crushed material is heated and a sudden increase in decrepitation of the inclusion cavities occurs as the filling temperature is exceeded (205).

Minute inclusions occur in quartz associated with the mineralized lenticles in the siliceous zones. Eight samples,

chosen by Lampard, were studied by Smith who reported (138); that very indistinct decrepigraphs were obtained. A number of sets of inclusions were present and one set possibly filled at 200-300°C. Smith concluded that additional work would probably not produce more significant data, and thus the method has not been pursued further.

g) Univariant points

(i) Quartz inversion

Basal sections of quartz etched by Lampard (138) and revealed features indicative of low quartz and consequent formation at <573°C at 1 atmos. (Possibly at a higher temperature under increased pressure).

(ii) Arsenopyrite and pyrite

The upper limit of stability for this assemblage is 491°C at 1 atmos. (The temperature increases by 18°C per Kb).

(iii) Native Bismuth

The melting point is 271°C, but is of dubious significance as the mode of occurrence indicates derivation from a melt at a higher temperature. The textures are compatible with a maximum metamorphic temperature of <350°C.

(iv) Galenobismutite

The melting point of 750°C suggests that crystallization took place below this temperature, and the textures indicate that galenobismutite may be an exsolution product.

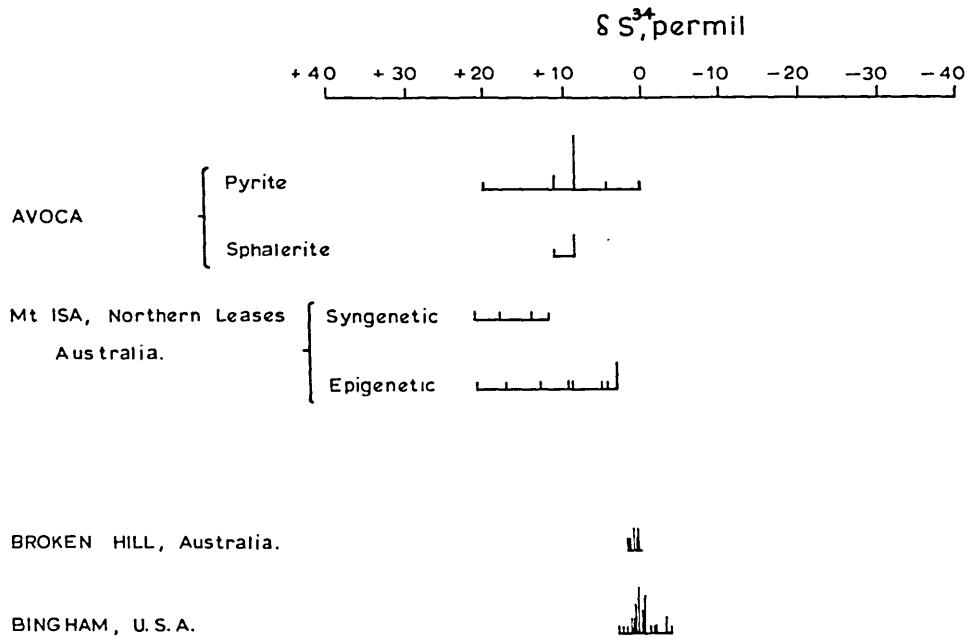
h) Sulphur Isotopes

Analysis of the isotopic composition of sulphur from twelve samples of pyrite and four samples of sphalerite from West Avoca by Jensen are in (138). These results are shown in Fig. 2.37A. There is a good correlation with results from ore deposits which have similar features and a tentative correlation with volcanism implied. Solomon et al. (210) have presented an analysis of isotopic data from metamorphosed conformable deposits around the world, and the data from Avoca conforms to the general pattern (Fig. 2.37B).

FIG 2.37

SULPHUR ISOTOPES

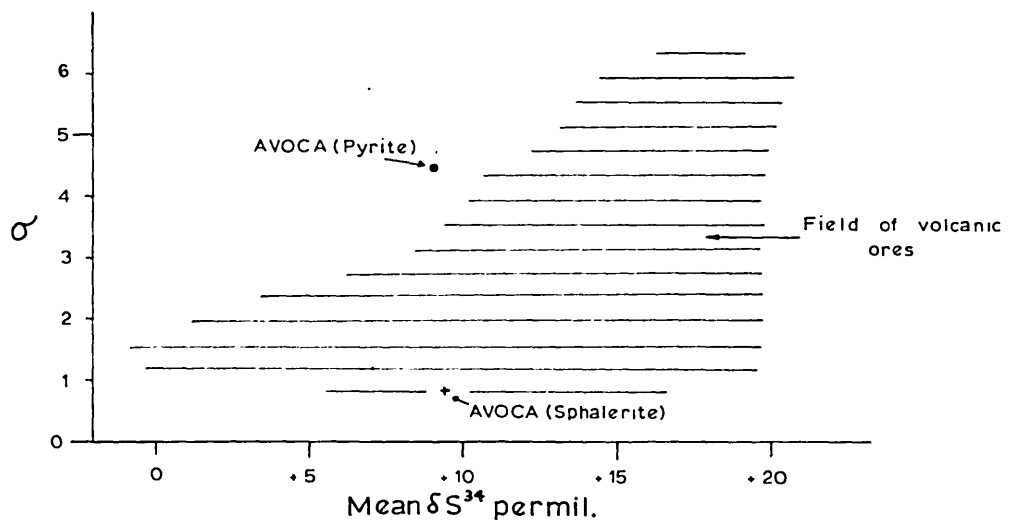
A. Isotopic ratios at Avoca contrasted with other deposits



(The length of vertical lines is directly proportional to the number of samples)

(After Jensen, 1967)

B. Mean and standard deviation for sulphide-sulphur δS^{34} for ores of volcanic association



(After Solomon et al., 1969)

i) Trace elements

Distribution coefficients of trace elements between coexisting phases and their geological significance has already been discussed.

j) Summary

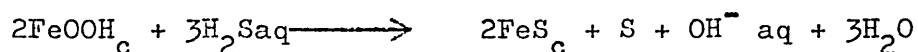
The geothermometric and geobarometric indicators in the Avoca ores are summarized in Fig. 2.38.

2.3.8.2. Phase relations as environmental indicatorsa) Pyrite

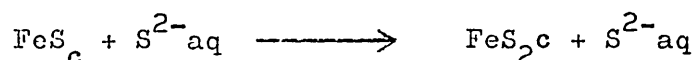
The textural features reveal contrasting types of pyrite and the differences are significant.

Pyrite is formed under a wide range of conditions and Rickard has ably discussed (186) the differing modes of formation.

In the normal marine sedimentary environment, (Fig. 2.33) the major form of reactant iron is goethite. Sulphidation of goethite takes place as follows; (D.T.Rickard, pers. comm.)



Mackinawite (FeS) is produced, which reacts with available polysulphide ions to form pyrite:-



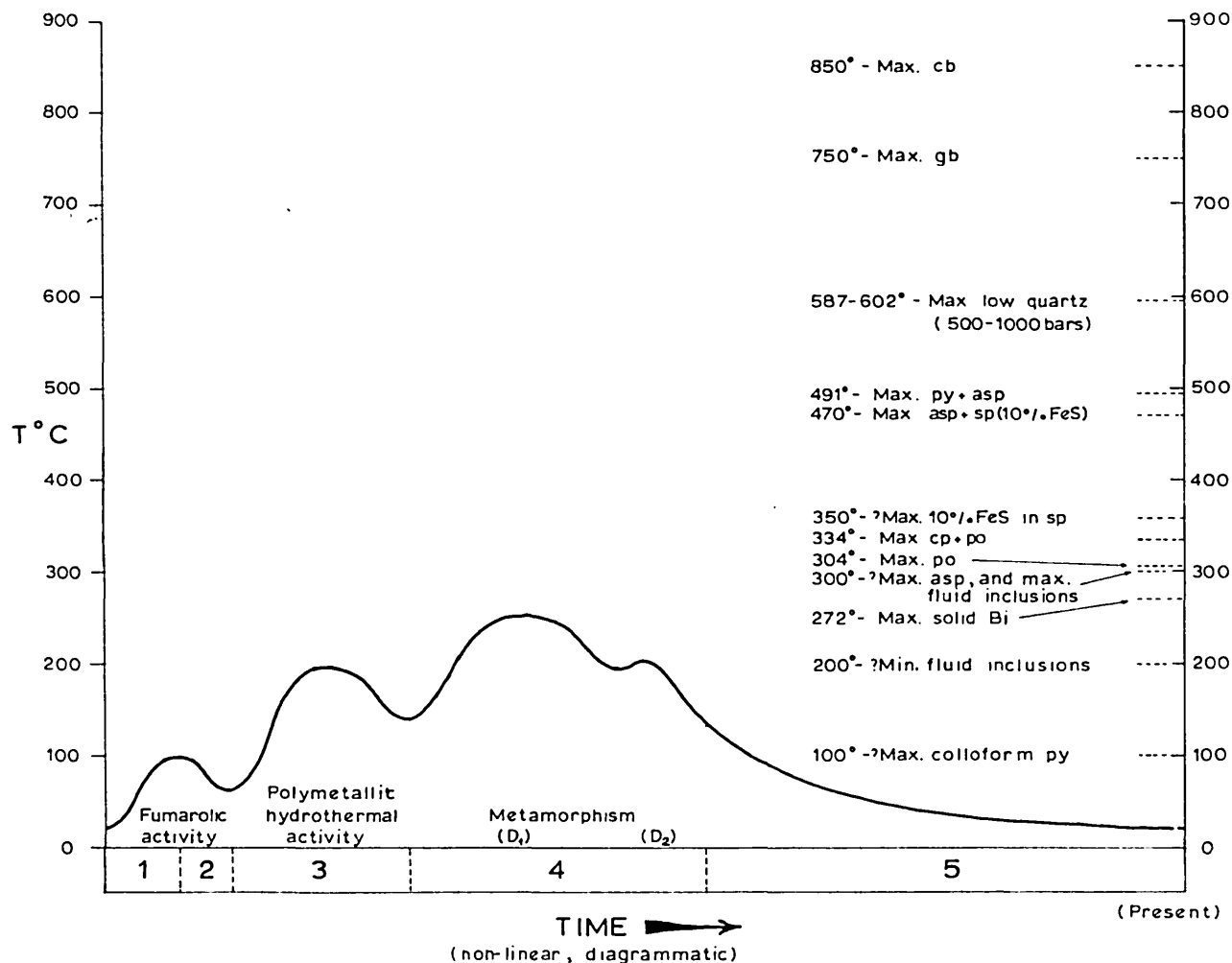
Simultaneously, further polysulphide ions are released and react with remaining mackinawite. Initially, fine crystals of pyrite (melnikovitic) are produced, because there is insufficient time for crystal organization as temperatures are low and the rate of growth is slow.

Primary, zoned, crystalline pyrite exhibits porphyroblastic forms and implies growth at a low temperature (<100°C) in an acid environment supersaturated with iron (compare Fig. 2.39 and 2.40A). The presence of melnikovitic pyrite at Avoca emphasizes the thermometric conclusion as it probably crystallizes at even lower temperatures.

Baas-Becking et al. (11) demonstrated that the pH of pore waters in most marine sediments occupied a restricted

FIG 2.38

TEMPERATURE VARIATION DURING FORMATION of the Avoca deposits



SEQUENCE :

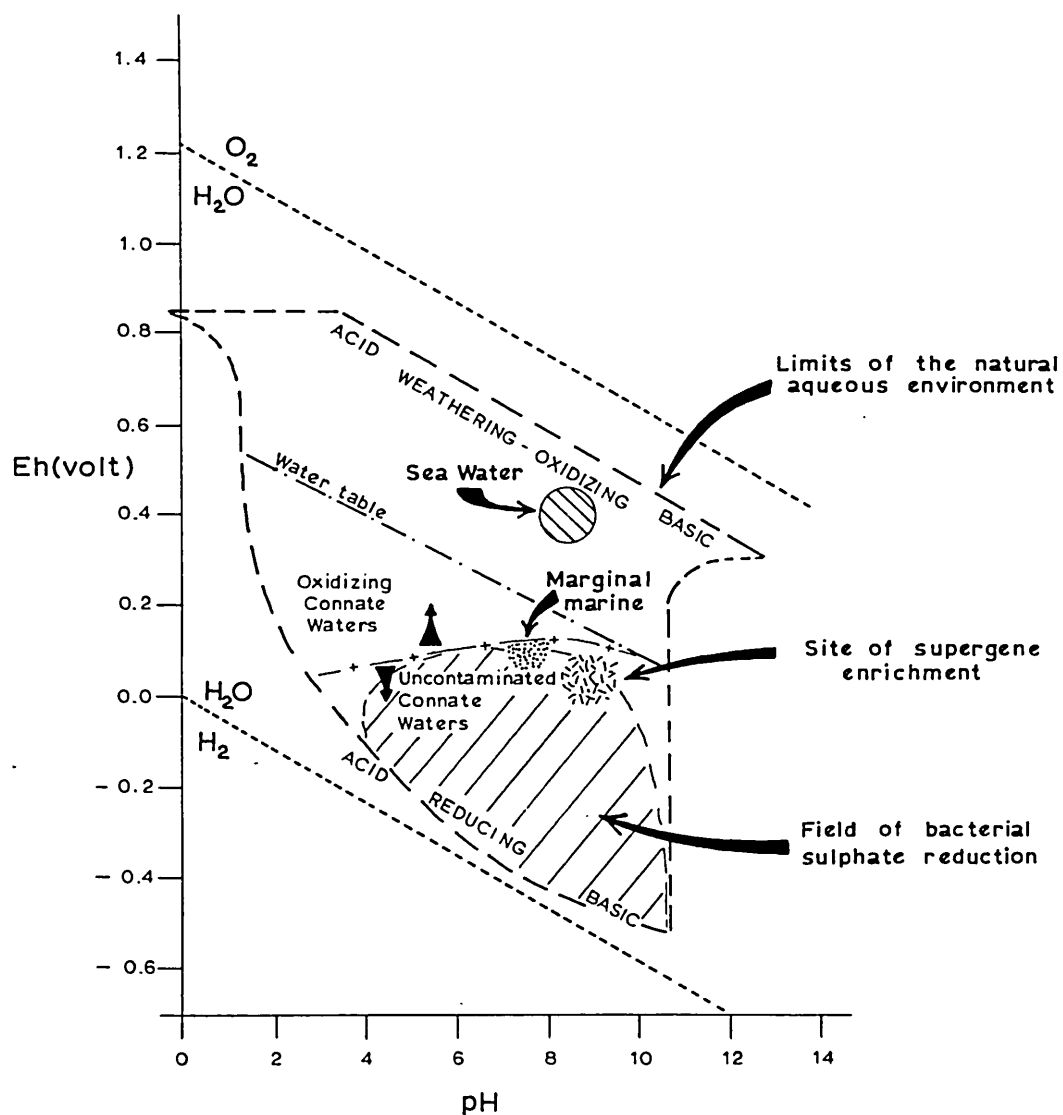
1. Sedimentation and fumarolic activity, with accumulation of carbonaceous and phosphatic horizons.
2. Diagenesis, and growth of pyrite followed by supergene effects (leaching).
3. Hydrothermal mineralization and wallrock alteration.
4. Metamorphism, and minor remobilization.
5. Late stage crustification and supergene effects.

(Mineral symbols in FIG 2.23)

FIG 2.39

STABILITY RELATIONS OF IRON (I)

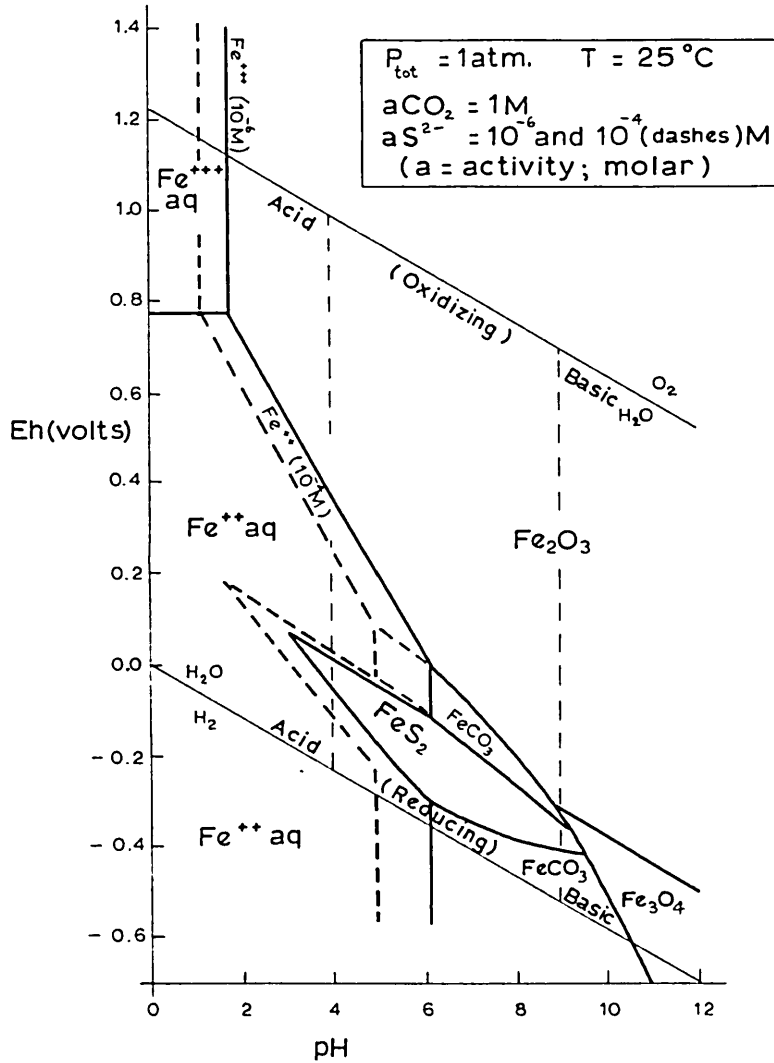
Eh and pH diagram illustrating the fields of near-surface environments.



(After Sato, 1960, Baas-Becking, 1960 and Krauskopf, 1967.)

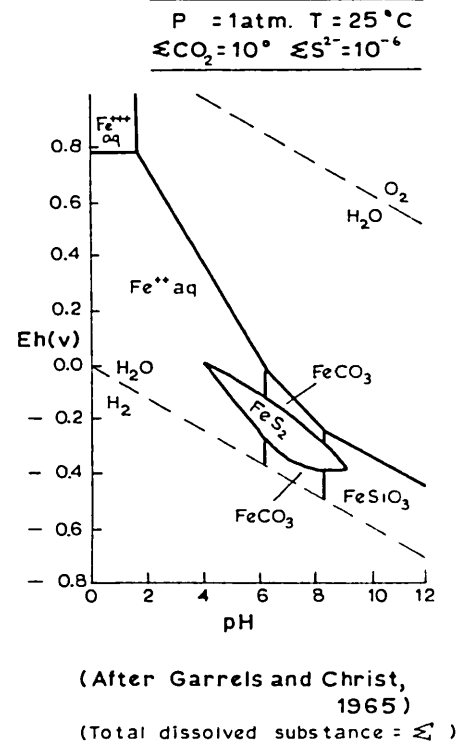
STABILITY RELATIONS OF IRON (II)

A.
Eh-pH relations of the iron species
in water

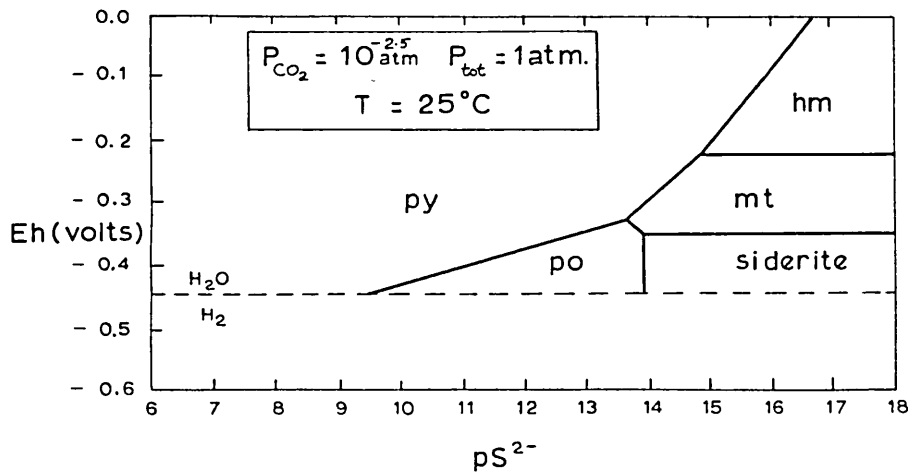


(After Garrels and Christ, 1965 and Krauskopf, 1967)

B.
Eh-pH relations of iron
in the presence of
water and excess silica



C.
Stability fields of iron species as a function of Eh and $p\text{S}^{2-}$ (-log $a_{\text{S}^{2-}}$)
in anaerobic marine sediments (pH=7.5)



(After Berner, 1970)

field (Fig. 2.39) in which the pH varied from 6.8-8.2, in the sea-water environment the pH varied from 7.6-8.3. In the present context, the relationships of the iron species as shown in Fig. 2.40A are therefore oversimplified. Berner (24) illustrated that concentration of hydrogen sulphide in pore waters during ore deposition is an important factor, and in accumulation of syn-sedimentary pyrite, would be critical. Formation of pyrite probably took place in an open system in which the sulphur, produced during sulphidation of goethite, would have been lost to the overlying water. This, combined with precipitation of iron sulphide, would have lowered the content of dissolved polysulphide. In this environment, new stability relations exist, exemplified by Fig. 2.40B, showing relationships at a pH of 7.5 (not unreasonable for pore waters) and demonstrates the wide field of pyrite stability. A large number of assumptions have to be made in applying these diagrams, but the dominance of the pyrite field in an aqueous medium similar to that expected in pore waters below the sediment water interface during the formation of the pyritic zones is obvious. This is amplified in the discussion of genesis.

Framboidal pyrite in carbonaceous shales indicates that strongly reducing conditions existed locally and that growth took place at low temperatures, possibly within gas vacuoles (187).

Unzoned crystalline pyrite occurs with pyrite showing primary growth fabrics. As it forms under so many divergent conditions, little can be deduced from its presence.

b) Iron oxides

The phase relationships of the oxides, carbonate and sulphides of iron in water at 25°C and 1 atmos. pressure are illustrated in Fig. 2.40A.

Coexisting magnetite and siderite with pyrite indicate fluctuating conditions. The field of siderite encloses strongly reducing conditions and requires greater than atmospheric amounts of carbon dioxide (Fig. 2.40C). The total dissolved carbonate must be $>10^{-3}$ otherwise, the siderite field

will disappear. Thus, magnetite and siderite in the Pond lode may indicate a local change in the amount of dissolved carbonate in the depositional environment, possibly due to an increase in carbon dioxide from fumaroles. The facies variations inherent in the presence of coexisting magnetite and hematite have already been discussed.

c) Base Metals

When the minor minerals are excluded, two major 'systems' of mineralization appear:

- (i) Pyrite and chalcopyrite
 - and (ii) Sphalerite and galena,
- which are both contained within a siliceous matrix.

These siliceous zones are crosscutting and have other features which point to an epigenetic origin. Textures indicate the corrosive nature of the metal-bearing siliceous media.

A great deal of research has been completed on the synthetic and natural sulphide systems, mainly by Kullerud and his co-workers. A summary appears in Barton and Skinner's paper (17).

(i) Pyrite and chalcopyrite with excess silica

The textural relationships are entirely consistent with Kullerud's work on the Cu-Fe-S system. Fig. 2.41B illustrates relations at temperatures close to those suggested by other indicators.

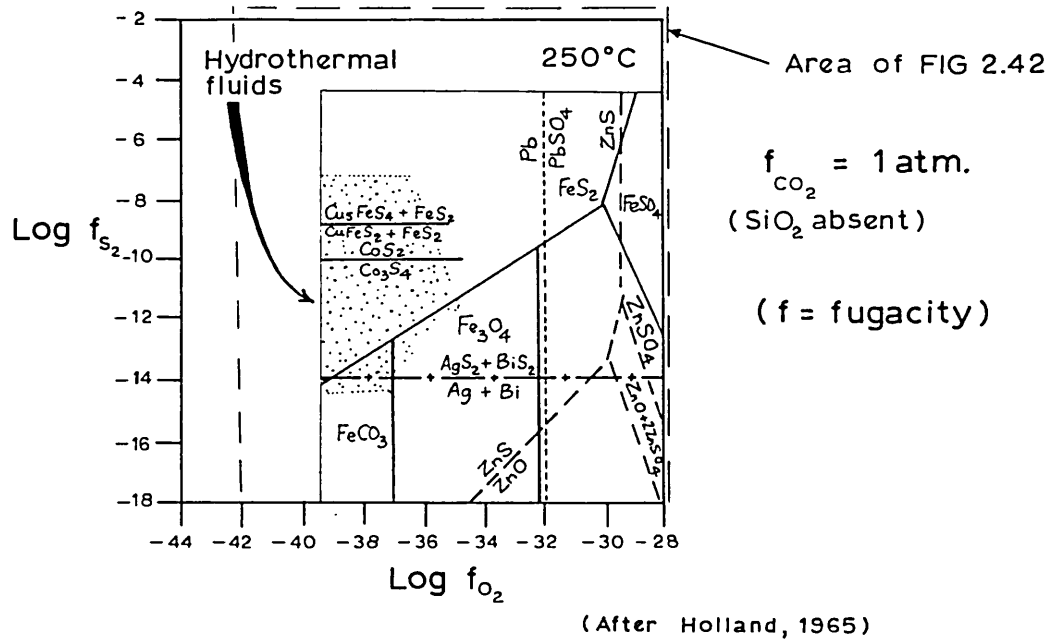
Holland's work (115) on the thermochemical stability of sulphide systems with respect to chloride-rich solutions is summarized in Fig. 2.41A. The field of 'hydrothermal fluids' includes the mineral assemblages at Avoca. The activity of silica determines whether or not silicate replaces the oxide field. Fig. 2.41A illustrates conditions in the absence of silica, but the hydrothermal fluids at Avoca probably contained excess silica and thus silicates may be expected.

(ii) Sphalerite and galena with excess silica

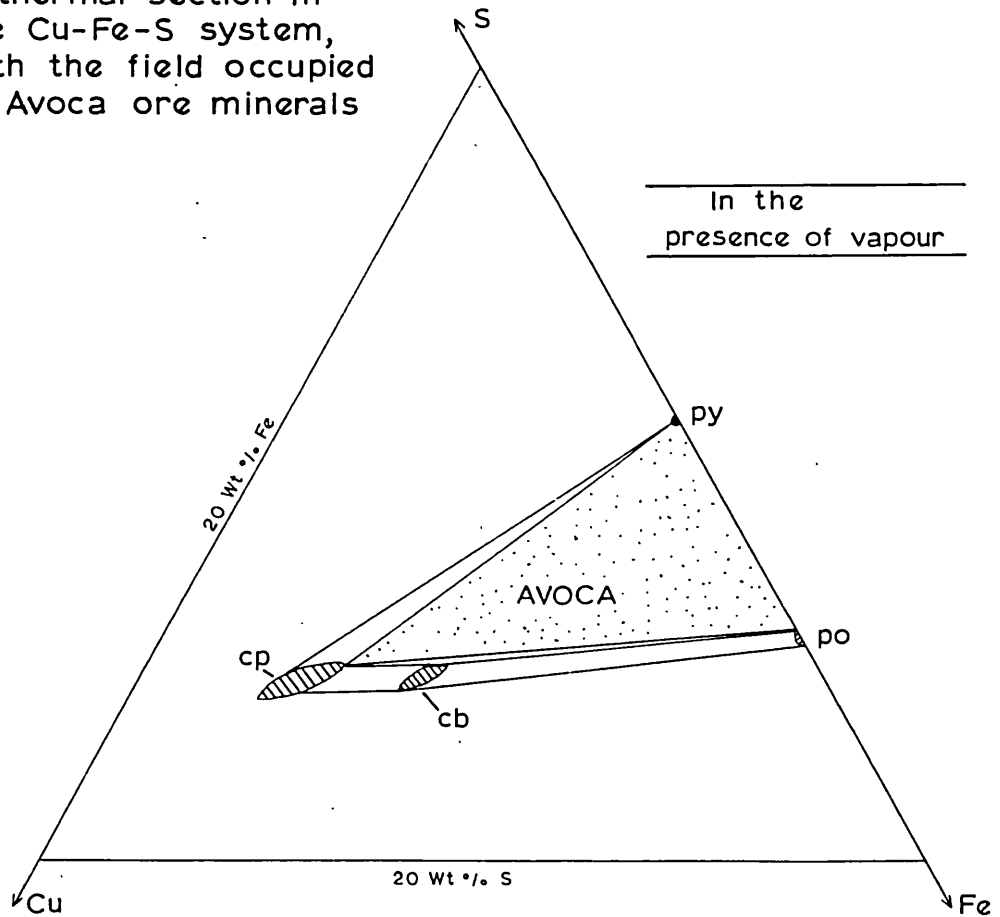
The synthetic systems and thermochemical predictions do not indicate any anomalous relationships in the mineral associations at Avoca.

FIG 2.41

A. Composition of liquid and vapour phases which can be in equilibrium with common mineral associations in hydrothermal ore deposits



B. Part of the 300°C isothermal section in the Cu-Fe-S system, with the field occupied by Avoca ore minerals



(After Yund and Kullerud, 1966)

d) Wallrock and base metal assemblage

Meyer and Hemley (151) in a discussion of wallrock alteration presented a diagram covering part of the field in Fig. 2.41A, and on which the mineralization and alteration at Avoca can be plotted (Fig. 2.42).

Field B illustrates the coexisting phases in the mine area assemblage, and diagrammatically the development path: early magnetite is followed by pyrite with or without coexisting chalcopyrite and finally exsolution of pyrrhotite occurred. The matrix is chlorite and minor sericite with excess silica. Excess total dissolved CO_2 is represented by siderite and late carbonates.

Field A diagrammatically represents the iron ore occurrences in which magnetite, hematite and minor pyrite and chalcopyrite coexist in chloritic wallrocks. The higher oxygen fugacity of this field may equate with a near surface environment, whereas, in the mine area, mineralization developed at a lower level.

2.3.9. Mineral and metal distribution

Mineralization in the Avoca deposits exhibits a crude zonal pattern. Certain mineralogical and elemental variations along the regional strike and down the dip, are examined in this section, and related to the structure and stratigraphy. The possible usefulness of the zonal pattern as a genetic or environmental indicator is then discussed.

2.3.9.1. Mineral distribution

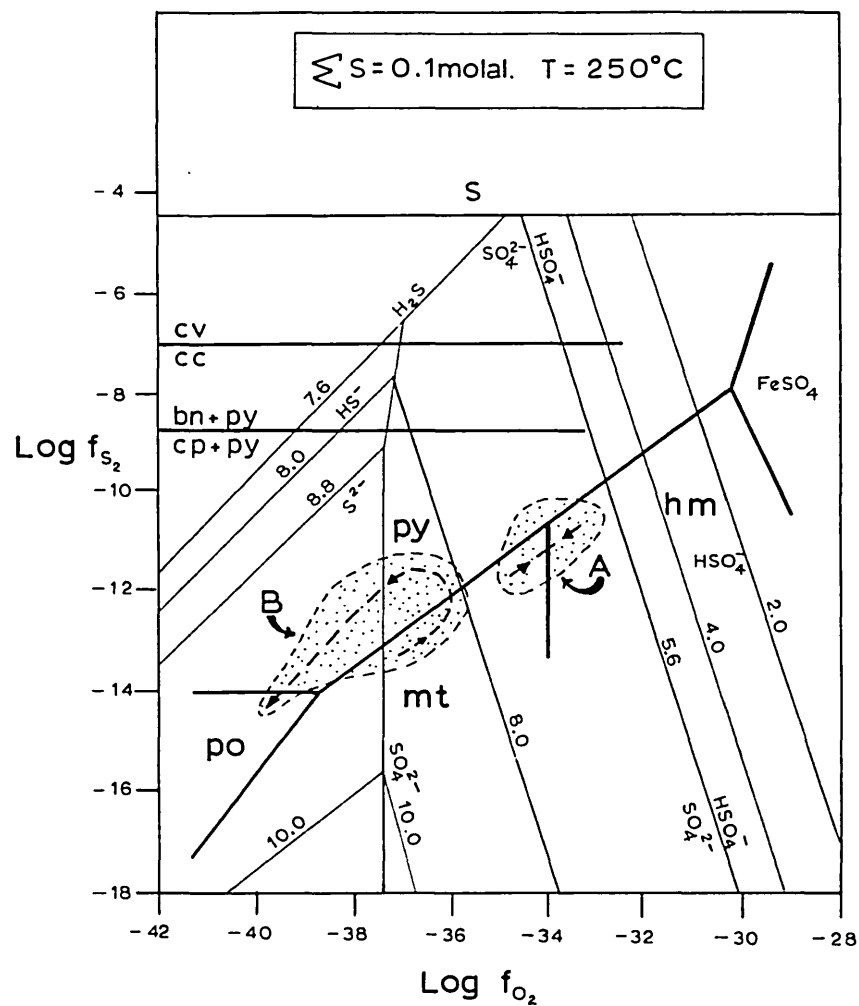
A direct consequence of using the S/Q logging method is that major mineral distributions can be graphically presented from the data contained in the log. Examples of this are shown in Maps 6 and 7, displaying distributions at West Avoca in a pyritic zone; the Pond lode, on the 1300 level, and a siliceous zone; the South lode on the 1670 level.

a) Pond lode (Map 7)

Quartz. A distinct concentration of disseminated and vein quartz occurs in the footwall of the ore zone and there are

FIG 2.42

FUGACITY - pH DIAGRAM OF PART OF
THE Cu-Fe-S-O SYSTEM



A : Field of mineralization and alteration
at outlying iron ore occurrences, Avoca district.

B : Field at Avoca mine.

- - - Diagrammatic development of the assemblages.

— Iso-pH contours.

ΣS Total aqueous sulphur.

(After Meyer and Hemley, 1967)

irregular concentrations in the hangingwall. The overall content of quartz in the ore zone is low.

Pyrite. A marked compound seam rich in pyrite occurs in the footwall of the ore zone and this correlates with the green-black chlorite schist horizon (Map 4).

Chalcopyrite. An even distribution of chalcopyrite exists in the footwall, and there is evidence of some concentration in the hangingwall.

Sphalerite and galena. Sphalerite is enriched in the hangingwall of the lode and galena has a sporadic distribution. Amounts of both minerals are low throughout, except for a concentration at the western limit, forming part of the Lead-zinc lode.

Lampard (138), in a statistical study of assay data, demonstrated that there was a decrease in the content of chalcopyrite, sphalerite and galena with increasing depth in the Pond lode. Concentration of sphalerite and galena occurred in the western portion of the lode, with enrichment in the upper levels on the hangingwall.

b) South lode. (Map 6)

Quartz. There are indistinct zones of anomalous quartz content on the hangingwall and footwall of the ore zone.

Pyrite. Medium to fine grained disseminated pyrite has a uniform distribution, with admixed chalcopyrite. A discontinuous zone of coarse grained pyrite occurs in the footwall, in the central and eastern portions. The hangingwall also contains a zone of coarse grained pyrite, which passes into medium and fine grained material with depth into the country rocks. (At the western limits, the presence of Central lode sulphide-rich lenticles is obvious.)

Chalcopyrite. An ubiquitous associate of vein quartz, chalcopyrite occurs as sporadic concentrations in the lode. Massive chalcopyrite seams tend to be more abundant in the hangingwall (e.g. Fig. A.1).

Sphalerite and galena. Sphalerite and galena are

mainly restricted to the eastern (hangingwall) limits of the lode lining fractures or shear voids or, rarely banded.

Lampard's results (138) were not at variance with these, and showed, in addition, that the footwall of the South lode was enriched in sphalerite and that the proportion of sphalerite and galena in the upper levels was sympathetic with sulphur content (largely represented by pyrite).

2.3.9.2. Metal ratios

Stanton (213) and Lampard (138) discussed the metal abundances at Avoca, and the following synthesis is drawn from their work.

a) Pond lode

Lampard demonstrated that the mean Zn:Pb ratio was $\sim 2.51:1$, and that copper and zinc were antipathetic, a fact also noted by Stanton.

Typical metal ratios from the pyritic zones at Avoca are shown in Fig. 2.43A. The dominance of zinc over lead, which holds throughout the ore zones, is obvious.

b) South lode

An increase of the Zn:Pb ratio with depth was noted by Lampard, from $\sim 3:1$ to $4:1$, but the paucity of data makes this conclusion dubious.

The metal ratios in the South lode, and typifying siliceous (lead-zinc free) mineralization are shown in Fig. 2.43B.

c) Lead-zinc lode

A mean Zn:Pb ratio of $\sim 2.5:1$ appears to typify the lead-zinc rich material at West Avoca (138) and is also characteristic of the East Avoca mineralization.

Metal ratios approximate to the distribution shown in Fig. 2.43C.

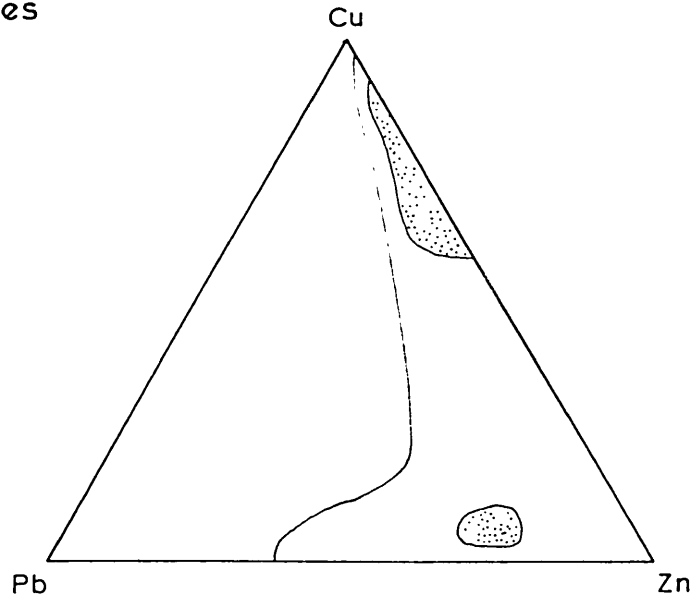
2.3.9.3. Relationship between mineral distribution and lode structure

Conolly (60) developed a method for illustrating the shape of a lode deposit which consists of selecting an arbitrary inclined reference plane and measuring the distance of a constant

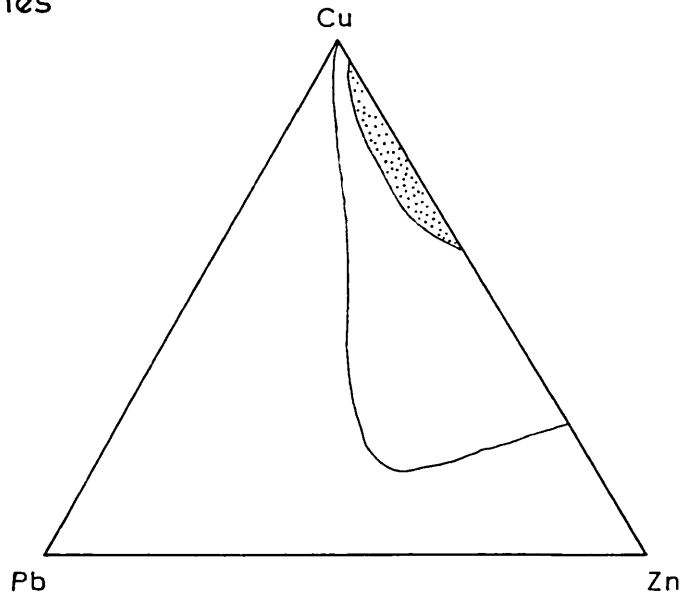
FIG 2.43

METAL RATIOS, WEST AVOCA

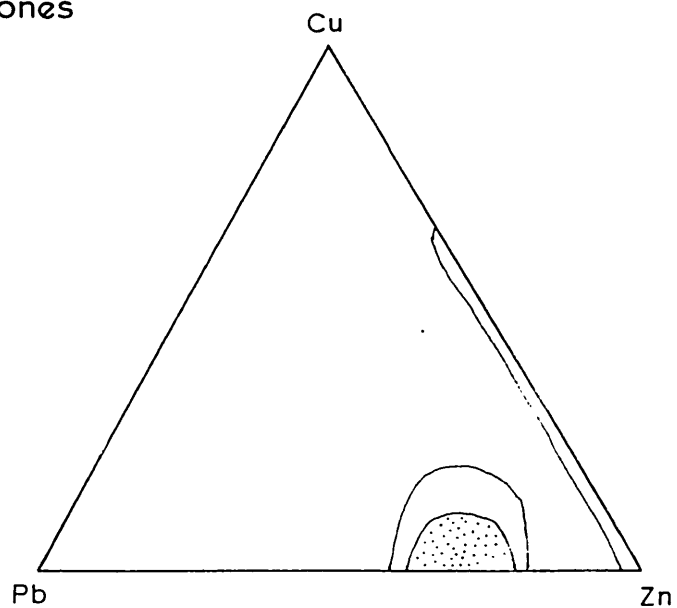
A. Pyritic zones



B. Siliceous zones



C. Lead-zinc zones



(Weight %.)

(After Lampard, 1960)

representative marker horizon in the lode from that plane. The distances are plotted on a longitudinal section, contoured, and produce a useful picture of the lode shape. Visual comparison of the Conolly contour diagram, on which major structural features are superimposed, with a contour plot of assay x width value, strikingly illustrates any relationship between lode structure and mineral (metal) distribution.

The lodes in the Avoca district are not true fissure veins, for which the Conolly diagram was initially devised, but data was collected for both the Pond and South lodes to discover whether any useful conclusions emerged. A plane inclined at 51° S with a bearing of 180° (T.N.) was chosen as the reference plane. A contour interval of 10ft was taken, as mine assay values are universally for 5 ft lengths.

a) South lode

A diagram showing contours of the distance between the footwall of the lode and the reference plane produces a uniform, featureless plot, and the metal value diagram merely outlines the limits of the mineralization, revealing no more than a conventional assay section.

b) Pond lode

Contours of the footwall of this lode illustrate some interesting features, (Map 8).

The Conolly diagram demonstrates the presence of two major domal areas (Map 8:A) which equate with areas rich in lead-zinc and poor in copper (Map 8:B). Marked change in slope of the contour surface coincides with faulting.

The Copper Value diagram illustrates the prominent pitch of maximum enrichment, 58° SW, corresponding to a plunge of 42° SW. The areas of low copper value, in relation to the overall mineral distribution, coincide with enrichment in lead-zinc. (The incoming of the Lead-zinc lode is indicated by a low at the western limit on the 1300 level. Below this level, the low enlarges and may equate with the presence of intrusive microdiorite dykes crosscutting the lode (Map 2)). Faulting causes a reduction in metal value, illustrated by the intersection

of the central fault zone with the lode.

2.3.9.4. Discussion

Spatial mineralogical and metal zonation in sulphide deposits has long been recognized (139) and many attempts have been made to correlate the observed sequences with hydrothermal and/or supergene effects. The primary objective of any study must be to determine which of these two processes has been active in producing the zonal arrangement, and this may provide significant genetic information.

The Avoca deposits are lenticular zones of banded, massive and disseminated ore, broadly conformable to the regional foliation, and as such may be termed stratiform (218). Stanton has enumerated the characteristics of this type of deposit (214). Occurrences in the Kupferschiefer and in the Zambian copper belt are termed normal stratiform deposits; being enclosed in a predominantly sedimentary sequence. Avoca, in common with many other deposits in the Appalachian-Caledonian orogenic belt, and similar eugeosynclinal sequences around the world, is typical of the volcanic category as it occurs within an essentially volcanic sequence. Mineralogically, these stratiform deposits consist of either pyrite or pyrrhotite with variable amounts of sphalerite, galena and chalcopyrite (213). Minor to trace amounts of arsenopyrite and sulphosalts also occur, making up a sequence equivalent to the assemblage at Avoca (with the exception of pyrrhotite). Zoning has been described within these deposits by several writers (5, 144, 191, 238) and the universal feature noted is the lack of correlation between enrichment in copper and that in lead-zinc.

Roscoe (191) and Lusk (144) found that zones of lead-zinc enrichment at the stratigraphic base of the Noranda and Heath Steele deposits were adjacent to porphyry rocks, possibly representing volcanic necks, and suggested a volcanic-exhalative genesis for the mineralization.

Zoning is a three dimensional feature and may be either lateral (approximately parallel to the foliation, in this case) or transverse (normal to the foliation). At Avoca the lateral

variations are marked by the incoming and dying-out of mineralized zones on a megascopic scale e.g. the qualitative changes in character of mineralization with depth at West Avoca. Transverse zoning becomes important on a mesoscopic scale within individual zones and this can be studied in detail through drillhole intersections. Interpretation of the ore textures indicates that the pyritic zones retain evidence of primary growth fabrics and have a syn-sedimentary origin, in part at least. The postulated structural scheme suggests that these pyritic zones are stratigraphically underlain by siliceous zones, representing stockworks. These siliceous zones exhibit crosscutting (epigenetic) relationships to the host rocks and have almost certainly been produced by hydrothermal ore fluids.

Copper is present in both the pyritic and siliceous zones as chalcopyrite, which predominantly has a recrystallized grain fabric: thus, its origin is in doubt. It is reasonable to suppose, however, that the copper in the siliceous zones is of hydrothermal origin, and the copper in the pyritic zones probably has a syn-sedimentary origin similar to the pyrite. The tenor of copper is remarkably uniform in the siliceous zones and shows local variations within the pyritic zones (emphasizing that a difference exists between the two types of mineralization). The siliceous, stockwork zones, probably formed during a relatively distinct period of mineralization and thus might be expected to contain an even distribution of copper. The bedded pyritic zones, on the other hand, show evidence of formation within a system rich in iron sulphide in which conditions fluctuated and were ideal for the production of local concentrations of copper. The latter might well be related to the acid sub-surface water movement and would therefore have a somewhat random distribution.

Enrichment in zinc and lead is generally confined to the margins of the ore zones at West Avoca, showing a statistical sympathy with sulphur content in certain areas (138). At East Avoca, appreciable zinc and lead also occur in the siliceous zones in addition to the marginal occurrence at Kilmacoo. Lampard (138) suggested that the distribution of zinc and lead

at West Avoca might be related in some way to the presence of pyritic bands and was probably superimposed on, but not influenced by, an earlier stage of pyrite-chalcopyrite mineralization. Detailed examination of the mineral fabrics supplies the key to the mechanism, by indicating that dissolution of the marginal portions of the sulphur-rich pyritic zones by circulating chloride-rich metal-laden fluids probably caused precipitation of the zinc and lead sulphides. These fluids were almost certainly genetically associated with the copper-rich fluids of the stockwork zones, and a mechanism for partitioning a lead-zinc rich fraction must be sought.

It is well known that ore deposition is not a simple phenomenon and the nature of ore forming solutions is poorly understood. If the ore fluids at Avoca were hydrothermal and chloride-rich, deposition of copper would have preceded zinc and lead (14) and the latter would only have been precipitated when the solubility of the fluid was radically altered. In this case, this criterion is provided by a sudden increase in dissolved sulphur on dissolution of pyrite. (This concept is elaborated in section 2.3.10).

To date, no satisfactory scheme to explain the lack of correlation observed between copper and lead-zinc enrichment has been put forward, but the mechanism outlined above may supply this requirement. In order to apply the theory to a specific volcanic stratiform deposit it is necessary to know the stratigraphic relationships, and to differentiate the zonal sequences in ore zones which are not of equivalent origin (e.g. at Rio Tinto, in 252).

The Avoca deposit is a type example where a hydrothermal (epigenetic) zonal sequence has been superimposed on an earlier, syn-sedimentary (supergene) zonal pattern. It is noteworthy that a similar situation exists at Tilt Cove, Newfoundland (26) where there is a volcanic-stratiform pyritic deposit in the continuation of the Caledonian mobile belt in North America.

2.3.10. Genesis

2.3.10.1. General

The genesis of the ores in the Avoca district depends heavily upon evidence for the depositional environment. Metamorphism effected the sulphide and silicate assemblages to a varying, but relatively minor degree. It is thus possible to make realistic proposals about the depositional environment and metallogenesis.

The country-rocks are a pyroclastic sequence with sedimentary intercalations and indicate a volcanic environment. There is no positive evidence that the source of the ore constituents was cogenetic with that of the enclosing rocks, but results from a study of trace elements in pyrite from the sediments and pyroclastics suggests that a similar genesis of the iron and sulphur is possible. Sulphur isotope studies (138) corroborate this and appear to negate an origin of the sulphur from sea-water sulphate.

Mineralogical study and macroscopic spatial relationships indicate the existence of a number of ore types. The genesis of each type is considered separately despite the fact that differing types of ore may occur close to one another.

2.3.10.2. Pyritic zones

The primary nature of the pyrite forming the bulk of these zones has been established through textural evidence. Intercalations of iron-rich chlorite signify derivation from a ferrous silicate (chamosite) during diagenesis, or from metamorphosed iron-rich tuffs or sediments. Regardless of the alternative chosen, a submarine environment appears likely. This notion receives support from the nearby presence of high energy sediments, graded tuffs, showing evidence of deposition from turbidity flows. The presence of phosphorites indicates that the depths of water were generally shallow (223).

Pyroclastic deposits associated with the iron-rich horizons indicate that rapid changes took place in the formational topography, the uplifted areas providing abundant material for

erosion. The sources of iron could therefore have been erosional, fumarolic or some combination of the two. The genesis of the sulphur was probably through the fumarolic exhalation of H_2S or SO_2 .

Regardless of the precise mode of discharge of iron and sulphur into the marine system, they would have been oxidized, forming goethite and sulphate anions, in the environment envisaged. Melnikovitic and zoned crystalline pyrite indicate growth at temperatures $\leq 100^\circ C$, it is noteworthy that the reported temperatures from effusive submarine brines in the Red Sea are $40-60^\circ C$ (29).

Goethite must have been accumulated, for dense pyritic layers to develop, freely or adsorbed on clay particles on the sea bottom. Redox potentials and pH conditions in this situation were no doubt continually fluctuating and the supply of iron was not constant. The pyritic layers are laterally continuous and show no evidence of disruption by sedimentary mechanisms, slumping etc. (Folding and displacement of iron sulphide seams can be shown to have occurred after lithification). Bottom currents have not affected the sulphide layers and there is an absence of abrasion amongst the pyrite grains. No suitable site for the accumulation of pyrite above the sediment-water interface is therefore indicated, a fact born out by Figs 2.39 and 40 and the thermodynamic calculations of Curtis and Spears (65). This study demonstrated that pyrite could only attain stability, in sediment masses.

The formation of the primary zoned and colloform pyrite is postulated as having taken place below the sediment-water interface, under requisite redox potential and pH conditions. The presence of abundant zoning in the pyrite grains implies slow growth, and changes in composition of the fluid medium in which the grains were growing, a situation compatible with growth within the sediment pore waters. Indication of local reducing environments are provided by intercalated horizons of carbonaceous material, and within these horizons, aqueous ionic sulphur may have been produced through the bacterial reduction of sea-water sulphate. Slow reaction, possibly during diagenesis, could have created the framboidal pyrite.

Sulphur isotope data support the notion that the sulphur was volcanic. Derivation of the iron and sulphur from surface, subsurface and/or submarine fumaroles appears feasible.

2.3.10.3. Siliceous zones

The siliceous zones stratigraphically underlie the pyritic zones. Crosscutting relationships are shown with the enclosing wallrocks and the mineralization has the characteristics of a stockwork below the conformable pyritic zones. An envelope of intensive silicification is common, sericitization is important and primary textures in pyrite are lacking. This ore-type is demonstrably epigenetic.

A distinctive suite of pyroclastic material (felsite), generally occurs stratigraphically below the siliceous zones. These represent large volumes of highly felsic magma, and the presence of a similar magma at depth appears reasonable. Burnham (44) stated that the aqueous phase from a felsic magma would become chloride-rich in the waning stages. He calculated that the initial fluid would contain 0.35 M NaCl, 0.2 M KCl, 0.04 M HCl, and 0.005 M CaCl₂, and at a temperature of 700-750°C and at pressures of 1,000-2,000 bars, would have a pH of 5-6. Furthermore, cooling below the solidus of a felsic magma in contact with quartzo-feldspathic rocks would decrease the amount of bonded K⁺ and H⁺, and the excess would become available for incorporation in hydrothermal fluids.

Additional evidence for a felsic magma chamber below the accumulating pile of eugeosynclinal sediments is afforded by the post-tectonic granodioritic complex at Croghan Kinshela, and the Leinster pluton. The sedimentary sequence is dominantly quartzo-feldspathic in character, and the sericitic alteration zone accompanying the siliceous mineralization testifies to the activity of potassium-rich fluids. Analyses of the felsites substantiate anomalous concentrations of potassium, and the relevance of Burnham's study is confirmed.

The ore constituents in the siliceous zones have certainly been deposited from fluids, and the source of these fluids is inferred to be related in some way to the products of the

aqueous hydrothermal phase of the underlying felsic magma.

Transport mechanisms of metals in ore formation have been studied experimentally in some detail recently. The solubility of the ore metals, demonstrated by Helgeson (113), is generally low, except in chloride-rich brines. It appears reasonable to suggest that the ore constituents at Avoca were transported in chloride-rich solutions.

The volcanic environment postulated for the accumulation of the pyritic zones was obviously an area of high geothermal activity and a suitable locus for the chloride solutions. The solutions may have moved to the surface through conduits related to the feeder channels for the magma, driven by a mechanism similar to that which operated at Wairakai (81). The chloride-rich, metal laden solutions would meet circulating connate and meteoric waters near the limits of their ascent to the surface. The zone of mixing of differing fluids would have been an ideal site for ore metal deposition.

The increase in porosity of the pyritic zones towards their base is evidence for the leaching activity of circulating pore waters following formation. This would have resulted in the pore waters having an increased acidity.

The chloride-rich metal brines would have been highly corrosive to the primary zoned and colloform pyrite. In the stratigraphically lower levels of the pyritic zones, mixing of the pore waters and the chloride solutions took place in the presence of pyrite. Strong corrosion of the pyrite resulted in a rapid increase of reduced sulphur species in the system, which would have reacted with the copper, zinc and lead from the metal brine to form sulphide. Iron from the replaced pyrite became incorporated in the sphalerite lattice, thus accounting for the high iron content of primary sphalerite. Sawkins (196) recently proposed that brecciation textures in pyrite from the Providencia Mine, Mexico, were due to the activity of a supersaturated hydrothermal solution. This suggests that leaching of pyrite by chloride-rich solutions may be of more frequent occurrence than is generally recognized.

The effects of fluid mixing, coupled with a sudden decrease in temperature and pressure resulted in the development of stockwork zones at lower levels. The presence of unzoned crystalline pyrite in these siliceous zones, its corroded nature and the absence of primary growth textures may indicate deposition at above 100°C, in the presence of a corrosive medium, possibly chloride-rich. This model is consistent with the temperatures recorded at depth within geothermal systems (200-300°C) (82). The stockwork mineralization at West Avoca was cupriferous and at East Avoca it was lead-zinc rich.

Burnham (44) stated that the ore metals would be deposited in the order: iron, copper, lead, and zinc from hydrothermal solutions. This conforms with the spatial distribution of ore types at West Avoca, where lead and zinc occur at the extremities of the mineralization. The picture at East Avoca is probably similar, but precise correlation will have to await the results of more drilling and development information.

The genetic development of the orebodies at Avoca is illustrated schematically in Fig. 2.22 (p.92).

The presence of the major economic mineralization in the centre of the mineralized belt may not be fortuitous. This may have delineated an area of incipient crustal weakness which provided the zone of dilatation in which the fumarolic and magmatic activity originated.

At either end of the mineralized belt are possible remnants of the eroded cores of basic to intermediate cone volcanoes. These may have provided the pyroclastic debris deposited in the intervening trough. Major mineralization occurs in a zone of increased pyroclastic deposition. (This supports the idea of a central zone of subsidence.)

The discussion has so far tacitly assumed the presence of anomalous silica and metal concentrations in the chloride-rich ore solutions. The source of the silica may be the felsic magma at depth or possibly hydrothermal leaching of the walls of the conduit through which the fluids rose to the surface. Similar reasoning applies to the source of the metals, iron, copper,

zinc and lead, minor metals and non-metals in the final elemental assemblage of the siliceous zones. Arsenic and bismuth are amongst the latter and are characteristic of volcanic exhalations (251), which supports the notion that the metals were derived from volcanic sources, possibly with additions from deep connate fluids contained in the sedimentary pile. Trace element contents of the Lower Palaeozoic sediments indicate that these were a potent source of metals (194).

2.3.10.4 Lead-zinc zones

Textures indicate that the primary colloform and zoned pyrite in the lead-zinc zones originated through a process identical to that described for the pyritic zones. The lead and zinc being brought to the surface within chloride-rich hydrothermal fluids. Deposition took place at the site of interaction between these fluids and pore waters in the presence of pyrite, which suffered extensive replacement.

2.3.10.5. Magnetite zones

The magnetite zones generally occur at the limits of the mineralization, outside the mine area, within similar rocks although pyroclastic material is less prominent. The source of the iron and the mechanism of its fixation in the sediments was almost certainly the same as for the pyritic zones. Magnetite, siderite and chamosite can only form under Eh and pH conditions that are typical of sediment pore waters (65). The siliceous (jasperoid) magnetite-hematite lenses probably originated from siliceous iron-rich sediments, below the sediment-water interface possibly during diagenesis.

2.3.10.6 Disseminated and vein-type mineralization

Disseminated pyrite in the sedimentary rocks probably developed from the sediment pore waters during lithification.

The siliceous veins carrying, lead, zinc and other metals which occur sporadically throughout the district may have originated from remobilized metal-rich fluids. These possibly developed, during folding, by the mixing of connate and juvenile waters

The crosscutting lead mineralization at Ballintemple has an equivalent age date to the deposits at the margin of the Leinster batholith. No genetic connexion exists between the Ballintemple mineralization and the Leinster granite, but remobilization of connate fluids in the surrounding sedimentary sequence may have occurred concomitant with the hydrothermal activity developed during consolidation of the pluton. The presence of encrusting dolomite and absence of pyrite, chalcopyrite and sphalerite at Ballintemple testifies to the unique nature of this late-stage paragenesis.

2.3.10.7. Post-depositional changes

The onset of metamorphism, folding and faulting post-dates the major mineralization at Avoca. The boundary between lithification, diagenesis and metamorphism is diachronous, but the effects of later deformation and associated metamorphism are easy to decipher. Minor remobilization of the sulphides took place, and chalcopyrite and galena migrated into pressure slacks. The crosscutting seams of dolomite associated with the Pond lode probably also originated at this stage.

Supergene effects have been produced by circulating groundwaters and surface weathering.

2.3.10.8. Summary

Mineralization within the Avoca district developed in two major, contrasting environments, and the formational sequence is diagrammatically illustrated in Fig. 2.22.

a) Iron accumulation in the sedimentary-diagenetic pore waters of a pyroclastic sequence produced conformable pyritic layers and magnetite (\pm hematite) horizons, under varying Eh and pH conditions.

b) At a later stage, siliceous mineralization developed from migrating chloride-rich metal laden fluids, localized where they mixed with connate and meteoric waters close to the pyritic zones.

The source of the ore constituents is a matter for

conjecture, but evidence from sulphur isotope and trace element studies favours a fumarolic origin for the iron and sulphur in the pyritic zones. The metals in the siliceous zones may be derived from partial fusion of the crystalline basement, or have been leached from previous sediments.

Metamorphism and folding resulted in localized small-scale remobilization and the development of minor crosscutting veins.

SECTION 3

OTHER DEPOSITS IN S.E. IRELAND3.1 Bunmahon, Co. Waterford3.1.1. Introduction

Mining in the Bunmahon district began in 1730 (58), with workings on veins occurring along the coast and inland around the villages of Bunmahon (Plate 50:A) and Annestown (Fig. 3.1). Operations ceased in 1878, and subsequent minor production took place during the period 1904-7. The total output was about 25,000 tons of shipped ore and concentrate (167). Prospecting is being carried on at present.

3.1.2. Stratigraphy

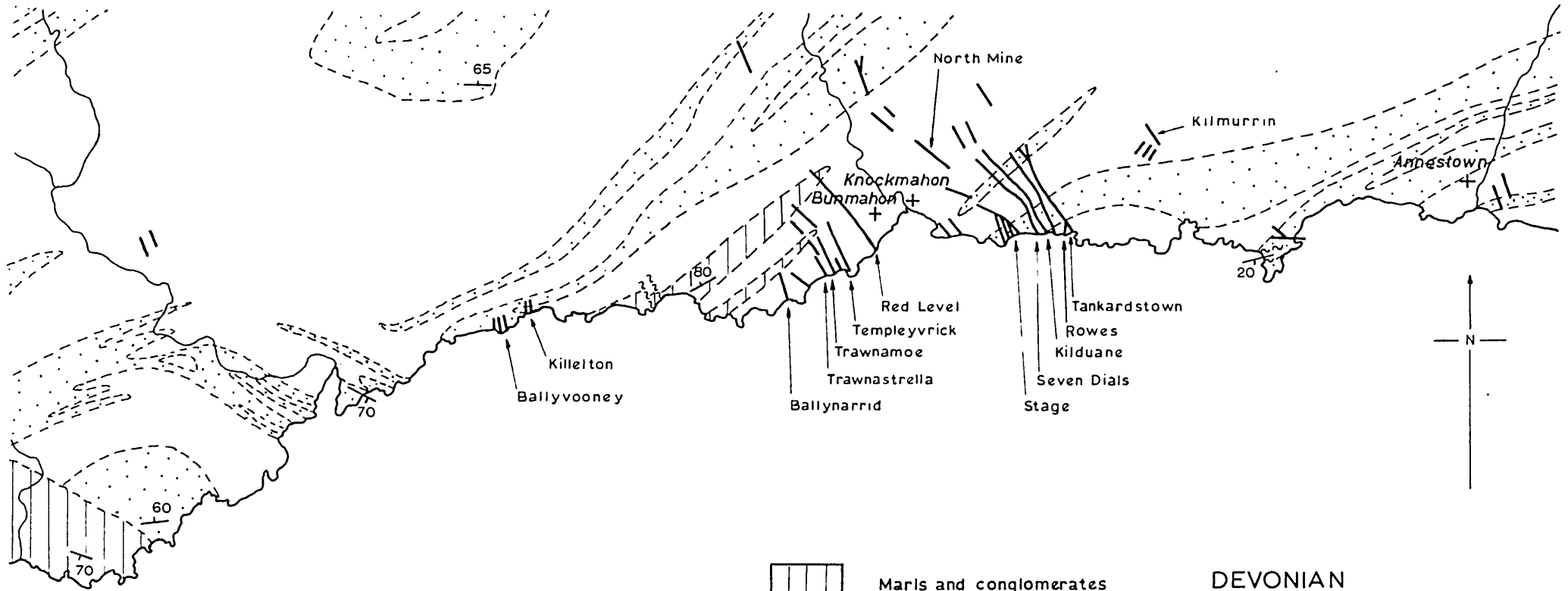
The district (Fig. 3.1) is at the southern limit of one of the two belts of (?) Caradocian volcanic rocks which occur in S.E. Ireland. Country-rocks are part of the Ballymoney Series (75), intruded by crosscutting dioritic dykes and overlain by Upper Old Red Sandstone conglomerates.

Detailed stratigraphic relationships are not clear, but a traverse from east to west along the coastal section summarizes the sequence (183). At Annestown, the sedimentary rocks are black shales with minor calcareous horizons. Felsitic rocks, consisting of interbedded tuffs and lavas become important towards the west. East of Knockmahon, shales and mudstones occur with interbedded tuffs and lavas. Volcanic rocks are abundant in the Bunmahon area, with interbedded shales. The total sequence is probably greater than 10,000 ft thick, post-dates Bala strata and is almost certainly Caradocian.

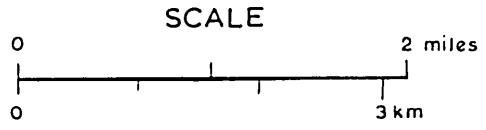
3.1.3. Lithology and Petrography


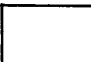
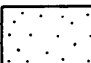


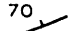

The sedimentary rocks are fine grained, evenly laminated shales and mudstones, purple, green and black in colour. Beds, 0.5-1.5 cm thick are separated by thin laminae 0.2-0.5 mm in width. Rare colour banding delineates the bedding. In thin section, the rocks consist of a microcrystalline aggregate of quartz and clay minerals with rare feldspar grains. The laminae

FIG 3.1



BUNMAHON DISTRICT
GEOLOGICAL SKETCH MAP



- | | | |
|---|----------------------------------|---|
|  | Marls and conglomerates | DEVONIAN |
|  | Tuffs and andesitic lavas | } ORDOVICIAN
Ballymoney
Series |
|  | Shales, mudstones and limestones | |
|  | Geological contact |  Fault |
|  | Dip and strike of bedding |  Vein / Lode |

(After Geological Survey : Sheet 178.)

are composed of a felty mass of clay minerals and these are sometimes reorientated parallel to the foliation.

The volcanic rocks are coarse, medium and fine grained tuffs with interspersed flows. Blue-grey, green and buff in colour, the lavas are often massive, flow banded and also show columnar jointing. Green, epidotic lavas with calcite impregnated vesicles occurring near Bunmahon have rude pillow-structures. In thin section, a felsophyric texture exists in the felsitic rocks, with phenocrysts of quartz and plagioclase feldspar set in a cryptocrystalline matrix containing scattered grains of epidote and leucoxene (Plate 50:F).

The tuffs are green to grey in colour and the pyroclasts are graded. The rocks, in thin section, consist essentially of feldspar, pyroxene, quartz, calcite, sericite and epidote with accessory iron oxides and leucoxene. Despite intense deuteric alteration, their fragmental nature is apparent (Plate 50:E).

3.1.4. Petrochemistry

Analytical data relating to the felsitic rocks has been published by Phillips (175), Hatch (107) and Reed (184). New analyses by the writer are shown in table 28.

Reed remarked that the felsites were generally potassic, with the exception of the analysis by Phillips which suggested that sodic varieties existed. Analysis B.21 in table 28, confirms the potassium enrichment. This feature is analagous to that described from the Avoca district and a similar mechanism for the generation of a potassium-rich, potentially explosive, magma fraction is proposed.

The andesitic tuffs (B. 2, 3 and 34 in table 28) have major oxide contents which only differ slightly from the values at Avoca. Their calc-alkaline affinities stress the petrological unity of the volcanic lineaments in S.E. Ireland.

Trace element contents of the rock-types illustrate comparable values to those at Avoca and are typical of the mean elemental abundance figures (228) for rhyolitic and andesitic igneous rocks.

Table 28 Partial analyses of rocks from the Bunmahon district, by X-ray fluorescence.

Major oxides: (%)	B.21	B.2	B.3	B.34
SiO ₂	72.20	51.80	50.60	53.50
Al ₂ O ₃	15.67	13.00	11.05	13.85
TiO ₂	0.31	0.87	0.66	0.79
Fe ₂ O ₃	1.31	0.24	1.15	1.82
FeO	1.04	6.76	6.80	4.59
MnO	0.03	0.27	0.15	0.18
MgO	1.35	6.12	10.45	5.66
CaO	0.34	3.60	3.96	6.04
Na ₂ O	1.15	5.00	3.72	4.00
K ₂ O	3.61	0.70	0.38	1.07
P ₂ O ₅	≠	0.14	0.08	0.10
Total S	0.03	0.16	0.17	0.14
H ₂ O +	—	—	—	—
H ₂ O -	—	—	—	—
Total	97.03	88.62	89.17	91.74

≠ not detected — not sought

Trace Elements: (ppm)	B.21	B.2	B.3	B.34
Co	≠	35	57	34
Ni	23	82	189	139
Cu	104	128	80	97
Zn	47	143	127	95
Rb	186	18	15	29
Sr	8	152	199	186
Pb	25	30	13	10

Analyst: C.J.V. Wheatley.

Description of samples:

- B.21 Felsite. Cliff section, 2,000 ft west of Tankardstown lode, Knockmahon.
- B.2. Tuff Footwall of Tankardstown lode, 100 ft from contact, Knockmahon
- B.3 Tuff Hangingwall of Tankardstown lode, 50 ft from contact, Knockmahon
- B.34 Tuff Hangingwall of Trawnamoe lode, 20 ft from contact, Bunmahon.

3.1.5. Wallrock alteration

The veins crosscut the intercalated volcanics and sediments, and wallrock alteration, restricted to within a few centimetres of the vein walls, consists of silicification and minor sericite and chlorite.

3.1.6. Environment of deposition

Interbedded sediments and pyroclastics make up the sequence. Marine conditions persisted during the deposition of shales and fossiliferous limestones, and the pyroclastics, ash-fall or ash-flow tuffs and lavas may be aerial or submarine. The graded beds suggest sub-aqueous deposition (85).

3.1.7. Intrusive rocks

Intrusive dyke rocks are well displayed in the coastal section (Plate 50:D) and range in composition from quartz-diorite to dolerite (184). Petrologically, these rocks are similar to those in the Avoca district.

3.1.8. Structure

3.1.8.1. Mesoscopic Structure

The current study only permitted reconnaissance work on the structure.

a) Planar

Bedding and cleavage are not coincident, but cut each other at a small angle. The cleavage is non-penetrative, becoming more prominent in the argillaceous members, with mean strike of 055° .

Minor kink bands and chevron folds develop close to faults.

Faulting may be considered under two categories, (i) vein infilled, and (ii) barren.

The vein-faults have two prominent directions:

- (i) $135-165^{\circ}$; infilled by quartz and chalcopyrite, sphalerite and galena.
- (ii) 070° ; infilled by quartz and chalcopyrite. Steep dips to the east and west are common ($65-85^{\circ}$).

Barren faults are often accompanied by a clay gouge zone up to 5 ft thick, have a trend of 035° , displace the vein faults and dip steeply to the east and west.

The vein faults may correspond to the steep normal faults at Avoca, which displace the ore zones. The barren faults are oblique strike slip faults. Fracture planes in the altered tuffs are often lined with epidote.

b) Linear

En echelon sigmoid tension gashes infilled by quartz are common adjacent to faults. An indistinct lineation develops by elongation of vesicles in the lavas within the plane of the cleavage, but is non-coincident with the fold axes. This is similar to the situation at Avoca.

Slickensides commonly occur on fracture planes, but the direction of movement could not be deduced.

3.1.8.2. Macroscopic Structure

A system of monoclinial folds about NE-SW axes facing northwest characterizes the regional structure (71). The folds vary from tight to open and are sometimes isoclinal. The productive veins crosscut the fold system and may infill a-c joints related to a tensional epoch of the Caledonian orogeny. Many similar examples have been figured by Weisser (255) from the North American Cordillera.

Tentative deductions about the regional stress distribution indicate a NW-SE compression, followed by NE-SW tension accompanied by metasomatic activity.

3.1.9. Mineralization

3.1.9.1. Form

The mineralization at Bunmahon consists of true lode-type fissure infillings (Plate 50:B,C). Two generalized ore types occur: a) siliceous veins with disseminated chalcopryrite and pyrite, and b) siliceous veins with sphalerite, galena and minor pyrite and chalcopryrite. Veins of type (a) are the commonest and the characteristics of the two types are given in table 29.

Table 29 Mineralization at Bunmahon

	A	B
Vein-type	Copper	Lead-zinc
Host-rocks	Tuffs and lavas (?Caradoc)	Tuffs and lavas (?Caradoc)
Orientation	135 - 165° Steep dips to East and West	165 - 175° Steep dips to East and West
Ore minerals	Chalcopyrite Pyrite	Sphalerite Galena Pyrite Chalcopyrite Tetrahedrite
Gangue minerals	Quartz	Quartz Calcite Dolomite Barite
Strike Length Max. Depth Av. Width	'short' 1000 ft ~10 ft	'short' shallow ~3 ft
Wallrock alteration	Minor silicification	Minor silicification
Examples	Major lodes at Bunmahon and Knockmahon	Kilmurrin and Ballynarrid

3.1.9.2. Ore Mineralogy

a) Primary Minerals

Disseminated pyrite euhedra occur in the vein material and the wallrocks. The grain size is variable : 1.0-0.05 mm and porphyroblastic crystals are rare. Etching does not reveal any zonal structures, indicating that the pyrite is probably stoichiometric (Plate 50:G). The morphology is cubic, and colloform and spheroidal textures are absent. Inclusions of chalcopyrite (c. 50 μ , in size) are minor.

Chalcopyrite fills the interstices between quartz grains as allotriomorphic masses. Etching reveals a recrystallized granular (?annealed) mosaic. The grain size is variable, 1.0-0.2 mm. Twinning is inconspicuous and inclusions are absent.

Sphalerite is a minor mineral which occurs, associated with galena, in the interstices between quartz and calcite grains. It is pale russet in colour, and etching reveals a recrystallized grain mosaic with equilibrium interfacial angles. The grain size varies from 1.0-0.2 mm. Ovoid blebs of chalcopyrite are common inclusions, and rare segregations of tetrahedrite occur at grain boundaries. Twinning exists (Plate 50:H).

Galena occurs with sphalerite, and etching reveals a recrystallized grain fabric, with a grain size of 1.0-0.5 mm. There are no inclusions.

Tetrahedrite, with sphalerite and galena, occurs in material from Ballynarrid. Allotriomorphic granular texture exists, and the grain size is 25 μ . Probe analysis indicates (Table 17) that it is an antimony-rich member with 1.6% Ag, and if extensive lead-zinc veins are located, tetrahedrite will be a significant source of silver.

b) Supergene minerals

Supergene copper minerals occur as surface coatings on oxidized vein material but are not important ore minerals.

c) Gangue minerals

Quartz is the major gangue mineral and contains abundant

fluid inclusions. Clear and milky varieties exist. Calcite, dolomite and rare barite become important in the lead-zinc veins.

The generalized paragenetic sequence is illustrated in table 30.

Table 30. Generalized paragenetic sequence at Bunmahon.

Ore Minerals:	Primary	
	Syngenetic	Epigenetic
Pyrite	-----	-----
Chalcopyrite		-----
Sphalerite		-----
Galena		-----
Tetrahedrite		-----
Gangue Minerals		
Quartz	-----	-----
Calcite		-----
Dolomite		-----

3.1.9.3. Trace element distribution

The trace elements in eight samples consisting of pyrite, chalcopyrite and galena are shown in table 31. Analysis was by spectrography, as described in section 2.3.7.2.

Values of Ti, Cr, Co, Ni and Mo in pyrite are low, seldom exceeding the detection limit, and together with manganese, the values are comparable with data from Avoca.

The elements in chalcopyrite are similar to those found at Avoca with the exception of tin, which decreases.

Titanium in galena is low, and the manganese content supports the notion that some manganese is in the galena lattice. 1180 ppm Ag confirms the presence of silver in solid solution in galena and the antimony content suggests the presence of contaminant tetrahedrite.

3.1.9.4. Genesis

Trace element indicators of ore genesis are not diagnostic. The Co:Ni ratio in pyrite is 0.33-1.42 and thus derivation

TABLE 31

SPECTROGRAPHIC ANALYSIS OF SULPHIDES, BUNMAHON AND CAIM

BUNMAHON

PYRITE

Sample No	Locality	Description	Contamination Indicators %			Trace Elements ppm					
			Cu	Zn	Pb	Ti	Cr	Mn	Co	Ni	Mo
A.1946	Tankardstown; Tankardstown lode, shore	Dissem.py and cp	*	*	*	25	*	88	10	30	39
1943	" ; Rows lode, shore	Dissem.py, cp & qtz	*	*	*	*	*	33	10	25	30
1625	Knockmahon; shore, E. of Boneyaught lode	Dissem.py	*	*	*	25	5	90	10	7	96
1945	" ; " , W. of Seven Dials lode	" "	*	*	*	*	*	90	10	9	30
		Detection Limit	0.25	1.0	0.25	25	5	5	10	2	30

The following elements were below detection (limits in ppm) : Ga(60), Ag(2), Cd(100), Sn(25), Sb(100).

CHALCOPYRITE

Sample No	Locality	Description	Zn	Pb	Ti	Mn	Co	Ag	Sn
			A.1795	Tankardstown; Tankardstown lode, shore	Mass. cp	*	*	245	510
1692	" ; Rows lode, shore	" "	*	*	43	5	10	2	52
1691	" ; Traunamoe lode, dump	Dissem.cp	*	*	79	5	*	2	*
		Detection Limit	1.0	0.25	25	5	10	2	25

The following elements were below detection (limits in ppm) : V(50), Cr(5), Ni(5), Ga(60), Mo(30), Cd(100), Sb(100).

GALENA

Sample No	Locality	Description	Fe	Cu	Zn	Ti	Mn	Ag	Sb
			A.1934	Ballycarrid ; Cliff Section	Dissem.gn, cp & qtz	1.0	1.0	*	10
		Detection Limit	0.05	0.25	1.0	10	5	2	100

The following elements were below detection (limits in ppm) : V(10), Cr(5), Co(10), Ni(5), Ga(10), Mo(10), Cd(100), In(10), Sn(30).

CAIM

CHALCOPYRITE

Sample No	Locality	Description	Zn	Pb	Ti	Mn	Ag
			A.1796	Engine Shaft, Dump	Dissem.cp, gn with qtz	*	*
		Detection Limit	1.0	0.25	25	5	2

The following elements were below detection (limits in ppm) : V(50), Cr(10), Co(10), Ni(5), Ga(10), Mo(30), Cd(100), Sn(25), Sb(100).

SPHALERITE

Sample No	Locality	Description	Cu	Pb	Fe	Ti	Mn	Ga	Ag	Cd
			A.1886	Engine Shaft, Dump	Dissem.gn. & sl with qtz	0.25	1.0	4.0	2300	960
		Detection Limit	0.25	0.25	0.05	10	5	10	2	100

The following elements were below detection (limits in ppm) : V(10), Cr(5), Co(10), Ni(5), Mo(10).

GALENA

Sample No	Locality	Description	Fe	Cu	Zn	Ti	Mn	Ag	Sb
			A.1867	Engine Shaft, Dump	Dissem.gn with qtz	0.88	*	M	500
		Detection Limit	0.05	0.25	1.0	10	5	2	100

The following elements were below detection (limits in ppm) : V(10), Cr(5), Co(10), Ni(5), Ga(10), Mo(10), Cd(100), Sn(30).

The following elements were below detection throughout (limits in appendix 3) : Ge, As, In, Ba, Pt, Au, Hg and Bi.

* = not detected

of the iron from hydrothermal (22) or volcanic sources (140) is a possibility. Ti, Mn, and Mo values in pyrite are all low, suggesting that the source of the iron may be hydrothermal (49) and the absence of vanadium also correlates a hydrothermal origin (3).

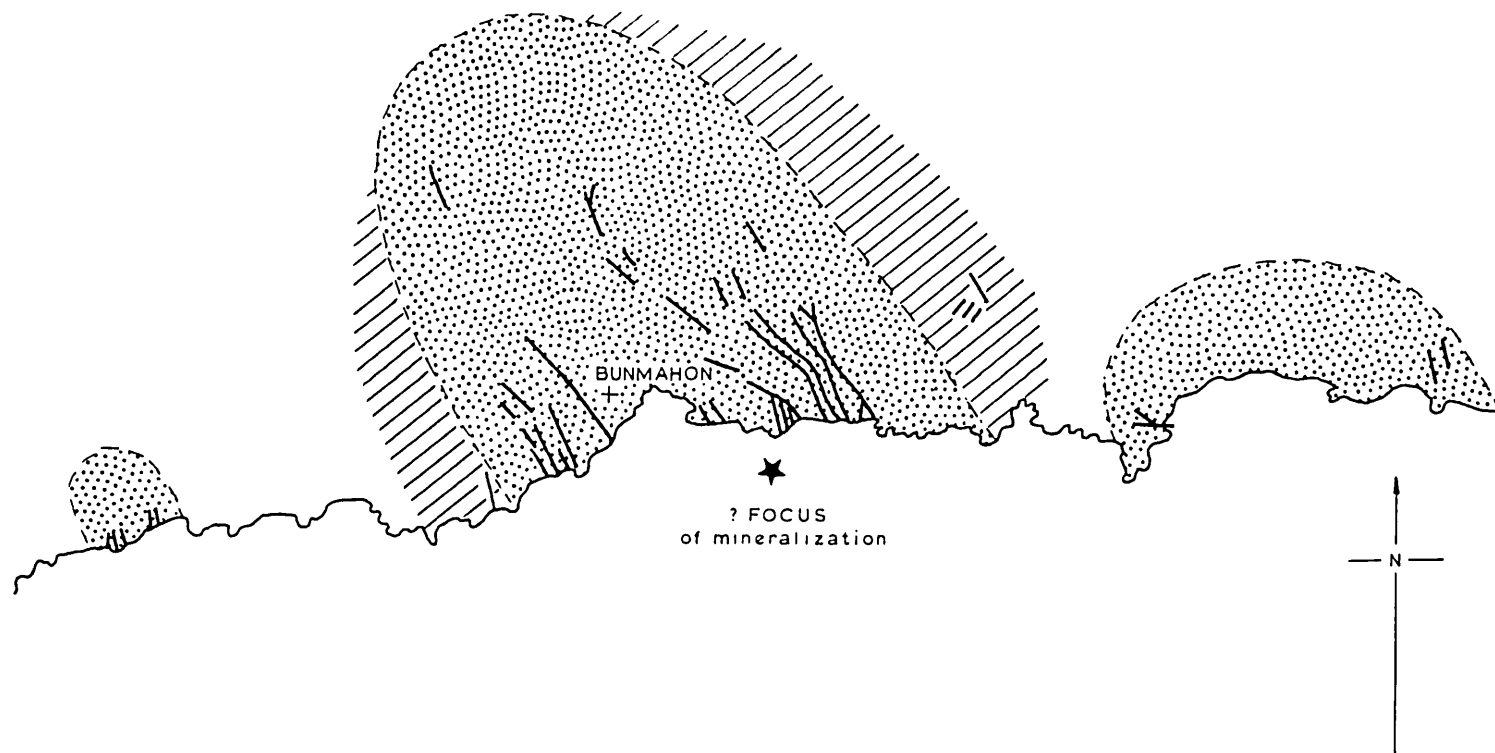
There are few geothermometric indicators in the mineral assemblage. The iron content of sphalerite (probe analysis) is 1.7%Fe, equivalent to 2.7 mole % FeS. The content of silver in galena suggests a relatively low temperature of origin (232). Application of exsolution textures indicate little, and the quartz appears to be the low temperature form.

The mineralization demonstrably post-dates the deposition and consolidation of the country-rocks, and this is substantiated by the lead isotope age determination (176) (300 m.y.) (cf. Fig. 2.2A). Structural relationships suggest that emplacement took place during a tensional phase of the Caledonian orogeny. The presence of abundant felsic pyroclastic activity, during the Caradocian implies the existence of a similar magma at depth, and it is not unreasonable to relate the hydrothermal activity, which produced the mineralization, to a final aqueous phase of the magma. The presence of abundant dyke rocks testifies to late stage magmatic activity.

A crude pattern of metal zoning exists in the Bunmahon district, with a central copper-rich zone fringed by one richer in lead and zinc, and this situation is paralleled amongst the gangue minerals:- calcite, dolomite and barite becoming important in the outer zone (Fig. 3.2). If this zonal scheme is correlated with patterns of epigenetic metal zoning elsewhere (e.g. 76), it may be that the focus of mineralization lies close to the Tankardstown/Stage lode complex.

In summary, mineralization at Bunmahon is leptothermal, epigenetic and may be the product of ramifying hydrothermal fluids which derived their contained metals from a magma phase, from connate fluids in the sedimentary pile, or a combination of these two sources.

FIG 3.2



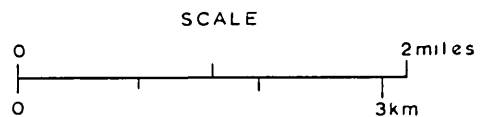
BUNMAHON DISTRICT
MEGASCOPIC METAL ZONING



COPPER ZONE



LEAD-ZINC ZONE



— Vein / Lode

3.2 Lead-zinc occurrences

3.2.1. Caim and Barrystown, Co Wexford

3.2.1.1. Geology

A sequence of mudstones, siltstones and sandstones probably of early Arenig age (Ribband Group) is cut at both these localities by a series of fault zones which have an approximate E-W trend crosscutting the regional NE-SW foliation, (Fig 2.24) and containing abandoned lead workings.

At Caim, about 5 miles from the margin of the Leinster granite, quartz veins infill sub-vertical fracture zones and also ramify through the wallrocks. A 'breccia ore' is produced, similar to that occurring in the Silvermines district (185). The lodes exist for over 400 ft in strike length and flooded workings extend to about 250 ft in depth (58). Mineralization consists of disseminated galena with sphalerite and minor chalcopryrite. The gangue minerals are quartz, calcite and siderite and wall rock alteration is slight, and limited to silicification.

At Barrystown, narrow fissures trending ESE-WNW are infilled by lodes which dip $40-60^{\circ}$ NNE (208). They have been worked for about 800 ft along the strike and to depths of about 300 ft (58). Mineralization consists of disseminated galena, sphalerite and minor chalcopryrite, in a gangue of quartz and calcite. Wallrock alteration is slight and confined to silicification.

Ore mineral textures are similar to those in siliceous vein-type mineralization at Avoca. The paragenetic sequence appears to be the same at Caim and Barrystown, and is shown below:

Table 32. Generalized paragenetic sequence: Caim and Barrystown.

Mineral	Time \longrightarrow
Pyrite	— — — —
Galena	—————
Sphalerite	—————
Chalcopryrite	— — — —
Quartz	—————
Calcite	—————

Spectrographic analyses of the trace elements in chalcopyrite, sphalerite and galena from Caim are in table 31. Low Ti, Mn and Ag in chalcopyrite correspond with the values in chalcopyrite from Avoca and Bunmahon.

In sphalerite, the high Ti supports the notion that it is present in sphalerite lattice and could not be supplied solely by contaminants. Mn and Ga have values similar to those recorded from Avoca. The silver value correlates with lead contaminants. The cadmium content of sphalerite is low, and 3.8% Fe is present.

In galena, the titanium value equates with that in galena at Avoca, and the manganese value is high, possibly due to impurity sphalerite, but almost certainly also present in the galena lattice. The silver content is below that at Avoca and Bunmahon and the presence of antimony suggests that tetrahedrite may be present, although none was observed. (At Barrystown 60-70 oz/t. Ag is reported in the lead concentrates - a high value).

3.2.1.2. Genesis

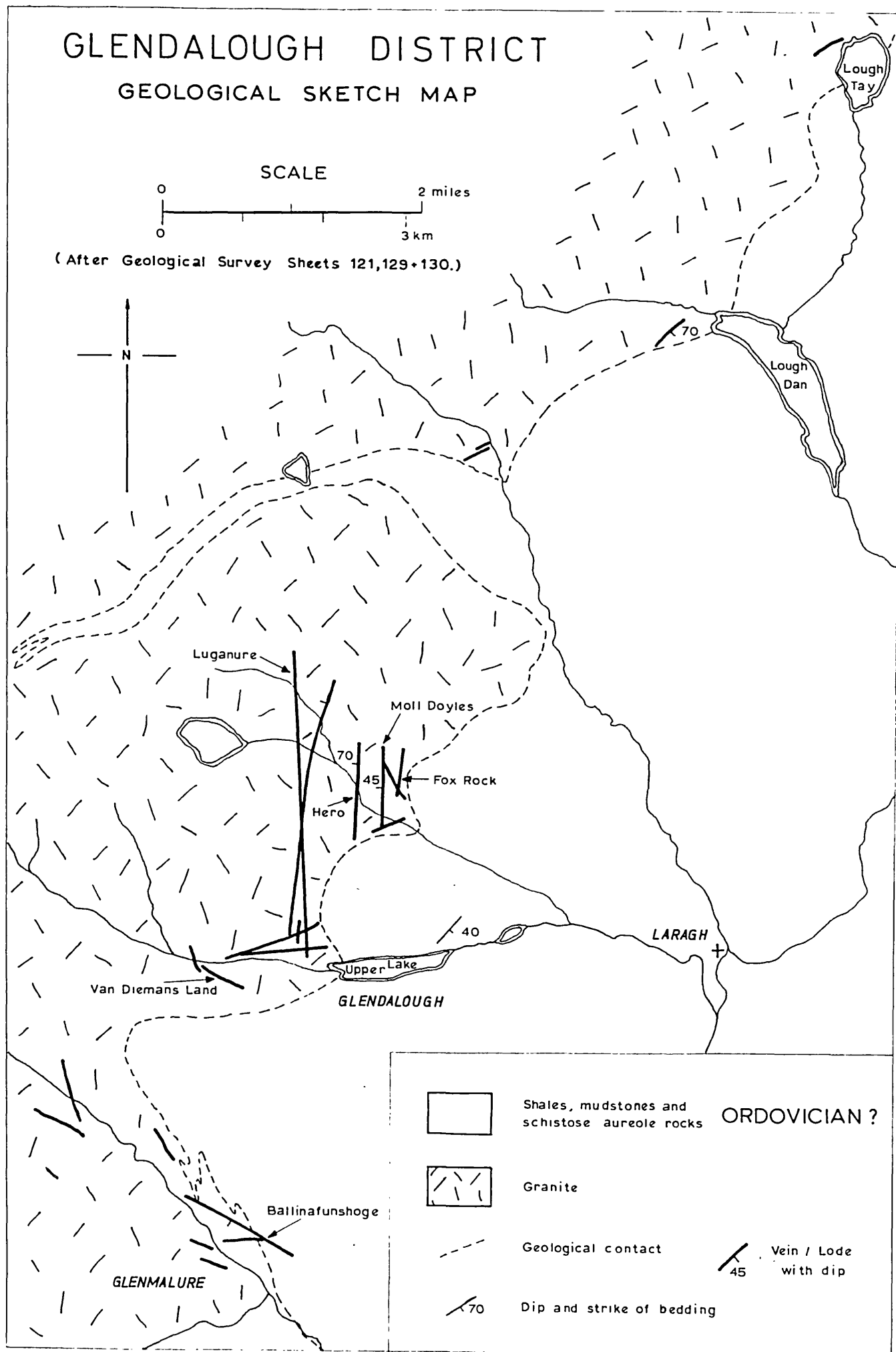
The veins crosscut the sediments and thus must post-date deposition of the rocks. Caim gives a B-type lead isotope age of 560 ± 30 m.y., and Barrystown a normal age of 280 ± 80 (176). Amongst the ore minerals and trace elements there is no precise genetic evidence, but the presence of fluid inclusions in the gangue quartz suggests that mineralization was from hydrothermal solutions. The mineral assemblage is leptothermal. The ore fluids may have originated within the sedimentary pile, and localization been contingent upon the presence of suitable structural openings.

3.2.2. Glendalough, Co. Wicklow

3.2.2.1. Geology

In this district, a number of narrow fissure veins occur at the margin of the Leinster pluton (Fig. 3.3). The geology of the area has been described by Smyth (208), Cole (58) and O'Brien (167). The veins trend north-south and east-west and are generally less than 3 ft in width. Individual

FIG 3.3



veins (Luganure lode) are up to 4,000 ft in length and have been worked to depths of 1,000 ft. Mineralization consists of disseminated galena with sphalerite, and minor chalcopyrite and pyrite within a gangue of quartz, calcite, dolomite and barite (208). Wallrock alteration is slight, consisting of kaolinization and development of sericite.

The textures of the ore minerals correspond with those in vein-type mineralization elsewhere. Allotriomorphic granular aggregates of galena occur (grain size: ~ 0.1 mm), with mutual boundaries against sphalerite. Chalcopyrite occurs as anhedral masses and also as exsolution blebs in sphalerite. Disseminated euhedral pyrite grains are common. The paragenetic sequence appears to be:

Table 33. Generalized paragenetic sequence, Glendalough.

Galena	—————
Sphalerite	—————
Pyrite	-----
Chalcopyrite	-----
Quartz	-----
Calcite	-----
Dolomite	?-----?
Barite	?-----?

Spectrographic analysis of trace elements in pyrite, chalcopyrite, sphalerite and galena from Glendalough are shown in tables 20, 22 and 23, section 2.3.7.

Contents of elements in pyrite are low and the Co:Ni ratio is 2.81. Chalcopyrite is similar to that at Avoca, values are generally low except for a high tin content (210 ppm).

Sphalerite contains high cadmium (3800 ppm) and low iron (0.7%). Ga and In. are relatively high, and silver content (260 ppm) is accompanied by 860 ppm antimony which suggests contaminant tetrahedrite, however, none was identified in polished section.

Galena contains low Ti, Mn, Co and Ga, and 185 ppm silver accompanied by 1250 ppm antimony suggests tetrahedrite contamination

3.2.2.2. Genesis

The mineralization is epigenetic and leptothermal, deduced from the coexisting ore and gangue minerals. The intimate spatial association with the Leinster granite supports the idea that ore deposition was related to a phase of hydrothermal activity associated with the cooling of the pluton. This notion is corroborated by the lead isotope age (220 m.y.) (176).

3.2.3. General

A similar suite of veins occurs at Glenmalure (Fig. 3.3) where mineralization consists of galena, sphalerite and pyrite with a gangue of quartz, barite and fluorite (208). At Ballycorus, Brownsford, Shankill and Killiney veins carrying galena and sphalerite have been recorded (58), and native silver occurred at Ballycorus (208) (Fig. 2.2A). At Corbally, a siliceous vein with galena and sphalerite cuts a dioritic intrusive which post-dates the consolidation of the nearby pluton and gives a lead isotope age of 150 ± 60 m.y. (176).

S E C T I O N 4

ANGLESEY4.1. Parys Mountain4.1.1. Introduction

Parys Mountain is in northeast Anglesey (Fig. 4.1, inset), about $1\frac{1}{2}$ miles south of the port of Amlwch. The 'mountain' rises to 484 ft above sea-level, is $1\frac{1}{2}$ miles long by $\frac{1}{2}$ mile wide, and elongated WSW-ENE.

Discovery of the mine was in 1768, and until 1883 the property was worked continuously and is reputed to have had the highest output of copper in the world for a time (148). The total quantity of ore mined was about $3\frac{1}{2}$ million tons, producing more than 100,000 tons of copper. The grade of the run of mine ore was $\sim 3\frac{1}{2}\%$ Cu and hand picking at the surface enriched this to about 5% Cu prior to transportation to Amlwch for smelting.

Intermittent activity followed over the next 60 years, copper being precipitated from mine water in settling ponds at Dyffryn Adda. A resurgence of prospecting activity occurred in 1957-8 and the workings above water-level were reopened, mapped and sampled. Northgate Exploration Ltd., through their subsidiary, Anglesey Copper Mines(UK) Ltd, drilled a series of inclined holes in 1961-62, north of the old workings to evaluate the deposit in depth. The option lapsed, and in 1966 Canadian Industrial Gas and Oil resumed drilling to complete the Northgate programme. Exploration is continuing.

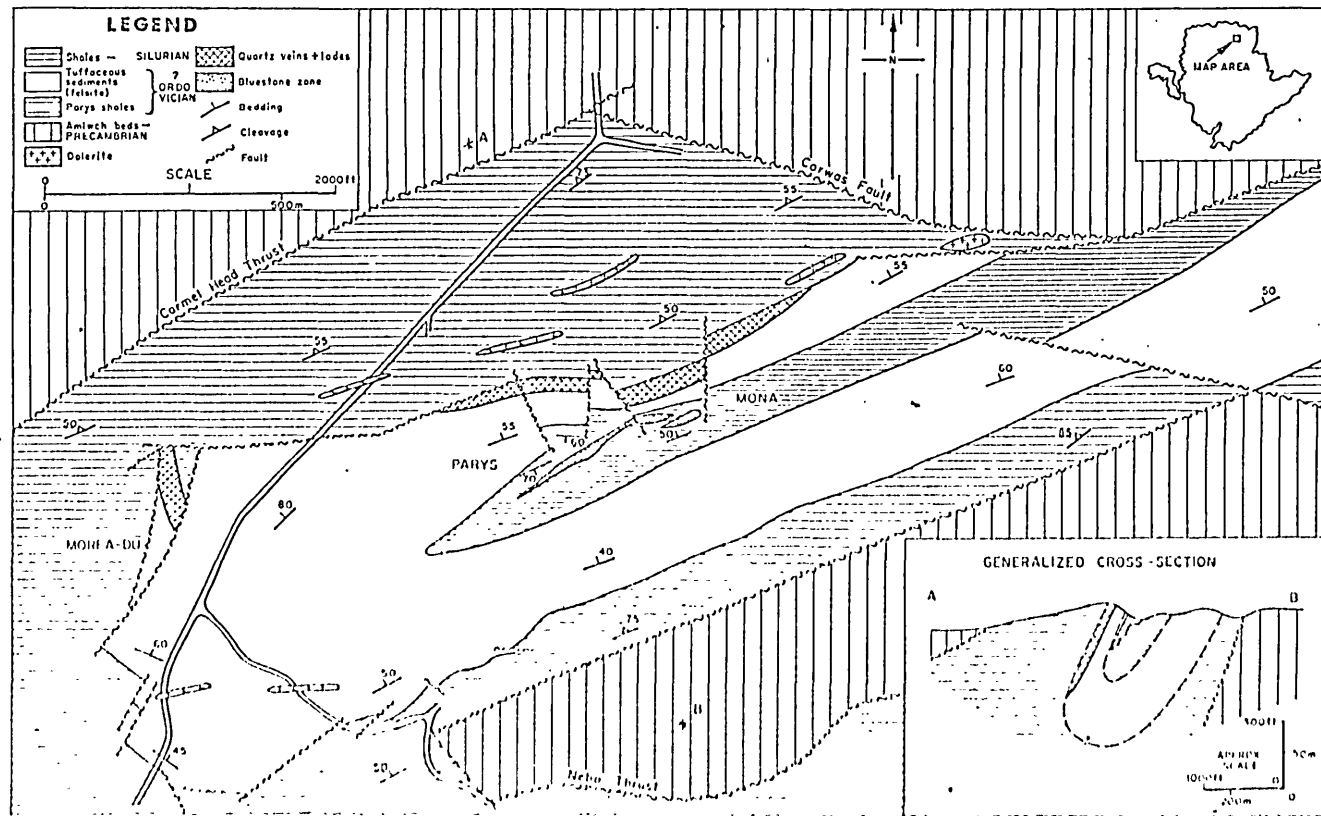
Aspects of the geology have been covered by several authors. Greenly (100) produced a comprehensive account of the geology of the district and Manning (148) described the mineralization. The stratigraphy and structure were discussed by Bates (20) and Hawkins (109), who also studied the petrology of the rock types.

4.1.2. Stratigraphy

The stratigraphic sequence is shown in table 34. Precise relations are not clear due to an absence of diagnostic fossils from the shale outcrop to the south of the felsite mass (Fig. 4.1),

FIG 4.1

Parys Mountain, geological sketch map and generalized cross-section.



(After Manning, 1959, Bates, 1964 and Hawkins, 1966)

and also in the Parys Shales.

No volcanic rocks are known to post-date the Caradoc, it is thus likely that the whole Ordovician sequence is of Caradoc age or earlier.

Table 34 Parys Mountain, stratigraphic relations

Age	Lithology	Thickness feet
Devonian	Conglomerates, sandstones and marls	500+
Silurian (Llandovery)	Grey Shales	?
— ? ————— ? ————— ? ————— ? —————		
	Rhyolitic suite: lavas and tuffs with intercalated sediments. (Felsite)	600+
ORDOVICIAN	Black shales	} Parys Shales 720
	Grey shales	
	Grey micaceous shales with sedimentary breccias	
————— THRUST —————		
PRECAMBRIAN	Pale green phyllites (Amlwch Beds)	?

(after Hawkins (109))

4.1.3. Lithology

The Precambrian Amlwch Beds are metasediments in the Bedded Series of the Mona Complex (201). The rocks consist of pale green and grey chlorite phyllites: altered shales, grits and mudstones. The beds are 1-2 cm thick and conglomeratic horizons occur, with pebbles up to 4 cm in length, of various lithologies, and are frequently deformed.

A sequence of blue-grey to black micaceous phyllites and shales occur at the base of the Ordovician (?) strata, intercalated with breccias which Hawkins (109) recognized as sedimentary.

These breccias contain assorted rock fragments in a fine grained mudstone matrix. Greywacke horizons also occur, with the beds varying in thickness from 5-50 cm. Blue-black, finely laminated shales complete the series, which has been termed the Parys Shales (Fig. 4.1)

The felsite is a rhyolitic suite, of tuffs, lavas and sediments. The rocks are greenish-grey to buff coloured, massive and flinty. Hawkins (109) initially identified tuff horizons at Parys Mountain, and these are the only recorded Ordovician volcanic rocks from Anglesey.

Silurian strata are blue-grey to black thinly laminated graptolitic shales. The shales to the south of the felsite mass are of similar lithology and have provided a meagre fauna, which Bates suggested might also be Ordovician (20).

Conglomerates, sandstones and marls of Devonian age, occurring south of the area, complete the succession.

Light to dark green, medium to fine grained intrusive dolerites occur at scattered localities in the mine area (Fig. 4.1).

4.1.4. Petrography

The sedimentary rocks consist of essential quartz, as a granular mosaic, and feldspar, as anhedral fragments, with the interstices filled by laths of sericite and chlorite.

The felsite is composed of rhyolites, tuffs and intercalated siltstones and mudstones. The rhyolites exhibit a well developed felsophyric texture in thin section, with a micro-to cryptocrystalline mosaic of quartz and feldspar set in a matrix of finely divided clay minerals. Spherulitic textures have been recorded (109), and in the less altered material eutaxitic textures have been identified (F.J. Fitch in 109), but the effects of devitrification and secondary silicification in the samples studied by the writer, make any dogmatic textural conclusions impossible (Plate 42:C-E).

The lithic tuffs contain angular pyroclasts of mudstone and siltstone (109), with rare feldspar grains, pyrite euhedra and leucoxene in a groundmass of chlorite and sericite.

Table 35 Partial analyses of felsites from Parys Mountain
by X-ray fluorescence

Major oxides:		
(%)		
SiO ₂	70.30	74.10
Al ₂ O ₃	16.84	14.05
TiO ₂	0.27	0.19
Fe ₂ O ₃	1.84	0.16
FeO	0.15	0.04
MnO	≠	≠
MgO	0.48	0.05
CaO	0.32	0.32
Na ₂ O	1.10	0.68
K ₂ O	8.20	9.78
P ₂ O ₅	0.01	0.01
Total S	0.16	0.20
H ₂ O+	-	-
H ₂ O-	-	-
Total	99.67	99.58

Trace Elements:
(ppm)

Co	≠	≠
Ni	45	27
Cu	96	108
Zn	35	122
Rb	207	211
Sr	35	12
Pb	314	9,450

≠ = not detected

- = not sought

Description of samples:

F.15. Felsite, Foel-newydd quarry, at northern end.

F.16. Felsite, Foel-newydd quarry, at southern end.

Analyst: C.J.V. Wheatley

The dolerites in thin section exhibit a rude trachytic texture with altered plagioclase laths 1-0.5 mm in length ophitically enclosing chlorite needles and grains of leucoxene (109).

4.1.5. Petrochemistry

Apart from analyses of the shales, (100), there is a complete lack of analytical data on rocks from Parys Mountain. The results of x-ray fluorescence analysis of two samples of rhyolite from the felsite suite are shown in table 35.

The rocks are petrochemically similar to felsite at Avoca. Contents of the major oxides are comparable and enrichment in potassium is noteworthy. Amongst the trace elements, there is a correspondence with values at Avoca, except for the anomalous lead content of F.16. Mineralization containing lead occurs close by, and thus contamination by disseminated galena is likely.

4.1.6. Petrogenesis

The felsites from Parys Mountain plot near the Q-Or edge in the Q-Or-Ab-H₂O system (Fig. 2.6A). The basement in Anglesey is essentially granitic, and following reasoning similar to that already given for the Avoca district, it is suggested that the felsite was a late stage product from partial fusion of the basement. Alkali-ion transfer was aided by a thermal gradient (implied by volcanism), and a vapour phase contributed by connate water at the base of the sedimentary pile. The mechanism for enrichment in potassium was probably similar to that at Avoca, and may have been increased by metasomatism associated with wallrock alteration.

4.1.7. Wallrock alteration

Intensive permeation by quartz veins produces extensive silicification, and sericite develops in the argillaceous units. Minor chlorite occurs.

4.1.8. Environment of deposition

Marine conditions predominated during the Ordovician and

interstratified pyroclastics appear at the top of the succession. It is not clear whether the tuffs were aerial or submarine. Marine, graptolitic shales occurred in the Silurian.

4.1.9. Structure

4.1.9.1. Mesosopic structure

a) Planar

Bedding(S_0), parallels the cleavage in the limbs of the macroscopic fold structure, and crosscuts the foliation at the southwest end of the mountain. The strike varies from $45-70^\circ$ and the dips range from $40-60^\circ$ NW. Bates (20) found a strike maxima at 65° dipping $50-60^\circ$ N, and a girdle about an axis plunging 20° NE.

Cleavage (S_1), the most prominent planar fabric in the rocks, is dominantly non-penetrative and locally produces phyllites. A well developed maxima with a strike of 70° and dip of 55° N was obtained by Bates (20).

Small-scale dislocation of the strata is common, and the importance of major faults is obvious from the geological map. The Carmel Head Thrust plane dips $30-60^\circ$ NNW and is sub-parallel to the cleavage and bedding. Associated with this structure, fractures developed in the incompetent felsitic rocks, and minor slip in the competent shales. These minor faults have a strike-slip sense of movement (20).

Late-stage normal faults, often with a wrench component occur with two major orientations: (a) 150° , dipping 80° NE and (b) 20° dipping steeply east and west (20). Sinistral movement occurs on the Carreg-y-doll crosscourse and dextral movement on the Great crosscourse.

Joints, sub-vertical and normal to the regional trend are typical a-c joints.

b) Linear

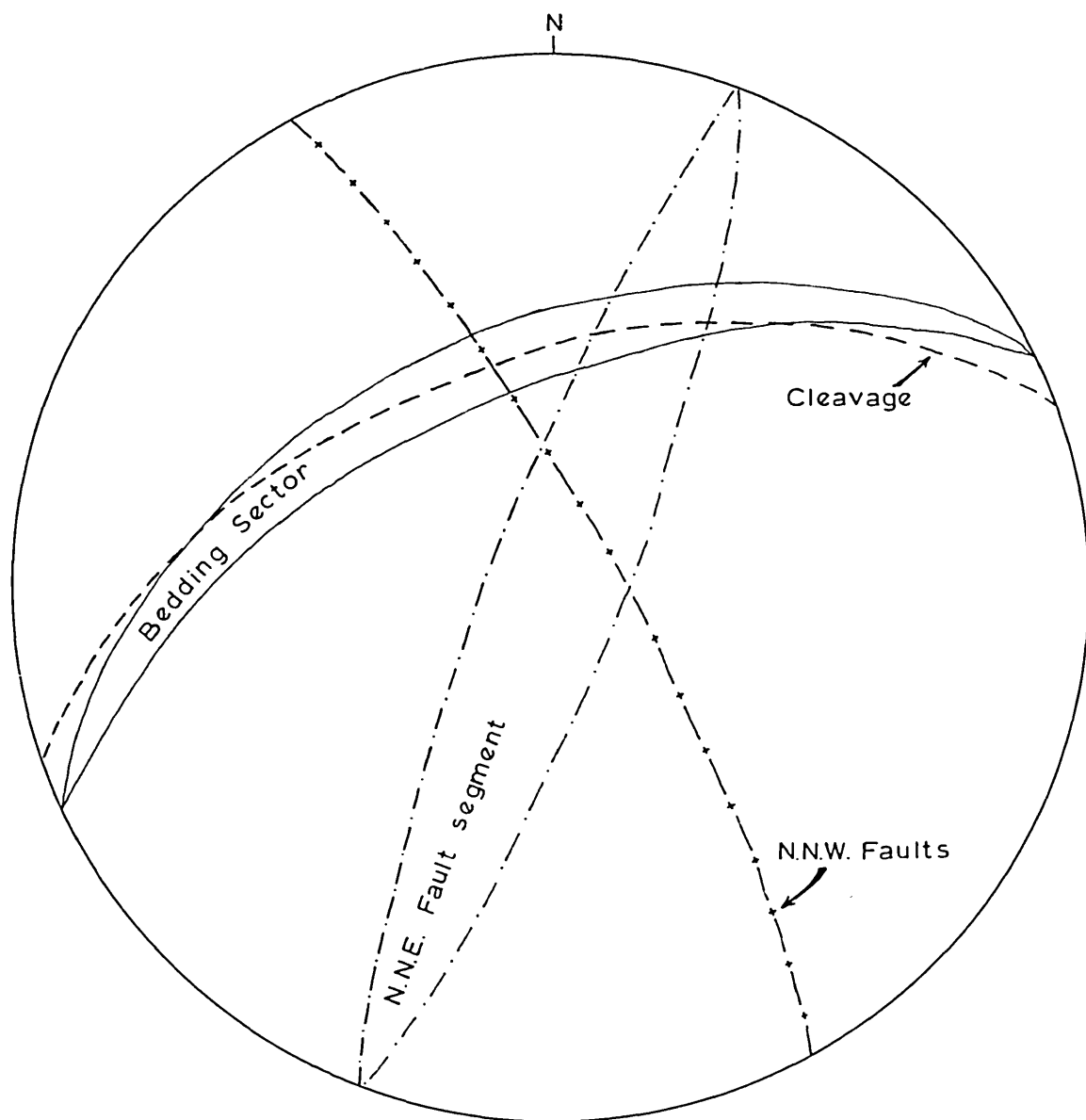
Axes of minor folds have a trend of $040-050^\circ$ plunging to the NE and SW at a small angle.

Crude boudinage of some of the quartzitic units in the

FIG 4.2

STRUCTURAL RELATIONSHIPS,
PARYS MOUNTAIN

Lower hemisphere equal area stereographic projection:



felsite suite exists, and the ductile sulphides, sphalerite and chalcopyrite migrate into the necks of the structures. There is no evidence of recrystallization or brecciation of the shale, simply plastic flow of the matrix sulphides.

Associated with the fracture zones, tension gashes and rectilinear systems of quartz veins developed. Slickensides occur on fault planes, often accompanied by clay gouge. The nature of the slickenside surfaces indicate that repeated movements took place.

The mesoscopic structures are summarized in Fig. 4.2.

4.1.9.2. Macroscopic Structure

The dearth of faunal evidence in the shales which occur to the south of the felsite mass results in disagreement over the macroscopic structure. Greenly (100) suggested that the felsite was a thick sill-like intrusion, and with the shales was later folded to give an overturned syncline containing Silurian rocks in the core (Fig. 4.3A). Manning (148) contended that the felsite might be a forked dyke (Fig. 4.3B) and that the Silurian shales occupied the core of an eroded fold. In the most recent interpretation Bates (20), considered the southerly shales were not Silurian, as inferred by Greenly, but possibly Ordovician, on the basis of a re-examination of the fauna and the structural evidence in the Hillside opencast. This suggestion makes the major structure a syncline, and is favoured by the writer (Fig. 4.1, inset) as this style of deformation is matched by the lithology and petrography of the rocks. The outcrop of the felsite delineates the model fold and the plunge of the syncline may change from northwest to southwest along the outcrop.

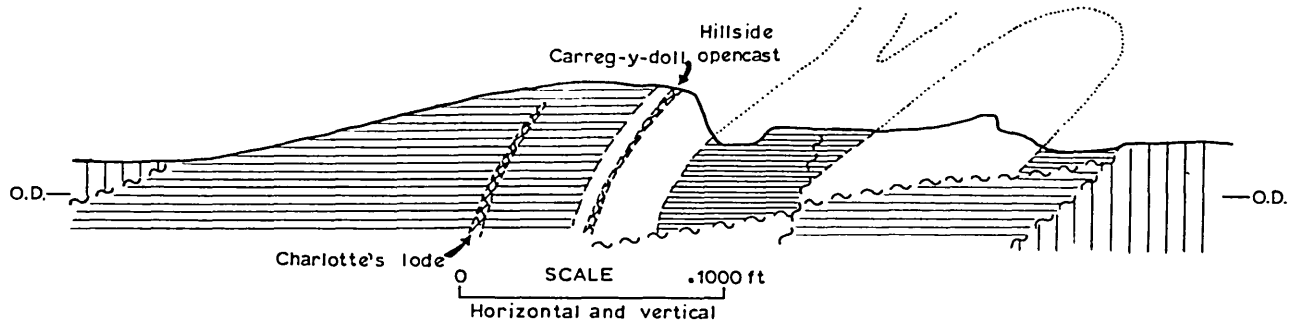
Boudins indicate marked contraction perpendicular to the bedding occurred adjacent to the felsite mass, evidence of the incompetence of the siliceous body relative to the more competent shales.

4.1.9.3. Stress Distribution

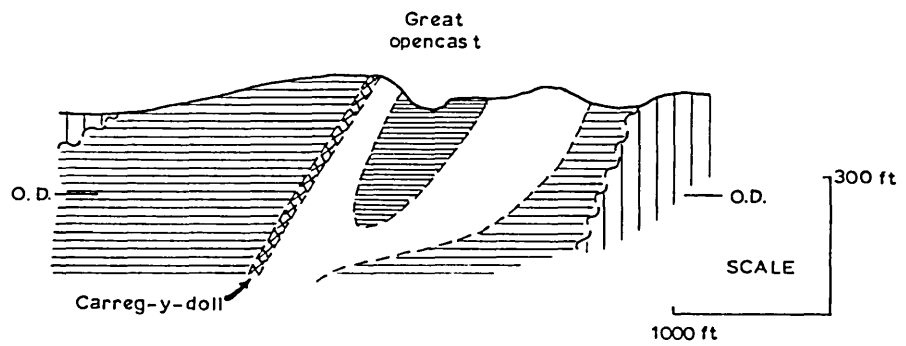
Bates (20) identified 160° as the principle stress direction

CROSS-SECTIONS, PARYS MOUNTAIN

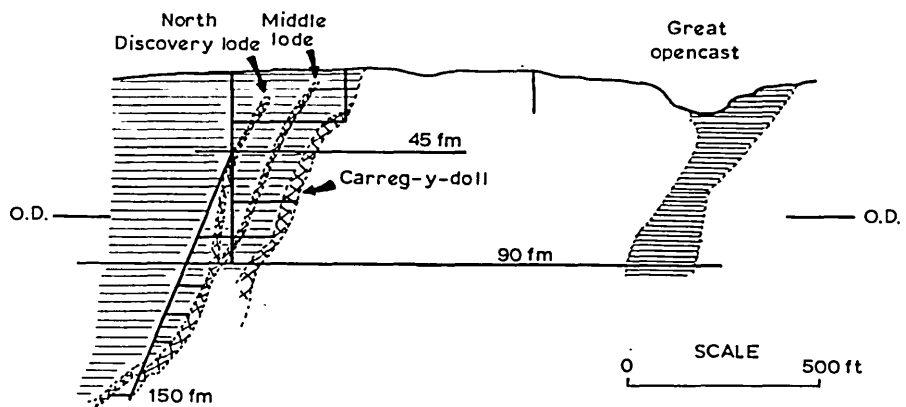
A. Section through central Parys Mountain (After Greenly, 1919):



B. Section through central Parys Mountain (After Manning, 1959):



C. Section showing the lode system and extent of workings:



(1 fm = 6 ft)

(After Manning 1959)

(LEGEND AS IN FIG 4.1)

for the area and suggested that a compressional phase giving folding was followed by a tensional phase accompanied by faulting. Precise interpretation is impossible because the macroscopic structure has to be assumed. Conjugate fracture systems do exist, but they have not yet been fully elucidated.

4.1.10. Mineralization

Manning (148) described the mineralization in general terms and Greenly (100) gave a list of ore minerals, but no details of the textures and ore mineralogy have been published. The writer examined a total of 30 polished sections of representative mineralization, from grab samples and diamond drill cores.

4.1.10.1. Nature of the ore zones

In common with Avoca, the zones of mineralization are termed lodes, but they are also not true fissure-fillings, a feature noted by Greenly (100). A series of eight lodes exist and the interrelationships between each of the zones is not clear because the critical workings are either caved or flooded. The lodes are broadly conformable with the enclosing strata, dipping 55-75°N, and their configuration is illustrated in Fig. 4.3C. The contact between felsite and Silurian shale is intensively silicified and mineralized, containing medium to fine grained disseminated pyrite with ramifying seams of chalcopryrite, sphalerite and galena. This forms the so-called Bluestone ground; site of the open pits (Plate 42:A,B). To the north are siliceous lodes made up of quartz seams with disseminated pyrite and chalcopryrite. The major representative is the Carreg-y-doll lode. The mineralization can be divided into a series of ore-types (Fig. 4.4) and these are remarkably similar to those at Avoca. The close correspondence between the mineralization at the two localities has been remarked upon by many writers (208, 84,100).

4.1.10.2. Ore Mineralogy

a) Primary minerals

The paragenetic sequence is illustrated in fig. 4.6.

(i) Pyrite. Pyrite is the commonest sulphide and occurs

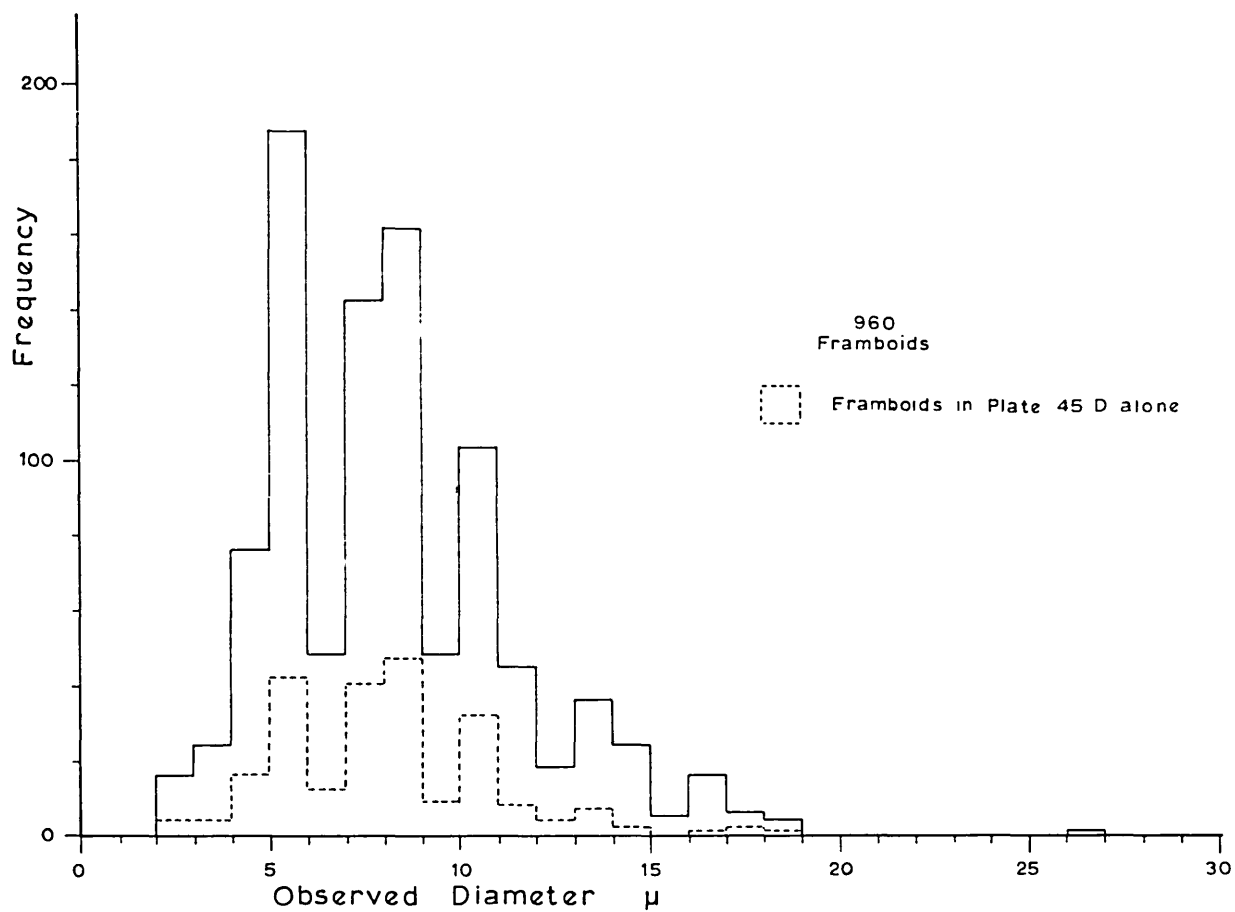
Fig. 4.4 Mineralization at Parys Mountain

Ore type	Host rock (matrix)	Mineralogy		Example
		Major	Minor	
Pyritic Zone	Black shale	Pyrite Chalcopyrite	Pyrrhotite Sphalerite Galena	Disseminated in shale units.
Siliceous Zone	Shales and tuffs (silicified)	Pyrite Chalcopyrite Sphalerite Galena	Pyrrhotite Tetrahedrite Bismuthinite Native Bismuth	Carreg-y-doll lode Golden Venture lode Charlottes lode. N. Discovery lode N. + S. Branch lodes.
Lead-zinc Zone	Shales and tuffs	Sphalerite Galena Pyrite Chalcopyrite	Tetrahedrite Bourmonite	Morfa-du and Black Rock lode. Clay Shaft lode (Bluestone)
Veins	Shales, tuffs and lavas.	Galena Sphalerite Chalcopyrite	Tetrahedrite	Great Crosscourse. Carreg-y-doll Crosscourse

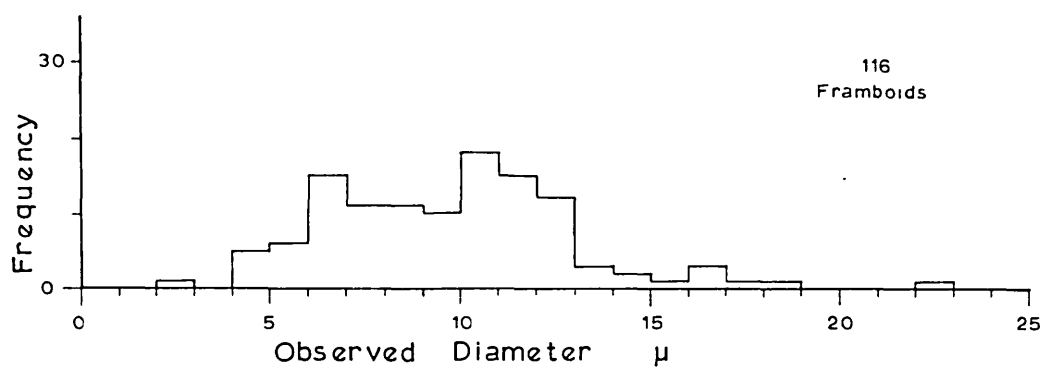
FIG 4.5

Size distribution of framboidal pyrite - Bluestone,
Parys Mountain.

A Bluestone adit dump, Hillside opencast.



B Morfa - du, Engine shaft dump.



PARYS MOUNTAIN

PARAGENETIC TABLE

NATURE OF THE ORE FORMING PROCESS

		SYNGENETIC	EPIGENETIC	REMOBILIZED	SUPERGENE
PRIMARY	Pyrite :				
	Framboidal	————			
	Colloform	————	- - - -		
	Zoned, crystalline	————	————		
	Unzoned, crystalline		————	- - - -	
	Chalcopyrite		- - - -	————	
	Sphalerite		————	- - - -	
	Galena		————	- - - -	
	Pyrrhotite			————	- - - -
	Tetrahedrite			————	
	Bournonite			————	
Native Bismuth			————		
Bismuthinite			————		
SUPERGENE	Goethite				————
	Covellite				————
	Native Silver				- - - -
	Native Copper				- - - -
	Malachite				————
	Chalcanthite				————
GANGUE	Quartz :				
	Grey	- - - -	————	- - - -	
	Milky		————	- - - -	
	Clear			————	- - - -
	Chlorite	- - - -	————	- - - -	
	Sericite		- - - -	————	
	Calcite			————	
	Barite			————	
	Siderite		- - - -		
	Leucoxene			- - - -	
	Gypsum	- - - -	————		

in each ore type except the late-stage veins. Pyrite is generally disseminated and rarely massive, with cubic and pyritohedral morphology. Euhedral to subhedral grains and crystal aggregates are common, with a variable grain size: 1.0-0.02 mm (predominantly 0.1 mm). Hawkins noted (109) that pyrite only occurred as pyritohedra in the black shale units and was cubic in all the other lithologies. He also showed a size differentiation, pyritohedra being ~ 0.5 mm diameter and cubic euhedra $\leq 0.5-2.0$ mm. This factor presumably reflects the availability of sulphur, iron and nucleation sites during grain growth.

Features of the pyrite fabric are illustrated in plates 43-45, and the similarity to pyrite from Avoca is obvious.

Zoning is present in many pyrite grains, from the pyritic and lead-zinc zones, but not as common as in similar material from Avoca. Colloform textures, as overgrowths on crystalline pyrite, are common (Plate 44) and the cores of colloform aggregates are preferentially replaced (Plate 43:I,J). Melnikovitic pyrite also occurs.

Spheroidal textures exist in the pyritic and lead-zinc zones (Plate 43:G,H). Atoll-like textures occur in the disseminated polymetallic sulphide zones and there are framboids in the bluestone zones. Analysis of the size distribution of apparent framboidal pyrite diameters from Parys Mountain is given in fig. 4.5. The distribution is unimodal and positively skewed with a maxima at 5.5μ , corresponding to a true diameter of 6.8μ , using Jackson's correction procedure (in 143). The outlines of the microcrystalline aggregates are spherical or subspherical (Plate 45). Single and dumbbell forms predominate and in clusters, the individuals tend to be of similar size. Amongst the internal characteristics, the size of the microcrystallites ranges from $0.5-2.0 \mu$ and ordering is common. Replacement of framboidal pyrite by chalcopyrite, sphalerite and galena occurs.

Evidence of cataclasis of pyrite is rare, except adjacent to fractures (Plate 43:E). The corroded grain boundaries

of pyrite are due to replacement by the matrix sulphides. In areas of pyrite devoid of matrix sulphides, euhedral forms are universal. Inclusions are rare, but emulsion blebs of chalcopryrite and pyrrhotite ($\leq 10 \mu$) do occur.

In summary, the textures in pyrite at Parys Mountain mirror those at Avoca.

(ii) Chalcopryrite. Chalcopryrite is the primary matrix sulphide at Parys Mountain and occurs as a cement to the pyrite grains in the cupriferous lenticles. Textures are shown in plate 46. Allotriomorphic masses are common, and the grain size, revealed by etching, is variable: 0.2-0.02 mm. The grains are generally equidimensional, but in pressure slacks, elongate grains occur. Twinning is ubiquitous and lamellar and polysynthetic forms are present, probably developing from crystallization within a stressed environment. Inclusions, blebs of sulphosalts and native bismuth, occur in chalcopryrite, concentrated at grain boundaries. Mutual boundary relations are shown against quartz, and chalcopryrite is replaced by sphalerite.

(iii) Sphalerite. Sphalerite is contemporaneous with, and also slightly post-dates, the crystallization of chalcopryrite, and occurs in every zonal type. The colour of sphalerite is russet and internal reflections are found. Etching (Plate 48) reveals a variable grain size: 0.6-0.05 mm. The common occurrence is as an aggregate of polygonal grains with a marked tendency for comminution at the margins of sphalerite seams (Plate 48:C-E). This is related to deformation possibly related to cooling. Twinning is universal and distortion of twin lamellae is illustrated in plate 48:C. Inclusions of chalcopryrite are common and concentrate at grain boundaries and along twin planes. A variety of exsolution patterns exist and are often related to grain growth and the crystal morphology (Plate 47:A-D). Replacement of sphalerite by exsolution chalcopryrite is common and mutual boundary relationships are shown against galena and sulphosalts. Sphalerite replaces zoned and melnikovitic pyrite (Plate 47:E and F).

(iv) Galena. Intimately associated with sphalerite, allotriomorphic masses of galena with cusped outlines are

common in the complex lead-zinc ore (Plate 48:F and H). Etching reveals a highly variable grain size: 0.3-0.05 mm, as granular mosaics (Plate 48:J). There are no inclusions. Mutual boundary relations are shown against quartz (Plate 48:I), and sulphosalts replace galena.

(v) Pyrrhotite. This rare mineral occurs as ovoid blebs (up to 25 μ in size) in pyrite.

(vi) Tetrahedrite. This mineral occurs in lead-zinc rich material associated with galena (Plate 49:A-E). Allotriomorphic masses are common and the grain size ranges from 25-50 μ . No inclusions are present, and twinning and deformation effects are absent. Analyses of representative samples (Table 2.17) indicate that the tetrahedrite from Parys Mountain is argentian. Tetrahedrite replaces zoned pyrite (Plate 49:E).

(vii) Bournonite. Trace quantities of bournonite occur as a marginal intergrowth with tetrahedrite and the grain size is $\leq 15 \mu$.

(viii) Native Bismuth. A minor mineral, associated with bismuthinite, native bismuth occurs as inclusions in chalcoppyrite (Plate 49:F,H).

(ix) Bismuthinite. Closely associated with native bismuth, bismuthinite occurs as allotriomorphic grains included in chalcoppyrite (Plate 49:F,H).

b) Supergene Minerals

A varied suite of supergene minerals is developed at Parys Mountain and Greenly (100) provided a list of the species found. Pyrite breaks down to form limonite, goethite and hematite, and derived from the copper content are native copper, covellite, malachite and chalcantite. The lead-rich ore gives rise to anglesite and minium, and the silver concentrates as native silver, which was recorded from the gossans (100).

c) Gangue Minerals

Quartz is the major gangue mineral and is primary and secondary, developed during the extensive silicification. Chlorite is minor, and sericite occurs as a prominent wallrock

alteration product associated with the siliceous zones. Talc, gypsum and barite are recorded by Greenly (100) but have not been identified by the writer.

d) Summary

In summary, the ore mineralogy at Parys Mountain is similar to that at Avoca, and an equivalent suite of ore textures exists. This suggests that a similar genesis may have operated.

4.1.10.3. Trace element distribution

Trace elements in samples of pyrite, chalcopyrite, sphalerite and galena have been analysed spectrographically using the method described in section 2.3.7.2. The results are in tables 36 and 37.

a) Pyrite

Ti, Cr, Mn, Ni and Mo contents are low. The erratic silver values reflect enrichment within the ores, although there is no correlation with lead, tetrahedrite does occur with pyrite (Plate 49) and this may contain the silver. Tin is absent except for a single specimen which may contain stannite inclusions. Bismuth minerals probably contribute the erratic bismuth values.

b) Chalcopyrite

Ti, Mn, Co, Ag and Sn contents are low, but a few high cobalt and manganese values exist. Nickel enrichment parallels that of cobalt, and the bismuth reflects the presence of bismuth minerals.

c) Sphalerite

Ti, Mn, Co, Ga and In are low. The high silver content is probably due to included tetrahedrite as the values are accompanied by an increase in antimony. The cadmium content (1400 ppm) confirms the geochemistry of this element. The erratic tin values may be due to contamination.

d) Galena

Ti, Mn and Co contents are low and the Ga value is erratic, the high value is not paralleled by zinc enrichment

TABLE 36

SPECTROGRAPHIC ANALYSIS OF PYRITE AND CHALCOPYRITE, PARYS MOUNTAIN

PYRITE

Sample No	Locality	Description	Contamination Indicators %			Trace Elements ppm									
			Cu	Zn	Pb	Ti	Cr	Mn	Co	Ni	Mo	Ag	Sn	Bi	Co/Ni
A.1779	W.opencast;Central boss	Dissem.py with qtz & sl & gn	0.5	1.0	1.0	45	5	11	10	17	30	41	*	*	0.59
1780	E.opencast;Bluestone Adit dump	Dissem.py, cp with qtz	0.5	2.0	1.0	29	5	19	14	8	30	74	*	2600	1.75
A.1733	DDH - M 1 C - 1207'	Dissem.py with cp, qtz & sl	0.5	1.0	0.25	25	*	45	270	21	52	5	*	500	12.86
1732	" "	Cp, py and qtz	*	1.0	1.0	210	*	52	180	100	30	21	*	3200	1.80
1841	" "	Banded py,sl in qtz with gn & cp	0.5	2.0	1.0	25	5	335	31	10	62	16	*	*	3.10
1906	" "	" " " " " "	0.5	2.0	0.5	25	*	260	45	7	70	18	*	*	6.43
1734	" "	Cp, py and qtz	5.0	1.0	0.25	25	8	96	410	11	30	34	365	500	37.27
1651	DDH - M 3 - 536'	Dissem.py, with qtz	*	*	*	88	*	37	270	24	30	2	*	*	11.25
1735	" "	Banded py with qtz, dissem.cp	0.5	*	*	32	5	17	290	13	30	2	*	*	22.30
1738	" "	Dissem.py with cp & qtz	1.5	*	*	45	5	16	350	18	30	4	*	*	19.44
1739	" "	Py stringer in phyllite with qtz	0.5	2.0	0.25	195	5	58	135	60	30	11	*	*	2.25
1744	" "	Dissem.py, with qtz & cp	0.5	*	*	36	5	33	260	5	30	2	*	*	52.00
1740	" "	Py, cp with qtz	2.25	1.0	*	38	5	31	10	2	30	22	*	*	5.00
A.1624	Rhosmynach;Exp.SW. of shaft	Banded py,cp,with qtz in greenstone +	3.4	*	*	75	5	5	390	7	30	18	*	*	55.71
		Detection Limit	0.25	1.0	0.25	25	5	5	10	2	30	2	25	500	

The following elements were below detection (limits in ppm) : V(50), Ga(60), Ge(20), As(800), Cd(100), In(700), Sb(100), Ba(100), Pt(50), Au(350) and Hg(500).

CHALCOPYRITE

Sample No	Locality	Description	Zn	Pb	Ti	Mn	Co	Ni	Ag	Sn	Bi
A.1640	W.opencast; N.wall	Dissem.cp	*	*	118	5	*	*	6	59	*
1873	W. " ; Central boss	Dissem.cp with py, gn & qtz	*	1.0	25	15	*	2	10	25	*
1874	E. " ; Bluestone Adit dump	Dissem.py, cp with qtz, sl & gn	2.0	0.75	25	5	*	2	36	120	500
1797	DDH - M 1 C - 454'	Dissem.cp, with py & qtz	*	0.25	40	31	10	*	8	25	*
1799	" "	Dissem.cp with py	*	*	108	237	10	*	3	71	*
1798	" "	" " with py & qtz	*	*	135	59	10	2	4	25	500
1800	" "	Dissem.py, cp with qtz, sl & gn	*	0.25	91	840	29	2	14	25	*
1801	" "	Cp, py & qtz	*	0.25	99	36	10	2	17	90	3100
1802	DDH - M 3 - 542'	Banded py with qtz, dissem.cp	*	*	137	82	210	7	9	25	*
1805	" "	Dissem.py with cp & qtz	*	*	380	275	135	10	13	25	*
1808	" "	Dissem.py, with qtz & cp	*	*	88	300	110	*	2	*	500
1806	" "	Py, cp with qtz	*	*	120	30	*	*	43	25	*
A.1639	Rhosmynach;Exp.SW. of shaft	Cp, py in sheared greenstone +	*	*	44	137	450	*	11	*	*
		Detection Limit	1.0	0.25	25	5	10	2	2	25	500

All samples have siliceous matrix except where noted +

The following elements were below detection (limits in ppm) : Cr(5), Ga(60), Ge(20), As(800), Mo(30), Cd(100), In(700), Sb(100), Ba(100), Pt(50), Au(350), and Hg(500). V. was found in A.1805(120 ppm) but was otherwise absent(50).

* = not detected

TABLE 37

SPECTROGRAPHIC ANALYSIS OF SPHALERITE AND GALENA, PARYS MOUNTAIN

SPHALERITE

Sample No	Locality	Description	Contamination Indicators %			Trace Elements ppm								
			Cu	Pb	Fe	Ti	Mn	Co	Ga	Ag	Cd	In	Sn	Sb
A.1887	W.opencast; central boss	Dissem.sl, gn & qtz with py +	2.8	1.0	6.3	10	115	10	58	53	1600	10	165	*
1888	E.opencast;Bluestone Adit dump	Banded sl, gn with py	2.8	0.75	3.6	45	140	18	61	390	1580	10	30	265
1889	" ; " "	" "	1.5	0.25	5.3	10	52	10	74	42	2050	10	500	100
1890	" ; " "	Dissem.sl in qtz with gn	0.75	0.5	5.3	10	190	10	90	280	1700	10	235	100
1897	Parys;Morfa-Du Eng.Shaft dump	Banded sl, gn & py	0.75	0.5	2.7	76	300	17	27	800	1360	*	*	1170
A.1879	" ; DDH - M 1 C - 1270'	Banded py, sl in qtz with gn & cp +	0.25	0.25	13.8	10	100	75	29	13	1420	58	*	*
1880	" " " - 1285'	Banded py, sl in qtz with gn +	3.0	1.0	17.0	10	80	10	10	135	*	*	*	*
		Detection Limit	0.25	0.25	0.05	10	5	10	10	2	100	10	30	100

The following elements were below detection (limits in ppm) : V(10), Cr(5), Ni(5), Ge(10), As(500), Mo(10-30), Ba(100), Pt(50), Au(350), Hg(500), and Bi(50).

GALENA

Sample No	Locality	Description	Fe	Cu	Zn	Ti	Mn	Co	Ga	Ag	Sn	Sb	Bi
A.1868	W.opencast; central boss	Dissem.sl, gn & qtz with py +	2.9	*	*	135	5	10	*	800	*	*	110
1869	E.opencast;Bluestone Adit dump	Banded sl, gn with py	1.7	*	2.0	138	8	12	10	550	113	188	*
1902	Parys;Morfa-Du Eng. Shaft dump	Banded sl, gn & py	5.8	*	*	10	97	28	210	920	*	345	*
A.1899	" ; DDH - M 1 C - 1285'	Banded py, sl in qtz with gn +	2.45	*	1.0	10	5	*	10	550	*	*	730
		Detection Limit	0.05	0.25	1.0	10	5	10	10	2	30	100	50

+ Samples with siliceous matrix & remainder with chlorite

The following elements were below detection (limits in ppm) : V(10), Cr(10), Ge(10), As(500), Cd(100), Mo(10-30), Ba(100), Pt(50), Au(350) and Hg(500). Ni was found in A.1902 (8 ppm) but was otherwise below detection(5).

* = not detected

and the source of the gallium is unknown. The mean silver content (~ 700 ppm) is higher than that at Avoca and the values correlate with antimony indicating impurity tetrahedrite. El Shazly et al (83) found only 50 ppm silver using semi-quantitative methods. The tin and bismuth values are erratic and probably due to inclusions.

c) Discussion

In general, the similarity of the trace element contents of sulphides to that described from Avoca is striking. The Co:Ni ratio is >1.0 (Table 36) and thus the sulphides may be associated with volcanism. There is no sulphur isotope data from Parys Mountain and the cadmium content of sphalerite is not 'granitophyle', but volcanogenic.

Evidence for the temperature of crystallization of the ores is minor. There is no constant partition of trace elements between coexisting sulphides, which suggests that the assemblage is not at equilibrium, supported by minor inhomogeneities amongst the sulphides e.g. zoning and twinning. The iron contents of sphalerite show a similar distribution to that at Avoca:

Table 38 Comparative analyses of iron contents in sphalerite, Parys Mountain.

		%Fe	
		Probe	Spec.
A.1887	Boss in Great opencast	2.0	6.3
1879	DDH M-1-C, 1270'	1.8	13.8*
1880	DDH M-1-C, 1285'	1.5	17.0*
P.97	DDH M-10, 1492'	1.8	-

* Specimen contaminated with CuFeS_2 and FeS_2 .

The cadmium content of sphalerite is non-diagnostic and the content of silver in galena ($0.08\% \text{Ag}_2\text{S}$) is within the expected limits as there are associated bismuth minerals (232).

In the context of metallogenic provinces, the presence of tin and molybdenum in pyrite is similar to that at Avoca, and thus the geochemical similarity between the two deposits is

highlighted. Work in progress on the geochemical atlas of Great Britain has delineated an anomalous tin area associated with copper at Parys Mountain, but the explanation for this is not fully understood (F.Urquidi, pers. comm.).

4.1.10.4. Mineral and metal distribution

A crude pattern of metal zoning exists at Parys Mountain, the pyritic zones are stratigraphically above the siliceous zones, and lead-zinc zones are associated with them.

a) Mineral distribution

Detailed analysis of diamond drill core using the S/Q logging method was not undertaken. Mineral variations were studied qualitatively.

(i) Pyrite. Amounts of pyrite are generally less than in the pyritic zones at Avoca, and the highest sulphur contents occur in the bluestone zones (~30%S).

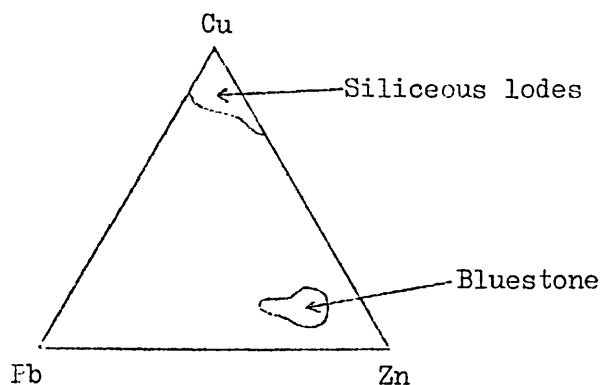
(ii) Chalcopyrite. Graphs of assay data from the Carreg-y-doll lode (W.Manning, pers. comm.) indicate minor concentration of copper on the hangingwall or stratigraphic base, of the lode, but the general distribution is uniform; similar to cupriferous siliceous zones at Avoca.

(iii) Sphalerite and galena. Bluestone ore contains the maximum concentrations of lead and zinc, but no quantitative data is available.

b) Metal ratios

The Zn:Pb ratio in bluestone ore is generally 3:1 -2:1 and is therefore broadly equivalent to that in kilmacooite (2.5:1), but the ratio at Parys Mountain sometimes becomes 1:1 and thus the overall lead content is higher. There is appreciable silver in the galena and therefore this factor is important.

Generalized metal ratios for the siliceous lodes are shown overleaf:



c) Relations between mineral distribution and lode structure

Insufficient data exists to construct a Conolly diagram for any of the ore zones. Level plans of the Carreg-y-doll lode indicate that the mineralization plunges steeply to the northwest (Fig. 4.7.). It is not clear to which structural element this elongation of values corresponds, but as at Avoca, the values plunge in the plane of the cleavage.

4.1.10.5. Genesis

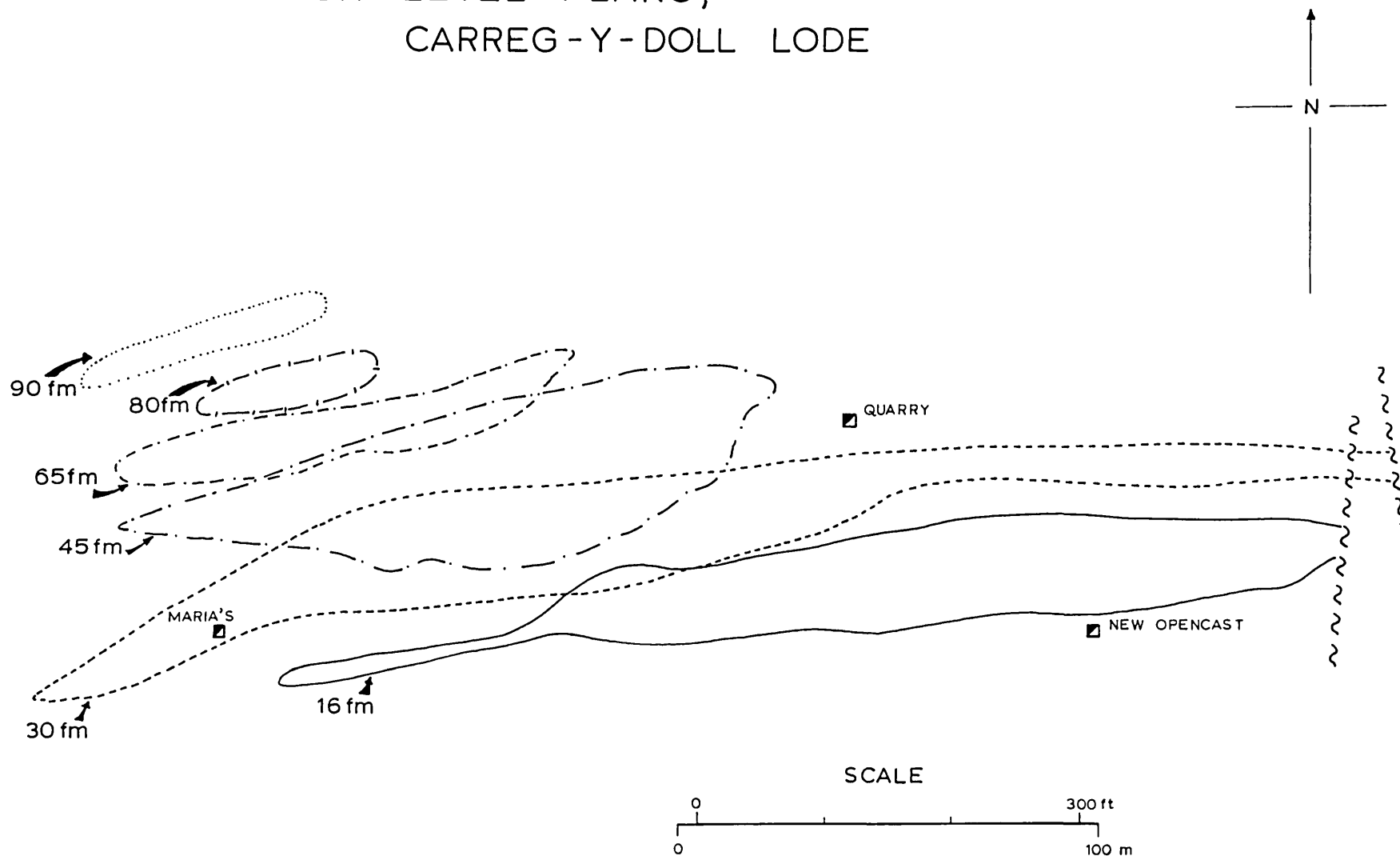
Geothermometric and geobarometric indicators amongst the ore minerals are inconclusive. The temperatures of ore deposition were leptothermal. Primary zoned pyrite suggests that growth took place at low temperatures ($\leq 100^{\circ}\text{C}$), in an environment supersaturated with iron, and melnikovitic pyrite emphasizes this conclusion. The occurrence of framboidal pyrite in the lead-zinc zones, indicates ore deposition at low temperatures.

As at Avoca, two major 'systems' of mineralization exist: a) Primary, bedded iron sulphide (pyrite) and b) iron, copper, lead and zinc polymetallic sulphides and sulphosalts, exhibiting crosscutting relationships to the wallrocks and demonstrably epigenetic. Each of the ore types at Parys Mountain has an analogue at Avoca, and it is reasonable to infer a similar origin.

Post-dating deposition of the argillaceous rocks, growth

FIG 4.7

SKETCH LEVEL PLANS,
CARREG-Y-DOLL LODE



of pyrite took place below the sediment water interface. The felsite exemplifies explosive felsic volcanicity and a salic magma fraction probably existed at depth. Hydrothermal fluids became active after the deposition of the Silurian shales, and were probably related to a cooling phase of the underlying magma. Increased heat flow provided by the cooling magma drove the fluids, which were probably chloride enriched, to the surface, possibly through dilatation zones related to the volcanic feeder channels or later intrusions. In the near-surface environment the fluids came into contact with circulating connate waters in the highly porous felsite, and stockwork copper-rich siliceous zones developed. The rapid change in the composition of the fluids on interaction with the pyritic zones caused precipitation of the sulphides and formation of complex lead-zinc rich material typical of this area. Potassic and silicic metasomatism of the wallrocks is evident from the development of sericite and quartz. During subsequent deformation, late-stage cross-cutting fractures were infilled by siliceous fluids charged with lead and zinc. This probably derived from connate water which possibly had leached the metals from the sedimentary pile.

4.2. Rhosnynach

Three narrow, shallow dipping lodes occur $1\frac{1}{2}$ miles west of Parys Mountain with an east-west trend in Silurian shales. The lodes, worked in about 1917, are of minor extent. A maximum strike length of 600 ft exists and abandoned workings extend to depths of 120 ft.

A body of felsite occurs on the hangingwall of the middle lode, and intrusive hornblendite has been recorded at depth (70). Mineralization consists of disseminated chalcopyrite and pyrite with minor sphalerite and galena. Native bismuth and bismuthinite occur and account for the bismuth content in trace element analysis of chalcopyrite (Table 36). Supergene native copper has been found (70). Gangue minerals are predominantly quartz and chlorite, and these are also the major wallrock alteration products.

Although little is known of the detailed geology, probably a similar genesis to that at Parys Mountain operated. Epigenetic, hydrothermal fluids enriched in silica probably produced ramifying stockwork zones in an area containing evident intrusive activity.

S E C T I O N 5

RELATED DEPOSITS5.1. The Southern Caledonides

The mineral deposits already discussed are only a selection from the Southern Caledonides of Great Britain and Ireland. There are numerous other occurrences in this belt of rocks (cf. Fig. 1.3) and the copper deposit at Coniston is on a linear extension of the metallogenetic belt which includes Bunmahon, Avoca and Parys Mountain. Coniston occurs in Ordovician volcanic rocks and as it may provide significant information about metallogenesis in the region, the deposit has been studied in reconnaissance.

5.1.1. Coniston

A series of steeply dipping fissure veins cut rhyolites and tuffs of the Borrowdale Volcanic Series (Fig. 5.1). The veins trend northwest-southeast at Paddy End and east-west at Seathwaite. Extensive workings testify to considerable mining activity in the last century and the Bonser Vein has been worked to a depth of about 1500 ft (77) (Plate 51 A-C). Recently an exploration programme was initiated on the property.

5.1.1.1. Lithology, petrology and petrogenesis

The country-rocks are dominantly green, medium grained pyroclastics, with ignimbrite horizons (156) and the lithology has been described by Mitchell (153) (Plate 51:D). Generalized descriptions of the petrography have been given (154) but no analytical data exist. Analyses of representative rock types by the writer are shown in table 39. The rocks are petrochemically similar to the suite at Bunmahon, but have an increased potash content, which is paralleled by the rubidium and strontium trace element content and reflects an increase in potash feldspar. This similarity reinforces the petrogenetic unity of the Ordovician volcanic lineament extending from the Lake District to S.E. Ireland.

5.1.1.2. Wallrock alteration

Wallrock alteration is slight, rarely extends for more

FIG 5.1

Geological sketch map,
Coniston district.

(After Eastwood 1959,
and Mitchell 1940,1963)

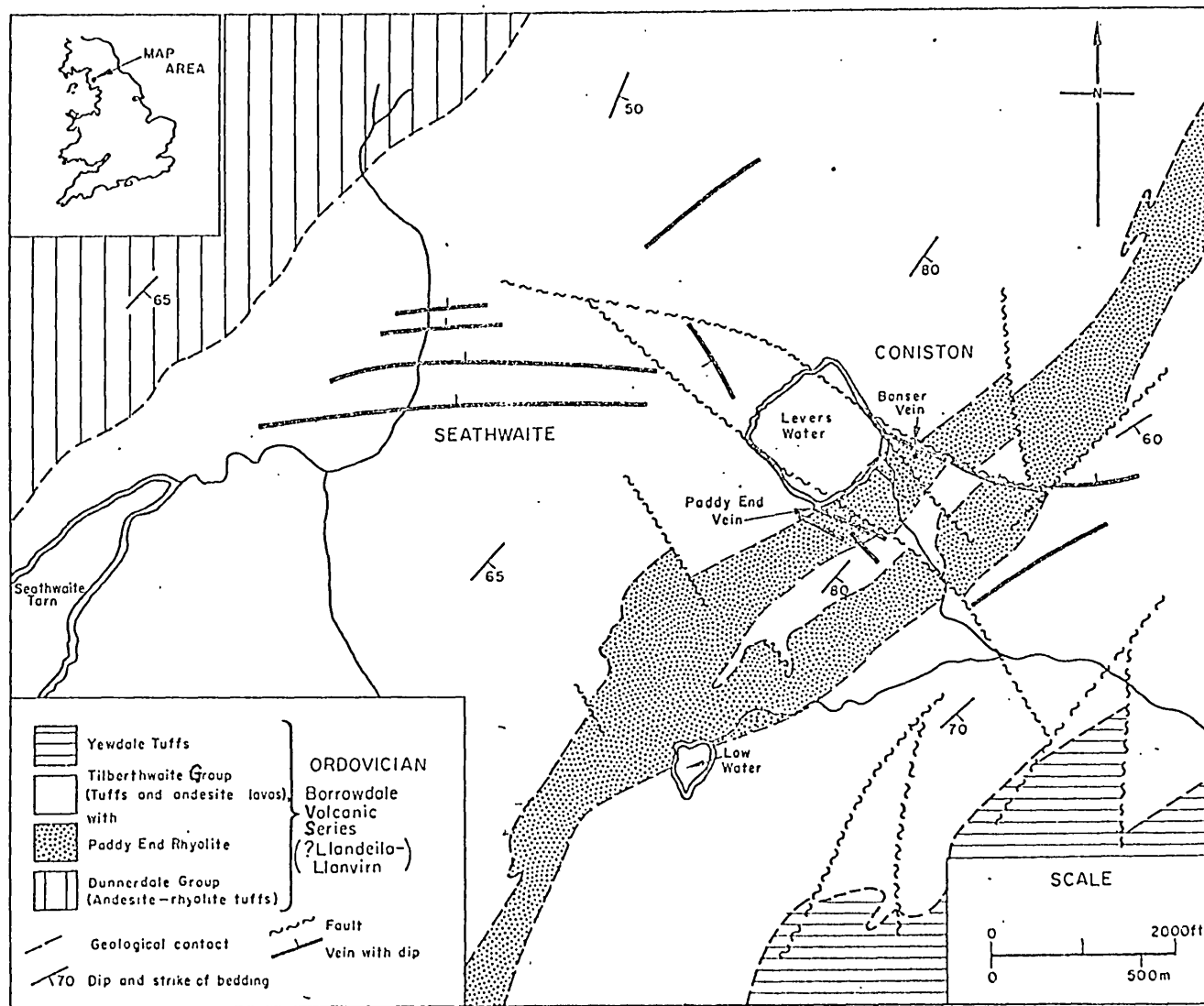


Table 39 Partial analyses of rocks from the Coniston district, by X-ray fluorescence.

Major oxides: (%)	C.1	C.2	C.3
SiO ₂	54.20	54.80	58.30
Al ₂ O ₃	15.03	16.52	11.98
TiO ₂	1.18	1.39	0.67
Fe ₂ O ₃	0.57	1.00	1.22
FeO	6.00	4.56	6.46
MnO	0.36	0.62	0.84
MgO	2.37	3.48	2.97
CaO	0.78	0.74	0.48
Na ₂ O	2.35	0.98	1.13
K ₂ O	7.58	8.03	5.68
P ₂ O ₅	0.42	0.12	0.16
Total S	0.03	0.04	0.05
H ₂ O+	-	-	-
H ₂ O-	-	-	-
Total	90.87	92.28	89.94

Trace Elements:
(ppm)

Co	12	12	15
Ni	≠	27	14
Cu	81	80	82
Zn	113	222	168
Rb	210	238	156
Sr	86	113	50
Pb	39	38	58

Analyst: C.J.V.Wheatley

≠ = not detected

- = not sought

Description of samples:

- C.1 Tuff. 200 ft east of Hospital adit portal, Paddy End, Coniston.
- C.2 Tuff. 200 ft west of Triddle vein surface pit, Paddy End, Coniston.
- C.3 Tuff. 800 ft northeast of Hospital adit portal, Paddy End, Coniston.

than a few centimetres from the vein walls and is limited to silicification.

5.1.1.3. Environment of deposition

The depositional environment may have been aerial or submarine, ash-fall tuffs and lavas exist (154).

5.1.1.4. Intrusive rocks

A narrow quartz-porphyry intrusive dyke occurs near Lever's Water and is the only evidence of intrusive activity. The trend of the dyke is close to that of the lodes, suggesting that intrusion and mineralization may have taken place whilst the same system of forces operated.

5.1.1.5. Structure

Pre-Bala deformation produced open NNE trending folds which are at 45° to the late Silurian folds and result in a dome-basin interference pattern in the Lake District. Broad late-stage folds have slaty cleavage of varying intensity.

5.1.1.6. Mineralization

The mineralization occurs as true lodes, and two vein-types can be recognized, emphasizing the similarity to the mineralization at Bunmahon : a) Siliceous veins with disseminated chalcopyrite and pyrite, and b) minor veins with galena and sphalerite. Magnetite also occurs at the vein margins (A.P. Millman pers. comm.) and appears to replace chlorite (Plate 51:E).

The ore minerals consist of chalcopyrite, pyrite, magnetite, and minor sphalerite and galena. Native bismuth and bismuthinite are associated with chalcopyrite (Plate 51:F). Arsenopyrite and nickel and cobalt minerals occur (77). The gangue minerals are quartz, calcite and dolomite.

The generalized paragenetic sequence is given below:

Table 40 Generalized paragenetic sequence, Coniston

Ore Minerals:	Syngenetic	Epigenetic
Magnetite		_____
Chalcopyrite		_____
Pyrite		— — —
Sphalerite		_____
Galena		_____
Arsenopyrite		? — — — ?
Native Bismuth		_____
Bismuthinite		_____
Quartz	— —	_____
Calcite		_____
Dolomite		_____

5.1.1.7. Trace element distribution

Trace elements in eight samples of pyrite, magnetite, chalcopyrite, sphalerite and galena are shown in table 41. Determination was by spectrography, as described in section 2.3.7.2.

In pyrite, values of Ti, Mn, Ni and Ag are low. The cobalt rises to 550 ppm, and the bismuth content is presumably contributed by bismuth minerals.

The elements in magnetite and chalcopyrite are similar to those found at Avoca, but the tin magnetite is markedly reduced.

In sphalerite, Ti, Mn, and In are low, and the high cobalt value and silver content are possibly due to impurities. The cadmium content (2360 ppm) is high and appreciable tin is present (180 ppm).

Manganese and cobalt are low in galena, and the silver content (1230 ppm) implies that there is some in solid solution. The presence of contaminant tetrahedrite is suggested by the antimony content and high tin value (87). The bismuth is probably due to contamination.

5.1.1.8. Genesis

Indicators of genesis amongst the trace element data are

TABLE 41

SPECTROGRAPHIC ANALYSIS OF SULPHIDES AND MAGNETITE, CONISTON DISTRICT

PYRITE

Sample No	Locality	Description	Contamination Indicators %			Trace Elements ppm						
			Cu	Zn	Pb	Ti	Mn	Co	Ni	Ag	Bi	Co:Ni
A.1767 1942	Paddy End;Hospital level,Dump " " "	Mass.py, dissem.cp	*	*	*	30	155	10	10	2	*	1.0
		Dissem.py with qtz	0.5	*	*	*	*	550	15	5	10000	36.7
		Detection Limit	0.25	1.0	0.25	25	5	10	2	2	500	

The following elements were below detection (limits in ppm) : V(50), Cd(100), In(700), Sn(25), Sb(100).

MAGNETITE

Sample No	Locality	Description	Cu	Zn	Pb	Ti	V	Mn	Ni	Sn
			A.1938	Paddy End;Hospital level,Dump	Mass.mt/hm, dissem.cp & qtz	3.0	*	*	340	440
		Detection Limit	0.25	1.0	0.25	25	50	5	5	25

The following elements were below detection (limits in ppm) : Co(10), Cd(100), In(700), Sb(100), and Bi(500).

CHALCOPYRITE

Sample No	Locality	Description	Zn	Pb	Ti	Mn	Co	Ni	Ag
			A.1939	Paddy End;Hospital level,Dump	Dissem.cp with py	*	*	25	19
		Detection Limit	1.0	0.25	25	5	10	5	2

The following elements were below detection (limits in ppm) : V(50), Cd(100), In(700), Sn(25), Sb(100) and Bi(500).

SPHALERITE

Sample No	Locality	Description	Cu	Pb	Fe	Ti	Mn	Co	Ag	Cd	In	Sn
			A.1930	Paddy End;Hospital level,Dump	Banded sl & gn with cp & qtz	0.25	*	2.6	10	425	107	7
		Detection Limit	0.25	0.25	0.05	10	5	10	2	100	10	30

The following elements were below detection (limits in ppm) : V(10), Ni(5), Mo(10), Sb(100), and Bi(50).

GALENA

Sample No	Locality	Description	Fe	Cu	Zn	Mn	Co	Ag	Sn	Sb	Bi
			A.1936	Paddy End;Hospital level,Dump	Banded sl & gn with cp & qtz	3.8	*	1.0	32	10	1230
		Detection Limit	0.05	0.25	0.25	5	10	2	30	100	50

The following elements were below detection (limits in ppm) : Ti(10), V(10), Ni(5), Cd(100) and In(10).

The following elements were below detection throughout (limits in appendix 3) : Cr, Ga, Ge, As, Mo, Ba, Pt, Au and Hg.

* = not detected

non-diagnostic. The Co : Ni ratio varies from 1 to 37 and this correlates with derivation from hydrothermal or volcanic sources. The low Ti, Mn and Mo content in pyrite and absence of vanadium may imply a hydrothermal origin (49, 3). The iron content of sphalerite varies from 2.6-7.0% Fe (4.3-11.0 mole % FeS), similar to the variation found elsewhere in the metallogenetic belt. The wallrock alteration is slight and compatible with ore deposition at temperatures of 200 - 300°C.

The relationship between the veins and the country-rocks indicates that ore deposition postdated deposition of the volcanics. The felsic volcanic activity exemplified by the Paddy End Rhyolites implies that a magma of similar composition existed at depth. This magma, as it cooled, would have been a locus for circulating connate fluids, which probably received additions from juvenile sources as they migrated upwards within fault fissures. These fissures probably developed in response to deformation related to the Caledonian orogeny. Elsewhere in the Lake District, the Shap Granite, intruded as a late stage pluton possibly derived from the same salic magma, has associated mineralization with chalcopyrite, pyrite, fluorite, bismuthinite, galena, sphalerite and barite (99). This suggests that the salic magma was a potent mineralizing source, and could have produced metal enriched hydrothermal activity.

5.1.2. Other deposits in the Southern Caledonides

The majority of deposits in the Southern Caledonides are vein-type lead-zinc deposits and copper deposits of economic significance are rare, being concentrated close to the median geanticline (cf Fig. 1.3). This feature produces a pattern of regional metal zoning, with an axial copper-rich belt bordered by areas rich in lead and zinc. This pattern, closely related to the symmetry of the geosyncline may also be genetically related to it, according to a genetic model recently suggested by the author (250)

5.2. World-wide

Mineralization at Avoca and Parys Mountain typifies

volcanic stratiform (or conformable) deposits, of which there are a large number around the world (218).

Bodies of cupriferous pyrite frequently occur within basic volcanic sequences, e.g. Cyprus (239), Norway (236), Turkey (219) and Greece (in 252). However, deposits of conformable pyrite with appreciable polymetallic sulphide and sulphosalt content, are invariably associated with acid volcanism, e.g. Spain and Portugal (252), Sweden (168), Japan (116), Canada (191) and Mt Lyell (149) and Mt Isa (62), Australia. The basic volcanic sequences are generally tholeiitic and the acid sequences calc-alkaline, typical of island arc regimes. These facts allow a primary subdivision of pyritic deposits, and Avoca and Parys Mountain fall in the group of polymetallic deposits in calc-alkaline provinces.

The acid volcanic rocks associated with polymetallic pyritic deposits are often pyroclastic and abnormally rich in potassium. The Mt Isa (62) and Noranda (191) districts illustrate this criterion, which also applies in Australia at Mt Lyell and Rosebery (H. Solomon, pers. comm.).

Depositional environments elsewhere correspond with that at Avoca, and the Iberian pyrite belt in Spain and Portugal is a good example (198). Interbedded carbonaceous horizons are commonplace and imply temporary reducing conditions during sedimentation. The recognition of phosphatic horizons as an environmental indicator is of recent origin (223), but sedimentary features in the pyroclastics point to deposition in shallow-water environments.

Wallrock alteration is generally minor, but as these deposits occur in eugeosynclinal terrain, succeeding orogeny often obscures the original relationships. Diagnostic features amongst the ore mineral fabric are obliterated by recrystallization and remobilization of the ductile minerals, but colloform textures in pyrite are often preserved. Alteration similar to that at Avoca occurs in the Skellefte district, Sweden (161) and the problem of deciding whether the potassic enrichment of the porphyries and wallrocks is primary, or due to wallrock

alteration is acute. An equivalent situation exists at Rio Tinto, Spain. (43).

The close relationship between the distribution of pyrite and chlorite has been frequently described (e.g. 47). To-date, few writers have questioned the nature of the chlorite, assigning it to wallrock alteration. Analysis may demonstrate that the chlorite could have derived from an authigenic iron silicate.

Quite commonly, the polymetallic pyritic deposits consist of a series of relatively distinct ore zones, e.g. Mt Lyell, Rio Tinto and the Kuroko ores of Japan. The genetic model developed for the Avoca district can equally be applied to many other deposits with only minor modifications. A thorough knowledge of the structure and primary configuration of the ore zones is a pre-requisite, but often this is lacking: e.g. Mt Lyell (47). The fact that pyritic zones are stratigraphically underlain by siliceous stockworks is well established e.g. Rio Tinto, Mt Lyell and the Kuroko ores. Intrusive activity, usually minor (porphyry dykes), post-dates formation of the pyritic bodies.

Many writers have noted the association between conformable pyritic deposits and the products of volcanism (3, 132, 142, 174, 252), and in Japan and Taiwan there is an obvious genetic relationship between recent ore deposition and hot spring and fumarolic activity (132).

Metallogenesis is an integral part of orogenic evolution, and Bilibin's work (27), amongst others, related the two processes. Markham (149) concluded that conformable pyritic deposits characterized the initial stages of development of a geosyncline, but this is certainly not so in the Caledonian geosyncline in Western Europe, nor elsewhere (252). As pyrite deposits occur at various stages throughout the geosynclinal sequence, there must be another metallogenetic control.

Conformable polymetallic pyritic deposits are undoubtedly related to volcanism, which is an expression of magmatic activity. Magma generation may therefore provide the key. Contemporaneous acid volcanism is often potassic and implies crustal contamination

of the magma. Crustal generation and destruction are intimately linked through plate tectonics. Plate destruction only occurs where an oceanic plate is being consumed at a continental margin by descending along a Benioff zone (72). An island arc environment is produced in this situation.

Lateral variations in magma type across island arcs are well known (136), and the calc-alkaline province develops in the region where crustal contamination is likely.

The writer therefore suggests that as the primary difference between polymetallic and non-polymetallic pyritic deposits is the nature of the accompanying volcanism, the polymetal content may derive from partial fusion of crystalline basement along a Benioff zone. Thus, the existence of a Benioff zone may be implied by the presence of conformable polymetallic pyritic deposits within a eugeosynclinal sequence.

S E C T I O N 6

CONCLUSIONS AND IMPLICATIONS6.1. Avoca Mineralized Belt

The country-rocks, a sequence of Ordovician sediments and volcanics, have been divided into a Lower Laminated Series (?Arenig) and an Upper Volcanic Series (?Caradoc-Ashgill). Granodioritic post-tectonic sheet intrusions, and stocks and dykes ranging from quartz-porphyry to appinite, occur.

A pyroclastic rock suite (felsite) is prominent at the base of the Upper Volcanic Series and is spatially associated with the mineralization. Analyses indicate abnormal potash content in the felsites, which may have derived from a potassic magma.

The host-rocks for the major mineralization are a series of tuffs and sediments, termed the Chlorite Zone, in the Upper Volcanic Series. Intercalated phosphate-rich and carbonaceous horizons occur and a shallow-water marine environment of deposition existed.

At least three periods of deformation affected the rocks and ore deposition pre-dates the earliest deformation. A regional monoclinial structure exists, and the pyritic lenses at West Avoca essentially occupy a single folded horizon which is parasitic upon the regional monocline.

Wallrock alteration consists of silicification and potassium metasomatism. Carbonatization developed during a subsequent deformation period. Analyses of chlorite imply that it may have derived from an authigenic iron silicate during metamorphism.

The mineralization is divided into a series of ore types, each with a distinct mineralogy and genesis. The major ore mineral is pyrite, with chalcopyrite, sphalerite, galena, magnetite and a suite of minor oxides, sulphides, sulphosalts and native metals. The paragenetic sequence may be polyascendant.

It is proposed that conformable lenticular pyrite zones formed in a marine environment, possibly during diagenesis with mineral growth taking place below the sediment-water interface. Trace element contents of the sulphides, sulphur isotope results and evidence for contemporaneous volcanicity support the idea that the supply of sulphur was fumarolic, and that the iron and copper probably derived from the same source. Magnetite zones developed under different Eh and pH conditions.

Stockworks containing appreciable polymetal content (copper and, in some cases, lead and zinc) were developed stratigraphically below the pyritic zones by hydrothermal metal-rich fluids at a later date. Siliceous and potassic wallrock alteration accompanied this mineralization. The hydrothermal fluids were probably chloride-rich, derived from the aqueous phase of an underlying magma, which may have been the source of the metals, with additions from connate fluids during ascent.

Complex lead-zinc-pyrite mineralization resulted from the reaction between the pyritic zones and the final fractions of the hydrothermal fluids.

This model may explain mineral zoning at the mine, and is consistent with temperatures of ore deposition indicated by the mineral assemblage.

During metamorphism and deformation, localized remobilization took place, and minor crosscutting veins formed.

6.2. S.E. Ireland

Crosscutting, vein-type cupriferous mineralization at Bunmahon, and the lead-zinc veins elsewhere, comprise a pulsatory metasomatic sequence closely related to deformation and plutonism.

6.3. Parys Mountain

The mineralization and geological environment at Parys Mountain is analogous to that at Avoca and a similar genetic model is put forward.

6.4. Related deposits

In the Southern Caledonides, mineralization at Coniston

is similar to that at Bunmahon.

Whole-rock analyses of pyroclastics throughout the region demonstrate the continuity of a calc-alkaline volcanic province extending from the Lake District to the Waterford coast.

The deposits at Avoca and Parys Mountain are environmentally similar to many other conformable polymetallic pyritic deposits. The relationship of these deposits to the tectonic cycle suggests that the polymetal content may derive from partial fusion of basement along a Benioff zone, with additions from connate fluids.

6.5. Implications

1) This study of mineralization in regionally metamorphosed terrain emphasizes the necessity to consider the whole geological environment. This enables deduction of the depositional environment and the milieu of syngenetic ore formation.

2) Different types of mineralization in close proximity to each other may have a separate genesis in folded rocks.

3) Mineral and metal zoning is important on all scales, providing patterns which are often related to genesis and thus may be an exploration tool.

4) The genetic model implies that polymetallic pyritic deposits are closely related to volcanic lineaments in eugeo-synclines, and their formation may be dependent upon crustal contamination in the magma source.

APPENDIX 1

Whole-rock x-ray fluorescence analytical method,
using close standardization

A series of eight representative samples from among the rocks were used as standards and analysed by both wet chemical and x-ray techniques. A series of international standards were also analysed by x-ray fluorescence as a check on the precision of the data. Element values were read from working curves using the standards.

(a) Standards (Wet chemical)

Major elements were determined using rapid methods (202). Silica was determined by a combined gravimetric-colorimetric method (122). The ammonium meta-vanadate method (253) was applied for ferrous iron and alumina was deduced by the classical difference method.

(b) Samples and Standards (X-ray fluorescence).

1.5 gm powder (-325 mesh) was compressed into a disc backed with 2 gm terephthalic acid using a method similar to that of Norrish and Chappell (165), and an 'infinitely thick' sample produced. Samples and standards were scanned on a Philips PW 1540 x-ray spectrograph using the operating conditions in table 42. Peak and background counts, corrected for instrumental drift, were recorded in triplicate and working curves constructed from the standards. The precision of the analyses is of the order of $\pm 1.5\%$, and reproducibility is high.

Table 42 X-ray fluorescence operating conditions (PW1540)

Element	2θ	X-ray tube	kV	mA	Analyser Crystal	Path	Collimator	Atten.	EHT (v)	Counter	P.H.A	
											Lower Level	Window
Si	79.08	Cr	40	20	PE	Vac.	160	2	1600	Flow	100	150
Al	115.08	Cr	50	20	PE	Vac.	480	2	1660	Flow	90	170
Ti	86.18	Cr	50	20	LiF ₁₀₀	Air	160	3	1650	Flow	230	210
Fe	57.50	Cr	40	20	LiF ₁₀₀	Air	160	3	830	Scin.	70	230
Mn	62.97	Au	40	20	LiF ₂₂₀	Air	160	3	850	Scin.	140	190
Mg	106.80	Cr	50	20	ADP	Vac.	480	2	1720	Flow	90	290
Ca	113.14	Cr	50	20	LiF ₁₀₀	Vac.	160	4	1750	Flow	240	310
Na	73.38	Cr	50	20	Gyp.	Vac.	480	3	1675	Flow	40	90
K	20.70	Au	40	20	PE	Vac.	160	1	1600	Flow	470	340
P	59.50	Cr	50	20	PE	Vac.	480	2	1640	Flow	110	160
S	45.93	Cr	50	20	PE	Vac.	480	2	1580	Flow	30	170
Co	78.10	Cr	50	20	LiF ₂₂₀	Air	480	2	1700	Flow	270	280
Ni	48.78	Cr	50	20	LiF ₁₀₀	Vac.	160	3	790	Scin.	80	140
Cu	65.58	Cr	50	20	LiF ₂₂₀	Air	480	3	200	Scin.	90	240
Zn	42.00	Cr	50	20	LiF ₁₀₀	Air	480	3	800	Scin.	40	250
Rb	38.05	Cr	50	20	LiF ₂₂₀	Air	480	3	800	Scin.	150	280
Sr	35.90	Cr	50	20	LiF ₂₂₀	Air	480	3	800	Scin.	150	280
Pb	34.20	Cr	50	20	LiF ₁₀₀	Air	160	2	1550	Flow	410	250
Se	45.85	Cr	50	20	LiF ₂₂₀	Air	480	3	780	Scin.	130	220

APPENDIX 2

Description of Samples in Table 1,
from Co. Wicklow, Ireland.

F.1	Felsite	Bell Rock, 450 ft S.S.E. of Ballygahan shaft, Avoca.
F.2	"	" " , 550 ft " " " " , "
F.3	"	" " 400 ft " " " " "
F.4	"	Tigroney, 800 ft E.S.E. of Ballygahan shaft, Avoca.
F.5	"	" , 900 ft " " " " "
F.6	"	Ballygahan upper, 500 ft N.N.W. of Ballygahan House Avoca.
F.7	"	Tigroney, 1200 ft northeast of Ballygahan shaft, Avoca.
F.8	"	" , 2200 ft east of Ballygahan shaft, Avoca.
F.9	"	Kilmacoo, 1800 ft northeast of Kilmacoo cross-roads, Avoca.
F.10	"	Ballymoneen, 5600 ft southwest of Ballygahan shaft, Avoca.
F.11	"	Castle Howard, 1500 ft northeast of Lions' Bridge, Avoca.
F.12	"	Tigroney, 1400 ft east of Ballygahan shaft, Avoca.
F.13	"	" 2200 ft northeast of Ballygahan shaft, Avoca.
F.14	"	Ballinabarny North, 5200 ft northeast of Kilmacoo cross-roads, Avoca.
G.1	Tuff	Aughrim road, 3600 ft northwest of Woodenbridge, Avoca.
G.2	"	" " , 4800 ft " " " "
JH.1	Felsite	Bell Rock, Avoca (125)
FH.5	"	Aughrim road, $1\frac{1}{4}$ miles northwest of Woodenbridge (107)
FH.6	"	Kilmacrea wood, $1\frac{3}{4}$ miles northwest of Redcross (107)
FH.8	"	1 mile southeast of Ballinacor cross-roads. (107)
FH.9	"	Aughrim road, $\frac{1}{4}$ mile east of Coatsbridge. (107)
FH.10	"	" " , $\frac{1}{2}$ mile northwest of Woodenbridge (107)
HG.1	Greenstone,	Westaston (125)
HG.2	"	" (125)
H.1	Leinster granite,	mean of 12 analyses in (125)
H.3	Granite,	Ballinaclash (125)
H.4	"	, Croghan Kinshela, head of Coolbawn brook (125)
H.5	"	, " " , summit (125)

APPENDIX 3

Lines used in spectrographic analysis

Element	Wavelength Å	Host Mineral		
		Pyrite, Chalcopyrite, Magnetite, Hematite	Sphalerite	Galena
Mn	2798.27(a)	5	5	5(a)
	2933.00(b)	>2000	30	15(b)
Pb	2833.07	75	10	-
Sn	2839.99	25	30	30
As	2860.45	800	500	500
Sb	2877.92	100	200	100
Fe	2929.00	-	500	500
Ga	2945.64	60	10	10
Pt	2997.97	50	50	50
Ge	3039.06	20	10	10
In	3039.36	700	10	10
Ni	3050.82	2	10	5
Bi	3067.72	500	15	15
Au	3122.22	350	350	350
Ti	3168.52	25	-	-
	3088.02	-	10	10
Mo	3170.34	30	10	10
V	3185.00	50	10	10
Cd	3261.06	-	100	20
Cu	3273.96(a)	10	5	5(a)
	2961.16(b)	>5000	-	- (b)
Zn	3345.02	500	-	500
Ag	3382.89	2	2	2
Co	3453.51	10	25	10
Cr	4254.35	15	10	5
Hg	4358.35	>500	>500	>500
Ba	4554.02	100	100	100

(a) Line used to determine low concentrations.

(b) Line used to determine high concentrations.

APPENDIX 4

The S/Q Logging MethodIntroduction:

A system of statistical core logging, initially devised by Booth and Dujardin of Canadian Superior Exploration Ltd., has been extensively applied by the writer during the current study. At present, no description of this method is available and the following account sets out the principles and practice.

Principles:

The S/Q (sulphide/quartz) logging method can be applied in the examination of drill core from deposits in which the following criteria apply:

1. Lenticular or massive mineralization which is generally concordant with the enclosing strata.

The system makes a macroscopic, visual record of the core and is not a chemical analysis. Partial continuity of mineral seams, either horizontally or vertically, is necessary for a meaningful assessment of mineralization per unit length of core. Disseminated mineralization is unsuitable.

2. Assay limits to the ore zone

Graphs of mineral distribution allow objective assessment of ore limits, efficient completion of drill holes and elimination of hundreds of feet of superfluous drilling.

3. Drill intersections approximately normal to the strike of the ore zone.

Less core is ground and a more complete intersection is obtained under these circumstances, which results in a higher degree of correlation between mineral graphs and assay data. Chalcopyrite, in the present context the economic sulphide, is relatively soft, and is one of the first minerals lost during grinding. This factor is therefore very important.

4. Simple mineralogy

The major minerals must be easily identified, of medium to

coarse grain size, and complex intergrowths should be absent, as these complicate the result.

5. Significant time-lag between completion of drill hole and receipt of assay results

A graphical representation of the mineralization is produced by the S/Q system and this gives a more complete representation of the mineralization than a normal, highly verbose, geological log. It is more readily utilized by an engineering department during a development programme. In exploration, drill samples are often dispatched to a central analytical laboratory and considerable time may elapse before results are received on the property. The mineral distribution graphs give a quick assessment of the ore zone and allow further holes to be accurately sited.

6. A detailed log is necessary

The complete S/Q log takes somewhat longer than conventional systems to apply, and is therefore more costly, however, it provides a more complete record of the core. This is especially important when whole core is assayed (often necessary with lenticular deposits, obviating errors incurred during core splitting.)

METHOD.

Core is boxed, numbered and labelled in the usual way, either underground or on surface.

A sampling interval is chosen; at Avoca this is five feet, and any other conventional unit e.g. one metre could be similarly applied.

The complete log consists of four parts:

1. S/Q (Sulphide/Quartz) log:

A frequency record count is made of the major units of the mineralization. At Avoca these were: barren quartz, Q_0 ; quartz with minor disseminated chalcopyrite, Q_1 ; quartz with major disseminated chalcopyrite, Q_2 ; pyrite alone, P_0 ; pyrite with minor chalcopyrite, P_1 ; pyrite with major chalcopyrite, P_2 ; disseminated chalcopyrite, C_0 ; and massive chalcopyrite C_1 .

Minor, disseminated or banded galena and sphalerite were included under 'others', together with carbonate and supergene minerals. The economic copper mineralization is highlighted by this procedure which can obviously be adapted to suit other parageneses.

During logging, the core is considered inch by inch, and each occurrence of Q_0 , Q_1 , Q_2 , P_0 , P_2 , C_0 and C_1 measured in inches parallel to the core is noted with its position. To speed plotting, the totals for each type may be visually summed within the sampling lengths, but this does not give a precise location to each mineralized lenticle. This may be of importance and the value of the log is consequently reduced. Minor disseminated material can be visually summed to give a total count.

Geological features are also noted, in a remarks column. The proforma used in the field note-book is shown below:

Footage	Q_0	Q_1	Q_2	P_0	P_1	P_2	C_0	C_1	Others	Geological Remarks
1.5										
6.3										
9.2										
etc.										

A summary S/Q log is next prepared in the office with values totalized over the sampling lengths using the proforma below:

Footage	Q_0	Q_1	Q_2	ΣQ	P_0	P_1	P_2	ΣP	Q_2+P_2	C_0	C_1	Others
0-5												
5-10												
etc.												

Values of Q_0 , Q_1 , P_0 and P_1 ≤ 0.4 inch over a sample interval at Avoca are inconsequential, and therefore neglected in the summary (they remain in the field note-book for reference). All values of Q_2 , P_2 , C_0 and C_1 ≥ 0.1 inch are plotted, as they contain measurable and significant quantities of copper, which in this case is the diagnostic element. Values of minor constituents are all noted.

A graph is then constructed of the summary S/Q data showing the values of the important units: Q_2 , P_2 , C_0 and C_1 for each drill hole. Representative graphs are shown in Fig. A.1.

$Q_0 + Q_1$ and $P_0 + P_1$ are also geologically important as they indicate the intensity of the mineralization and combined with the plotted units may illustrate mineralogical trends along or across the strike of the ore zones (Maps 6 and 7).

The S/Q data and graph are kept abreast of drilling and an objective visual estimate of the progress of the hole through the ore zone, and a guide to grade can be obtained. Where no prominent lithological marker exists at the ore limits, as soon as the intensity of mineralization falls below a base level, on the graph determined through previous experience, the drill hole may be confidently stopped and drilling efficiency increased.

Graphs shown in Fig. A.1, A and B, show cuts through typical South and Pond orebody material. The correspondence between the S/Q graphs and the later assay returns is noteworthy. Absolute values vary between individual geologists carrying out logging, but the form of the graph has a consistent relation to the assay value.

2. Summary geological log

This is a concise form of a normal log. At Avoca, lithological divisions form the main rock units. The need to describe the mineralization in detail is no longer necessary as the S/Q data contains this information. The general nature of the mineralization is described together with salient structural, sedimentological etc., notes. (The original geological remarks from the S/Q log are useful in this respect, but the core is usually quickly re-examined.)

3. Data Sheet

The data sheet illustrates pertinent engineering data; dates drilled, bearing of the hole, co-ordinates of the collar, name of geologist, etc.

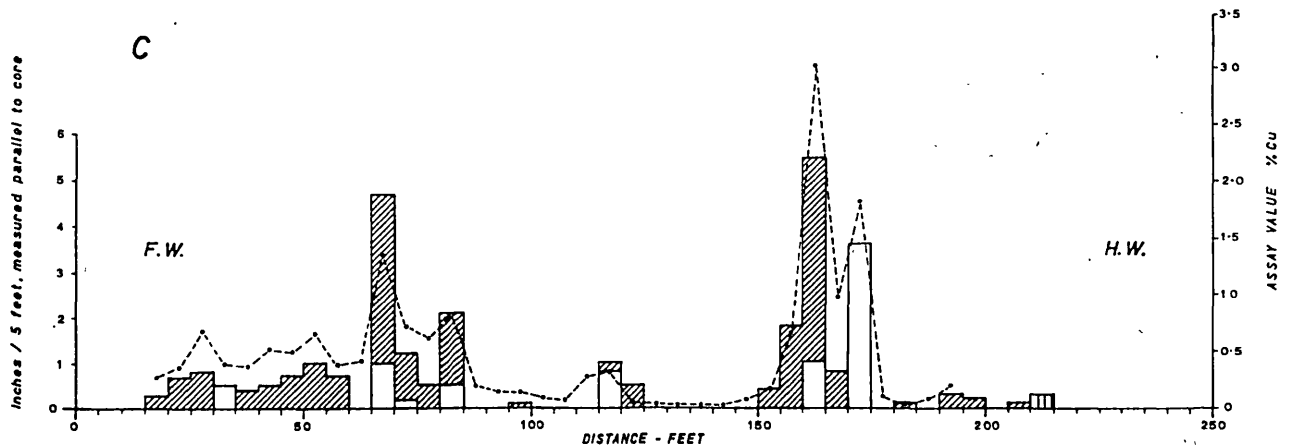
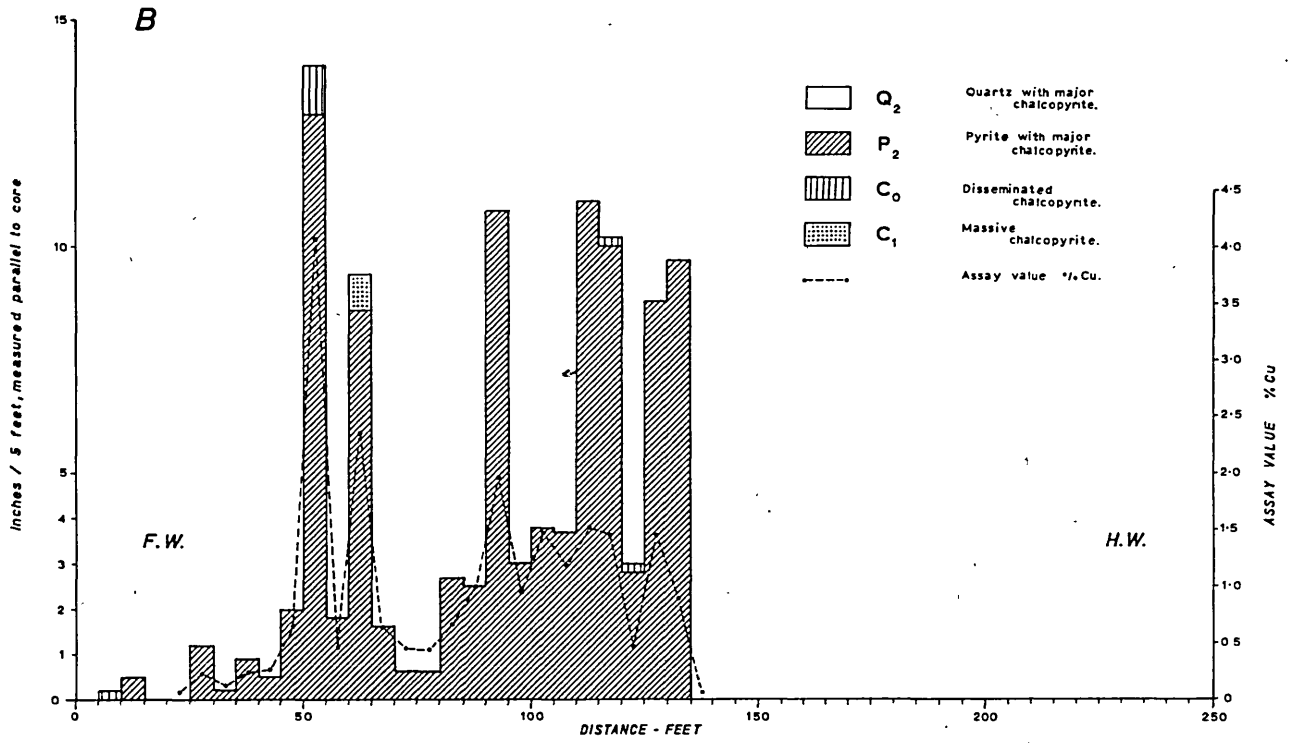
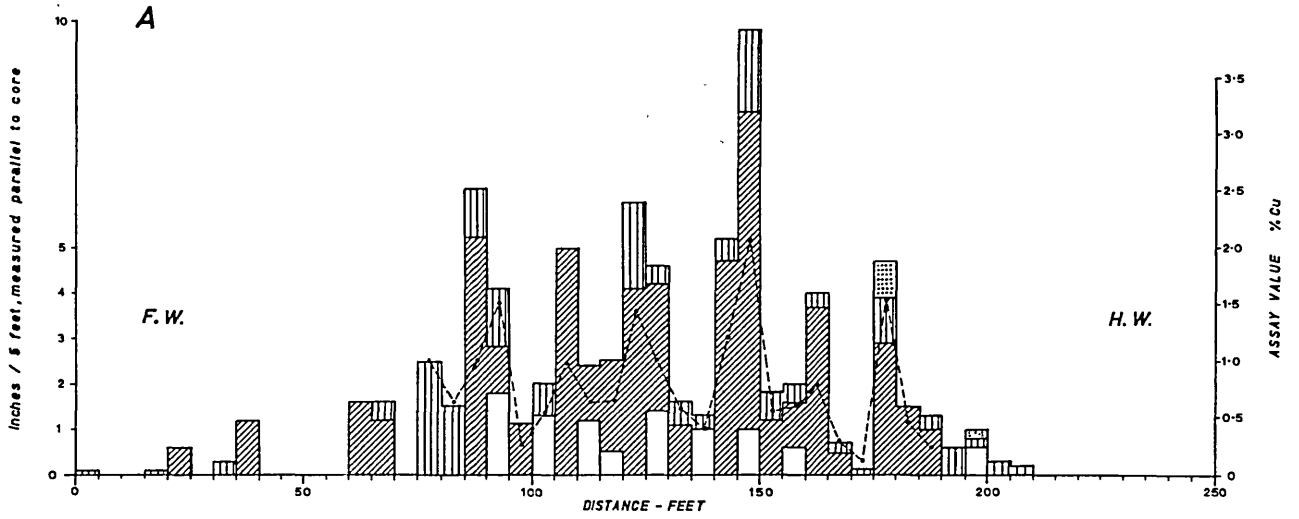
4. Assay values

These are tabulated in the normal manner and contrasted with the S/Q data on the final graph (Fig. A1.).

FIG A.1

WEST AVOCA MINERAL DISTRIBUTION GRAPHS

OF S/Q LOG DATA WITH BANDS COMBINED OVER FIVE FEET SAMPLING INTERVAL.



REFERENCES

1. Ahrens L.H. and Taylor S.R. Spectrochemical analysis 2nd ed. (London, etc.: Pergamon, 1961) 454p.
2. Albee A.L. Relationships between the mineral association, chemical composition and physical properties of the chlorite series. *Am. Miner.* 47, 1962, 851-70.
3. Anderson C.A. Massive sulfide deposits and volcanism, *Econ. Geol.* 64, 1969, 129-46.
4. Anderson E.M. The dynamics of faulting. (Edinburgh : Oliver and Boyd, 1951) 206 p.
5. Anger G. et al. Sulfur isotopes in the Rammelsberg ore deposit (Germany). *Econ. Geol.* 61, 1966, 511-36.
6. Angus N.S. and Brindley J.C. A swarm of Caledonian dolerite intrusions in the Tallaght Hills, Co. Dublin. *Proc. R.Ir. Acad.* 69B, 1970, 165-78.
7. Argall P.H. Notes on the ancient and recent mining operations in East Ovoca district. *J.R.geol. Soc. Ireland*, 5, 1879, 150-64.
8. Arnold R.G. Equilibrium relations between pyrrhotite and pyrite from 325 to 743°C. *Econ. Geol.* 57, 1962. 72-90.
9. Arnold R.G. Pyrrhotite phase relations below $304 \pm 6^\circ\text{C}$ <1 Atm. total pressure. *Econ.Geol.* 64, 1969, 405-19.
10. Auger P.E. Zoning and district variations of the minor elements in pyrite of Canadian gold deposits. *Econ.Geol.* 36, 1941, 401-23.
11. Baas-Becking L.G.M., Kaplan I.R. and Moore D. Limits of the natural environment in terms of pH and oxidation-reduction potentials. *J.Geol.* 68, 1960, 243-84.
12. Baker J.W. The petrology of the Carnsore granite intrusion, Co. Wexford. *Proc.R.Ir. Acad.* 67B, 1968, 159-76.
13. Baker J.W. Correlation problems of metamorphosed Pre-Cambrian rocks in Wales and S.E. Ireland. *Geol.Mag.* 106, 1969, 249-59.
14. Barnes H.L. and Czamanske G.K. Solubilities and transport of ore minerals. In; *Geochemistry of Hydrothermal Ore deposits*, Barnes H.L. (ed) (New York: Holt, Rinehart and Winston, 1967) 334-78.

15. Barton P.B. Thermochemical study of the system Fe-As-S. *Geochim. Cosmochim. Acta*, 33, 1969, 841-57.
16. Barton P.B., Bethke P.M. and Toulmin P. Equilibrium in ore deposits. *Mineral.Soc,Am.,Spec.Paper No.1*, 1963, 171-85.
17. Barton P.B. and Skinner B.J. Sulphide mineral stabilities. In, *Geochemistry of hydrothermal ore deposits*, Barnes H.L. ed. (New York etc. : Holt, Rinehart and Winston 1967), 236-333.
18. Barton P.B. and Toulmin P. Phase relations involving sphalerite in the system Fe-Zn-S. *Econ.Geol.*, 61, 1966, 815-849.
19. Bateman A.M. *Economic mineral deposits: 2nd.ed.*, (New York, etc.: Wiley 1950) 916p.
20. Bates D.E.B. *The Lower Palaeozoic rocks of Anglesey. Ph.D. thesis, University of Belfast, 1964.*
21. Beavon R.V. et al. Nomenclature and diagnostic characters of ignimbrites with reference to Snowdonia. *Lpool Mancr geol.J.*, 2, 1961, 600-11.
22. Berg G. and Friedensberg F. *Nickel und Kobalt. Die Metallischen Rohstoffe, ihre Lagerungsverhältnisse und ihre wirtschaftliche. Bedeutung.* (Stuttgart:Enke, 1944) 280p.
23. Bergenfelt S. Om forekimsten av selen i skeleftefallets sulfidmalmer. *Geol.Forens.Forhandl.* 75, 1953, 327-59.
24. Berner R.A. Iron, in *Handbook of Geochemistry.* Wedepohl K.H. ed. (Berlin, etc.: Springer-Verlag 1969) 26-G, 1-8.
25. Berry L.G. and Thompson R.M. X-ray powder data for ore minerals. *Geol. Soc. Am.; Mem.85*, 1962, 281p.
26. Bichan W.J. The origins of the massive sulphides. *Can.Min.J.* 1960, 73-78.
27. Bilibin Yu.A. *Metallogenetic provinces and epochs.* Ges-geoltekhizdat, Moscow. Translated by Canadian Geological Survey, 1955.
28. Billings M.P. *Structural geology.* (New Jersey : Prentice-Hall, 1954) 514p.

29. Bischoff J.L. Red Sea geothermal brine deposits, their mineralogy, chemistry and genesis. In Hot brines and recent heavy metal deposits in the Red Sea, Degens E.T. and Ross D.A. (eds)(New York etc.: Springer-Verlag, 1969) 368-401.
30. Bishopp D.W. et al. The geology of Eastern Ireland II : the geology of the Dublin district. 18th. Int. Geol.Cong.London, 1948,35p.
31. Blundell D.J. et al. Sedimentary basin in the south Irish Sea. Nature,219, 1968, 55-56.
32. Boorman R.S. Subsolidus studies in the ZnS-FeS-FeS₂ system. Econ.Geol., 62, 1967, 614-31.
33. Borchert H. Uber entmischungen in system Cu-Fe-S und ihre bedeutung als "geologische thermometer". Chem. der Erde, 9, 1934, 145-72.
34. Boyle R.W. On the colour of black and grey quartz from Yellowknife, Northwest Territories, Canada. Am.Miner. 38, 1953, 528-35.
35. Boyle R.W. Geology, geochemistry and origin of the lead-zinc-silver deposits of the Keno Hill-Galena Hill area, Yukon Territory. Geol. Surv.Canada Bull. 111, 1965, 302p.
36. Boyle R.W. and Jambor J.L. The geochemistry and geothermometry of sphalerite in the lead-zinc-silver lodes of the Keno Hill-Galena Hill area, Yukon. Can.Miner. 7, 1963, 479-96.
37. Bray J.M. Spectroscopic distribution of minor elements in igneous rocks from Jamestown, Colorado. Bull.geol.Soc.Am. 53, 1942, 765-814.
38. Brenchley P.J. and Treagus J.E. The stratigraphy and structure of the Ordovician rocks between Courtown and Kilmichael point, Co.Wexford. Proc.R.Ir.Acad. 69B, 1970, 83-102.
39. Brett F.R. Experimental data from the Cu-Fe-S system and their bearing on exsolution textures in ores. Econ.Geol., 59, 1964, 1241-69.
40. Brindley J.C. Caledonian and Pre-Cambrian intrusive rocks of Ireland. In North Atlantic-Geology and Continental Drift, Kay M.(Ed.), Mem.12.An. Assoc.Petrol.Geol. 1969, 336-53.
41. Brindley J.C. Appinitic intrusions associated with the Leinster granite, Ireland. Proc.R.Ir.Acad. 70B, 1970, 93-104.

42. Buerger N.W. The unmixing of chalcopyrite from sphalerite. *Am.Miner.* 19, 1934, 37-61.
43. Burnham C.W. Metallogenic provinces of the southwestern U.S. and northern Mexico. *New Mexico Bur. Mines Bull.* 65, 1959, 76p.
44. Burnham C.W. Hydrothermal fluids at the magmatic stage. In *Geochemistry of hydrothermal ore deposits.* Barnes H.L. (ed)(New York etc.: Holt, Rinehart and Winston 1967), 34-76.
45. Burns R.G. Mineralogical applications of crystal field theory. (Cambridge: Cambridge Univ.Press, 1970)222p.
46. Butler J.R. Private report to St.Patrick's Copper Mines Ltd. 1961.
47. Bystron A. Monoclinic magnetic pyrites. *Arkiv.Kemi. Min.Geol.* 19, 1945, 1-8.
48. Cambel B. and Jarkovsky J. The possibility of using the nickel and cobalt in pyrites as indicators of ore genesis. *Geol.sbornik*, XVII, 1966, 17-34.
49. Cambel B. and Jarkovsky J. On the character of the distribution of manganese, vanadium, molybdenum and titanium in pyrites. *Geol.sbornik* 18, 1967, 11-25.
50. Cambel B. and Jarkovsky J. Geochemie der Pyrite einiger Lagerstätten der Tschechoslowakei (Bratislava: Slovenska Akademia Vied, 1967) 493p.
51. Carmichael I.S.E. The petrology of Thingmuli, a Tertiary volcano in Eastern Iceland. *J.Petrol.* 5, 1964, 435-60.
52. Carstens C.W. Zur Geochemie einiger norwegischen Kivsvorkommen. *Kgl. Norsk.Vidensk.Selskab Forh.* 14, 1941, 36.
53. Carstens C.W. Über den Co-Ni-Gehalt norwegischer Schwefelkiesvorkommen. *Kgl.Norske.Vidensk. Selskab Forh.* 15, 1943, 165-68
54. Chernyshev L.V. and Anfilogov V.N. Subsolidus phase relations in the ZnS-FeS-FeS₂ system. *Econ. Geol.* 63, 1968, 841-43.
55. Chinnery M.A. Secondary faulting. *Can.J.Earth Sci.* 3, 1966, 163-90.

56. Clark L.A. The Fe-As-S system; phase relations and application. *Econ.Geol.* 55, 1960, 1345-81 and 1631-52
57. Clark L.A. The Fe-As-S system. *Carnegie Inst.Wash. Yearbook* 59, 1960, 127-30.
58. Cole G.A.J. Memoir and map of localities of minerals of economic importance and metalliferous mines in Ireland. *Mem.geol.Surv.Ireland.* (Dublin : The Stationery Office, 1922) 154p.
59. Coleman R.G. and Delevaux M. Occurrence of selenium in sulfides from some sedimentary rocks of the western United States.*Econ.Geol.* 52, 1957, 499-527.
60. Conolly H.J.C. A contour method of revealing some ore structures. *Econ.Geol.* 31, 1936, 259-71.
61. Crines T.P. and Crossley J.C. The stratigraphy, sedimentology, ichnology and structure of the Lower Palaeozoic rocks of part of northeastern Co. Wexford. *Proc.R.Ir.Acad.* 67B, 1968, 185-215.
62. Croxford N.J.W. Origin and significance of volcanic potash-rich rocks from Mount Isa. *Trans. Instn.Min.Metall.* 74, 1964, 33-43.
63. Croxford N.J.W. Discussion in *Proc. CSIRO Symp. on Iron Sulphides*, CSIRO Division of Min.Chemistry Investig.Rpt. 305R, 1969, p.33.
64. Curtis C.D. Applications of the crystal-field theory to the inclusion of trace transition elements in minerals during magmatic differentiation. *Geochim.Cosmochim.Acta* 28, 1964, 389-402.
65. Curtis C.D. and Spears D.A. The formation of sedimentary iron minerals. *Econ.Geol.* 63, 1968, 257-70.
66. Davidson C.F. On the cobalt : nickel ratio in ore deposits. *Mining Mag.*, 106, 1962, 78-85.
67. Deer W.A., Howie R.A. and Zussman J. *Rock-Forming Minerals Vols 1-5.* (London: Longmans, 1962).
68. Desborough G.A. and Carpenter R.H. Phase relations of pyrrhotite. *Econ.Geol.* 60, 1965, 1431-50.
69. Desborough G.A. and Sainsbury C.L. Cassiterite as an exsolution product in magnetite, Lost River Tin Mine, Alaska. *Econ.Geol.* 65, 1970, 1004-05.

70. Dewey H. and Eastwood T. Copper ores of the Midlands, Wales, the Lake District and the Isle of Man. *Mem.geol.Surv.Gt.Brit.Min.Res.* 30, 1925, 87p.
71. Dewey J.F. Structure and sequence in Paratectonic British Caledonides. In *North Atlantic-Geology and continental Drift*, Kay M.(ed.). Mem.12, *Am.Assoc.Petrol.Geol.* 1969, 309-35.
72. Dewey J.F. and Bird J.M. Plate tectonics and geosynclines. *Tectonophysics*, 10, 1970, 625-38.
73. Downie C. and Tremlett W.E. Micropalaeontological evidence on the age of the Clara Group (Southeast Ireland) *Geol.Mag.* 105, 1968, 401.
74. Drummond A.D., Trotter J., Thompson R.M. and Gower J.A. Neyite, a new sulphosalt from Alice Arm, British Columbia. *Can.Miner.* 10, 1969, 90-96.
75. Du Hoyer G.V. Explanatory memoir to accompany sheets 167, 168, 178, and 179. *Mem.Geol.Surv. Ireland (Dublin 1865)* 94p.
76. Dunham K.C. Epigenetic mineralisation in Yorkshire. *Proc.Yorks.Geol.Soc.* 32, 1-29.
77. Eastwood T. The Lake District mining field, in the future of non-ferrous mining in Great Britain and Ireland (London :Institution of Mining and Metallurgy, 1959) 149-74.
78. Edwards A.B. and Carlos G.C. The selenium content of some Australian sulphide deposits. *Proc.Aust. Inst.Min.Met.*, No.172, 1954, 31-64.
79. Einaudi M.T. Sphalerite-pyrrhotite-pyrite equilibria-a re-evaluation. *Econ-Geol.* 63, 1968, 832-34.
80. Einaudi M.T. Copper zoning in pyrite from Cerro de Pasco Peru. *Am.Miner.* 53, 1968, 1748-52.
81. Elder J.W. Physical processes in geothermal areas. In *Terrestrial heat flow. Monogr.Am.Geophys. Union No.8*, 1965, 211-39.
82. Ellis A.J. Present-day hydrothermal systems and mineral deposition. In *Mining and Petroleum geology (London : Institution of Mining and Metallurgy, 1970)* 211-40 (Proc. 9th. Commonw.Min.Metall. Congr. 1969, vol.2)
83. El Shazly E.M., Webb J.S. and Williams D. Trace elements in sphalerite, galena and associated minerals from the British Isles. *Trans. Instn.Min.Metal.* 66, 1957, 241-271.

84. Finlayson A.M. The metallogeny of the British Isles. Q.J. geol.Soc.Lond. 66, 1910, 281-98
85. Fiske R.S. Subaqueous pyroclastic flows in the Ohanapecosh Formation, Washington. Bull. Geol. Soc. Am. 74, 1963, 391-406.
86. Fitton J.G. and Hughes D.J. Volcanism and plate tectonics in the British Ordovician. Earth Plan. Sci. Lett. 8, 1970, 223-28.
87. Fleischer M. Minor elements in some sulfide minerals. Econ. Geol. 50th Anniv. Vol, 1955, 970-1024.
88. Garrels R.M. and Christ C.L. Solutions, minerals and equilibria. (New York: Harper and Row, 1965) 450p.
89. Gavelin S. and Gabrielson O. Spectrochemical investigations of sulphide minerals from the ores of the Skelleftea district. Sveriges Geol. Undersoka 41, 1947, 1-45.
90. Gay H.C. The composition of gold from the Barberton mountain land. Trans. geol. Soc. S. Afr. Vol. 71, 1968, 273-89.
91. Gilbey J.W.G. The mineralogy, paragenesis and structure of the ores of the Dolgellau gold belt, Merionethshire, and associated wallrock alteration. Ph.D. thesis, University of London 1968.
92. Goldschmidt V.M. and Hefter O. Zur Geochemie der Selen Nacr. Ges. Wiss. Gottingen, 2, 1933, 245-52.
93. Goldschmidt V.M. and Strock L. Zur Geochemie der Selen. II. Nacr. Ges. Wiss. Gottingen, 1, 1935, 123-42.
94. Goldschmidt V.M. The principles of distribution of chemical elements in minerals and rocks. J. Chem. Soc., 1937, 655-72.
95. Goldschmidt V.M. Crystal chemistry and geochemistry. Chem. Prod., 7, 1944, 29-34.
96. Goldschmidt V.M. Geochemistry. (London: Oxford Univ. Press, 1954) 720p.
97. Gordon-Smith J. Private reports to St. Patrick's Copper Mines Ltd. 1961-1962.
98. Graf J.L. (Jr) and Skinner B.J. Strength and deformation of pyrite and pyrrhotite. Econ. Geol. 65, 1970, 206-15.
99. Grantham D.R. The petrology of the Shap Granite. Proc. Geol. Assoc. 39, 1928, 299-331.

100. Greenly E. The geology of Anglesey. *Mem.geol.Surv. Gt.Brit.*, 2 vols. 1919, 980p.
101. Groves D.I. and Loftus-Hills G. Cadmium in Tasmanian sphalerites. *Proc.Aust.Inst.Min.Met.*, No.228, 1968, 43-51.
102. Hall A. Regional variation in the composition of British Caledonian granites. *Jour.Geology*, 77, 1969, 466-81.
103. Hamaguchi H. and Kuroda R. In, *Handbook of Geochemistry*. Wedepohl K.H. (ed.)(Berlin, etc.: Springer-Verlag, 1969) 50D, 1-7.
104. Harper C.T. Potassium-Argon ages of slates from the Southern Caledonides of the British Isles. *Nature*, 212, 1966, 1339-41.
105. Harris D.C., Jambor J.L., Lachance G.R. and Thorpe R.I. Tintinaite, the antimony analogue of Kobellite. *Can.Mineral.* 9, 1968, 371-82.
106. Hatch F.H. Notes on the Wicklow greenstones. *Geol.Mag.* 6, 1889, 261-65.
107. Hatch F.H. On the Lower Silurian felsites of the southeast of Ireland. *Geol.Mag.* 6, 1889, 545-549.
108. Haughton S.F. *The Mines of Wicklow* (London : C.H.Law, 1856).
109. Hawkins T.R.W. Boreholes at Parys Mountain, near Amlwch, Anglesey. *Bull.geol.Surv.Gt.Brit.* 24, 1966, 7-17
110. Hawley J.E. and Nichol I. Selenium in some Canadian sulfides. *Econ.Geol.* 54, 1959, 608-28.
111. Hawley J.E. and Nichol I. Trace elements in pyrite, pyrrhotite and chalcopyrite of different ores. *Econ.Geol.* 56, 1961, 467-87.
112. Hegemann F. Die geochemische Bedeutung von Kobalt und Nickel im Pyrit. *Zeitschr. f. angew. Mineral.* 4, 1943, 121-239.
113. Holgeson R.C. Complexing and hydrothermal ore deposition. (New York etc.: Pergamon, 1964), 128p.
114. Hey M.H. A new review of the chlorites. *Mineral Mag.* 30, 1954, 277-92.
115. Holland H.D. Some applications of thermochemical data to problems of ore deposits. *Econ.Geol.* 60, 1965, 1101-66.

116. Horikoshi Ei. Volcanic activity related to the formation of the Kuroko-type deposits in the Kosaka district, Japan. *Mineral.Deposita*, 4, 1969, 321-45.
117. Hull E., Cruise R.J. and Hatch F.H. Explanatory memoir to accompany sheets 138 and 139. *Men.geol. Surv.Ireland.*(Dublin: Stationery Office, 1888) 59p.
118. Ivanov V.V. Distribution of cadmium in ore deposits. *Geochemistry*. 4, 1964, 757-68.
119. James C.H. A review of the geochemistry of mercury (excluding analytical aspects) and its application to geochemical prospecting. *Tech.Comm. Imp.Coll.Sci.Tech.Geochem. Prosp.Res.Centre no.41*, 1962, 42p.
120. James C.H. and Webb J.S. Sensitive mercury vapour meter for use in geochemical prospecting. *Trans. Instn.Min.Metall.* 73, 1964, 633-41.
121. James H.L. Chemistry of the iron-rich sedimentary rocks. In *Data of Geochemistry*, 6th edn. *Prof.Pap.U.S. geol.Surv.* 440-W, 1963, 60p.
122. Jeffrey J.L. and Wilson A.D. A combined gravimetric and photometric procedure for determining silica in silicate rocks and minerals. *Analyst, Lond.* 85, 1960, 478-86.
123. Jensen M.L. Sulfur isotopes and mineral genesis. In *Geochemistry of Hydrothermal ore deposits*, Barnes H.L.(ed.)(New York etc.; Holt, Rinehart and Winston, 1967), 143-65.
124. Jones W.R. The mining district of Avoca, Co. Wicklow. *Private Rpt. to Mianrai Teoranta.* 1947.
125. Jukes J.B. and Haughton S. On the Lower Palaeozoic rocks of the south-east of Ireland and their associated igneous rocks. *Trans.R.Ir.Acad.* 23, 1859, 564-621.
126. Jukes J.B. and Du Noyer G.V. Explanations to accompany sheets 121 and 130. *Men.Geol.Surv.Ireland.* (Dublin: Stationery Office, 1859) 49p.
127. Kalliokoski J. and Cathles L. Morphology, mode of formation and diagenetic changes in framboids. *Bull.Geol.Soc.Finland.* 41, 1968, 125-33.

128. Kaplan I.R., Sweeney R.E. and Nissenbaum A. Sulfur isotope studies on Red Sea geothermal brines and sediments. In Hot brines and recent heavy metal deposits in the Red Sea. Degens E.T. and Ross D.A. (eds.) (New York, etc.: Springer-Verlag, 1969) 474-98.
129. Kelly W.C. and Turneure F.S. Mineralogy, paragenesis and geothermometry of the tin and tungsten deposits of the Eastern Andes, Bolivia. *Econ. Geol.* 65, 1970, 609-80.
130. Kinahan G.H. A manual of the geology of Ireland. (London : Keagan Paul, 1878) 444p.
131. Kinahan G.H. Economic geology of Ireland. *J.R.geol.Soc. Ireland*, 18, 1889, 1-122.
132. Kinkel A.R. Jr. Massive pyritic deposits related to volcanism and possible methods of emplacement. *Econ.Geol.* 61, 1966, 673-94.
133. Krauskopf K.B. Introduction to geochemistry. (New York, etc.: McGraw-Hill 1967) 721p.
134. Kullerud G. The FeS-ZnS system, a geological thermometer. *Norsk.Geol.Tidsskr.* 32, 1953, 61-147.
135. Kulp J.L. et al. Potassium-argon and rubidium-strontium ages of some granites of Britain and Eire, *Nature*, 185, 1960, 495-497.
136. Kuno H. Lateral variation in basalt magma type across continental margins and island arcs. *Can.Geol. Surv. Paper* 66-15, 1966, 317-336.
137. Lacy E.D. Melts of granitic composition, their structure, properties and behaviour. *Rpt.Internat.Geol. Cong.Norden*, 14, 1960, 7-15.
138. Lampard W.J. Mineralization at West Avoca Co.Wicklow, Ireland. Ph.D. thesis, University of London, 1960, 272p.
139. Lindgren W. Mineral deposits : 4th ed. (New York, etc.: McGraw-Hill 1933) 930p.
140. Loftus-Hills G. and Solomon M. Cobalt, nickel and selenium in sulphides as indicators of ore genesis. *Mineral.Deposita*, 2, 1967, 228-42.
141. Loftus-Hills G., Groves D.I. and Solomon M. The Selenium content of some Tasmanian sulphides. *Proc. Aust.Inst.Min.Met.*, No.232. 1969, 55-65.

142. Loginov V.P. Genetic relation between sulfur-sulfide and typical pyrite deposits. Dokl.Akad.Nauk. SSSR., 189, 1969, 601-4 (Eng.Transl.)
143. Love L.G. and Amstutz G.C. Review of microscopic pyrite from Devonian Chattanooga Shale and Rammelsberg Bandertz. Fortschr.Mineral. 43, 1966, 273-309.
144. Lusk J. Base metal zoning in the Heath Steele B-1 orebody, New Brunswick, Canada. Econ.Geol., 64, 1969, 509-18.
145. Mackay H.S. Private reports to Electrolytic Copper Company at Avoca. 1917-20.
146. McDonald J.A. Some effects of deformation on sulfide-rich layers in lead-zinc ore bodies, Mount Isa, Queensland. Econ.Geol. 65, 1970, 273-98.
147. Manning P.G. Absorption spectra of Fe(III) in octahedral sites in sphalerite Can.Mineral. 9, 1967, 57-64.
148. Manning W. The Parys and Mona mines in Anglesey. In The future of non-ferrous mining in Great Britain and Ireland. (London:Institution of Mining and Metallurgy, 1959) 313-28.
149. Markham N.L. Some genetic aspects of the Mt. Lyell mineralisation. Mineral.Deposita, 3, 1968, 199-221.
150. Harno V. On the use of ore minerals in the interpretation of the stage of metamorphism within the amphibolite and saussurite facies. Norsk.Geol.Tidsskr., 32, 1953, 156-61.
151. Meyer C. and Hemley J.J. Wallrock alteration. In Geochemistry of Hydrothermal ore deposits, Barnes H.L. (ed.)(New York, etc.: Holt, Rinehart and Winston, 1967), 166-235.
152. Millman A.P. Ore microscopy data tables of reflectivity and microhardness. In Mineral exploitation and economic geology, Proc. Intercoll.Colloq. Cardiff, 1970, 64p.
153. Mitchell G.H. The Borrowdale Volcanic Series of Coniston, Lancashire.Q.J.geol.Soc.Lond., 96, 1940, 301-19.
154. Mitchell G.H. The geological history of the Lake District. Proc.Yorks.Geol.Soc., 30, 1956, 407-63.
155. Mitchell G.H. The Borrowdale volcanic rocks of the Seathwaite Fells, Lancashire. Lpool.Manchr. geol.J. 3, 1963, 289-300.

156. Mitchell G.H. The Lake District. Geol. Assoc. Guide No. 2., 1970, 42p.
157. Moorbath S. Lead isotope abundance studies on mineral occurrences in the British Isles and their geological significance. Phil. Trans. R. Soc., 254A, 1962, 295-360.
158. Murphy G.J. The Avoca enterprise 2. The geology of the mineralised area. Min. Q. Eng. 25, 1959, 330-38
159. Nickel E.H. The application of ligand field concepts to an understanding of the structural stabilities and solid solution limits of sulphides and related minerals. Chem. Geol. 5, 1970, 233-42.
160. Nicolaou M. and Hakli T.A. The presence of aikinite in the Aberdeen area of the Kirki mine, Western Thrace, Greece. Bull. Geol. Soc. Finland. 42, 1970, 53-55.
161. Willson C.A. Wallrock alteration at the Bolicea deposit, Sweden. Econ. Geol. 63, 1968, 472-94.
162. Nockolds S.R. Average chemical composition of some igneous rocks. Bull. geol. Soc. Am. 65, 1954, 1007-32.
163. Noddack I and Noddack W. Die geochemie des Rheniums. Z. physik. Chem., A, 154, 1931, 207.
164. Noddack I. and Noddack W. Die geochemischen Verteilungskoeffizienten der Elemente. Svensk Kem. Tid. 46, 1934, 173.
165. Norrish K. and Chappell B. X-ray fluorescence spectrography. In Physical Methods in determinative mineralogy. Zussman J. (ed) (London, etc.: Academic Press, 1967) 161-214.
166. O'Brien M.V. Private report to Mianrai Teoranta. 1951.
167. O'Brien M.V. The future of non-ferrous mining in Ireland, in the future of non-ferrous mining in Great Britain and Ireland (London: Institution of Mining and Metallurgy, 1959) 5-26.
168. Odman O.H. Geology and ores of the Boliden deposit, Sweden. Svergeol. Unders. ser. C., no. 438, 1941, 190p.
169. Odman O.H. Report on a microscopic examination of rocks and ores from the Avoca mines. Priv. Rpt. to Mianrai Teoranta, 1946, 11p.

170. Orville P.M. Alkali ion exchange between vapour and feldspar phases. *An.J.Sci.*261, 1963, 201-237.
171. Oversby V.M. The isotopic composition of lead in iron meteorites. *Geochim.Cosmochim.Acta*, 34, 1970, 64-75.
172. Palache C., Berman H. and Frondel C. The system of mineralogy. Vols 1 and 2, 7th ed. (New York etc.: Wiley).
173. Patterson J.M. Geology and mineralization of the Keel area Co. Longford, Republic of Ireland. Ph.D. thesis, University of London, 1970. 274p.
174. Pereira J. Further reflections on ore genesis and exploration. *Min.Mag.Lond.* 109, 1963, 265-80.
175. Phillips J.A. In, Occurrence of soda-felsites (keratophyres) in Ireland. *Geol.Mag.* 6, 188g, 288.
176. Pockley R.P.C. Lead isotope and age studies of uranium and lead from the British Isles and France. D.Phil. thesis, University of Oxford, 1961.
177. Price N.J. Fault and joint development in brittle and semi-brittle rock. (New York, etc. : Pergamon 1966) 176p.
178. Price N.J. Laws of rock behaviour in the Earth's Crust 1970 (in press).
179. Ramdohr F. The ore minerals and their intergrowths. (Oxford.: Pergamon 1969) 1174p.
180. Ramsay J.G. Folding and fracturing of rocks. (New York, etc.: McGraw-Hill, 1967) 568p.
181. Rankama K. and Sahama Th.G. Geochemistry. (Chicago: Univ.of Chicago Press, 1950) 912p.
182. Read R.A. Deformation and metamorphism of the San Dionisio pyritic orebody, Riotinto, Spain. Ph.D. thesis, University of London, 1967.
183. Reed F.R.C. The Lower Palaeozoic bedded rocks of County Waterford. *Q.J.geol.Soc.Lond.* 55, 1899, 718-73.
184. Reed F.R.C. The igneous rocks of the coast of County Waterford. *Q.J.geol.Soc.Lond.* 56, 1900, 657-92.
185. Rhoden H.N. Structure and economic mineralization of the Silvermines District, County Tipperary, Eirc. *Trans.Instn.Min.Metall.* 1958, 67-94.

186. Rickard D.T. The chemistry of iron sulphide formation at low temperatures. *Stockholm Contr.in Geol.*, 20, 1969, 67-95.
187. Rickard D.T. The origin of framboids. *Lithos*, 3, 1970, 269-93.
188. Robertson E.C. Experimental study of the strength of rocks. *Bull.Geol.Soc.Am.* 66, 1955, 1275-1314.
189. Roedder E. Studies of primary fluid inclusions in sphalerite crystals from the OH vein, Creede, Colorado (abs.) *Econ.Geol.*, 55, 1960, 1337.
190. Roedder E. Fluid inclusions as samples of ore fluids. In *Geochemistry of Hydrothermal Ore deposits*, Barnes H.L.(ed.)(New York etc., : Holt, Rinehart and Winston, 1967), 515-74.
191. Roscoe S.M. Geochemical and isotopic studies, Noranda and Matagami Areas, *Can.Min.Met.Bull.* 58, 1965, 467-87.
192. Rose A.W. Origin of trace element distribution patterns in sulfides of the Central and Bingham Districts, Western U.S.A. *Mineral Deposita* 5, 1970, 157-63.
193. Rowe J. The eastern extension orebody, Tynagh Mine, Co. Galway, Ireland. BSc. treatise, R.S.M. Imp. Coll.London. 1970.
194. Russell M.J. Structural controls of base metal mineralization in Ireland in relation to continental drift. *Trans. Instn.Min.Metall.* 77, 1968, B 117-28.
195. Sato H. Geochemical environments in terms of Eh and pH. *Econ.Geol.* 55, 1960, 928-61.
196. Sawkins F.J. Preliminary fluid inclusion studies of the mineralization associated with the Hercynian granites of southwest England, *Trans.Instn.Min. Metal.* 75, 1966, 109-12.
197. Sawkins F.J. Chemical brecciation, an unrecognized mechanism for breccia formation? *Econ.Geol.* 64, 1969, 613-17.
198. Schermerhorn L.J.G. The deposition of volcanics and pyritite in the Iberian pyrite belt. *Mineral. Deposita*, 5, 1970, 273-79.
199. Schreyer W., Kullerud G. and Ramdohr P. Metamorphic conditions of ore and country rock of the Bodenmais, Bavaria, sulfide deposit *Neues Jahrb.Mineral.Abhandl.*, 101(1), 1964, 1-26.

200. Scott S.D. and Barnes H.L. Sphalerite geothermometry at 330° - 580°C(abs). *Econ.Geol.* 62, 1967, 874-75.
201. Shackleton R.M. The Pre-Cambrian rocks of Wales. In, *The Pre-Cambrian and Lower Palaeozoic rocks of Wales.* Wood A.(Ed)(Cardiff; University of Wales Press, 1969) 1-22.
202. Shapiro L and Brannock W.W. Rapid analysis of silicate, carbonate and phosphate rocks. *U.S.G.S.Bull.* 1144A, 1962, 56p.
203. Sindeeva N.D. Mineralogy and types of deposits of selenium and tellurium (New York, etc.: Wiley, 1964) 363p.
204. Singh D.S. Measurement of spectral reflectivity with the Reichert Microphotometer. *Trans.Instn.Min. Metall.* 74, part 14, 1965, 901-16.
205. Skinner B.J. Effect of manganese on the sphalerite geothermometer (abs.). *Bull.Geol.Soc.Am.*, 70, 1959, 1676.
206. Smith F.G. Determination of the temperature and pressure of formation of minerals by the decrepitative method. *Min.Engineer.* 4, 1952, 703-8.
207. Smyth L.D. et al. The geology of South-East Ireland, together with parts of Limerick, Clare and Galway. *Proc.Geol.Ass.* 50, 1939, 287-351.
208. Smyth W.W. On the mines of Wicklow and Wexford. *Rec. School of Mines Vol I* (London : Longman, 1853) 349-412.
209. Sollas W.J. Contributions to a knowledge of the granites of Leinster. *Trans.R.Ir.Acad.* 29, 1891, 427-513.
210. Solomon M., Rafter T.A. and Jensen M.L. Isotope studies on the Rosebery, Mount Farrell and Mount Lyell ores, Tasmania. *Mineral.Depositn* 4, 1969, 172-99.
211. Springer G. Electron probe analyses of tetrahedrite. *N.Jb.Mineral. Mh.*, 1969, 24-32.
212. Spry A. *Metamorphic textures.* (Oxford, etc.: Pergamon, 1969) 350p.
213. Stanton R.L. Abundances of copper zinc and lead in some sulfide deposits. *J.Geol.*, 66, 1958, 484-502.
214. Stanton R.L. General features of the conformable 'pyritic' orebodies - Pt.2; *Mineralogy.Bull.Can.Instn. Min.Metall.*, 53, 1960, 28-36.

215. Stanton R.L. Mineral interfaces in stratiform ores.
Trans.Instn.Min.Metall. 74, part 2, 1964, 45-79.
216. Stanton R.L. Discussion in Proc. CSIRO Symp. on Iron Sulphides, CSIRO Division of Min.Chemistry Investig.Rpt. 305R, 1969, p.42.
217. Stanton R.L. and Gornan H.A. A phenomenological of grain boundary migration in some common sulphides.
Econ.Geol. 63, 1968, 907-23.
218. Stanton R.L. and Rafter T.A. The isotopic composition of sulphur in some stratiform lead-zinc sulphide ores. Mineral.Deposita, 1, 1966, 16-29.
219. Suffel G.G. Remarks on some sulphide deposits in volcanic extrusives. Bull.Can.Inst.Min.Metall., 58, 1965, 1057-63.
220. Suzuki T. A geochemical study of selenium in volcanic exhalation and sulphur deposits. Chem.Soc. Japan, B, 37, 1964, 1200-06.
221. Taylor S.R. The application of trace element data to problems in petrology. Phys.Chem.Earth, 6, 1964, 133-214.
222. Templeman-Kluit D.J. The relationship between sulfide grain size and metamorphic grade of host rocks in some strata-bound pyritic ores. Can.J.Earth Sci. 7, 1970, 1339-45.
223. Tooms J.S., Summerhayes C.P. and Cronan D.S. Geochemistry of marine phosphate and manganese deposits. Oceanogr.Mar.Biol.Ann.Rev. 7, 1969, 49-100.
224. Tremlett W.E. The Pre-Cambrian rocks of southern Co. Wicklow (Ireland) Geol.Mag. 96, 1959, 58-68.
225. Tremlett W.E. The structure of the Lower Palaeozoic rocks of the Arklow District (Ireland). Q.J. geol.Soc.Lond., 115, 1959, 17-40.
226. Troshin Y.P. and Troshina G.M. On the stability of distribution of trace elements during the formation of polymetallic deposits. Geochemistry, 2, 1965, 42-46.
227. Turner F.S. Metamorphic petrology. (New York, etc.: McGraw-Hill, 1968) 403p.
228. Turikian K.K. and Wedepohl K.H. Distribution of the elements in some major units of the earth's crust. Bull.geol.Soc.Am., 72, 1961, 175-92.

229. Tuttle O.F. and Bowen N.L. Origin of granite in the light of experimental studies in the system $\text{NaAlSi}_3\text{O}_8 - \text{KAlSi}_3\text{O}_8 - \text{SiO}_2 - \text{H}_2\text{O}$. Geol.Soc. Am.Mem. 74, 1952, 153p.
230. Uytendogaardt W. Tables for microscopic identification of ore minerals. (Princeton Univ.Press 1951) 242p.
231. Vallentyne J.R. A chemical study of pyrite spherules isolated from sediments of Little Round Lake, Ontario. In Jensen M.L. (ed.) Biogeochemistry of sulphur isotopes. Nat.Sci.Found.Symp. (Yale Univ.Press, New Haven 1963) 144-52.
232. Van Hook H.J. The ternary system $\text{Ag}_2\text{S}-\text{Bi}_2\text{S}_3-\text{PbS}$. Econ. Geol. 55, 1960, 759-88.
233. Vaughan D.J. Zonal variation in bravoite. Am. Miner. 54, 1969, 1075-83.
234. Velikoborets T.A. Crystal morphology and the cobalt content of pyrite. Doklady Akad.Nank SSSR. 189, 1969, 139-41.
235. Vine J.D. Element distribution in some shelf and eugiosynclinal black shales. U.S.Geol. Survey Bull. 1214-E, 1966, 31p.
236. Vokes F.M. Mines in south and central Norway. Guide to Excursion C.10 XXI Intl.geol.Cong.Norden, 1960, 73p.
237. Vokes F.M. Mineral parageneses of the massive pyritic orebodies of the Caledonides of Norway. Econ. Geol. 57, 1962, 890-903.
238. Vokes F.M. Geological studies on the Caledonian pyritic zinc-lead orebody at Bleikvassli, Nordland, Norway. Norges geol.unders., 222, 1963.
239. Vokes F.M. Pyrite-copper deposits in Cyprus. Tidsskr. fur.Kjemi, Bergr. od.Metall. 24, 1964, 172-77.
240. Vokes F.M. Regional metamorphism of the Palaeozoic geosynclinal sulphide ore deposits of Norway. Trans.Instn.Min.Metall. 77, 1968, B53-B59.
241. Vokes F.M. A review of the metamorphism of sulphide deposits. Earth Sci.Rev. 5, 1969, 99-143.
242. Wager L.R. and Mitchell R.L. The distribution of trace elements during strong fractionation of basic magma-a further study of the Skaergaard intrusion, East Greenland. Geochim,Cosmochim.Acta, 1, 1951, 129-208.

243. Waltham A.C. The geology of the Folldal massive sulphide deposits, Norway. Ph.D. thesis, University of London, 1968, 198p.
244. Warren H.V. and Thompson R.M. Sphalerites from Western Canada. *Econ.Geol.* 40, 1945, 309-35.
245. Weaver T. The geological relations of the East of Ireland. *Trans.geol.Soc.Lond.*, 5, 1821, 117-304.
246. Webber C.R. Second report of analytical data for CAAS syenite and sulphide standards. *Geochim. Cosmochim.Acta*, 29, 1965, 229-48.
247. Wedepohl K.H. Chemical fractionation in the sedimentary environment. In, *Proceedings of a Symposium on Origin and distribution of the elements.* Ahrens L.H.(ed)(London etc.: Pergamon, 1968) 889p.
248. Wedepohl K.H. *Handbook of Geochemistry.* (Berlin, etc.: Springer-Verlag 1969).
249. Welin E. Notes on the mineralogy of Sweden 5. Bismuth-bearing sulphosalts from Gladhammer, a revision. *Ark.Min.Geol.* 4, No.13, 1967, 377-86.
250. Wheatley C.J.V. Aspects of metallogenesis within the Southern Caledonides of Great Britain and Ireland. *Trans.Instn.Min.Metall.* 80, 1971, B.211-223.
251. White D.E. and Waring G.A. Volcanic emanations. In *Data of Geochemistry*, 6th ed., U.S.Geol. Survey Prof. Paper 440-K, 1963, 29p.
252. Williams D. Volcanism and ore deposits. *Freiberger. Forschft.* C210, 1966, 93-111.
253. Wilson A.D. A new method for the determination of ferrous iron in rocks and minerals. *Bull.Geol.Surv. Gt.Brit.*, 9, 1955, 56-58.
254. Wilson W.R. An account of the exploration of the Avoca mines, County Wicklow, Ireland. *Trans.Instn. Min.Metall.* 65, 1956, 209-28.
255. Wisser E.H. Relation of ore deposition to doming in the North American Cordillera. *Mem.geol.Soc.Am.* 77, 1960, 117p.
256. *World Mining*, December 1968, 52-53.
257. Wynne L.C. Report on the Avoca Mines. Private Rpt. to Mianrai Teoranta 1945.

258. Young B.B. and Millman A.P. Microhardness and deformation characteristics of ore minerals. Trans.Instn. Min.Metall. 73, 1964, 437-66.
259. Yund R.A. and Kullerud G. Thermal stability of assemblages in the Cu-Fe-S system. J.Petrol. 7, 1966, 454-88.
260. Yund R.A. and Hall H.T. Hexagonal and monoclinic pyrrhotites. Econ.Geol. 64, 420-23.
261. Northern Miner, March 4th 1971.